

10-25-2021

Development of an Ultra-High Performance Concrete Joint Detail for Short-Span Bridges

Francisco De Jesus Chitty Gozalo
fchit001@fiu.edu

Follow this and additional works at: <https://digitalcommons.fiu.edu/etd>



Part of the [Civil Engineering Commons](#), [Construction Engineering and Management Commons](#), [Structural Engineering Commons](#), and the [Transportation Engineering Commons](#)

Recommended Citation

Chitty Gozalo, Francisco De Jesus, "Development of an Ultra-High Performance Concrete Joint Detail for Short-Span Bridges" (2021). *FIU Electronic Theses and Dissertations*. 4896.
<https://digitalcommons.fiu.edu/etd/4896>

This work is brought to you for free and open access by the University Graduate School at FIU Digital Commons. It has been accepted for inclusion in FIU Electronic Theses and Dissertations by an authorized administrator of FIU Digital Commons. For more information, please contact dcc@fiu.edu.

FLORIDA INTERNATIONAL UNIVERSITY

Miami, Florida

DEVELOPMENT OF AN ULTRA-HIGH PERFORMANCE CONCRETE JOINT
DETAIL FOR SHORT-SPAN BRIDGES

A dissertation submitted in partial fulfillment of the

requirements for the degree of

DOCTOR OF PHILOSOPHY

in

CIVIL ENGINEERING

by

Francisco De Jesus Chitty Gozalo

2021

To: Dean John L. Volakis
College of Engineering and Computing

This dissertation, written by Francisco De Jesus Chitty Gozalo, and entitled Development of an Ultra-High Performance Concrete Joint Detail for Short-Span Bridges, having been approved in respect to style and intellectual content, is referred to you for judgment.

We have read this dissertation and recommend that it be approved.

Walled Orabi

Atorod Azizinamini

Seung Jae Lee

Kingsley Lau

David Garber, Major Professor

Date of Defense: October 25, 2021

The dissertation of Francisco De Jesus Chitty Gozalo is approved.

Dean John L. Volakis
College of Engineering and Computing

Andres G. Gil
Vice President for Research and Economic Development
and Dean of the University Graduate School

Florida International University, 2021

© Copyright 2021 by Francisco De Jesus Chitty Gozalo
All rights reserved.

DEDICATION

To my mother, Isabel M. Gozalo. For her persistent encouragement, understanding, and unconditional love, which made the fruition of the project and the writing of this dissertation a reality.

ACKNOWLEDGMENTS

I would like to express the deepest appreciation to my Major Advisor, Dr. David Garber, for his unconditional support, patience, insightful guidance, and confidence in my abilities to not only complete all the project tasks, but to complete them with excellence throughout this long journey.

I would like to thank my project manager, Christina Freeman, for her valuable advice and crucial contribution over the years of concept development, design, and testing. I also want to acknowledge the expert guidance and contribution from the FDOT Structures Research Center staff: William Potter, Stephen Eudy, Justin Robertson, Sam Adeniji, Sandra Bell, Miguel Ramirez, Paul Tighe, Ben Allen, Ariana Morales, and Bruno Vasconcelos. This project was supported by the Florida Department of Transportation. The opinions, findings, and conclusions expressed here are those of the authors and not necessarily those of the Florida Department of Transportation or the U.S. Department of Transportation.

Sincere thanks to the members of my doctoral committee, Dr. Atorod Azizinamini, Dr. Kingsley Lau, Dr. Seung Jae Lee, and Dr. Wallied Orabi for their input, valuable discussions, and accessibility.

Last, but not least, I would like to thank my uncle, Julio F. Gozalo, for giving me the opportunity to come to the US, and for his continuous encouragement in pursuing my goal; thanks also to my aunt Laura and my cousins Carlo, Isabel, and Sophia for their continuous support and motivation; and I thank my dearest friends Fatima Vieira and Isabella Zapata for their constant support, good humor, and unconditional friendship that nourished me during my graduate student years and now future career life.

ABSTRACT OF THE DISSERTATION

DEVELOPMENT OF AN ULTRA-HIGH PERFORMANCE CONCRETE JOINT
DETAIL FOR SHORT-SPAN BRIDGES

by

Francisco De Jesus Chitty Gozalo

Florida International University, 2021

Miami, Florida

Professor David Garber, Major Professor

Slab beam superstructures have been used for short-span bridges since prestressed concrete began to be used in the US. Poor joint performance of these superstructures led to recent revisions to design standards; one example being the Florida Slab Beam (FSB). The FSB and other similar slab beam systems include a composite cast-in-place (CIP) reinforced concrete deck and joint between adjacent beams. An optimized joint design has been developed to accelerate the construction times and eliminate the need for a CIP deck by using ultra-high performance concrete (UHPC) in the longitudinal closure pour to connect the precast members.

The optimized joint design was first developed from eight different cross-section and joint reinforcement details (four 18-inch deep specimens including the control, and four 12-inch deep specimens), investigating the joint transverse service and strength behavior in a small-scale experimental testing protocol. All the specimens were transversely supported and tested under a three-point load setup, applying the load

adjacently to the joint region. All 18-inch deep joints performed similar to the current FSB design, while the 12-inch deep specimen with the lowest joint reinforcement placement had the largest transverse strength capacity among those of the same thickness.

The best joint geometry performer from the 12-inch deep specimens in the small-scale protocol was selected to investigate further the overall joint behavior with 30-foot length specimens. Two two-beam test configurations with UHPC joints were developed and experimentally tested under strength and cyclic performance with different loading schemes and support conditions, investigating the load transfer mechanisms, and the demand on the precast concrete, joint reinforcement, and joint interface.

The joint performed well with no observed joint distress or deterioration in performance through the permit service load testing, more than four million cycles of load, and ultimate strength testing of the two-beam systems. Results from these tests and numerical models were used to guide in the subsequent design and construction aids of the new FSB system for accelerated construction to replace aging short-span bridges.

TABLE OF CONTENTS

| CHAPTER | PAGE |
|--|------|
| 1. INTRODUCTION | 1 |
| 1.1 Overview | 1 |
| 1.2 Research Objectives | 2 |
| 1.3 Research Scope | 3 |
| 1.4 Thesis Organization..... | 4 |
| 2. BACKGROUND | 7 |
| 2.1 Overview | 7 |
| 2.2 Current Bridge Inventory Status | 9 |
| 2.3 Concrete Short-Span Bridge Solutions | 10 |
| 2.3.1 Adjacent Box Beams..... | 11 |
| 2.3.2 New England Extreme Tee (NEXT) Beam | 18 |
| 2.3.3 Poutre-Dalle System and Minnesota Modification..... | 24 |
| 2.3.4 Inverted-T Prestressed Beams..... | 29 |
| 2.3.5 Florida Slab Beam..... | 34 |
| 2.4 Longitudinal and Transverse Joints..... | 38 |
| 2.4.1 Non-UHPC Joints | 40 |
| 2.4.2 UHPC Joints..... | 46 |
| 2.5 Joint Materials | 55 |
| 2.5.1 Non-UHPC Materials..... | 55 |
| 2.5.2 UHPC Materials..... | 57 |
| 2.5.3 UHPC Mixing and Casting Procedure | 62 |
| 2.6 Other UHPC Bridge Superstructure Applications | 64 |
| 2.6.1 UHPC Overlays | 64 |
| 2.6.2 UHPC Members..... | 65 |
| 2.7 Summary | 65 |
| 3. RESEARCH METHODOLOGY..... | 67 |
| 4. NUMERICAL STUDY OF SHORT-SPAN BRIDGE SOLUTIONS..... | 69 |
| 4.1 Overview | 69 |
| 4.2 Selection of Short-Span Bridge Deck Members | 69 |
| 4.3 Analytical Investigation | 71 |
| 4.3.1 Background..... | 71 |
| 4.3.2 Effects of Section Depths and Strand Number | 72 |
| 4.4 Numerical Investigation | 74 |
| 4.4.1 Numerical Methods..... | 74 |
| 4.4.2 Specimen Geometries and Loading Configurations | 76 |
| 4.4.3 Meshing and Material Models | 78 |
| 4.5 Numerical Results and Discussion..... | 80 |
| 4.5.1 Effects of Distribution Factors..... | 80 |

| | | |
|-------|--|-----|
| 4.5.2 | Effects on Transverse Section and Joint Demand..... | 82 |
| 4.6 | Conclusions and Recommendations..... | 86 |
| 4.7 | Data Availability Statement | 88 |
| 4.8 | Acknowledgement..... | 88 |
| | | |
| 5. | JOINT DESIGN OPTIMIZATION FOR ACCELERATED BRIDGE CONSTRUCTION OF SLAB BEAM BRIDGES..... | 89 |
| 5.1 | Abstract | 89 |
| 5.2 | Introduction | 90 |
| 5.2.1 | Slab Beam Superstructures | 91 |
| 5.2.2 | Research Motivation, Objective, and Significance..... | 94 |
| 5.2.3 | Previously Investigated Joint Details with UHPC..... | 95 |
| 5.3 | Development of UHPC Joint Geometry and Reinforcement Detail | 96 |
| 5.4 | Numerical Investigation | 99 |
| 5.4.1 | Numerical Methods..... | 99 |
| 5.4.2 | Specimen Geometry..... | 100 |
| 5.4.3 | Meshing and Material Models | 101 |
| 5.4.4 | Transverse Joint Capacity..... | 102 |
| 5.5 | Experimental Investigation | 105 |
| 5.5.1 | Specimen Design and Material Properties..... | 105 |
| 5.5.2 | Test Setup and Loading Protocol..... | 108 |
| 5.5.3 | Instrumentation | 111 |
| 5.6 | Experimental Results and Discussion | 111 |
| 5.6.1 | Performance of Numerical Modeling | 113 |
| 5.6.2 | Performance of Current FSB Joint Detail..... | 114 |
| 5.6.3 | Performance of Developed Joint Details | 117 |
| 5.6.4 | Interface Surface Finish and Bond to UHPC..... | 120 |
| 5.6.5 | Fatigue Performance of Joint Specimens..... | 122 |
| 5.7 | Conclusions | 125 |
| 5.8 | Notations | 126 |
| 5.9 | Data Availability Statement | 127 |
| 5.10 | Acknowledgements | 127 |
| | | |
| 6. | FULL-SCALE TESTING OF SLAB-BEAM BRIDGE SYSTEM FOR ACCELERATED BRIDGE CONSTRUCTION..... | 128 |
| 6.1 | Abstract | 128 |
| 6.2 | Introduction | 129 |
| 6.2.1 | Research Motivation, Objective, and Significance..... | 133 |
| 6.3 | Experimental Program..... | 133 |
| 6.3.1 | Specimen Design and Material Properties..... | 135 |
| 6.3.2 | Test Setups and Loading Protocols..... | 137 |
| 6.3.3 | Instrumentation | 144 |
| 6.4 | Experimental Results and Discussion | 145 |
| 6.4.1 | Effect of Cyclic Loading..... | 145 |
| 6.4.2 | Effect of Intermediate Support..... | 147 |

| | | |
|-------|--|-----|
| 6.4.3 | Joint Demand for Continuous Beams | 149 |
| 6.4.4 | Effect of Cracking on Joint Demand | 151 |
| 6.4.5 | Ultimate Strength Behavior | 153 |
| 6.5 | Conclusions | 156 |
| 6.6 | Data Availability Statement | 158 |
| 6.7 | Acknowledgements | 158 |
| 7. | SUMMARY, CONCLUSIONS, AND RECOMMENDATIONS..... | 159 |
| 7.1 | Conclusions and Recommendations..... | 160 |
| 7.1.1 | Analytical Study of Precast Concrete Superstructure Systems..... | 160 |
| 7.1.2 | Joint Design Optimization and Small-Scale Testing Protocol..... | 161 |
| 7.1.3 | Full-Scale Testing Protocol..... | 162 |
| 7.1.4 | Constructions and Design Recommendations | 164 |
| 7.2 | Recommendations for Future Work..... | 166 |
| | REFERENCES | 168 |
| | APPENDIX..... | 176 |
| | VITA..... | 221 |

LIST OF TABLES

| TABLE | PAGE |
|--|------|
| Table 2.1: 3 rd Generation bridges built in Minnesota [47]..... | 28 |
| Table 2.2: Ultimate load capacity for each Specimen [36]..... | 31 |
| Table 2.3: FSB Property Table. (Beam's widths are from 4' to 5') | 36 |
| Table 2.4: Commercial and Non-commercial grout materials [64]..... | 56 |
| Table 2.5: Non-commercial grout materials [64] | 57 |
| Table 2.6: Typical Composition of UHPC [65]..... | 58 |
| Table 2.7: Typical field-cast UHPC material properties [4]..... | 58 |
| Table 2.8: Typical ranges of UHPC non-proprietary mixtures with fine aggregates (not including steel fibers) (based on data from Graybeal [66])..... | 61 |
| Table 2.9: Cost of material per volume of low cost UHPC [66] | 61 |
| Table 4.2: Section depths with strand numbers for each span length and section widths with corresponding efficiency factors (units: mm, 1 mm = 0.0394 in. = 0.00328 feet) ... | 73 |
| Table 4.3: Summary of concrete and steel materials models used | 80 |
| Table 4.4: Section parameters and distribution factor summary | 80 |
| Table 5.1: Design values for UHPC connections (based on [4])..... | 96 |
| Table 5.2: Summary of concrete and steel material models used..... | 102 |
| Table 5.3: Material properties for experimental specimens..... | 107 |
| Table 6.1: Service, fatigue, and strength testing schedule for FIU-4/5 | 143 |

LIST OF FIGURES

| FIGURES | PAGE |
|---|------|
| Figure 2.1: Total US National Bridge Inventory [12] less than 22.9 m (75 ft.) by: (a) bridge condition, (b) bridge age, and (c) number of lanes (units: m, 1 m = 3.281 ft.) | 10 |
| Figure 2.2: Prestressed concrete box beam construction per year [39] | 12 |
| Figure 2.3: Typical box girder sections: (a) regular, non-composite section and (b) composite section [38] | 13 |
| Figure 2.4: Box girder configurations: (a) adjacent configuration and (b) spread configuration [39] | 15 |
| Figure 2.5: Hawk Lake Bridge [42] | 16 |
| Figure 2.6: Shear keys [43]: (a) Partial depth shear key and (b) full-depth shear key systems | 17 |
| Figure 2.7: High-level railroad platform [5] | 18 |
| Figure 2.8: Typical configurations for NEXT beams [44] | 20 |
| Figure 2.9: Typical reinforcement for NEXT beams [44] | 21 |
| Figure 2.10: Types of joint detail for NEXT D beam [44] | 22 |
| Figure 2.11: NEXT beam section at Dailey Precast plant, Shaftsbury, Vermont [5] | 23 |
| Figure 2.12: Poutre-Dalle Section [45] | 24 |
| Figure 2.13: Colocation detail of Poutre-Dalle System [45] | 24 |
| Figure 2.14: New type of developed joints [47]: (a) joint between PCSS panels (90-degree hooks) and (b) drop-in reinforced cage | 26 |
| Figure 2.15: (a) Typical transverse section of a bridge with PCSS system; (b) typical MnDOT PCSS [47] | 27 |
| Figure 2.16: Erection of Bridge 04002 located on MN Highway 72 over the Tamarac River near the rural, northern Minnesota town of Waskish. [47] | 28 |
| Figure 2.17: (a) 3D FEM representation of an inverted-tee section with straight web, (b) Side view FEM representation of an inverted-tee section with straight web [36] | 30 |

| | |
|---|----|
| Figure 2.18: (a) Typical composite cross-section and (b) typical reinforcing details [50]..... | 32 |
| Figure 2.19: Connection detail [50]..... | 32 |
| Figure 2.20: Phase construction of US 360 bridge [50]..... | 33 |
| Figure 2.21: Florida Slab Beam Superstructure system..... | 35 |
| Figure 2.22: Typical FSB Section [51]..... | 36 |
| Figure 2.23: (a) Placement of FSBs adjacent to each other and (b) finished pilot project SRS 373 [51]..... | 37 |
| Figure 2.24: Shear force at joint | 38 |
| Figure 2.25: Bending moment at joint | 39 |
| Figure 2.26: (a) Most common non-UHPC connection detail (Adapted from Biswas [56]) and (b) most common UHPC connection detail (adapted from Graybeal [3]) | 40 |
| Figure 2.27: Sample joint details for (a) PCSS (Minnesota), (b) inverted-T (Virginia), and (c) Florida slab beam (FSB) (Florida)..... | 42 |
| Figure 2.28: Transverse Joint Between precast slabs [56]..... | 43 |
| Figure 2.29: Two types of mechanical connectors: welded connection detail [57] and grouted HSS pocket connection [58] | 44 |
| Figure 2.30: Additional reinforcement required in (a) transverse direction [59] and (b) extending from side of members [60]..... | 45 |
| Figure 2.31: UHPC joint connection examples adapted from: (a) Royce [61] and (b) Aaleti and Sritharan [62]..... | 46 |
| Figure 2.32: Joint developed by FHWA [63] | 47 |
| Figure 2.33: (a) Traditional solution with post-tensioning and (b) UHPC connection solution without post-tensioning [63] | 48 |
| Figure 2.34: (a) Conventional shear key specimen and (b) UHPC shear key specimen [63]..... | 49 |
| Figure 2.35: Forced Cracking [63]..... | 49 |

| | |
|---|----|
| Figure 2.36: Sollars Road Bridge cross-section [63]..... | 50 |
| Figure 2.37: (a) Longitudinal joint detail and (b) shear key dowel detail [63]..... | 51 |
| Figure 2.38: (a) UHPC connection between precast deck panels as deployed by NYSDOT on CR47 over Trout Brook, (b) UHPC adjacent box beam connection detail , and (c) combined UHPC deck-level and composite connections as deployed by NYSDOT on I-81 near Syracuse, NY [4]..... | 52 |
| Figure 2.39: Panel-to-panel and panel-to-girder connection [62]..... | 52 |
| Figure 2.40: Common panel-to-panel UHPC connection details: (a) waffle deck panel-to-panel connection detail, (b) panel-to-panel headed connection detail, (c) panel-to-panel straight connection detail, and (d) panel-to-panel hairpin reinforcement [62] | 53 |
| Figure 2.41: Shear key connection in Wapello County Bridge [62]..... | 54 |
| Figure 2.42: (a) Compressive UHPC behavior, (b) Tensile UHPC behavior [65] | 58 |
| Figure 2.43: General procedure for mixing and casting UHPC [65]..... | 63 |
| Figure 2.44: Cast-in-place UHPC overlay, immediately (a) before and (b) after placement [65] | 64 |
| Figure 2.45: (a) Mars Hill Bridge girder comparison [65] and (b) Pi girder used in Jakway Park Bridge [6]..... | 65 |
| Figure 3.1: Research methodology flowchart..... | 68 |
| Figure 4.1: Selected bridge shapes with available widths (W) and depths (H): (a) Northeast DBT beam, (b) NEXT D beam, (c) AASHTO BI for ABC, and (d) Florida Slab Beam for ABC (units: mm, 1 mm = 0.0394 in.)..... | 70 |
| Figure 4.2: Summary of UHPC joint shapes for: (a) decked girders, (b) AASHTO BI, and (c) Florida Slab Beam (units: mm, 1 mm = 0.0394 in.)..... | 70 |
| Figure 4.3: Example bridge using Florida Slab Beam (not to scale; units: m, 1 m = 3.281 ft.)..... | 71 |
| Figure 4.4: 1219-mm (48-inch) width sections comparison: (a) maximum span length versus required section depth and (b) maximum span length versus number of 15-mm (0.6-inch) diameter strands | 74 |

| | |
|---|-----|
| Figure 4.5: Schematics of example bridge for FEA analysis: (a) half-bridge model with boundary conditions, (b) load patch pattern, and (c) load cases (FSB shown, others similar; not to scale; units: m, 1 m = 3.281 ft.)..... | 77 |
| Figure 4.6: Mesh examples: (a) superstructure and (b) joint detail | 79 |
| Figure 4.7: Maximum principal stress map at midspan for Load Case 3 – NEXT D section: (a) full width cross section, (b) zoomed in precast-joint region (other side similar), and (c) joint A and B cross-section stress maps (1 MPa = 0.15 ksi)..... | 83 |
| Figure 4.8: Maximum principal stress map at midspan for Load Case 3 – DBT section: (a) full width cross section, (b) zoomed in precast-joint region (other side similar), and (c) joint B and C cross-section stress maps (1 MPa = 0.15 ksi) | 84 |
| Figure 4.9: Maximum principal stress map at midspan for Load Case 2 – FSB section: (a) full width cross section, (b) zoomed in precast-joint region (other side similar), and (c) joint A and B cross-section stress maps (1 MPa = 0.15 ksi) | 85 |
| Figure 4.10: Maximum principal stress map at midspan for Load Case 2 – AASHTO BI section: (a) full width cross section, (b) zoomed in precast-joint region (other side similar), and (c) joint A and B cross-section stress maps (1 MPa = 0.15 ksi)..... | 86 |
| Figure 5.1: Slab beam system evolution in Florida: (a) prestressed rectangular slab unit (1955), (b) prestressed keyed slab unit (1958), (c) prestressed voided slab units – Sonovoid (1958), (d) prestressed slab unit – PSU (2008), (e) Florida Slab Beam – FSB (2015), based on Goldsberry [51], and (f) precast composite slab span system – PCSS (2005)..... | 93 |
| Figure 5.2: Details for joint: (a) FDOT 1 (F1), (b) FDOT 2 (F2), (c) Alternate 1 (A1), and (d) Alternate 2 (A2). (units: mm, 1 mm = 0.0394 in) | 98 |
| Figure 5.3: Specimen details for analytical and experimental program. (units: mm, 1 mm =0.0394 in)..... | 100 |
| Figure 5.4: Transverse capacity evaluation: (a) applied load relative to joint and supports, (b) top view of wheel patch location, (c) 18F1 top and bottom expected cracking pattern before failure (others similar), and (d) 18F1 estimated load-deflection response (others similar). (length units: mm, 1 mm = 0.0394 in)..... | 104 |
| Figure 5.5: Maximum principal stress at the load point in 305-mm (12-inch) deep specimens from FEA at (a) service load of 35.6 kN (8 kips) and (b) ultimate load (load dependent on joint type) with cracking in the plane shown in black (1 MPa = 0.15 ksi) | 105 |

| | |
|--|-----|
| Figure 5.6: Construction of joint specimens: (a) precast specimen concrete pour, (b) delivery of slab-beam specimens to FDOT SRC, (c) casting of field-cast UHPC, and (d) FSB deck casting..... | 108 |
| Figure 5.7: Testing frame layout: (a) supports elevation and specimen layout and (b) supports plan layout (actuator centerline parallel to longitudinal joint). (units: mm, 1 mm = 0.0394 in)..... | 109 |
| Figure 5.8: Ultimate flexural strength comparison. (1 kN-m = 0.738 k-ft)..... | 112 |
| Figure 5.9: Load versus deflection responses with maximum loads for (a) 457-mm (18-inch) deep and (b) 305-mm (12-inch) deep specimens; *Monolithic response after fatigue testing completed | 113 |
| Figure 5.10: FSB joint performance: (a) load versus deflection response (b) specified joint detail with 64-mm bend diameter for hooks and (c) actual joint reinforcement with larger than 64-mm bend diameter for hooks. (length units: mm, 1 mm = 0.0394 in) | 116 |
| Figure 5.11: Failure mechanism observed during testing: (a) pullout of hooked reinforcement in FSB-1 (hooked joint reinforcement shown), (b) pullout of straight joint reinforcement caused by splitting crack in 12F1-1 (splitting crack shown after unloading), (c) pullout of straight joint reinforcement in 18F1-1 (bottom view shown), (d) pullout of straight joint reinforcement with conical failure in 12F2-2, and (e) crushing of concrete in top of section in 12A2-1..... | 119 |
| Figure 5.12: Impact of joint surface finish on performance: (a) surface finish obtained using heavy sandblasting, (b) debonding during testing of 18A1-1 (occurred in majority of these specimens with sandblasted finish), (c) failure plane of 18A1-1 after specimen removed from test setup, (d) surface finish obtained using paste retarder on forms for 12A2-2, (e) failure of 12A2-2..... | 122 |
| Figure 5.13: Normalized absolute stiffness every thousandth cycle of system for joints (a) 12F1-2, (b) 12A1-2, and (c) 12A2-2. *Cracked specimen due to accidental load.... | 124 |
| Figure 6.1: Joint system and CIP concrete topping system construction for: (a) Poutre-Dalle (French slab beam), (b) Minnesota PCSS, (c) Virginia inverted-tee, and (d) Florida Slab Beam..... | 132 |
| Figure 6.2: Slab-beam section details for two-beam system tests: (a) keyway detail, (b) side-joint detail, and (c) cross-section reinforcement detail. Note: design is for 9150-mm beam length (units: mm, 1 mm = 0.0394 in.)..... | 134 |
| Figure 6.3: Slab beam and joint construction process: (a) reinforcement cage and wood formwork with painted paste retarder, (b) concrete cast in beams, (c) exposed | |

| | |
|--|-----|
| aggregate finish, (d) joint geometry with non-contact lap spliced rebar, baker rod and leakage sealer, (e) wooden strips for UHPC overpour, and (f) top joint form closure application..... | 137 |
| Figure 6.4: Testing frame layout for LC 2-4 (service loading) and LC 2-1 (ultimate strength) (units: mm, 1 mm = 0.0394 in.)..... | 138 |
| Figure 6.5: Test setup for configurations: (a) FC 2-5 plan/elevation views, (b) reverse sinusoidal load protocol for FC 2-5, (c) static transverse cracking load protocol for FC 2-5cr, (d) FC 2-6 plan/elevation views, (e) reverse sinusoidal load protocol for FC 2-6, and (f) static load protocol for FC 2-6st. (units: mm, 1 mm = 0.0394 in.)..... | 141 |
| Figure 6.6: Testing frame layout for LC 2-7 (continuous span) (units: mm, 1 mm = 0.0394 in.)..... | 142 |
| Figure 6.7: (a) Normalized stiffness at midspan versus fatigue cycles and (b) load versus midspan deflection before and after FC 2-5 fatigue loading (1 kN = 0.225 kips; 1 mm = 0.0394 in.)..... | 146 |
| Figure 6.8: (a) Strain change of top transverse CSGs per change in applied load versus number of cycles and (b) load versus strain in top transverse CSGs before and after FC 2-5 fatigue loading (1 kN = 0.225 kips; 1 mm = 0.0394 in.)..... | 147 |
| Figure 6.9: (a) Load versus displacement for FIU-4/5 with LC 2-4 and FC 2-6st load configurations and (b) load versus longitudinal concrete strain for longitudinal CSGs on bottom of system at midspan (1 kN = 0.2248 kips; 1 mm = 0.0394 in.)..... | 148 |
| Figure 6.10: Load versus average strain across the joint for FIU-4/5 on top of the system measured using CDTs using (a) LC 2-4 and (b) FC 2-6st load configurations (1 kN = 0.2248 kips)..... | 149 |
| Figure 6.11: (a) Load versus displacement for FIU-4/5 with LC 2-4 and LC 2-7 load configurations and (b) load versus average curvature found using CSGs on top and bottom of system toward beam ends and midspan (1 kN = 0.2248 kips; 1 mm = 0.0394 in.)..... | 150 |
| Figure 6.12: Load versus transverse concrete strain on top of FIU-4/5 for (a) LC 2-4 and (b) LC 2-7 (1 kN = 0.2248 kips)..... | 151 |
| Figure 6.13: (a) Load versus displacement for FIU-4/5 with FC 2-5cr and FC 2-6cr load configurations and (b) load versus longitudinal concrete strain for longitudinal CSGs on bottom of system at midspan of beams (1 kN = 0.2248 kips; 1 mm = 0.0394 in.)..... | 152 |

Figure 6.14: Load versus average strain across the joint for FIU-4/5 on top of the system measured using CDTs using FC 2-5cr (a) before (LR 10-1) and (b) after (LR 15-1) transverse cracking and subsequent fatigue loading (1 kN = 0.2248 kips)..... 153

Figure 6.15: (a) Load versus displacement for ultimate strength tests on FIU-1/2 and FIU-4/5, (b) failure of FIU-1/2, and (c) failure of FIU-4/5 (1 kN = 0.2248 kips; 1 mm = 0.0394 in.)..... 154

Figure 6.16: Crack patterns from cores at center region: (a) plan location of cores, (b) core location at boundary region, (c) north side core, (d) center side core, and (e) south side core. (units: mm, 1 mm = 0.0394 in.)..... 155

Figure 6.17: Load versus joint reinforcement strain for joint reinforcement region extending from FIU-1 in the center region for (a) LC 2-4 service load testing and (b) ultimate strength testing (1 kN = 0.2248 kips; 1 mm = 0.0394 in.)..... 156

Figure 7.1: Proposed joint geometry based on small-scale joint testing and two-beam system tests (units: mm, 1 mm = 0.0394 in.)..... 160

ABBREVIATIONS AND ACRONYMS

| | |
|--------|---|
| AASHTO | American Association of State Highway Officials |
| ASCE | American Society of Civil Engineers |
| FDOT | Florida Department of Transportation |
| FEA | Finite Element Analysis |
| FHWA | Federal Highway Administration |
| FSB | Florida Slab Beam |
| GDF | Girder Distribution Factors |
| PBES | Prefabricated Bridge Elements and Systems |
| PCI | Precast/Prestressed Concrete Institute |
| SCC | Self-Consolidating Concrete |
| UHPC | Ultra-High Performance Concrete |

1. INTRODUCTION

1.1 Overview

Structural joints are necessary to transfer load between bridge elements in superstructure constructions, and they must be designed for strength and ductility requirements with proper detailing to withstand the demand over the bridge service life. Most of the joint applications in bridge superstructures have been to connect precast members (e.g., slabs to beams and slabs, adjacent beams, caps to columns, etc.). When connecting adjacent elements such as precast panels, prestressed decked tee beams, or slab beams, a range of connection materials and systems have been implemented, like wide reinforced concrete closure pours, transverse tie bars in sleeves, transverse posttensioning systems, grouted shear keys, welded plates, among others.

However, a decay in service performance has been documented with these connection systems as they start to lose the load transfer mechanism between members in some cases immediately after joint construction. This decay can be caused by superstructure movement due to thermal effects and service loads and results in reflective cracks in the riding surface immediately above the joint. These cracks can lead to further performance decay by allowing the intrusion of moisture resulting in corrosion of the reinforcement in the connection matrix, exacerbating the loss of the load transfer mechanism in the superstructure.

Many bridge owners have been testing and deploying Ultra-High Performance Concrete (UHPC) in bridge joints around North America and Europe as a solution to diminish the occurrence of joint cracks, while enhancing the capacity of the load transfer mechanism.

UHPC has become more widely used in bridge joint applications due to its well-known superior performance, including high compressive and tensile strength, long-term durability, low permeability, high flowability, and low water-to-cement ratio (all compared to current conventional concrete) [1], [2]. It also increases the precast-to-UHPC bond by providing a stronger connection than the precast element itself, and it reduces large reinforcement densities by eliminating the usage of a cast-in-place (CIP) deck when UHPC joints are used.

Although this material has been implemented in bridge connections with adjacent precast panels [3], [4], prestressed decked tee beams [3], [5], [6], and prestressed box girders [7], [8], a thorough review of the literature indicated that this implementation has not been focused on slab-beam systems for short span bridges.

1.2 Research Objectives

The main objective of this research was to develop a resilient, slab-beam system with accelerated on site construction times utilizing a UHPC connection between precast members. The development of the joint detail included the following secondary objectives:

- Identify precast concrete superstructure systems for accelerated construction with UHPC connections
- Develop cross-section and joint region details for short- to medium-span slab-beam bridges for use with accelerated construction,
- Compare analytically the developed slab-beam system to other precast concrete systems for accelerated construction,

- Assess transverse strength, fatigue, and service performance of cross-section and joint using small-scale joint testing,
- Assess longitudinal and transverse strength, fatigue, and service performance of developed slab-beam joint detail by conducting full-scale structural tests.

1.3 Research Scope

The above objectives were achieved through the following primary research tasks:

- Task 1: Involved an extensive literature review to develop the appropriate background in precast, prestressed bridge superstructure systems for short-span bridges, focusing on connection mechanisms, joints material performance, and UHPC joints,
- Task 2: Identified potential joint cross-section geometries and reinforcement arrangement following a review of past work to optimize the current slab-beam cross-section and joint design,
- Task 3: Determined feasible span lengths with different slab-beam section depths and prestressing strand patterns, comparing it with other common prestressed superstructure systems,
- Task 4: Designed and built several different cross-section and joint details to investigate further in the small-scale experimental testing, focusing on joint transverse behavior in strength and service performance,
- Task 5: Based on the selected best performer joint detail from Task 4 to investigate the overall superstructure behavior in the large-scale experimental testing, focusing

on the assessment of two two-beam systems with different loading schemes and support conditions.

The summation of the work will provide designers with a slab-beam system with UHPC joint that could be used effectively for accelerated construction of short-span bridges, providing a performance for 100 years of service life without debonding or distress at the precast-joint boundary region.

1.4 Thesis Organization

This dissertation is written based on the format of ‘Thesis Containing Journal Papers’. The dissertation includes the research background and methodology, one manuscript to be submitted for scholarly journals, one published journal paper, and one submitted manuscript under review. Additional chapters are provided to complete the dissertation and summarize work not adequately captured in the two unpublished manuscripts. The organization is as follow:

- ***Chapter 2 – Background:*** This chapter introduces the background on the current national bridge inventory status, existing precast, prestressed superstructure systems for short-span bridges, and reviewing also existing longitudinal and transverse connections including joint materials.
- ***Chapter 3 – Research Methodology:*** This chapter discusses the research methodology followed to carried out the development of a UHPC joint detail for slab-beam bridges.
- ***Chapter 4 – Numerical Study of Short-Span Bridge Solutions (to be submitted to Engineering Structures Journal) [9]:*** A discussion of four different precast,

prestressed concrete sections suitable for accelerated construction of short span bridges is presented. It includes a parametric study of different variables such as span length, section depth, strand number, and efficiency factor. Also, a numerical analysis of the joint connection demand is discussed for all superstructure systems.

- **Chapter 5 – “Joint Design Optimization for Accelerated Bridge Construction of Slab Beam Bridges”** (published on *ASCE Bridge Engineering Journal*) [10]: This paper discusses results from small-scale testing conducted at the FDOT Structures Research Center (SRC). It includes numerical and experimental results of eight small-scale UHPC joint connections between 16 56-inch long and 60-inch wide slab-beam elements (connecting two precast specimens with one longitudinal joint), and design and construction recommendations for large-scale specimens.
- **Chapter 6 – “Full-Scale Testing of Slab-Beam Bridge System for Accelerated Bridge Construction”** (submitted to *ASCE Bridge Engineering Journal*) [11]: The final papers describes the results from the large-scale testing conducted at the FDOT Structures Research Center (SRC). It includes experimental results of two large-scale UHPC joint connections between four 30-foot long and four-foot wide slab-beam specimens (connecting two precast specimens with one longitudinal joint), and design and construction recommendations for bridge implementation. Also, this chapter discusses four different precast, prestressed concrete sections suitable for accelerated construction of short span bridges. It includes a parametric study of different variables such as span length, section depth, strand number, and efficiency factor. A numerical analysis of the joint connection demand is also discussed for all superstructure systems.

- *Chapter 7 – Summary, Conclusions, and Recommendations*: A conclusions section is then provided to summarize conclusions and propose recommended future work from all three papers.

2. BACKGROUND

2.1 Overview

Many of the nation's bridges have reached or are nearing the end of their functional design lives and need repair, rehabilitation, or replacement. Prefabricated bridge elements (PBEs) are almost exclusively used in these scenarios to reduce construction times, minimize the impact on the public, and improve durability performance. There are many different short-span bridge options available in the United States and also in Florida. Each option has its advantages and disadvantages, and each have different requirements for connecting adjacent elements.

Based on the latest National Bridge Inventory (NBI) data, the United States has 618,456 bridges built across the country with approximately 80-percent having a maximum span length less than 22.9 m (75 ft.) [12]. The condition of these bridges was evaluated in the latest infrastructure report card published in 2021 by the American Society of Civil Engineers (ASCE), where the nation's bridges received a C grade, identifying more than seven percent of them as structurally deficient, requiring maintenance, rehabilitation, or replacement [13]. Efforts have been made by state bridge officials to reduce the number of structurally deficient bridges as the percentage decreased by almost two percent since the last report in 2017 [14]. However, at the current rate of enhancements, it would take more than 50 years to repair all of these bridges with existing practices [13], not to mention the bridges now approaching to the end of their design life, with some above 70 years old.

Departments of Transportation (DOTs) have worked towards the development of bridge replacement programs to aid the aging infrastructure and decrease its vulnerability to the

traveling public. According to Doolen et al. [15], AASHTO and FHWA have encouraged the development and use of various accelerated bridge construction (ABC) strategies such as PBEs, state-of-the-art construction equipment, new material technologies, and innovative contracting methods to rapidly address the damaged conditions of bridges. These efforts by DOTs and FHWA have led to many different programs to encourage ABC, e.g., “Everyday Counts” (EDC) and associated cost studies by the FHWA [16], [17], and research efforts.

Rodenberry and Servos [18] investigated PBES among all state DOT’s standard bridge sections suited for ABC, identifying Minnesota’s inverted-tee beam and the PCI Northeast Xtreme Tee (NEXT) Beam as promising bridge superstructure standards for use in a bridge replacement program. Chavel and Yadlosky [19] developed a framework that couples significant bridge issues that occurred during construction and in service with new designs to enhance the performance and understanding of failure mechanisms. Other researchers [20]–[24], [7], [25] have identified construction materials that can enhance structural performance and durability such as innovative prestressing materials [22], high-performance grouts for structural joints [7], [20], [25], and precast/prestressed girders made of ultra-high performance concrete (UHPC) [24].

There are several focuses of the following background review. First, a discussion on the current national bridge inventory status is presented. Second, some of the more commonly used and more recently developed short-span bridge solutions are introduced. Following this introduction on short-span bridge solutions is an overview of the various types of longitudinal and transverse joints that have been used to connect adjacent members.

Finally, a summary of the material types and properties for the materials used in these joints is presented.

2.2 Current Bridge Inventory Status¹

The current US National Bridge Inventory (NBI) [12] consists of 618,456 bridges as of 2020, and the majority of the inventory (more than 79 percent) are short-span bridges, with length of maximum spans of 22.9 m (75 ft.). Of those short-span bridges number, less than eight percent (39,042) bridges are classified as Poor, having either the deck, superstructure, or substructure condition rated 4 or worse [26]. The highest number of the bridges deemed as Poor have a maximum span length between 7.6 m and 15.2 m (25 and 50 ft.), as shown in Figure 2.1 (a). Another characteristic of the total short-span bridge inventory is that more than 19 percent (94,508) are older than 70 years, as shown in Figure 2.1 (b), indicating that they are approaching to the end of their service life and would likely need major bridge repairs or replacement. Also, over 82 percent (402,707) of short-span bridges have a two-lane configuration, as shown in Figure 2.1 (c), and more than 90 percent (441,355) span over waterways.

¹ This section is from “Precast Concrete Superstructure Systems for Accelerated Construction of Short-Span Bridges”, to be submitted to Engineering Structures Journal

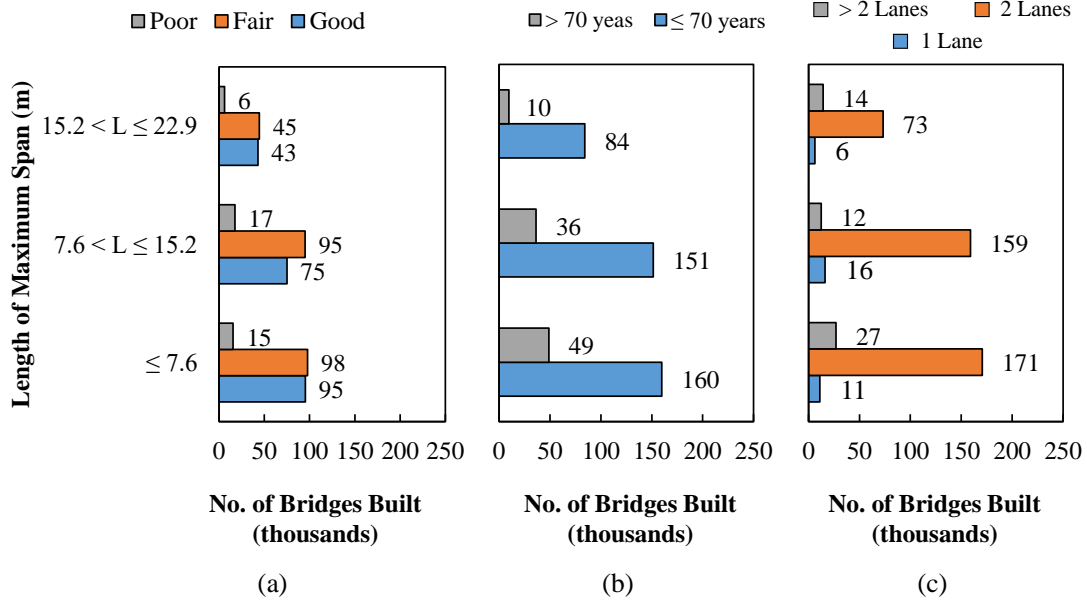


Figure 2.1: Total US National Bridge Inventory [12] less than 22.9 m (75 ft.) by: (a) bridge condition, (b) bridge age, and (c) number of lanes (units: m, 1 m = 3.281 ft.)

2.3 Concrete Short-Span Bridge Solutions

There are several different reinforced and prestressed concrete short-span bridge solutions that are being used across the US. These solutions have traditionally fallen into two main categories:

1. *Stemmed decked members*, including decked bulb tee and decked double tee beams (e.g., decked bulb-tee girders [27], Northeast Deck Bulb Tee for adjacent configurations [28], composite Florida Inverted Tee for adjacent configurations [29], composite Nebraska Inverted Tee [30], PCI double-tee beams [31], Northeast Extreme Tee beam [27], and second generation Pi-Girder shape [32]).
2. *Flat decked members*, including box beams and flat slabs (e.g., PCI box-beam systems [33], Texas box-beam systems [34], Ohio box-beam systems [35], Texas

decked slab beam [34], Minnesota Precast Slab-Span system [45], Virginia slab-beam system [36], and Florida Slab-Beam system [10]).

Five common cross sections were selected for further review from these two categories based on:

- *Construction benefits*: possessing increased on-site construction quality while reducing on-site construction activities [37];
- *Section popularity*: documented successful deployments by different state bridge officials and contractors [37], or with proven advances in the ABC state of the practice;
- *Bridge modularity*: consisting of prefabricated section geometries with deck systems and longitudinal joint details.

Specific cases of these types of short-span bridge solutions will be introduced and discussed in more detail in the following sections. Although there are many more prefabricated concrete elements in the field, the ones discussed are relevant to this research due to their resemblances to the FSB in terms of behavior, technology, and applicability.

2.3.1 Adjacent Box Beams

2.3.1.1 Background

According to Bender and Kriesel [38], the use of box girders began in the late 1940's or early 1950's in the US. Their first introduction is traced back to Pennsylvania and Tennessee; they were used primarily in short-span applications and were basically voided slabs. Basic research by the Portland Cement Association (PCA) and several universities

was done to verify and improve their strength and durability. This research resulted in sections capable of spanning from 20 to 120 feet. Avendaño et al. [39] created a chart that shows the number of prestressed concrete box beam bridges built over the last 55 years, as shown in Figure 2.2. The section had a peak of use between 1990 and 1995, when about 16% of all bridges built were box beams. Since its peak, box beam usage has been declining.

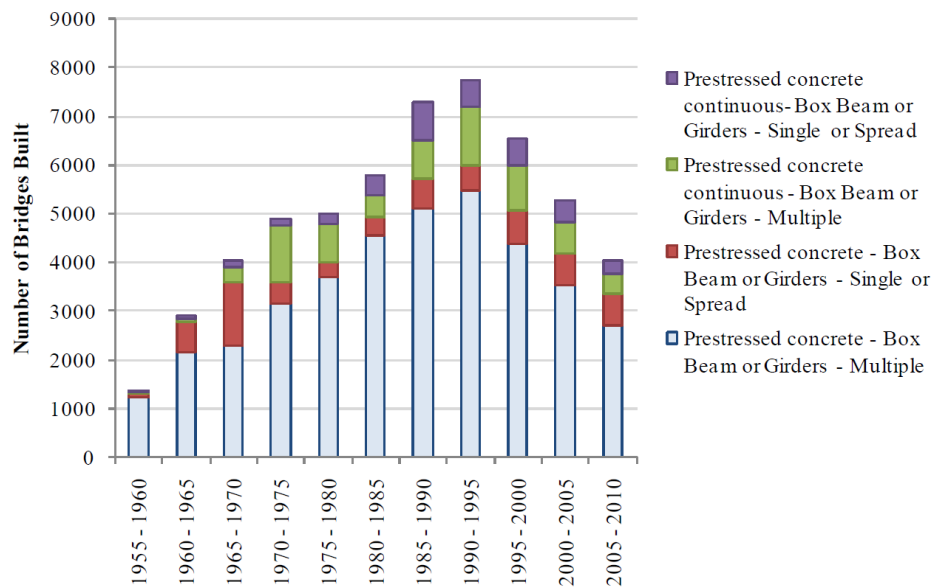


Figure 2.2: Prestressed concrete box beam construction per year [39]

2.3.1.2 Details

According to Bender and Kriesel [38], there are two typical cross-section types for short-span, box girders: (1) regular, non-composite box beams and (2) composite box beams, as shown in Figure 2.3. While dimensions of specific box girder shapes vary from state to state, the general design principles are consistent.

Box beams designed in a regular, non-composite fashion, shown in Figure 2.3 (a), are designed to withstand their share of lane loads and dead loads from the wearing surface without any composite slab cast on top. This type of construction is preferred as it allows for shorter construction times, less field labor, excellent span-to-depth ratios, and good load distribution. Proper detailing of the joint region is extremely important for this type of construction.

Composite box beams, shown in Figure 2.3 (b), are slightly different due to a minimum 4-inch cast-in-place (CIP) deck poured on top of the section. Box beams used in this fashion have protruding stirrups to ensure proper composite action between the precast box beam and the CIP deck. Because the box beams are placed side-by-side, the top of the beams serves as the lower formwork, which allows for quicker construction than spread configurations. The CIP deck will also improve the joint performance between adjacent members.

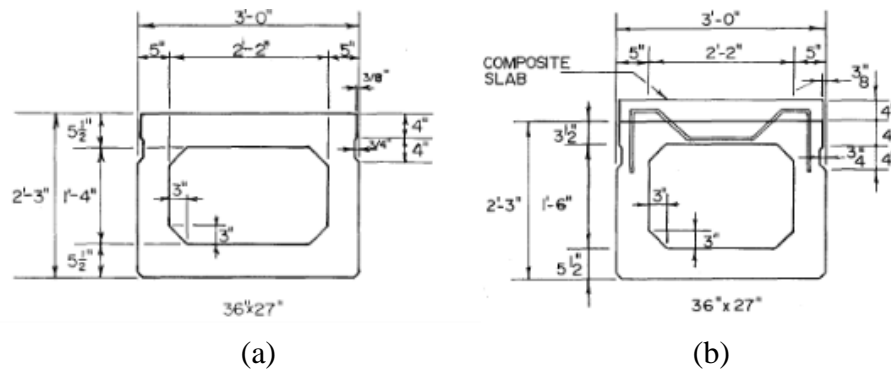


Figure 2.3: Typical box girder sections: (a) regular, non-composite section and (b) composite section [38]

In addition to the variation in section shape, short-span box girders can be used in two basic bridge configurations: (1) adjacent beam and (2) spread beam structures, as shown in

Figure 2.4. An adjacent beam configuration is where the box beams are placed immediately next to one another and no space is left between adjacent members. These adjacent members are connected using longitudinal shear keys and the bonding action of either passive high-strength rods or post-tensioning cables in the transverse direction. In spread beam configurations, the girders are placed several feet apart and driving surface is made of a full-depth, CIP deck and an asphalt overlay in some cases. Because beams in the spread configuration are not immediately adjacent to one another, neither shear keys nor transverse post-tensioning are required. Having spread box girders requires a deeper section than adjacent configurations and also requires additional prestressing strand to handle the additional loads [39].

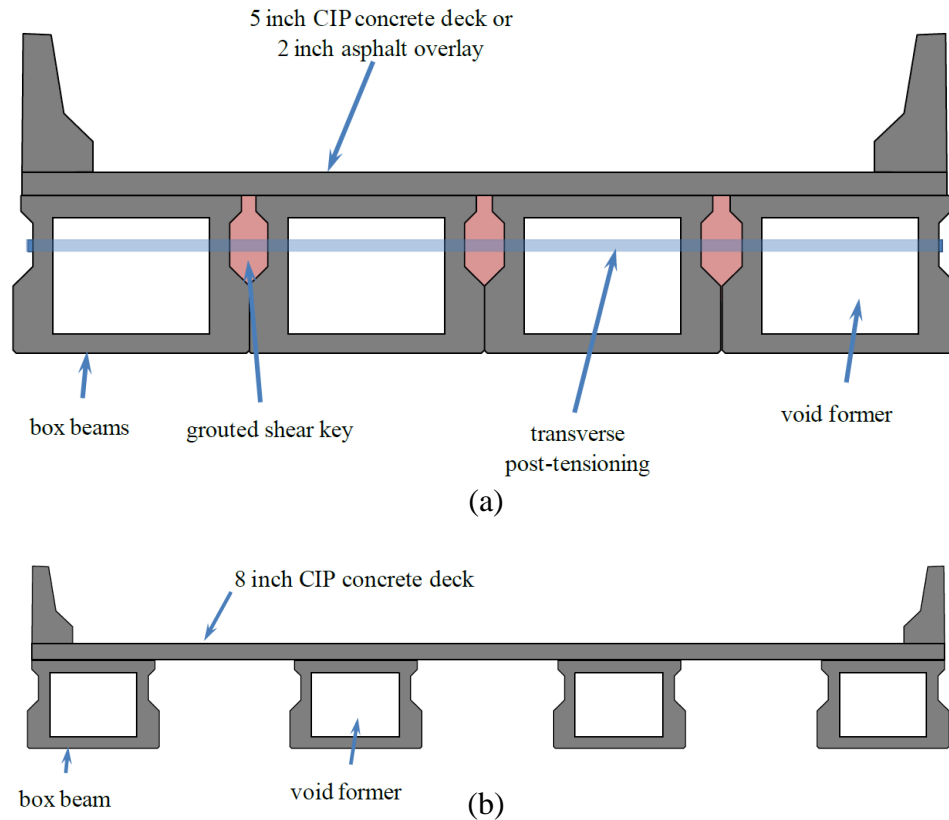


Figure 2.4: Box girder configurations: (a) adjacent configuration and (b) spread configuration [39]

For an improved box girder detail and design considerations for short-span applications, see research done by Bender and Kriesel [38], Avendaño et al. [39], Hanna et al. [40], and Corvin [41].

2.3.1.3 Current Uses

Box girder bridges are used in many states across the US for many different applications: to carry typical automotive traffic, as pedestrian bridges, as railroad bridges and even in bridge widening applications. A well-known example of an aesthetically pleasing box beam bridge is the Hawk Lake Bridge, located in Ontario, Canada (Figure 2.5). It is located over an existing Canadian Pacific Railway (CPR) rail line and is situated over elevated

train tracks, so clearance height was an important part of the design. The single-span bridge (13.8m wide x 27.2m long) has 12 side-by-side precast box girders, 11 joints, approach slabs and guardrail curbs. It received in 2010 a PCA Concrete Bridge Award which is a biennial competition that distinguishes quality in design and construction of concrete bridges.



Figure 2.5: Hawk Lake Bridge [42]

2.3.1.4 Challenges

There are a few challenges that the designer has to tackle in order to guarantee the proper behavior of the section. According to Avendaño et al. [39], if the bottom slab of the girder is too flexible, the transfer of forces transversely across the bottom section might be ineffective and the prestressing force placed in the bottom slab might not be transferred appropriately into the webs.

These researchers also highlighted the issue unique to wide girders at both ends when bridges are oriented at a skew angle. If we depict the two webs acting as two simply supported beams, the beam with the shorter span is stiffer and therefore will attract a higher fraction of the load towards the support than the beam with the larger span. The greater the skew angle, the greater the difference in the stiffness between the two webs.

As previously mentioned, challenges also arise in the area of the joint region between adjacent members. Lall, Alampalli, and DiCocco [43] highlights these challenges associated with the shear key geometries implemented in box girders. In the study, field personnel reported that longitudinal cracks were appearing shortly after construction in adjacent box beam bridges of various configurations. This longitudinal cracking can lead to premature spalling and water intrusion. According to a 1990 study [43], 54% of adjacent box beam bridges between 1985 and 1990 had developed longitudinal cracks over the shear keys. The issue was addressed by suggesting the implementation of full-depth shear keys (see Figure 2.6), full-width bearing pads, higher reinforcement ratio in the concrete deck overlay, and higher transverse post-tensioning forces and two tendons over the depth of the beam at each tendon locations. Cracking between adjacent box beams is still an issue today.

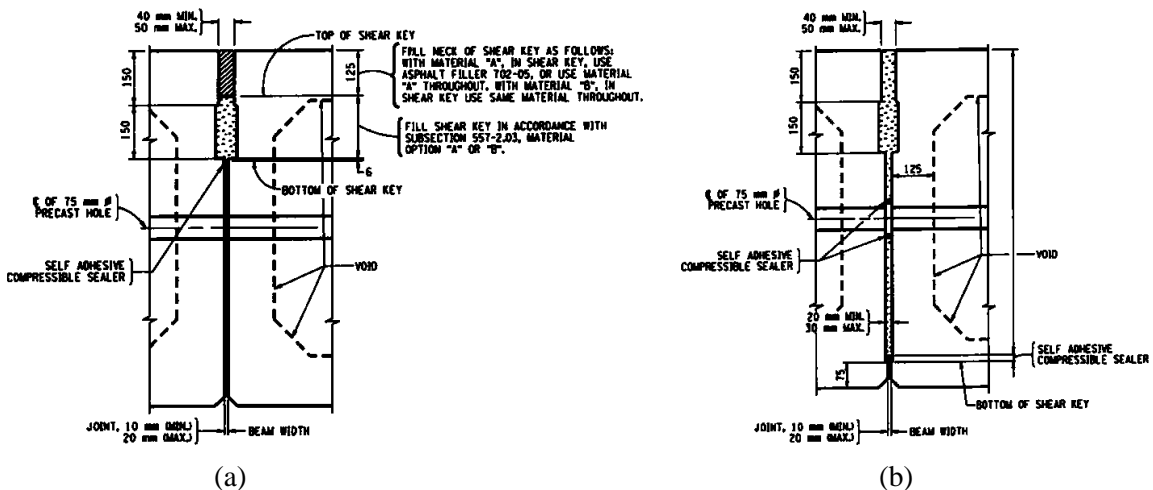


Figure 2.6: Shear keys [43]: (a) Partial depth shear key and (b) full-depth shear key systems

Finally, the box beam has associated durability concerns. Box beams are designed to have a void on the interior that is generally constructed using a Styrofoam, stay-in-place form.

This formed void typically somehow catches water, which has led to accelerated deterioration and corrosion concerns. The issues related to this deterioration are exacerbated as there is no way to easily inspect the inside conditions of a typical box beam.

2.3.2 New England Extreme Tee (NEXT) Beam

2.3.2.1 Background

The New England Extreme Tee (NEXT) beam is another short-span bridge solution implemented as an improvement over box beams. It is basically a modification of a concrete precast section originally developed for high-level railroad platform segment in the northeast (see Figure 2.7).



Figure 2.7: High-level railroad platform [5]

Different parameters were established in the design guidelines of the NEXT beam according to Culmo and Seraderian [5]:

- Bridge spans from 45 to 90 feet
- Section depths vary from 24 to 36 inches
- Widths varies from 8 to 12 feet

- Weight limit of section set to about 120 kip (due to shipment and handling concerns)
- Top flange thickness is constant at 4 inches (avoiding the need for deck forming)

2.3.2.2 Details

The Precast/Prestressed Concrete Institute (PCI) Northeast has established three types of NEXT beams, as shown in Figure 2.8 and Figure 2.9. NEXT F beams require a minimum 8-inch deep CIP concrete deck, but do not require a special longitudinal connection detail. NEXT E beams require only a 4.5-inch deep CIP deck that includes a closure pour detail to ensure proper connection between adjacent members. The top flange of the NEXT D beam doubles as the wearing surface, so only a closure pour is required to connect adjacent members and create the bridge span. The NEXT D beam is the best solution for Accelerated Bridge Construction (ABC) applications because the only on-site casting required is a narrow reinforced closure pour typically made with ultra-high performance concrete (UHPC) or non-shrink grout.

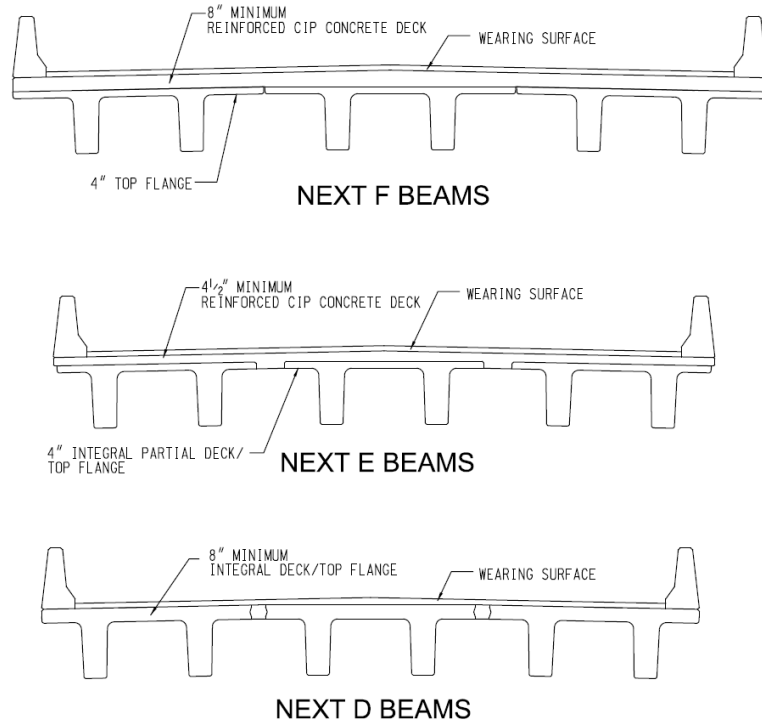


Figure 2.8: Typical configurations for NEXT beams [44]

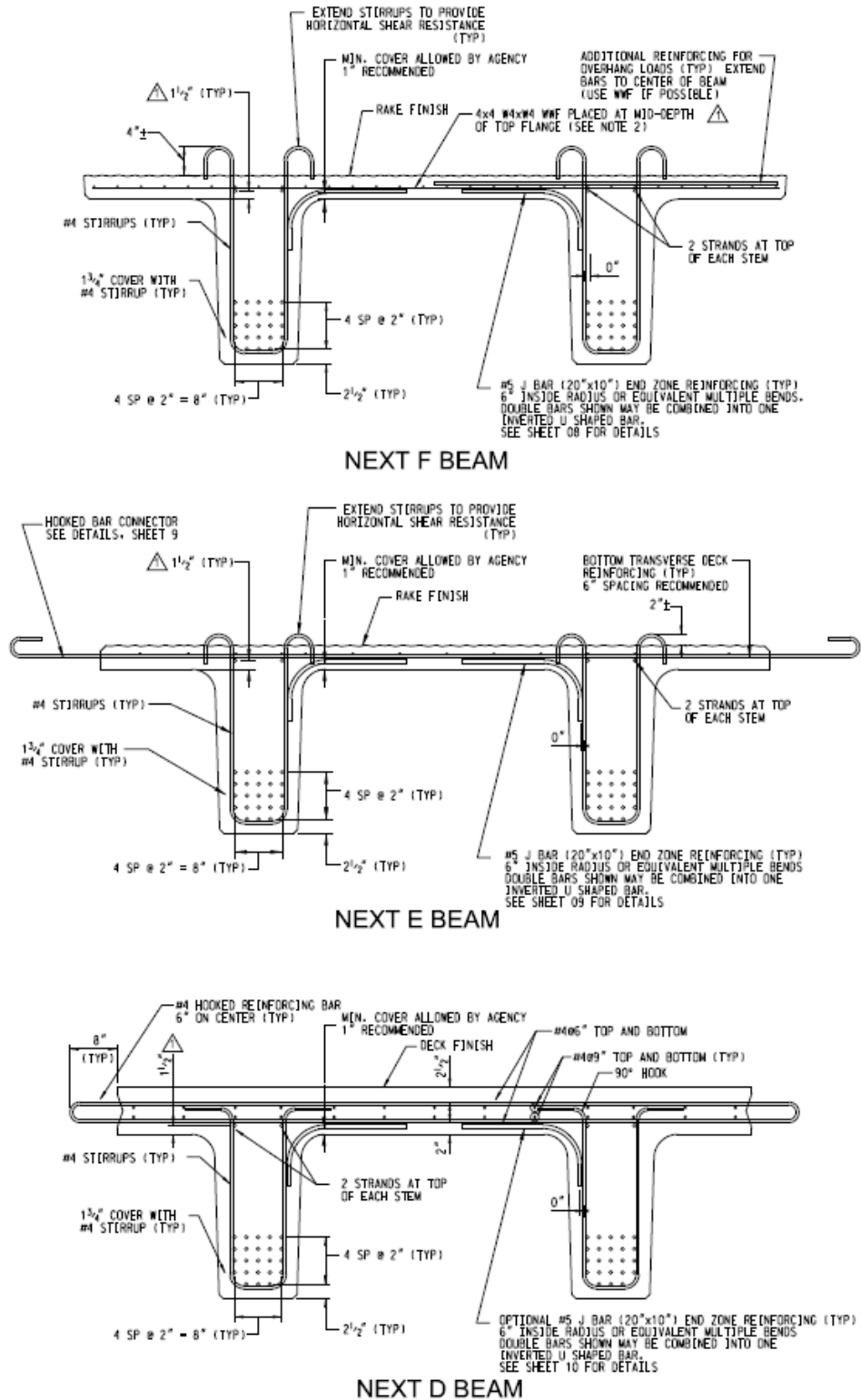


Figure 2.9: Typical reinforcement for NEXT beams [44]

It should be highlighted that for NEXT D beam, the flange connections can be designed in two ways: (1) using hooked bars with non-shrink grout or (2) using straight bars with UHPC, as shown in Figure 2.10. Hooked bars are not required when using UHPC because using UHPC greatly decreases the development length of reinforcement.

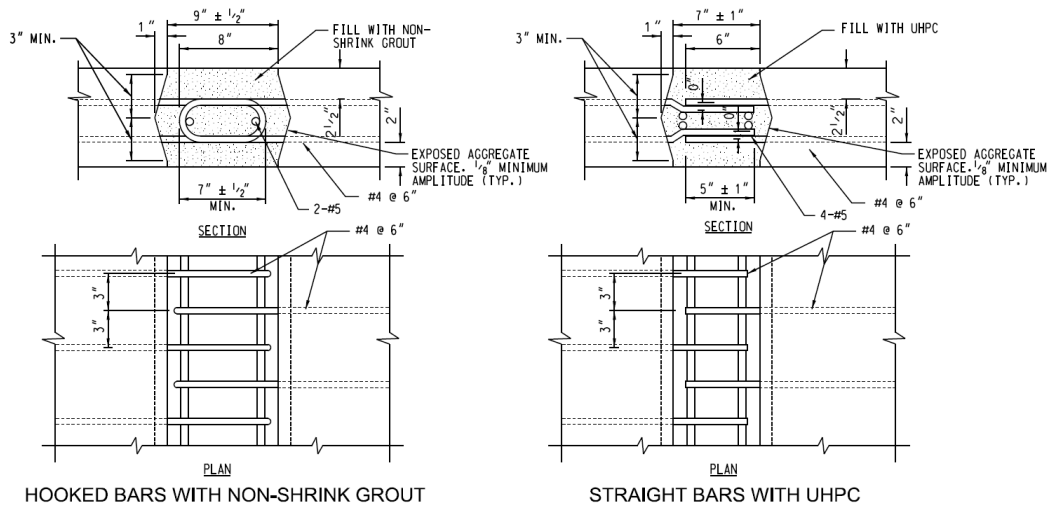


Figure 2.10: Types of joint detail for NEXT D beam [44]

2.3.2.3 Current Uses

Because the system is relatively new, the first NEXT beam project was built in 2010 in Maine. As with many short-span bridge solutions, this one was used to completely replace the New Bridge on Route 103 in York, Maine. The Maine DOT had the additional challenges of maintaining the existing profile and navigational clearances, so the bridge section was designed accordingly. A photograph from casting of the NEXT F beams used in this project is shown in Figure 2.11.



Figure 2.11: NEXT beam section at Dailey Precast plant, Shaftsbury, Vermont [5]

2.3.2.4 Challenges

Because the NEXT beam is relatively new (with the first bridge built in 2010), there have not been any long-term issues reported that affect the integrity of the girder. However, PCI Northeast has highlighted in their design guidelines possible difficulties that the designer might encounter. NEXT F beams require more CIP concrete and two layers of deck reinforcing, so there is an increased cost. There is also the possibility of having longitudinal cracks along the inner face of the stem, especially when there is greater than 20 degrees skew. NEXT E beams requires forming of larger closure pours that can also increase the cost of construction. It is also a possibility to have longitudinal cracking along the inner face of the stem when there is larger than 20 degrees skew. NEXT D beams also require forming of closure pours. Because it is a complete section (i.e., they do not require CIP concrete deck), it is more difficult to accommodate vertical curves. Lastly, this section requires the use of UHPC which can increase the up-front cost of the superstructure but decreases long term expenses due to future retrofits.

2.3.3 Poutre-Dalle System and Minnesota Modification

2.3.3.1 Background

The Poutre-Dalle (“Beam Slab”) System originally from France showed promise in innovation of rapid bridge construction. It consists of shallow precast concrete inverted-T beams that are laid down in place one next to the other. They have transverse 180-degree looped bars that ensure the transferring of forces either longitudinally or transversely depending on the configuration (See Figure 2.12).

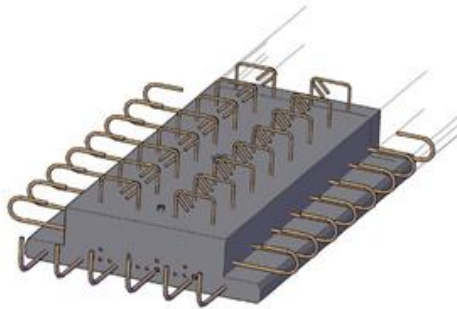


Figure 2.12: Poutre-Dalle Section [45]

After they are laid down in parallel, concrete is poured in the inner joints and continued with a top deck all in one single cast. The bottom flanges of the beams are butted up next to each other eliminating the need for formwork. The construction sequence for these members is shown in Figure 2.13.

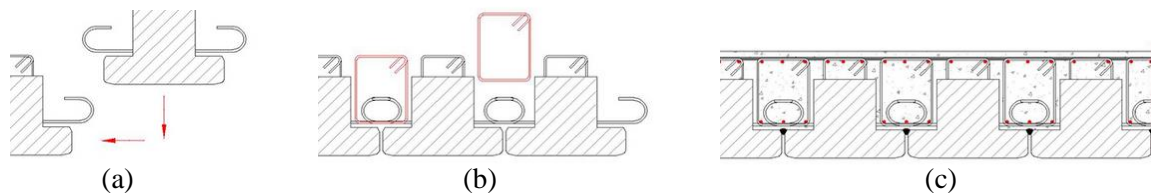


Figure 2.13: Colocation detail of Poutre-Dalle System [45]

According to Mercer [46], the system was first introduced in the US when a group of engineers sponsored by the Federal Highway Administration (FHWA) and the American Association of State Highway and Transportation Officials (AASHTO) investigated new technologies on prefabricated bridge systems in France, Japan, and Germany in 2004. This structure came out as a suitable solution for the rapid replacement of short-span bridges. Captivated with the Poutre-Dalle section, the Minnesota Department of Transportation (MnDOT) was the first to start developing a similar CIP slab span system in 2005.

The study began with a partnership between MnDOT and the University of Minnesota. Mercer (2012) states that the team tested a series of connection details to better improve its structural behavior. The major outcome in the study performed was the modification of the 180-degree hooked bars used in France to 90-degree hooked bars (see Figure 2.14). By this modification, one can now add a pre-tied reinforced cage to better resist shear forces along the joint. This drop-in reinforcement cage serves to control reflective cracks at the joint line. The new section is called Precast Composite Slab Span (PCSS) system by MnDOT.

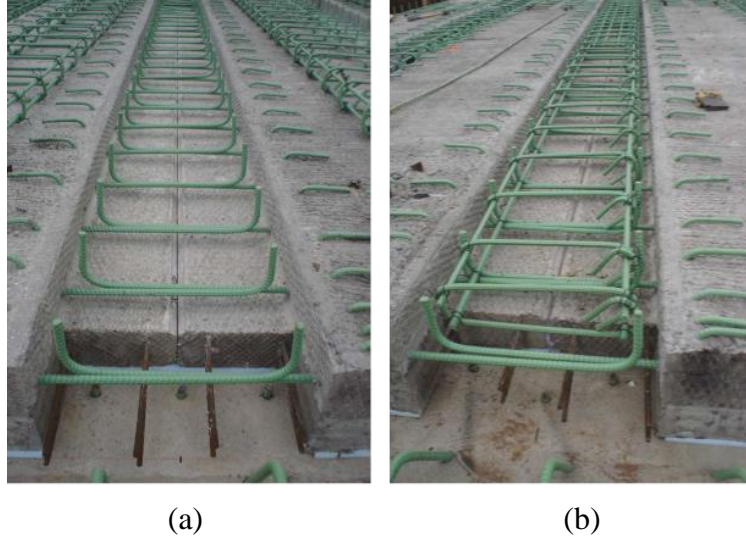


Figure 2.14: New type of developed joints [47]: (a) joint between PCSS panels (90-degree hooks) and (b) drop-in reinforced cage

For an improved PCSS detail of development and testing, see papers published by French et al. [48] and Piccinin and Schultz [49].

2.3.3.2 Details

The new PCSS is a combination of precast, prestressed concrete beams and the traditional concrete slab-span system. A general view of the cross-section developed by MnDOT is shown in Figure 2.15. This section is currently used for short-span bridges ranging from 20 to 65 feet. A roughened concrete surface and 90-degree hooks help to guarantee proper composite action between the girder and deck concrete, as shown in Figure 2.15 (b).

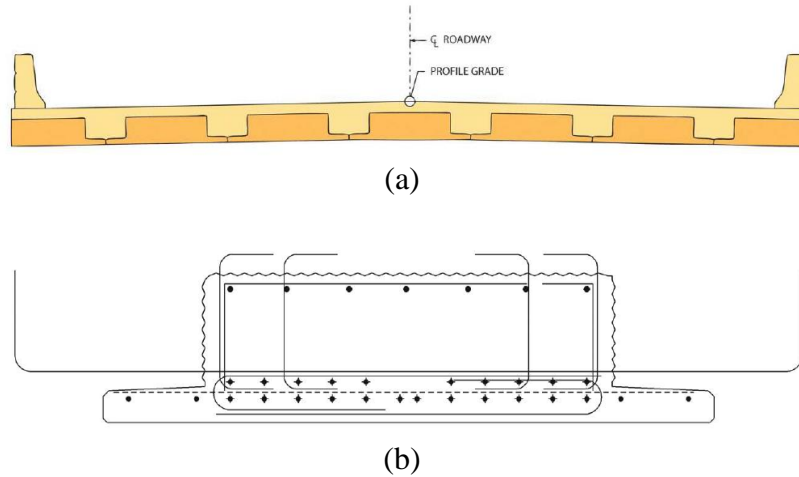


Figure 2.15: (a) Typical transverse section of a bridge with PCSS system; (b) typical MnDOT PCSS [47]

2.3.3.3 Current Uses

MnDOT first implemented the described section in two pilot bridge projects over two water crossings. The bridges served as calibration sites so that results of the field and adjustment data from laboratory tests could confirm the system's durability and verify the first PCSS design assumptions. The bridges are Bridge No. 04002 located on MN Highway 72 over the Tamarac River and Bridge No. 13004 on U.S. Highway 8 over Center Lake Channel. The erection of the bridge is shown in Figure 2.16.



Figure 2.16: Erection of Bridge 04002 located on MN Highway 72 over the Tamarac River near the rural, northern Minnesota town of Waskish. [47]

The successful implementation of the section in this first pilot project led to six more PCSS bridges being designed and built in Minnesota. The first group of three bridges or “2nd generation bridges” were built in 2007. By 2009, a group of three more bridges or “3rd generation bridges” were also erected. Some of the main characteristics of the 3rd generation bridges are shown in Table 2.1.

Table 2.1: 3rd Generation bridges built in Minnesota [47]

| | | | | |
|---|--|---|---|--|
| Bridge No., Trunk Highway No., Bridge Name, and Location | 6679, T.H. 76 over the South Fork of the Root River, Houston Co. | 49007, T.H. 238 over the Swan River, Morrison Co. | 49036, T.H. 238 over Pike Creek, Morrison Co. | 66004, T.H. 60 over the Cannon River, Rice Co. |
| Year Built | 2007 | 2009 | 2009 | 2009 |
| Total Length | n/a | 104'-2" | 72'-2" | 124'-5" |
| Width | 30'-0" | 39'-4" | 43'-4" | 47'-4" |
| Span Lengths | 19'-0" | 34'-1", 34'-10", 34'-1" | 23'-5", 24'-2", 23'-5" | 40'-5", 40'-10", 40'-5" |
| f_c Precast and CIP, psi | 4000, 4000 | 6500, 4000 | 6000, 4000 | 6000, 4000 |
| Fabricator (PCI-certified producer) | County Materials, Roberts, Wis. | Cretex Concrete Products Maple Grove, Minn. | Cretex Concrete Products Maple Grove, Minn. | Cretex Concrete Products Maple Grove, Minn. |
| Contractor | MnDOT Bridge Maintenance | Lunda Construction Co., Black River Falls, Wis. | Lunda Construction Co., Black River Falls, Wis. | Minnowa Construction Harmony, Minn. |

2.3.3.4 Challenges

There have been several issues reported by the researchers related to the PCSS section. [49] noted that standardized I-sections might be more economical and practical than PCSS sections for spans longer than 62 feet, which would correspond to a PCSS depth deeper than 25 inches. Further research regarding economic feasibility of the PCSS is needed.

Reflective cracks were observed during the pilot project at two specific locations: along the longitudinal joints and transverse joints at piers. These cracks were determined to be a result of thermal gradient effects [47]. The designers made several improvements to the geometry of the system; this cracking was reduced but not eliminated with these improvements. The University of Minnesota is still monitoring the constructed bridges to better understand the nature of the cracks and their effect on durability.

2.3.4 Inverted-T Prestressed Beams

2.3.4.1 Background

Another inverted-T section for short-to medium-span application is the solution created in Virginia. This inverted-T system was developed with the goal of decreasing reflective cracks along longitudinal joints, which is a big concern associated with such systems. The section has the advantage of a thick CIP topping and the profile is adjusted to reduce stress concentrations. [36] proposed a modification to the straight web shape from the section of Minnesota. They stated that this geometry was creating entrant corners with 90 degree angles, which are a source for crack initiation once the CIP topping is poured.

One of the main design issues tackled in this research was the transverse load distribution. Once the system is fully loaded, a two-way plate bending action takes place. The finite

element model developed by the researchers to study the transverse load behavior specifically is shown in Figure 2.17.

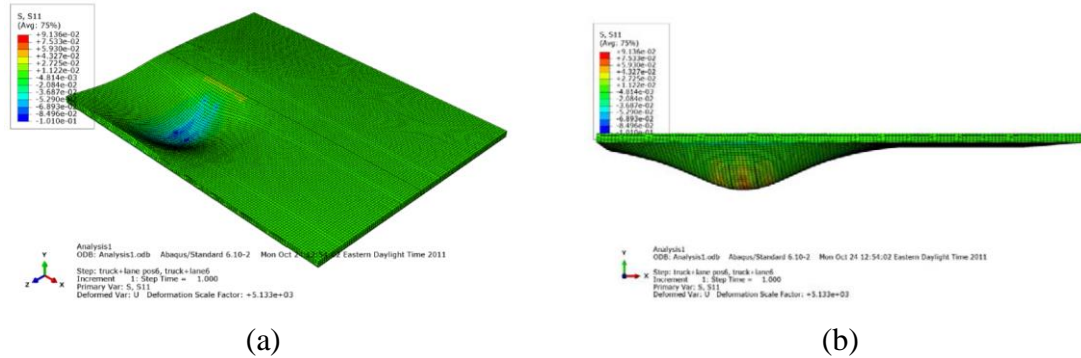


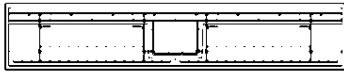
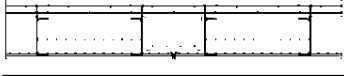
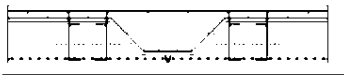
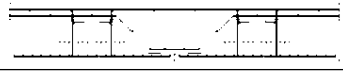
Figure 2.17: (a) 3D FEM representation of an inverted-tee section with straight web, (b) Side view FEM representation of an inverted-tee section with straight web [36]

Menkulasi et al. [36] performed an analytical and experimental study to test four specimens with different cross-section configuration:

- Specimen #1 – Straight web with extended bars (similar to University of Minnesota Section)
- Specimen #2 – Straight web with embedded plate connection
- Specimen #3 – Tapered web with embedded plate connection
- Specimen #4 – tapered web no connection

Each specimen was loaded in increments of 5 kips up to 30 kips, simulating the load that creates transverse flexural stresses. Preliminary results from these tests are shown in Table 2.2.

Table 2.2: Ultimate load capacity for each Specimen [36]

| Specimen Description | Cracking Load (kips)* | Ratio** | Ultimate Load (kips) |
|---|-----------------------|------------|---|
| Straight Web with extended bars  | 90 | 2.5 | 260 Many cracks in all directions |
| Straight web with embedded plate connection  | 100 | 2.7 | 225 Fracture of weld at one location and rebar at another |
| Tapered web with embedded plate connection  | 110 | 3.0 | Test stopped at 300 due to capacity of the loading frame. |
| Tapered web with no connection  | 60 | 1.8 | 90 (Large Crack Through Precast Section) |

The researchers concluded that tapering the webs to reduce straight angles provided necessary integrity between members and deck and prevented cracking due to service loads in the transverse direction. This detail also happened to be the cheapest of the options.

2.3.4.2 Details.

The new section consists of adjacent precast inverted-T beams with tapered webs covered with a CIP topping as shown in Figure 2.18.

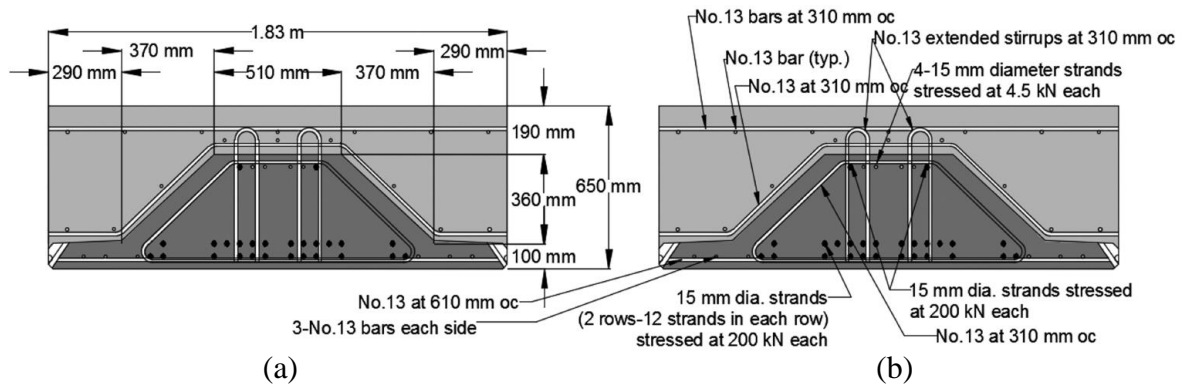


Figure 2.18: (a) Typical composite cross-section and (b) typical reinforcing details [50]

The connection detail between adjacent sections is shown in Figure 2.19. This belongs to the first bridge built in Virginia on US 360 near Richmond using the proposed technology. It is shown that the tee beams feature discrete embedded steel plates and welded bars.

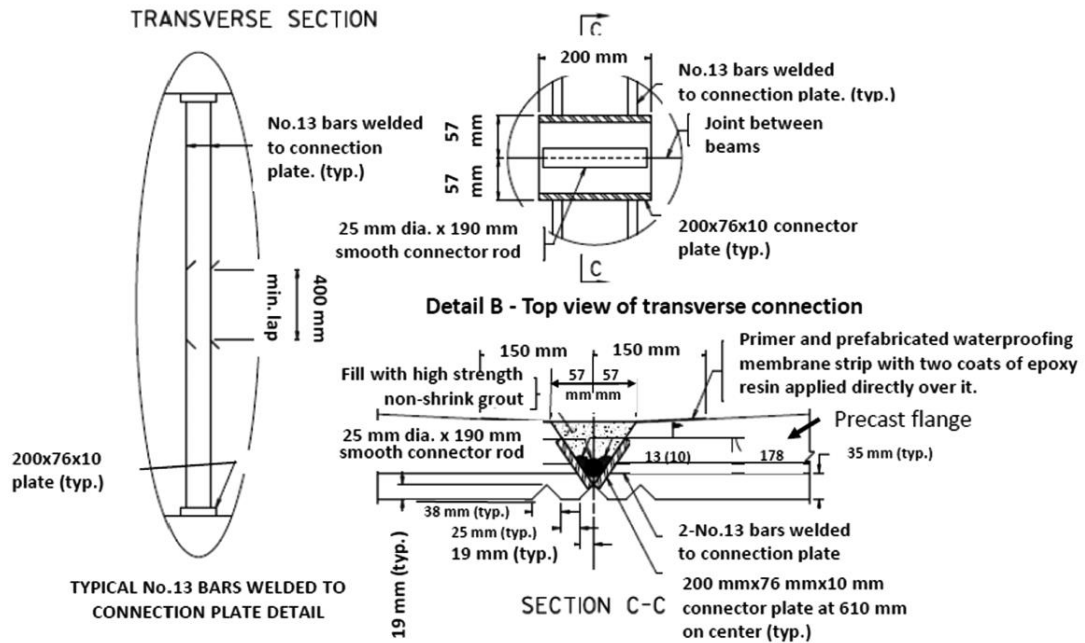


Figure 2.19: Connection detail [50]

2.3.4.3 Current Uses

This section was first implemented in a bridge built in Virginia on US 360 near Richmond.

The construction phases of this project are shown in Figure 2.20.

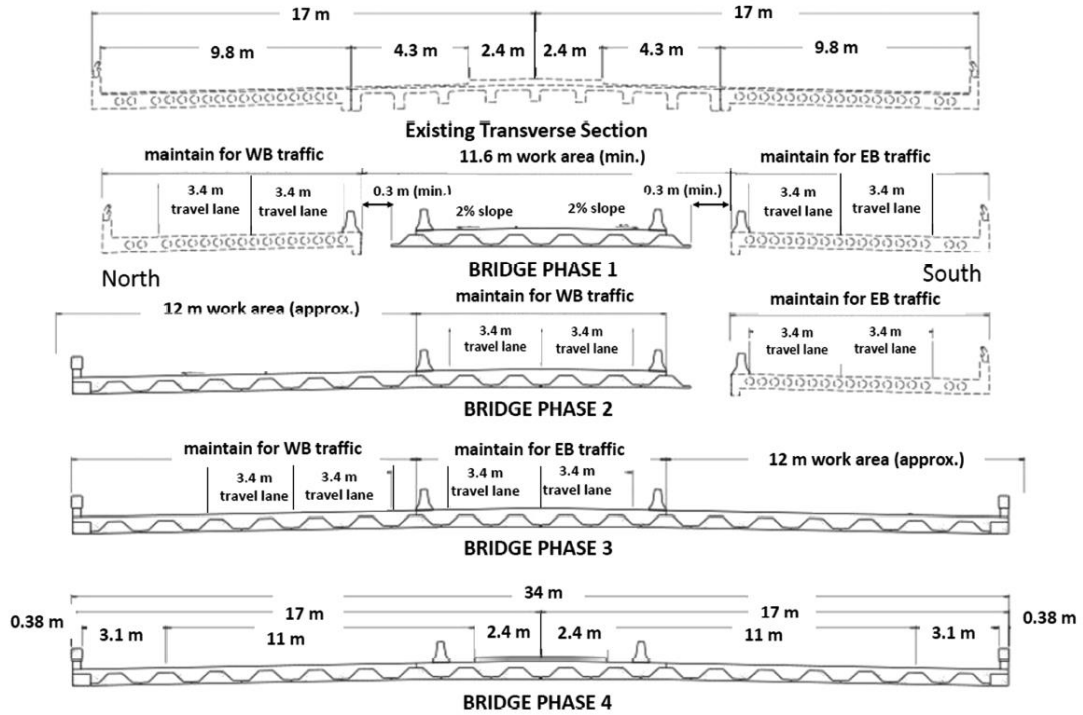


Figure 2.20: Phase construction of US 360 bridge [50]

2.3.4.4 Challenges

Due to the relatively young age of the system, there have not been any challenges reported using this type of section. However, it can be improved, according to [36], by increasing the size and reducing the spacing of the transverse reinforcement in the flanges.

2.3.5 Florida Slab Beam

2.3.5.1 Background

The development of the Florida Slab Beam (FSB) has its roots in the Minnesota FCSS. It is also a precast, prestressed, flat slab beam that requires a composite concrete deck topping and longitudinal reinforced concrete joints between beams.

Florida Department of Transportation (FDOT) has worked with precast slab beam units since the late 1940s [51], [52]. The systems have gone through several design modifications, especially to achieve a design that tackles cracking in the longitudinal direction. The FSB system has evolved from prestressed beam superstructures that were employed by FDOT and used in the mid to late 1950s. On November 9, 1984, FDOT released a memorandum to consultants and precast designers with the sole request of discontinuing the use of the precast prestressed slab units made in that period. The memorandum stated that they had modified this system several times to reduce reflective cracks through the topping at the precast slab interfaces without satisfactory results. A modification was proposed utilizing additional post-tensioning in the transverse direction. These modifications were made in hopes of causing the slab units to act as a monolithic structure and have the proper live load distribution [53].

In January 2006, FDOT introduced another iteration to the FSB system, which was presented in the Developmental Design Standards Indexes D20450 through D20453 and the associated Instructions for Developmental Design Standards as an alternative solution for short-span bridges. After several additional changes to its design, the FSB has been established to be used in off-system bridges with low Average Daily Traffic (ADT) and

low Average Daily Truck Traffic (ADTT). In March 2016, the Index D20450 Series Florida Slab Beam was officially presented. The design criteria follows current AASHTO LRFD Bridge Design Specifications, Structure Design Guidelines (SDG), and Structures Detailing Manual (SDM) [54], [55].

2.3.5.2 Details

The FSB superstructure system implemented by FDOT is shown in Figure 2.21. The components of the FSB superstructure are the FSB itself, a CIP reinforced concrete topping, and the railing system.

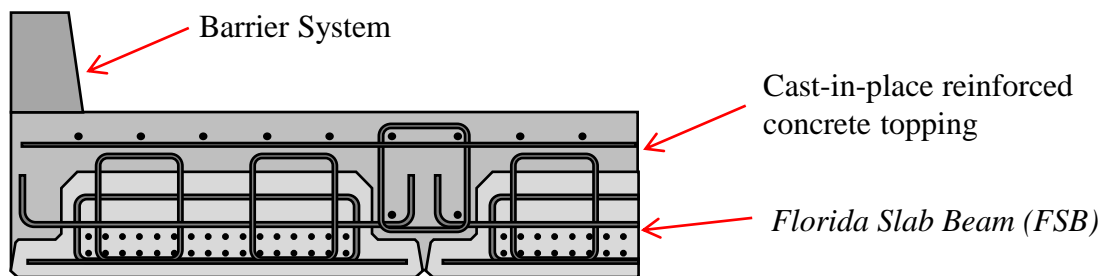


Figure 2.21: Florida Slab Beam Superstructure system

The three different types of FSB members are presented in Table 2.3 with a typical FSB cross section shown in Figure 2.22. Three FSB section depths are currently available: 12, 15, and 18-inch depths. Similar to the Minnesota FCSS, FSBs have square edges with transverse reinforcing bars that protrude from the sides. Unlike the FCSS, however, these reinforcing bars do not extend beyond the edges of the FSB flanges, which facilitates placement. A 2-inch chamfer is used at the top of the precast section to minimize abrupt changes section. This design detail is aimed at eliminating the formation of longitudinal reflective cracks that have traditionally formed at the joint locations.

Table 2.3: FSB Property Table. (Beam's widths are from 4' to 5')

| Index No. | FSB Depth | Span Length |
|-----------|-----------|--------------|
| D20451 | 12" | 30 to 50 ft. |
| D20452 | 15" | |
| D20453 | 18" | |

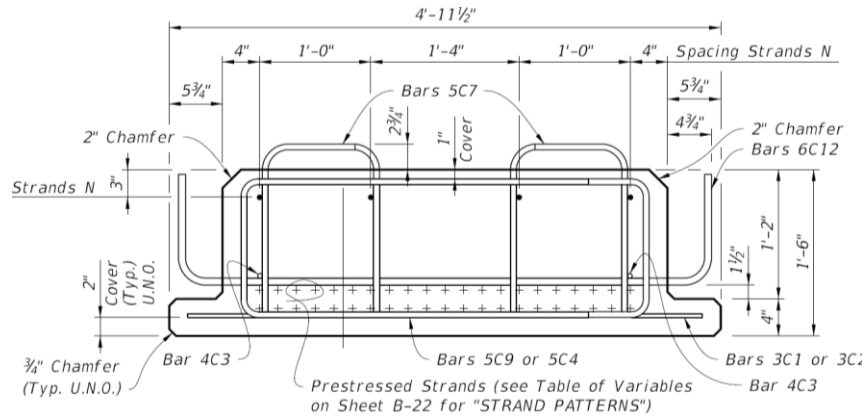


Figure 2.22: Typical FSB Section [51]

Cracking can be further reduced by saturating the FSB with water for at least 12 hours prior to casting of the concrete topping, creating a saturated surface condition. FDOT requires the inclusion of a shrinkage reducing admixture into the concrete mixture for the composite topping [54].

2.3.5.3 Current Uses

The system is intended to be used to replace Prestressed Slab Units [54]. As mentioned before, the FSB superstructure system is currently recommended for off-system bridges with low ADT and ADTT. The pilot project for this system was the SR 373 (Orange Avenue) over St. Marks Trail (District Three, Leon County; Tallahassee, Florida). The road closure was for seven weeks; from June 2nd to July 20th of 2014. The designers of this

project were the FDOT State Structures Design Office (superstructure and GRS), and George & Associates (roadway, drainage, utilities, and permitting). The placement of the FSB members and the finished bridge are shown in Figure 2.23 (a) and (b), respectively.



Figure 2.23: (a) Placement of FSBs adjacent to each other and (b) finished pilot project SRS 373 [51]

As of now, the FSB system is limited to 12, 15, and 18-inch beam depths spanning between 30 and 60 feet. There is also a required minimum 6-inch CIP topping made of conventional concrete.

2.3.5.4 Challenges

There were a few lessons learned in the previously mentioned pilot project. The skewness was one hassle for the construction stage. Damage was seen at the corners of the larger length of the members (due to its reduced stiffness). A lower skew angle was recommended for future projects [51]. Additionally, backer rods between the beam joints were improperly sized and resulted in some of the concrete leaking between the adjacent members during casting of the CIP deck. Finally, the manufacturer of the tie bars suggested decreasing the size of the hoop bars in the joint pockets between members be reduced to #5 bars (from the

#6 bars used in the pilot project). There are no other reported issues, but this may be a result of it only being recently released for use.

2.4 Longitudinal and Transverse Joints

The increased use of prefabricated bridge elements has caused joints to become a greater area of interest. The joint regions have traditionally been the weakest link in the bridge structure and thus dictate the bridge's strength and durability performance. Joints must be designed to restrict vertical movement between members and suitably transfer forces due to traffic loads between adjacent members. Under these traffic loads, a joint region (transverse or longitudinal) experiences two types of forces:

1. **Vertical Shear Forces:** These forces attempt to break the bond between the filling material (Grout, Epoxy, Ultra High Performance Concrete, etc.) and the adjacent concrete elements.

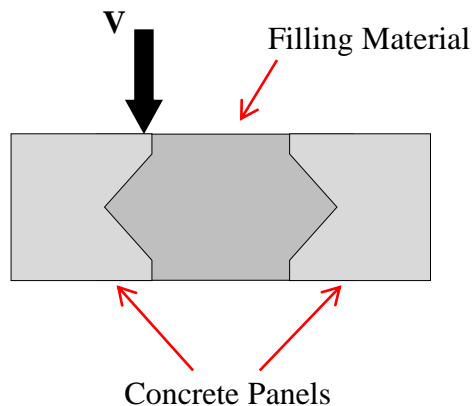


Figure 2.24: Shear force at joint

2. **Bending Moments:** A bending moment that engages compression in the top half of the joint and tension in the bottom half. Some type of reinforcement is required to carry these developed tension stresses in the joint.

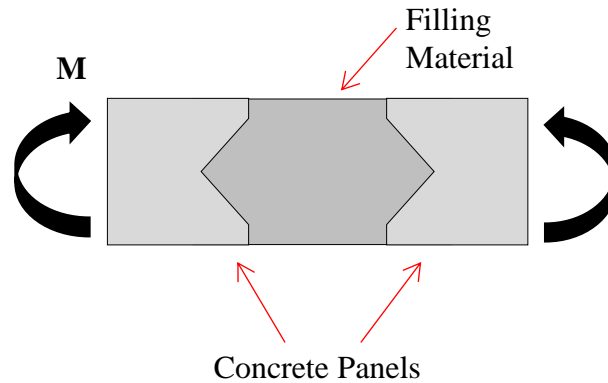


Figure 2.25: Bending moment at joint

Each of the short-span bridge solutions described in §2.3 required the use of some type of transverse or longitudinal joint between members to carry the vertical shear forces and bending moments. This section will introduce some of these typical joint details. The overview will start with non-UHPC connection details (including conventional concrete, grout, transverse post-tensioned, etc.) and move to UHPC connection details. The most common non-UHPC and UHPC connection details are provided in Figure 2.26 (a) and (b), respectively.

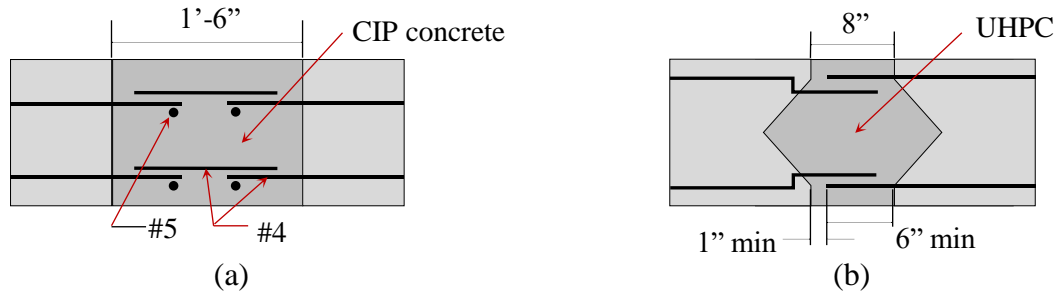


Figure 2.26: (a) Most common non-UHPC connection detail (Adapted from Biswas [56]) and (b) most common UHPC connection detail (adapted from Graybeal [3])

The goal of this summary is not to report on all of the types of connections between precast bridge superstructure elements, but to show a sample of the most commonly used details in US bridges. Special attention will be paid to both non-UHPC and UHPC joint details that connect prefabricated elements including: full-depth precast concrete deck panels, members with precast full-depth decks (e.g. decked bulb-Tees), adjacent box beams, and other similar details. Other joints (e.g., between columns and bent caps) will not be covered in this section.

2.4.1 Non-UHPC Joints

Prior to UHPC there were several commonly used details utilizing conventional concrete, grout, and even mechanical features like transverse post-tensioning. Some of the more common non-UHPC details will be covered in this section.

2.4.1.1 Non-Post-Tensioned Joint Details

Non-post-tensioned (non-PT) joints were the first put in use in both new and rehabilitated bridges with precast panels primarily due to their low cost and easier constructability (when compared to similar post-tensioned details). An example of a standard non-PT joint detail is shown in Figure 2.26 (a), from the Pintala Creek Bridge built by the Montgomery County

Commission from Alabama in 1973. The detail involved straight #4 reinforcing bars spliced in an 18-inch joint with #5 reinforcing bars laid down parallel to the joint providing confinement. The connection region was filled later with CIP concrete.

Later non-PT connection details involved the use of either headed reinforcing bars or hooked bars; these details were primarily used to connect precast panels. The use of headed or hooked reinforcement decreases the development length, which allows for decreased joint widths and overall improvement in the joint region behavior [56].

Non-PT joints are also utilized in the several slab-beam designs that were discussed above (e.g., Poutre-Dalle System, inverted-T beam system used by Virginia DOT, and the Florida Slab Beam). Typically, these sections serve as the formwork for a CIP deck. The CIP deck then serves as both the deck and the agent to join the adjacent beams together. Sample details for the joint regions of three such members are shown in Figure 2.27.

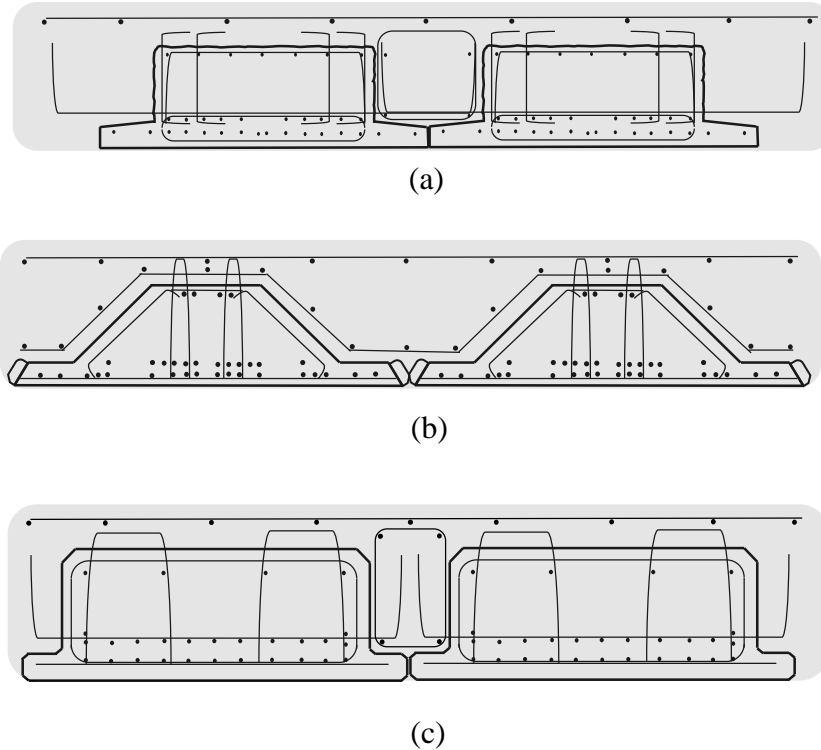


Figure 2.27: Sample joint details for (a) PCSS (Minnesota), (b) inverted-T (Virginia), and (c) Florida slab beam (FSB) (Florida)

2.4.1.2 Post-Tensioned Joint Details

Another popular non-UHPC joint is constructed using transverse post-tension. Post-tensioning bridge deck joints helps to have better structural performance and ensures the correct distribution of live loads. Post-tensioning of adjacent members and precast panels has been used since the 1970s. The Big Blue River Bridge over Indiana State Road 140 (near Knightstown, IN) has panels that were transversely pretensioned in the longitudinal direction. Also, the Bean Blossom Creek Bridge on Indiana State Road 37 (near Bloomington, IN) used the same method for the replacement of deteriorating deck panels. These connections have performed fairly well, although there have been partial failures of some of the joints at slab-to-slab interfaces.

Most of the joint details for these post-tensioned joints are similar to that shown in Figure 2.28, which is from the Amsterdam Interchange Bridge in New York City (built in 1973). Here precast deck panels were conventionally reinforced. The joint was then cast using one part epoxy to two parts of sand to provide a flowable mixture [56].

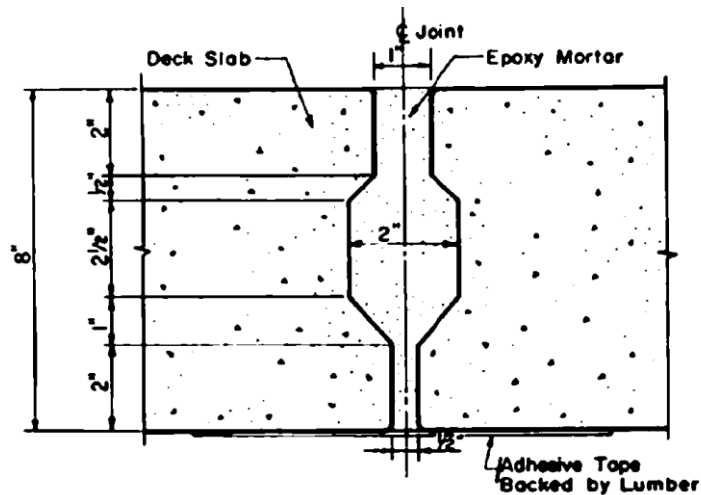


Figure 2.28: Transverse Joint Between precast slabs [56]

Post-tensioned joints have been used to connect adjacent box beam superstructures. These systems have typically not performed well, as discussed in §2.3.1.

2.4.1.3 Mechanical Connectors

There are several different types of mechanical connectors that have been designed and implemented. Mechanical connectors are required for carrying tensile loads between the girders because of shrinkage and torsional effects and because of shear due to differential camber between girders. Two examples are shown in Figure 2.29: the Washington DOT's standard mechanical connection detail [57] and the grouted HSS connection detail from the NCHRP Report 584 [58].

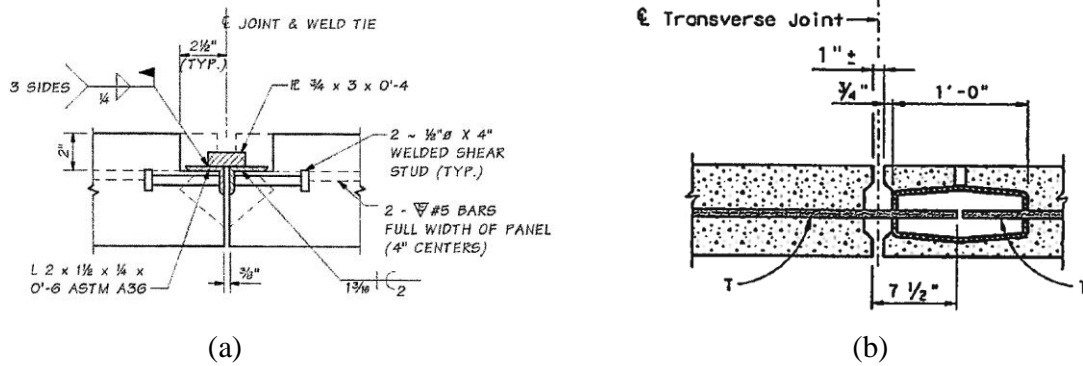


Figure 2.29: Two types of mechanical connectors: welded connection detail [57] and grouted HSS pocket connection [58]

2.4.1.4 Field Performance and Observations

Non-UHPC joints can offer satisfactory performance if they are designed and detailed properly. Most non-PT non-UHPC joint details require large amounts of reinforcement protruding from the precast members. This reinforcement is oftentimes challenging to place, which will result in higher labor costs. Additionally, many of details described above require the placement of additional reinforcement in the joint, both transverse (to aid in development lengths) and longitudinal (to improve confinement), as shown in Figure 2.30 (a). In some details, reinforcement bars were required to be threaded through 180-degree hooks, as shown in Figure 2.30 (b). Simpler non-UHPC joint details (in terms of reinforcement) require PT, which is also labor intensive.



Figure 2.30: Additional reinforcement required in (a) transverse direction [59] and (b) extending from side of members [60]

Many of these joints do lead to cracking along the joint boundaries. These cracks can lead to water intrusion and affect the durability performance of the connection detail. This cracking can be exacerbated if there are poor construction practices. One example of this is the Harriman Interchange Ramp (New York) in which the contractor used an epoxy mortar of unsatisfactory quality at some joint locations with evidence of improper proportioning.

2.4.1.5 Summary

There are many different types of non-UHPC joint details that both require and do not require the use of post tensioning. Non-PT joints generally require large amounts of reinforcement both at the precast plant and at the bridge site. These joints also often require inclusion of at least a partial-depth CIP deck included in the deck cast. Post-tensioned, non-UHPC joints are also used in many applications, but require the extra labor costs and constructability issues associated with field post-tensioning.

2.4.2 UHPC Joints

Accelerated bridge construction (ABC) techniques are becoming much more commonplace, which has encouraged the pursuit of innovative alternative joint details to expedite construction. The transverse deck cracking that is often present in the traditional joints discussed above has also encouraged the search for new joint details. The discovery of ultra-high performance concrete (UHPC) has allowed for a new group of joint details to be created. Two such joint details are shown in Figure 2.31.

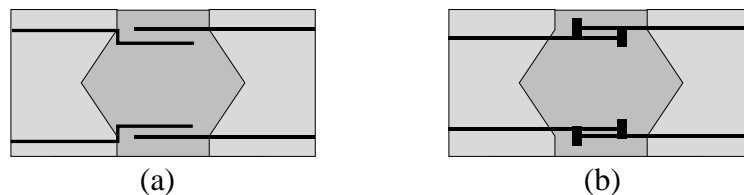


Figure 2.31: UHPC joint connection examples adapted from: (a) Royce [61] and (b) Aaleti and Sritharan [62]

UHPC has been utilized in many different applications since the mid-1990s in Europe. While UHPC is used in many different applications (e.g., overlays, full bridge elements, joints, etc.), the focus of this section will be on uses of UHPC in joints between adjacent elements or precast deck panels. This material has enabled significant simplification in the design of field-cast connections and allowed easy field assembly of prefabricated bridge components.

2.4.2.1 Graybeal (2008)

In 2008, Graybeal et al. [63] developed a joint detail to be used between adjacent box beams, with the objective of enhancing the performance of the longitudinal connection

detail. The concept was dependent on the use of UHPC. Specific details for the developed joint are shown in Figure 2.32.

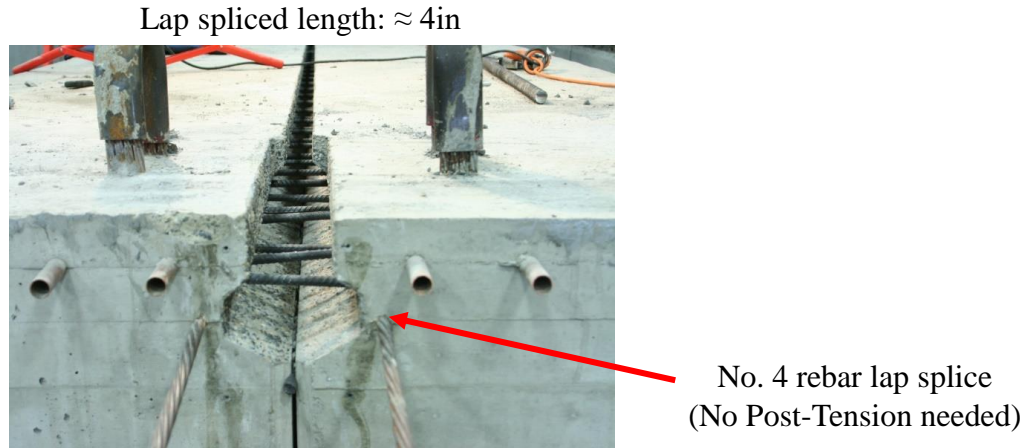


Figure 2.32: Joint developed by FHWA [63]

Before the development of the UHPC connection, there were two primarily used female-to-female connection details used to connect adjacent members, as shown in Figure 2.33 (a). Both of these options required the use of transverse post-tensioning (as discussed above). Graybeal [63] developed a simpler joint detail using UHPC that required no transverse post-tensioning, shown in Figure 2.33 (b).

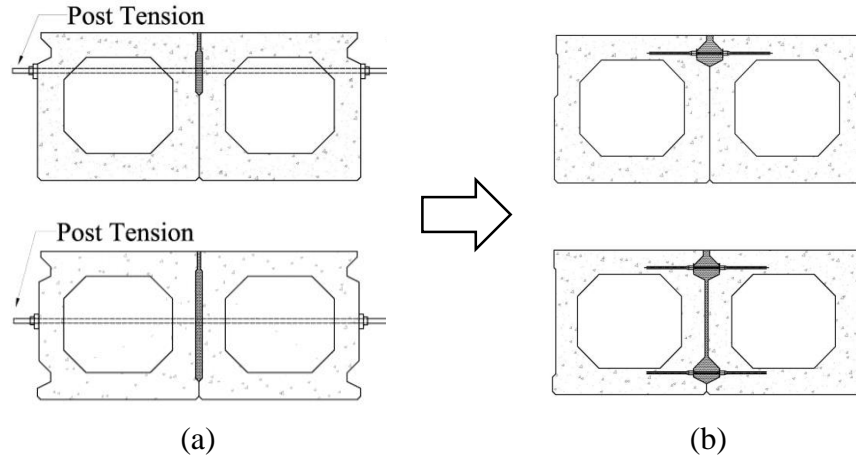


Figure 2.33: (a) Traditional solution with post-tensioning and (b) UHPC connection solution without post-tensioning [63]

These joint details were developed through an extensive experimental program involving both small-scale testing (focused on the joint development) and full-scale testing (focused on the performance of the joint detail in two adjacent girders). Two of the full-scale configurations used in the experimental program are shown in Figure 2.34. The current shear key configuration utilizing conventional grout materials and transverse post-tensioning tendons, shown in Figure 2.34 (a), was used to develop a baseline performance to start as a comparison point for testing. The developed UHPC connection detail, shown in Figure 2.34 (b), required the use of #4 reinforcement extended 5.5 inches into the joint, which provided a 4-inches splice length. The surface was prepared by using a retarding agent on the formwork and then sandblasting the surface; this created an exposed aggregate finish in the joint and improved the bond performance.



Figure 2.34: (a) Conventional shear key specimen and (b) UHPC shear key specimen [63]

Two different loading protocols were used in the full-scale experimental program: (1) simply-supported and (2) simply-supported with restrained deflections on one specimen at midspan. Neither of the loading protocols were able to create distress in the connection region for the UHPC connection details. To see the post-cracking behavior of the joint detail, cracking of the joint was caused by placing a transverse load on the girders, as shown in Figure 2.35.

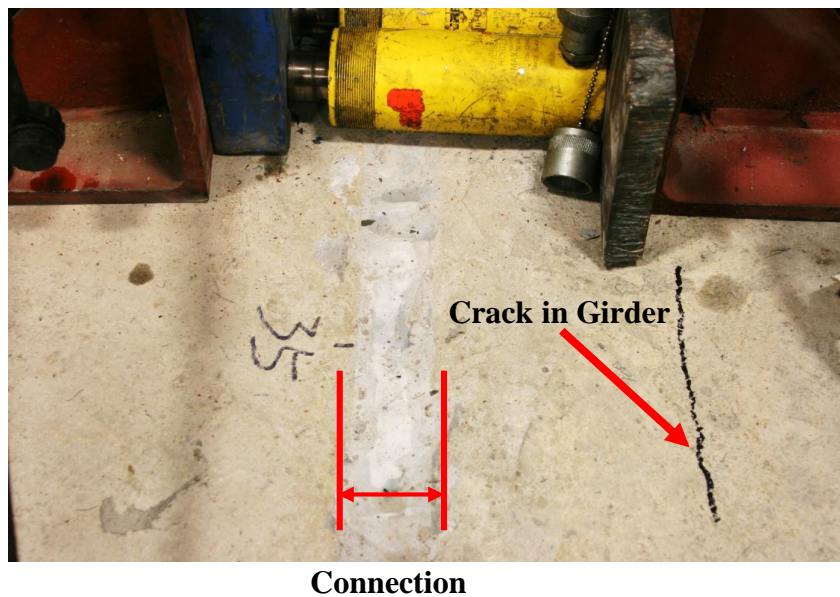


Figure 2.35: Forced Cracking [63]

Graybeal found [63] found that the transverse PT did not prevent crack propagation after initiation. They found that the UHPC connections, on the other hand, performed very well and created a robust joint region.

Because of the positive results of the FHWA testing, several bridges have been constructed using the proposed UHPC joint detail. One example is the Sollars Road Bridge built in Fayette County (Ohio). The Sollars Road Bridge consists of seven adjacent precast, prestressed box beams, shown in Figure 2.36. The bridge was constructed without any transverse post-tensioning and without any composite deck, relying fully on the UHPC joints for compatibility and load transfer between members. The use of these joints with the prefabricated box beams allowed the construction project to be completed fairly quickly, with construction starting on May 28th and the bridge being opened to traffic on August 13th (both of 2014). Details of the joint region used in this project are shown in Figure 2.37.

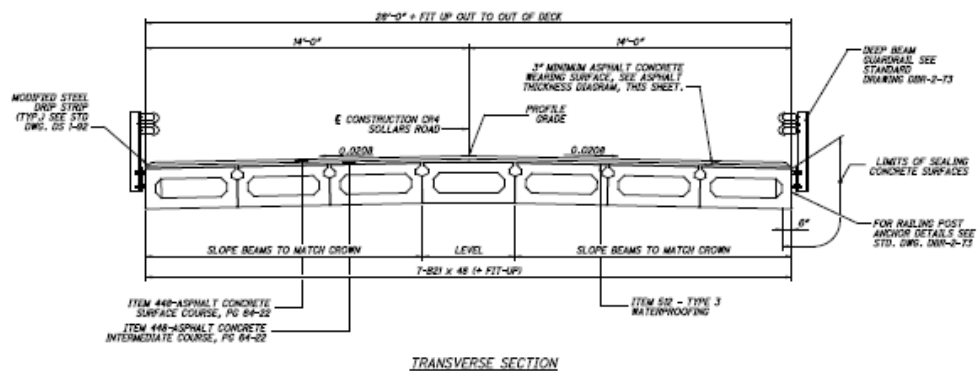


Figure 2.36: Sollars Road Bridge cross-section [63]

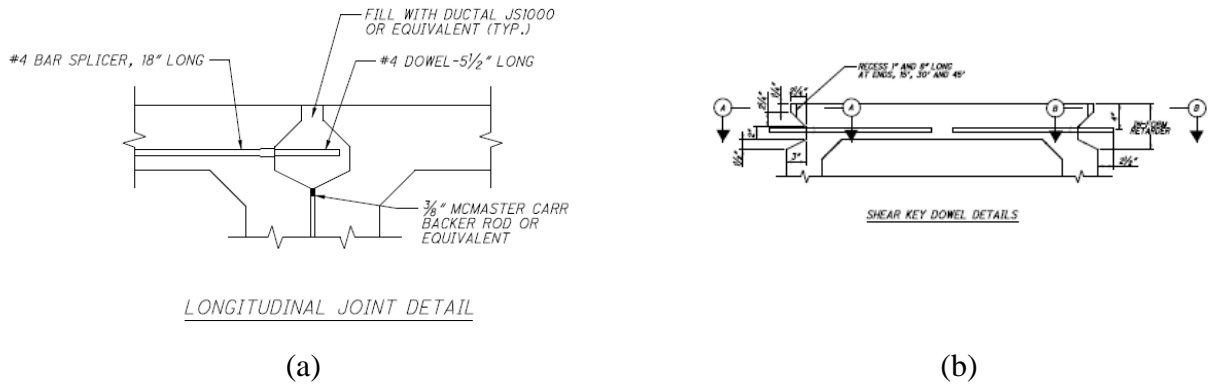


Figure 2.37: (a) Longitudinal joint detail and (b) shear key dowel detail [63]

To facilitate the use of UHPC joints and summarize the results of the work done by the FHWA, Graybeal [4] released a technical note on UHPC bridge connections. The note includes details for several different types of connections as well as the properties of several different available UHPC materials. Some of the developed details are shown in Figure 2.38.

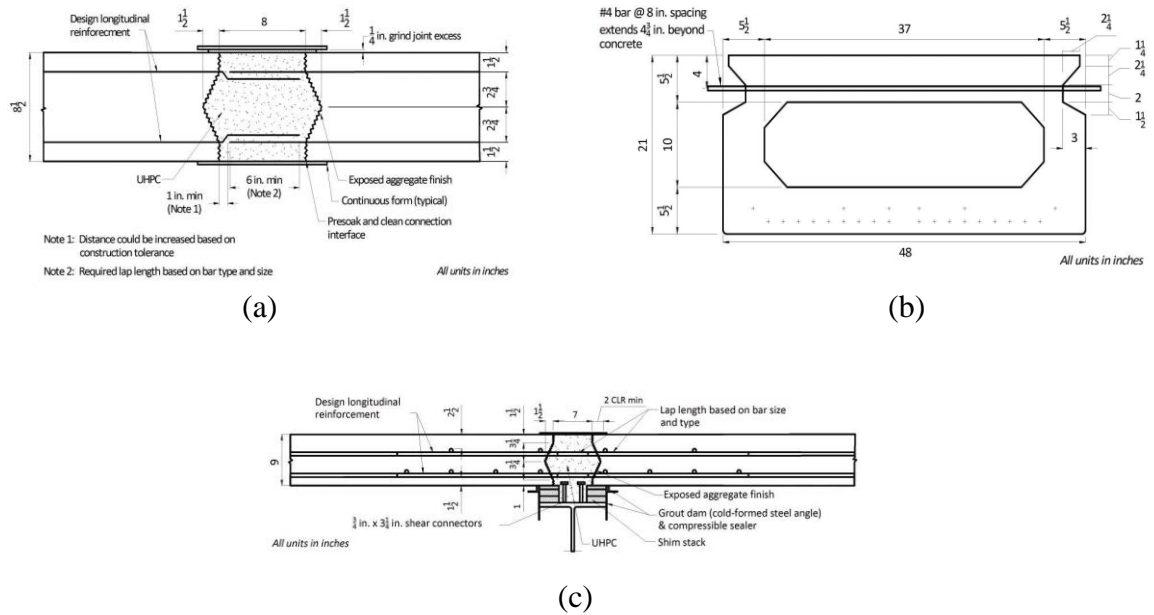


Figure 2.38: (a) UHPC connection between precast deck panels as deployed by NYSDOT on CR47 over Trout Brook, (b) UHPC adjacent box beam connection detail, and (c) combined UHPC deck-level and composite connections as deployed by NYSDOT on I-81 near Syracuse, NY [4]

2.4.2.2 Aaleti and Sritharan (2014)

Another UHPC joint detail recently developed was to connect full-depth, precast, UHPC waffle-deck panels [62]. The details of this joint region are shown in Figure 2.39.

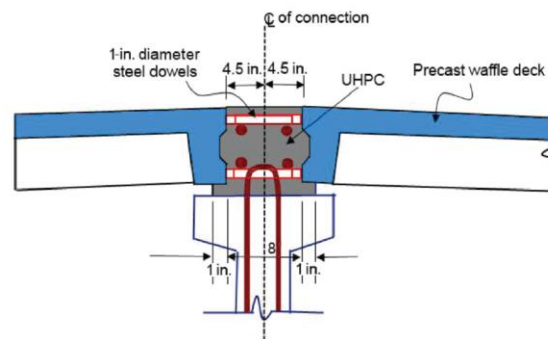


Figure 2.39: Panel-to-panel and panel-to-girder connection [62]

This UHPC joint detail was developed through a full-scale experimental program involving the testing (with service, ultimate, and fatigue loads) of adjacent panels connected using several different UHPC joint details, as shown in Figure 2.40. Two different joint geometries were tested with four different reinforcement details. A joint geometry similar to that developed by Graybeal et al. (2008), introduced above, was used with straight headed reinforcement, hairpin reinforcement, and straight reinforcement. A shallower joint that was self-forming and only used one layer of reinforcement was also tested.

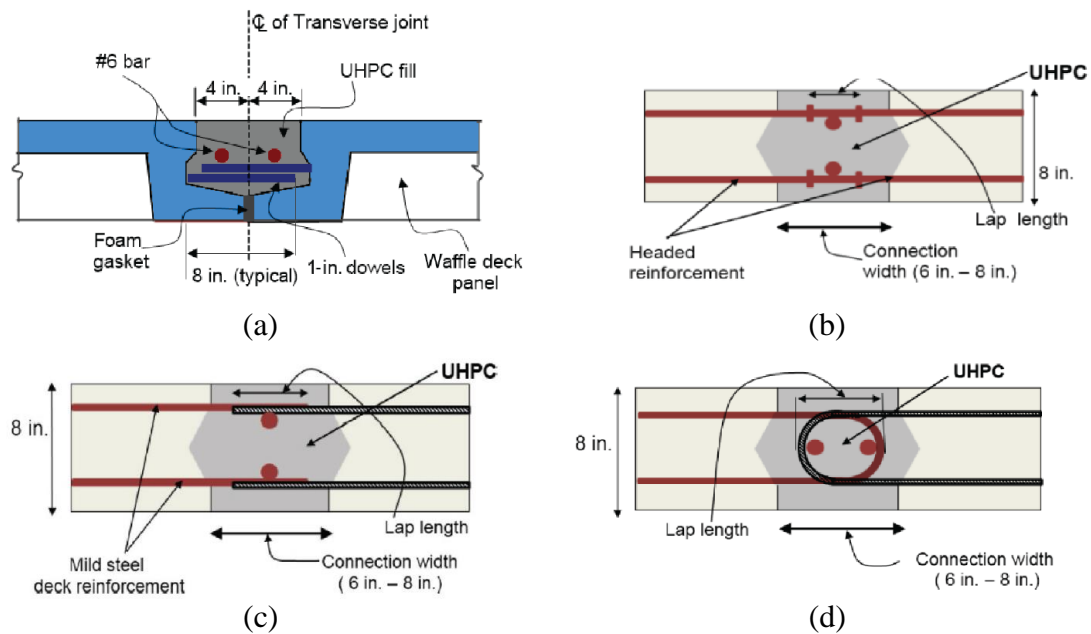


Figure 2.40: Common panel-to-panel UHPC connection details: (a) waffle deck panel-to-panel connection detail, (b) panel-to-panel headed connection detail, (c) panel-to-panel straight connection detail, and (d) panel-to-panel hairpin reinforcement [62]

The results of these tests led to the final joint geometry and reinforcement configuration shown in Figure 2.39. The main feature of this joint are straight dowel bars extending from the panels, shear hooks extending from the girder, longitudinal reinforcement running along the length of the joint, and UHPC to finish the joint.

This UHPC joint detail was used in the Little Cedar Creek Bridge (Wapello County, Iowa) as part of the FHWA Highways for LIFE program. The UHPC joint detail was used in both the transverse and longitudinal directions to connect the waffle slab panels, as shown in Figure 2.41.

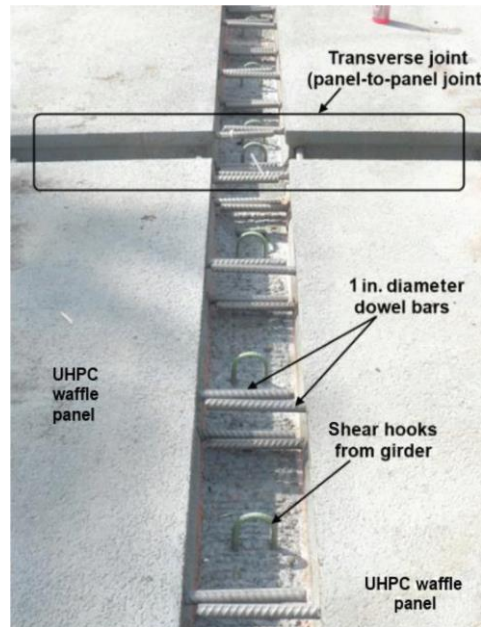


Figure 2.41: Shear key connection in Wapello County Bridge [62]

Other state DOTs have expressed interest in UHPC waffle deck components and the developed joint detail for aging bridge replacements.

2.4.2.3 Field Performance and Observations

The bridge industry is becoming more interested in the use of prefabricated bridge components designed to incorporate UHPC joint details as they both accelerate construction and are thought to improve long-term durability. While there is a fair amount of research on the joint details and some durability testing of UHPC materials, the use of UHPC joints in field applications is too recent to be able to gain any true insights on long-

term performance. The use of UHPC joints has been shown to ease and accelerate construction, as many of the details require no reinforcement be placed at the construction site.

2.5 Joint Materials

There are several different types of materials that are utilized in the joint regions described above. Each joint material has its own composition and properties that make it better suited for certain applications. Some of the primary materials that are used in these joints are: conventional concrete, self-consolidating concrete, cementitious grout, and UHPC.

2.5.1 Non-UHPC Materials

Many different non-UHPC materials are used in joint regions: conventional concrete, self-consolidating concrete, and cementitious grout are the primary three. Conventional and self-consolidating concretes are typically used in non-PT connections, with either a wide joint region with large amounts of reinforcement or in situations where the joint is cast with a CIP deck. Conventional and self-consolidating concretes are non-proprietary, although some of their components are proprietary products (e.g., some admixtures or supplementary cementitious materials).

Cementitious grout is the material typically used in the shear pockets of joints with transverse post-tensioning. While conventional and self-consolidating concretes are non-proprietary, grouts are normally proprietary and come in prepackaged bags. According to Badie et al. [64], grouts are used in these joints for several reasons:

- Relatively high strength at young age

- Minimal shrinkage deformation
- Low permeability
- Increased bonding capabilities with hardened concrete surfaces

The following table, Table 2.4 and Table 2.5, describe some of the commercial and non-commercial grout products.

Table 2.4: Commercial and Non-commercial grout materials [64]

| COMMERCIAL GROUT PRODUCTS | |
|---------------------------------------|--|
| Name | Characteristics |
| <i>SET-45</i> | It is a one-component concrete repair and anchoring material, which sets in 15 minutes approximately. For use in ambient temperatures below 85° F (29° C). |
| <i>SET-45 Hot Weather (HW)</i> | Same one-component concrete repair and anchoring material with same setting time. For use in ambient temperatures below 85-100°F (29-38°C). |
| <i>SET GROUT</i> | Natural aggregate non-shrink grout: Portland cement-based product, non-catalyzed, multi-purpose construction grout containing mineral aggregate. |
| <i>EMACO 2020</i> | It is a methyl methacrylate (MMA), polymer concrete system designed for the protection and rehabilitation of horizontal, formed vertical or overhead concrete surfaces. It consists of three parts denominated A, B, and C, for binder, aggregate and initiator, respectively. |
| <i>EMACO 2041</i> | Bonding agent for EMACO 2020: It is a one-component, moisture-tolerant acrylic bonding agent applied to concrete or steel prior to the placement of EMACO 2020. |

Table 2.5: Non-commercial grout materials [64]

| NON-COMMERCIAL GROUT PRODUCTS | |
|--|---|
| Name | Characteristics |
| <i>Hydraulic Cement Concrete (HCC)</i> | This mix was used on some bridges built prior 1972. It has a minimum concrete strength of 4,000 psi (27.6 MPa), relatively high slump (about 6 in), and maximum aggregate size of ½ in. |
| <i>Latex Modified Concrete (LMC)</i> | It consists of a latex emulsion added to an HCC mix. The latex forms a thin film on the aggregate surface, which enhances the bond between the past and the aggregate and results in high compressive strength and less permeable concrete mix. |
| <i>Type K- Cement Concrete Mix</i> | This concrete mix has a specified concrete strength of 4,000 psi (27.6 MPa) and only cement type K is used in the mix. The concrete has no fly ash, and the maximum aggregate size is 3/8 in. Type K cement is an expansive cement that contains anhydrous calcium aluminatupon, which being mixed with water, forms a paste, that during the early hydrating period occurring after setting, increases in volume significantly more than does Portland cement paste. |

2.5.2 UHPC Materials

UHPC is a cementitious composite material first developed in the 1990s and commercially available in the US since the early 2000s. It is typically acquired from a merchant in three separate components: a pre-bagged cementitious powder, chemical admixtures, and steel fiber reinforcement. Water is the last ingredient added at the construction site. Afterwards, the mixture is placed into the formwork using standard construction equipment.

This material is known for its superior performance such as high compressive strength (above 18 psi), long-term durability, low permeability, high usable tensile strength, and low water-to-cement ratio (all of them are compared to conventional concrete). The typical composition of UHPC is presented in Table 2.6. Current compressive and tensile behavior are shown in Figure 2.42. Typical field-cast properties are shown in Table 2.7.

Table 2.6: Typical Composition of UHPC [65]

| Component | Amount | % by Weight |
|------------------|-------------------------|-------------|
| Portland Cement | 1200 lb/yd ³ | 28.5 |
| Silica Fume | 390 lb/yd ³ | 9.3 |
| Fine Sand | 1720 lb/yd ³ | 41.0 |
| Ground Quartz | 355 lb/yd ³ | 8.5 |
| Superplasticizer | 51 lb/yd ³ | 1.2 |
| Water | 218 lb/yd ³ | 5.2 |
| Steel Fibers | 263 lb/yd ³ | 6.3 |

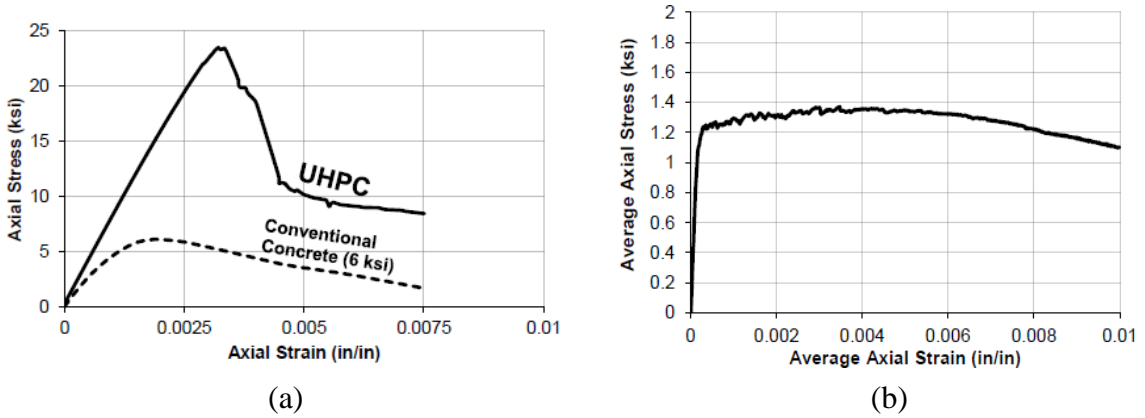


Figure 2.42: (a) Compressive UHPC behavior, (b) Tensile UHPC behavior [65]

Table 2.7: Typical field-cast UHPC material properties [4]

| Material Characteristic | Average Result |
|--|------------------------|
| Density | 155 lb/ft ³ |
| Compressive strength (ASTM C39, 28-day) | 24 ksi |
| Modulus of elasticity (ASTM C469, 28 day) | 7,000 ksi |
| Direct tension cracking strength (uniaxial tension with multiple cracking) | 1.2 ksi |
| Split cylinder cracking strength (ASTM C496) | 1.3 ksi |

| Material Characteristic | Average Result |
|--|---------------------------------|
| Prism flexure cracking strength (ASTM C1018, 12-inch span) | ksi |
| Tensile strain capacity before crack localization and fiber debond | > 0.003 |
| Long-term creep coefficient (ASTM C512; 11.2 ksi load) | 0.78 |
| Long-term shrinkage (ASTM C157; initial reading after set) | 555 microstrain |
| Total shrinkage (embedded vibrating wire gage) | 790 microstrain |
| Coefficient of thermal expansion (AASHTO T259; 0.5-inch depth) | 8.2×10^{-6} in./in./°F |
| Chloride ion penetrability (ASTM C1202, 28-day test) | 360 coulombs |
| Chloride ion permeability (AASHTO T259; 0.5-inch depth) | < 0.10 lb/yd ³ |
| Scaling resistance (ASTM C672) | No scaling |
| Abrasion resistance (ASTM C944 2x weight; ground surface) | 0.026 oz. lost |
| Freeze-thaw resistance (ASTM C 666A; 600 cycles) | RDM = 99 percent |
| Alkali-silica reaction (ASTM C1260; tested for 28 days) | Innocuous |

2.5.2.1 Proprietary UHPC Materials

There are a number of commercially available UHPC materials in the US. The following list of proprietary UHPCs have been shown to align with the needs of typical UHPC joint projects [4]:

- BCV[®] (Beton Composite Vicat produced by VICAT)
- BSI[®] (Beton Special Industriel produced by EIFFAGE)
- Cor-tuf[®] (produced by The US Army Corps of Engineers – Engineer Research and Development Center)
- CRC[®] (Compact Reinforced Composite by Hi-Con)
- Densit[®] (produced by Densit Aps)

- Ductal[®] (produced by Lafarge Holcim)

Lafarge Holcim (producer of Ductal[®]) has developed a proprietary UHPC mixture specifically for joint solutions. The product is called Ductal[®] JS1000 and is advertised as a field-cast joint fill solution for precast deck panel bridges. The main components of this Ductal[®] JS1000 mixture are:

- **Premixture:** Silica fume ground quartz, sand, and cement
- **High tensile steel fibers:** 0.2mm (0.008 in) diameter x 14 mm (0.5 in) long (>2000 MPa/290 psi).
- **Admixture:** High range water reducer/3rd generation
- **Water and/or ice**

These proprietary UHPC materials are expensive but offer more consistent wet and hardened properties than can normally be achieved with locally available materials.

2.5.2.2 Non-Proprietary UHPC Materials

Due to the high cost of the proprietary UHPC products and limitations that have been presented with “buy America” contract clauses, many states have conducted research to develop non-proprietary UHPC mixtures. Typical ranges for the mixture proportions for these non-proprietary UHPC mixtures are shown in Table 2.8; these values are the ranges of four different non-proprietary UHPC mixtures summarized by [66].

Table 2.8: Typical ranges of UHPC non-proprietary mixtures with fine aggregates (not including steel fibers) (based on data from Graybeal [66])

| Component | Typical Range |
|--|---------------|
| White Cement (lb/yd ³) | 1248 to 1311 |
| Silica Fume (lb/yd ³) | 312 to 328 |
| Fly Ash (lb/yd ³) | 303 to 318 |
| HRWR (lb/yd ³) | 45 to 48 |
| Fine Aggregate (lb/yd ³) | 1871 to 1966 |
| Aggregate-to-cement ratio | 1.5 |
| w/cm ratio | 0.23 to 0.24 |
| Spread (inch) | 10.4 to 12.4 |
| Avg. Compressive Strength at 28 days (ksi) | 23.5 to 29.0 |
| Cost (\$/yd ³) | 472 to 652 |

Graybeal [66] also investigated the cost of each of the components in the UHPC mixture, as shown in Table 2.9. He found that the steel fibers are by far the most expensive component of the UHPC mixture. The cost of the UHPC mixture is increased by about \$470 per cubic yard when 1.5-percent by volume of fiber reinforcement is added to the mixture.

Table 2.9: Cost of material per volume of low cost UHPC [66]

| Material | Cost (\$/yd ³) |
|------------------------|----------------------------|
| Portland Cement (II/V) | 73.66 |
| Silica Fume | 82.57 |
| Fly Ash | 7.54 |
| HRWR | 103.60 |
| Fine Aggregate | 12.82 |
| Fibers (1.5%) | 472.39 |

| Material | Cost (\$/yd³) |
|-----------------|---------------------------------|
| Total | 751.59 |

2.5.3 UHPC Mixing and Casting Procedure

Mixing of UHPC materials is done slightly different than conventional concrete materials. The full casting procedure is shown in Figure 2.43. One of the main differences with regard to mixing is that UHPC requires a large amount of shear energy to mix properly. This means that either a high-shear mixer must be used, or a long amount of mixing time is required. The mixing time and energy required for UHPC is one of the major limitations of the material. After the UHPC is properly mixed, it behaves similarly to a self-consolidating concrete. The UHPC can be placed in one location and allowed to flow down the member and joint. It should be noted that fiber reinforcement will align in the direction of the flow, so care should be taken to ensure that fibers are correctly oriented for the application. Steam curing will improve early age strength, but top forming or moist curing will result in satisfactory behavior for most applications. Finally, the UHPC can be used as the riding surface but requires grinding if it is to be used without an asphalt overlay.

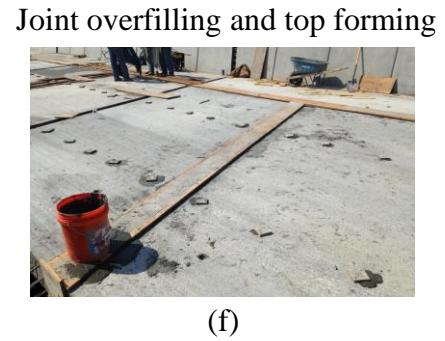
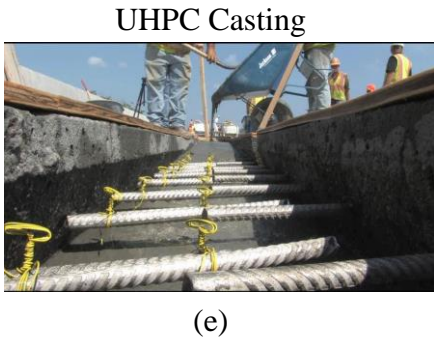
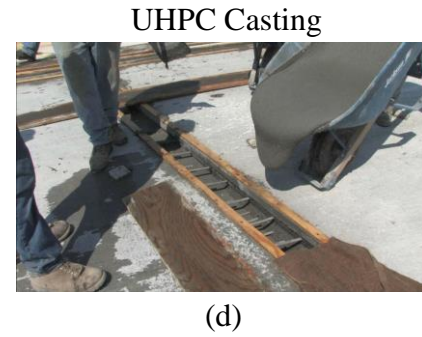
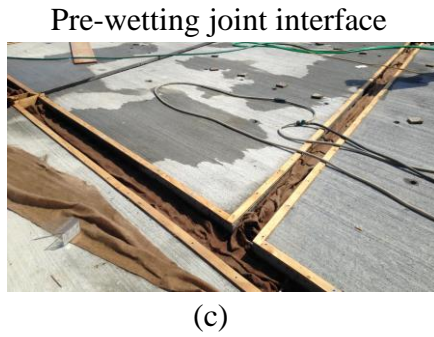
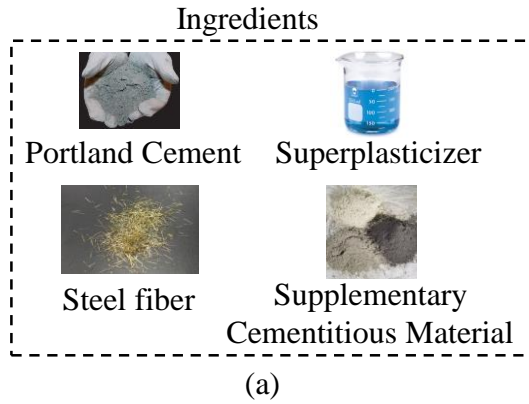


Figure 2.43: General procedure for mixing and casting UHPC [65]

2.6 Other UHPC Bridge Superstructure Applications

The benefits of UHPC have been extended to other applications in bridge superstructures. Two of these applications (as overlays and full members) will be briefly introduced in this section.

2.6.1 UHPC Overlays

Overlays made of UHPC are being used to rehabilitate decks of aging bridges. One example is the Chillon Viaduct near Lausanne (Switzerland), as shown in Figure 2.44. The deck was replaced with a CIP UHPC overlay in order to improve the durability of the riding surface and protect the existing structure underneath [67].

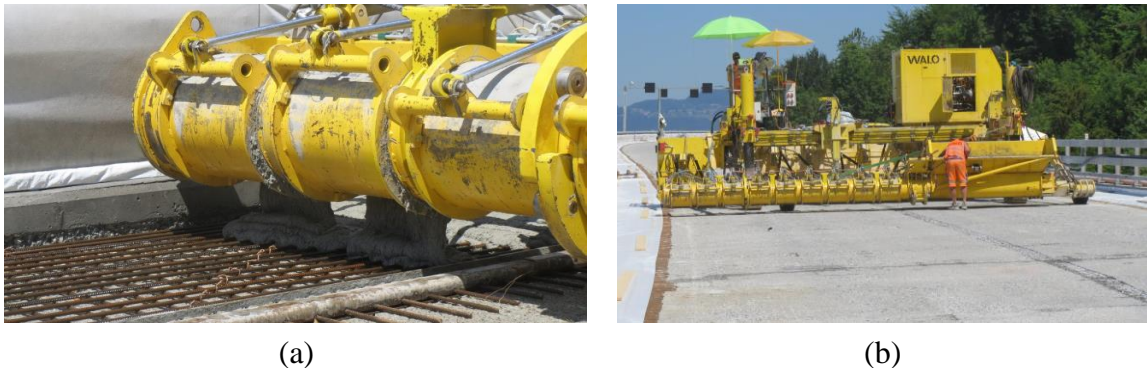


Figure 2.44: Cast-in-place UHPC overlay, immediately (a) before and (b) after placement [65]

There have been many other research efforts looking into the use of UHPC for overlay applications, but it is not yet being widely used in field applications. There are still concerns with the integrity of the UHPC with the remaining deck and with how existing corroded reinforcement behaves after being sealed by the material.

2.6.2 UHPC Members

UHPC has also been used in other bridge members such as deck panels ([62], [68]), piles [69], and bridge girders ([6], [65], [70]). The use of UHPC in these members allows for optimized section dimensions and decreased amounts of steel. For example, shear reinforcement in bridge girders has been completely eliminated in some applications. Two examples of UHPC girder sections are shown in Figure 2.45: The Mars Hill Bridge (Iowa) and the Jakway Park Bridge (Iowa). The use of UHPC in these projects allowed for lighter superstructures, which in turn decreased the loading on the substructure elements.

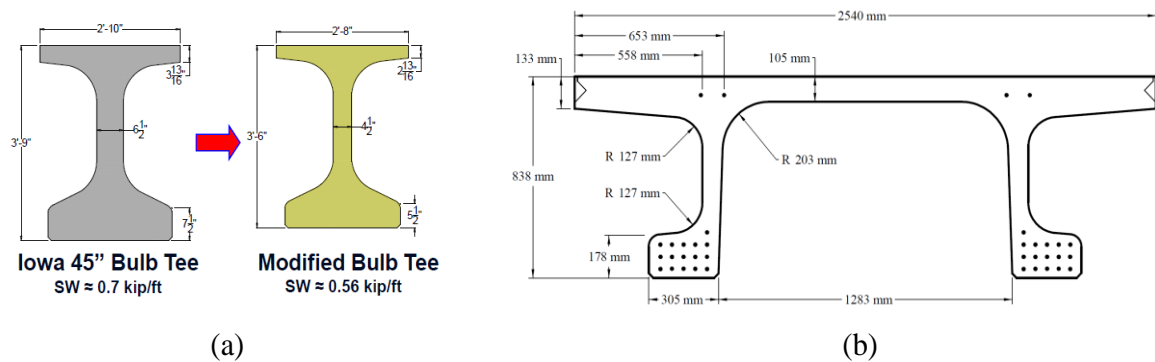


Figure 2.45: (a) Mars Hill Bridge girder comparison [65] and (b) Pi girder used in Jakway Park Bridge [6]

2.7 Summary

Fundamental concepts and background information about the current National bridge inventory status, and precast, prestressed superstructure systems for short-span bridges in America and Europe, including their connection mechanisms, joints material performance, and UHPC joints for ABC implementations were presented in this chapter. Although these superstructure systems have vastly different documented long-term performance in accelerated construction deployments, the specific case of slab-beam bridges with

optimized joints for UHPC usage has not been a focus of study. The objective of this research was to advance the state of practice by developing and testing a UHPC joint detail for slab-beam bridges, investigating further the strength, fatigue, and service performance for a 100-year service life span.

3. RESEARCH METHODOLOGY

The methodology followed to develop the UHPC joint detail for short-span bridges is shown in Figure 3.1. The current bridge inventory status, available superstructure systems for short-span bridges, and connection types and materials were first identified through a comprehensive review of the literature with respect to state-of-the-art practices in accelerated bridge construction. Three major studies were conducted based on the background reviewed:

1. Analytical and numerical study based on four typical superstructure types for ABC of short-span bridges, identifying the niche for slab-beam bridges with UHPC joints,
2. Joint design optimization for ABC of slab-beam bridges, developing UHPC joint specimens for small-scale strength and fatigue assessments and,
3. Full-scale testing of the developed UHPC joint detail for accelerated construction, assessing the service, fatigue, and strength performance of the connection.

Testing to address the first topic included an analytical and numerical FEM study to assess the analyses using commercially available software (i.e., ATENA and PGSuper) and analysis tools developed by state department of transportations (i.e., Prestressed Beam v5.1 developed by FDOT). Testing to address the second topic included an initial numerical FEM study (i.e., ATENA) to assess the strength capacities of the different joint designs and evaluate the specimen dimensions, and laboratory component tests to assess the capacity of a small-scale joint region of a full superstructure width (providing the adequate boundary conditions). Lastly, testing to address the third topic included an initial numerical

FEM study (i.e., ATENA) to assess the service and strength capacities of a full-bridge design incorporating the developed joint system, while testing different loading configurations and boundary conditions; a laboratory experiment was then assessed to two two-beam configurations with one joint each, testing the service, strength, and fatigue performance of a full-size joint section under different loading protocols. To maintain the tests simplicity, no barrier nor riding surfaces were included in the laboratory tests.

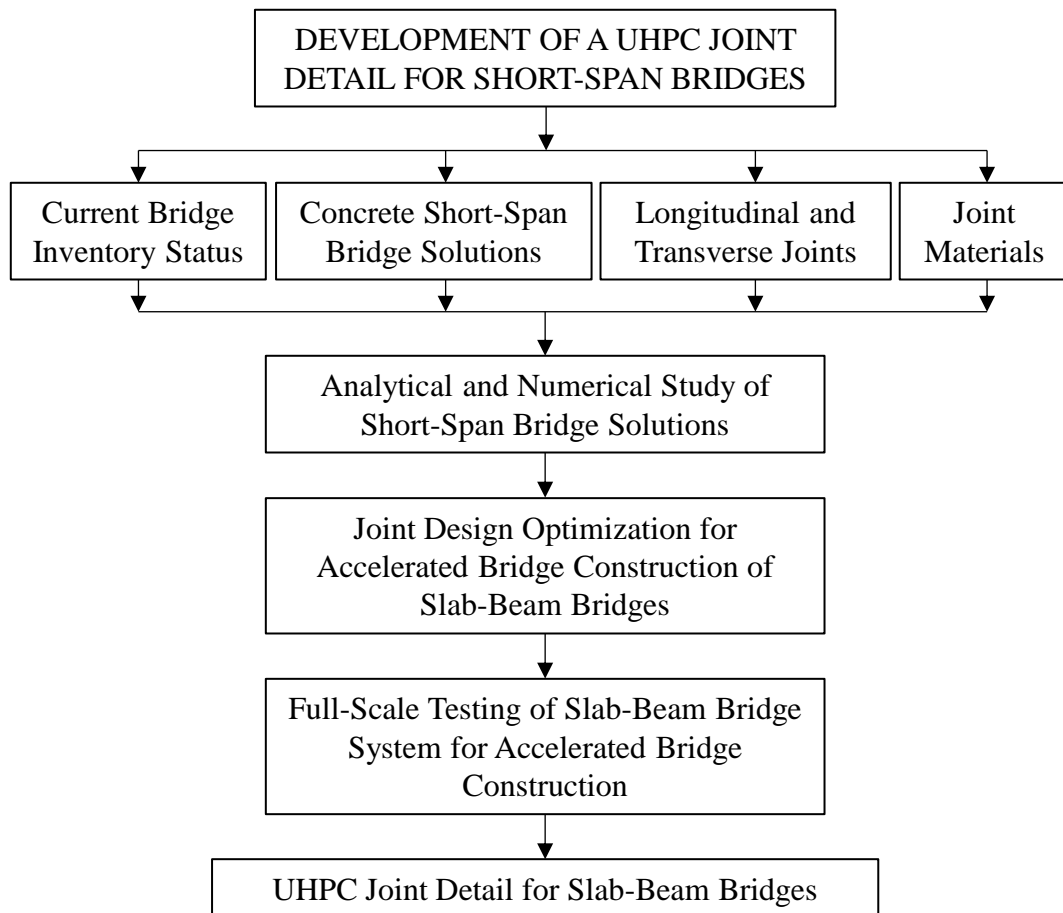


Figure 3.1: Research methodology flowchart

The definitive product of this dissertation is a connection detail for slab-beam bridges that satisfies the load demands of 100 years of service life

4. NUMERICAL STUDY OF SHORT-SPAN BRIDGE SOLUTIONS¹

4.1 Overview

Based on the reviewed background about the current bridge inventory status §2.2 and concrete short-span bridge solutions §2.3, a parametric analysis of popular adjacent precast/prestressed deck beam elements for rapid replacement of short-span bridges (less than 22.9 m [75 ft.] long) was executed. Four main groups of superstructure systems were selected for the analysis: deck-bulb tee beams, adjacent double-tee beams, adjacent box beams, and slab-beam girders. The parameters considered in the comparison matrix and finite element analysis were based on depth of section, structural efficiency, strand number, distribution factors, flexural capacity based on span length, and transverse capacity based on joint demand under truck traffic loading. The main goal of this study was to determine precast concrete short-span bridge solutions that can be used with ABC and numerically evaluate the performance of typical longitudinal joints between adjacent members.

4.2 Selection of Short-Span Bridge Deck Members

The sections selected for the comparison analysis were (a) the Northeast Deck Bulb Tee (DBT) [28], (b) the Northeast Extreme Tee (NEXT) D beam [5], (c) the AASHTO/PCI box beam type B (BI) [33], and (d) the untopped Florida Slab Beam (FSB) [10], as shown in Figure 4.1. Several different section depths and widths for each cross section were investigated in this research.

¹ This chapter is based on material from “Precast Concrete Superstructure Systems for Accelerated Construction of Short-Span Bridges”, to be submitted to Engineering Structures Journal

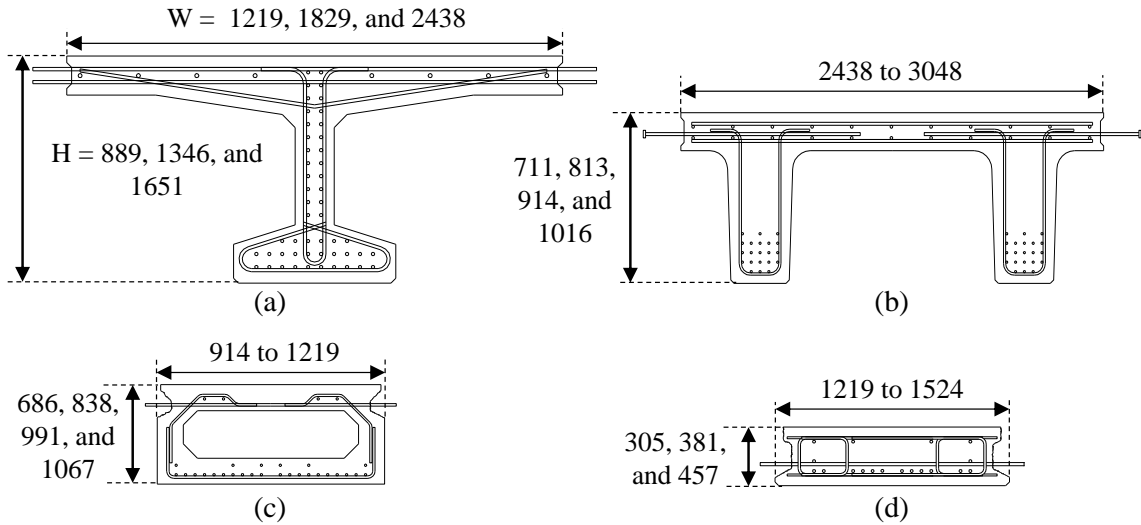


Figure 4.1: Selected bridge shapes with available widths (W) and depths (H): (a) Northeast DBT beam, (b) NEXT D beam, (c) AASHTO BI for ABC, and (d) Florida Slab Beam for ABC (units: mm, 1 mm = 0.0394 in.)

UHPC longitudinal joint configurations were used for all cross sections to connect adjacent members. The joints used in this study were based on available design standards [2], [4] and previous research [7], [71], [72], [10]. A summary of the joints used between the members is shown in Figure 4.2.

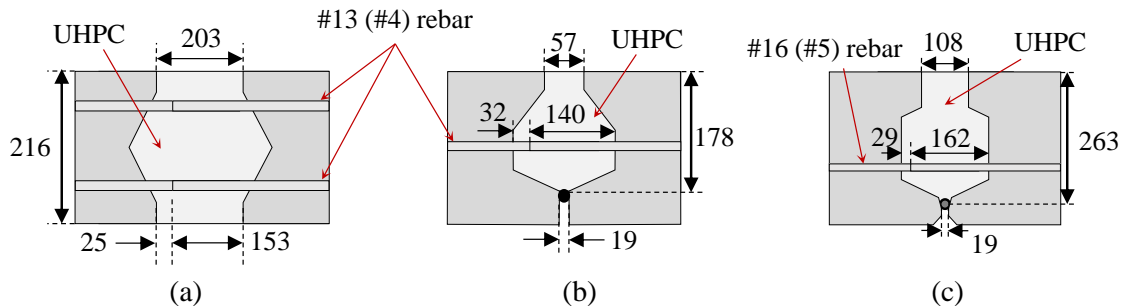


Figure 4.2: Summary of UHPC joint shapes for: (a) decked girders, (b) AASHTO BI, and (c) Florida Slab Beam (units: mm, 1 mm = 0.0394 in.)

Details on concept development, design optimization and full-scale testing of FSB joint geometry are provided in chapters §5 and §6, respectively

4.3 Analytical Investigation

4.3.1 Background

The first component of the investigation was made through a flexure parametric analysis designing a typical two-lane bridge configuration with barriers and shoulders, as shown in Figure 4.3, with varying span lengths from 6.1 to 24.4 m (20 to 80 ft.). The bridge width was kept consistent throughout all analyses at approximately 10 m (33 ft.); this width varied slightly based on the superstructure type based on standard beam widths and UHPC joint geometries. Flexural designs were conducted based on strength and service limit states specified in the AASHTO LRFD Bridge Design specifications [73]. The design for each case was optimized based on the shallowest section capable of meeting the flexural design requirements. The number of strands were accommodated from the bottommost layer to the top layers until the capacity was achieved for a certain span.

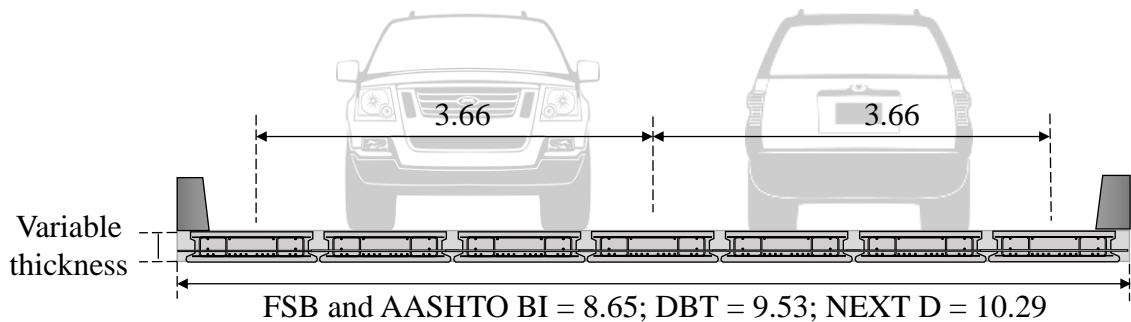


Figure 4.3: Example bridge using Florida Slab Beam (not to scale; units: m, 1 m = 3.281 ft.)

The design assumptions made for the parametric analysis were based on typical flexural design and include: exterior beam design, aggressive corrosive environment, beam concrete strength equal to 41.4 MPa (6 ksi) at release and 58.6 MPa (8.5 ksi) at 28 days, 15-mm (0.6-inch) diameter low-relaxation strands, 51-mm (2-in.) non-composite wearing

surface with 27.6 MPa (4 ksi) at 28 days, beams with sufficient connectivity to make them act as a unit without transverse posttensioning mechanism, and HL-93 live load truck as per AASHTO LRFD Bridge Design specifications [73]. The Decked NEBT beam and AASHTO box beam for ABC were designed using BridgeLink software [74]. The FSB for ABC was designed using FDOT Prestressed Beam – LRFD [75] Mathcad sheet with a modified joint geometry for proper section inertia and weight calculations. The NEXT D beam parameters were based on PCI Manual design aids [31].

As flexural stresses typically control the design of prestressed concrete girders, the key for an efficient design is the use of a girder section geometry with a large section modulus and small area. An efficiency factor (Equation 1) developed by Guyon [76] and discussed by many others [77]–[79] is based on maximizing section moduli for top and bottom fibers for a given cross-sectional area. This efficiency factor was used to compare the efficiency of the different cross section geometries; a larger efficiency factor means a more efficient section.

$$\rho = \frac{I}{Ay_b y_t} = \frac{r^2}{y_b y_t} \quad \text{Equation 1}$$

where: ρ = efficiency factor of section; I = moment of inertia of girder (in.⁴); A = area of cross section (in.²), y_b = distance from centroid of section to bottom fiber (in.); y_t = distance from centroid of section to top fiber (in.); and r = radius of gyration of section (in.).

4.3.2 Effects of Section Depths and Strand Number

A summary of the selected girder types with required strand numbers and depths versus span lengths is shown in Table 4.1. The average efficiency factors (ρ_{avg}) for each section

are included at the end of the table for comparison. The average efficiency factor was taken when a section varied in thickness per span length. The section widths and strand numbers that were further investigated in the numerical investigation are underlined in Table 4.1.

Table 4.1: Section depths with strand numbers for each span length and section widths with corresponding efficiency factors (units: mm, 1 mm = 0.0394 in. = 0.00328 feet)

| Span (m) | DBT 35 | | | NEXT D | | AASHTO BI | | FSB | |
|--------------|---------------------|---------------------|---------------------|---------------------|---------------------|--------------------|---------------------|---------------------|---------------------|
| | <u>1219</u> wide | <u>1829</u> wide | <u>2438</u> wide | <u>2438</u> wide | <u>3048</u> wide | <u>914</u> wide | <u>1219</u> wide | <u>1219</u> wide | <u>1524</u> wide |
| 6.1 | 889 (4) | 889 (4) | 889 (4) | 711 (8) | 711 (10) | 686 (3) | 686 (3) | 305 (8) | 305 (9) |
| 9.1 | 889 (6) | 889 (6) | 889 (8) | 711 (12) | 711 (14) | 686 (5) | 686 (5) | 305 (12) | 305 (15) |
| 12.2 | 889 (8) | 889 (8) | 889 (12) | 711 (16) | 711 (20) | 686 (7) | 686 (9) | 381 (15) | 381 (18) |
| 15.2 | <u>889</u> (8) | 889 (10) | 889 (14) | <u>711</u> (22) | 711 (28) | 686 (9) | 686 (11) | <u>457</u> (16) | 457 (21) |
| 18.3 | 889 (12) | 889 (16) | 889 (20) | 711 (30) | 813 (32) | 686 (11) | 686 (15) | 533 (22)* | 533 (26)* |
| 21.3 | 889 (16) | 889 (22) | 889 (28) | 813 (36) | 914 (36) | 686 (15) | 686 (21) | 610 (27)* | 610 (33)* |
| 24.4 | 889 (22) | 889 (28) | 889 (40) | 914 (40) | 1016 (42) | 686 (20) | 686 (26) | 762 (33)* | 686 (43)* |
| ρ_{avg} | 0.511 | 0.512 | 0.504 | 0.367 | 0.369 | 0.490 | 0.520 | 0.346 | 0.350 |

*Note: Section widths and depths in millimeters. Strand numbers in parenthesis, *Non-standard thickness.*

When comparing sections of same 1219-mm (48-in.) widths, the most efficient sections from the analysis were the DBT and AASHTO BI beam with efficiency factors of 0.511 and 0.520, respectively. The solid slab shape (FSB) and NEXT D beam had the lowest efficiency, with efficiency factors of 0.346 and 0.367, respectively.

The maximum span length versus required section depths for all 1219-mm (48-in.) width beam families is shown in Figure 4.4 (a). The FSB section allowed for the shallowest depths from 6.1 to 21.3-m (20 to 70-ft.) span lengths; the DBT and AASHTO BI beams only have one available section depth for this span length range. The shallowest available

NEXT D beam section (711 mm [28 in.]) can span up to 18.3 m (60 ft.); this section depth increases for spans of 21.3 m and 24.4 m (70 ft. and 80 ft.).

The maximum span length versus required number of strands for all 1219-mm (48-in.) width beam families is shown in Figure 4.4 (b). For comparison, the 1219-mm-wide (48-inch-wide) sections can be compared to half of the 2438-mm (96-inch) wide NEXT D beam section. The DBT, AASHTO BI, and NEXT D beam sections all required a similar number of strands per 1219-mm (48-in.) width. The solid slab beam (FSB) section required the most strands per 1219-mm (48-in.) width.

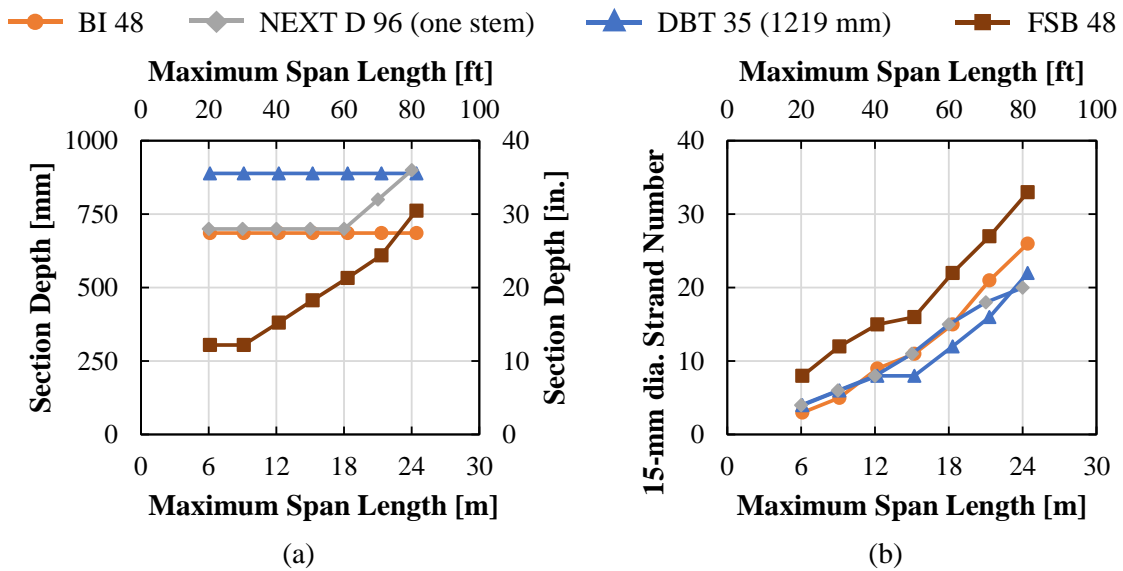


Figure 4.4: 1219-mm (48-inch) width sections comparison: (a) maximum span length versus required section depth and (b) maximum span length versus number of 15-mm (0.6-inch) diameter strands

4.4 Numerical Investigation

4.4.1 Numerical Methods

The second component of the analytical and numerical investigation involved non-linear finite element analysis (FEA) of the same simply supported bridge superstructure shown

in Figure 4.1 with different section shapes and a 15.2-m (50-ft.) length; barriers were not included to decrease the computing processing time. The response of all the numerical models were estimated using a commercial non-linear FEA package specifically designed for modeling reinforced concrete elements in the elastic, post-cracking, and ultimate capacity ranges. The software uses the Fracture-Plastic Constitutive Model: tensile and compressive behavior [80], which is suitable to simulate concrete cracking, crushing under high confinement, and crack closure due to crushing in other material directions.

Girder distribution factors (GDF_i) were determined from the FEA results following a similar approach used by past researchers [20], [81], [7]. This approach is based on the ratio of bottom longitudinal strain in a single girder to the summation of bottom longitudinal strains in all the girders, as shown in Equation 2. Therefore, longitudinal strain monitors were defined at the central bottommost region of each precast section to calculate the moment distribution factors.

$$GDF_i = \frac{M_i}{\sum_{j=1}^k M_j} = \frac{ES_i \varepsilon_i}{\sum_{j=1}^k ES_j \varepsilon_j} = \frac{\frac{S_i}{S_l} \varepsilon_i}{\sum_{j=1}^k \frac{S_j}{S_l} \varepsilon_j} = \frac{\varepsilon_i \omega_i}{\sum_{j=1}^k \varepsilon_j \omega_j} \quad \text{Equation 2}$$

where: M_i = bending moment at the i -th girder; E = modulus of elasticity, S_i = section modulus of the i -th girder; S_l = typical interior section modulus, ε_j = maximum bottom-flange static strain at the j -th girder; ω_j = ratio of the section modulus of the j -th girder to that of a typical interior girder.

These distribution factors were compared to those found using AASHTO LRFD Bridge Design specifications [73]. Distributions factors for interior ($g_{interior}$) and exterior ($g_{exterior}$)

beams were based on Table 4.6.2.2.2b-1 and Table 4.6.2.2.2d-1 [73] respectively. Additional guidance was obtained from FDOT Structures Design Guidelines [82] for slab beam bridges §2.9.A.1 and §2.9.A.2 and provisions from PCI and PCINE for DBT [28] and NEXT D [44] beams. Additional load configurations with rear-axle truck loading placed at different locations across the bridge width were used to investigate the performance of the longitudinal joints between adjacent beams.

Stresses were also monitored in the beams and joints during all the numerical analyses. These were used to compare the overall performance of the superstructure systems and joints.

4.4.2 Specimen Geometries and Loading Configurations

The schematics of the bridge model, load application pattern, and load cases used in the numerical analyses are shown in Figure 4.5. Each bridge geometry was modeled as a half-bridge model to decrease the computational demand required for the analysis; the model consisted of a pinned support under the bearing on one end of the bridge and a restraint against rotation but allowing vertical deflection on the other support, as shown in Figure 4.5 (a). Each bridge was loaded using one HS-20 rear axle geometry located at midspan based on the AASHTO LRFD Bridge Design Specifications [73] oriented in the direction of traffic parallel to the joints. A half rear-axle with two wheel patches (508 mm by 254 mm [20 in. by 10 in.]) was used in the model since only half of the bridge was modeled, as shown in Figure 4.5 (b). The total applied load per patch was determined based on a FL120 Permit Truck, described in Chapter 2 of the FDOT Bridge Load Rating Manual [83], with an equivalent weight of 1.67 times an HS20 truck, or 533.8 kN (120 kips), with one FL120

rear axle load being 237.1 kN (53.3 kips). The load was increased by 15 percent for Dynamic Load Allowance as per AASHTO LRFD Bridge Design Specifications (§3.6.2.1) [73]. The total load applied per load patch was 136.6 kN (30.7 kips). Three load cases were identified to create the largest transverse demands in the joints and precast sections, as shown in Figure 4.5 (c). Case 1 consisted of loading one lane by locating the exterior load patch boundary at the farthestmost exterior location of the system, maximizing transverse tensile stresses in the opposite top region. Case 2 consisted of aligning the centerline of the axle with the centerline of the bridge at midspan, maximizing the tensile stresses on the underside of the bridge. Case 3 consisted of loading two lanes by aligning both exterior load patches boundaries with the exterior lane limits, increasing transverse tensile stresses at the centerline of the bridge.

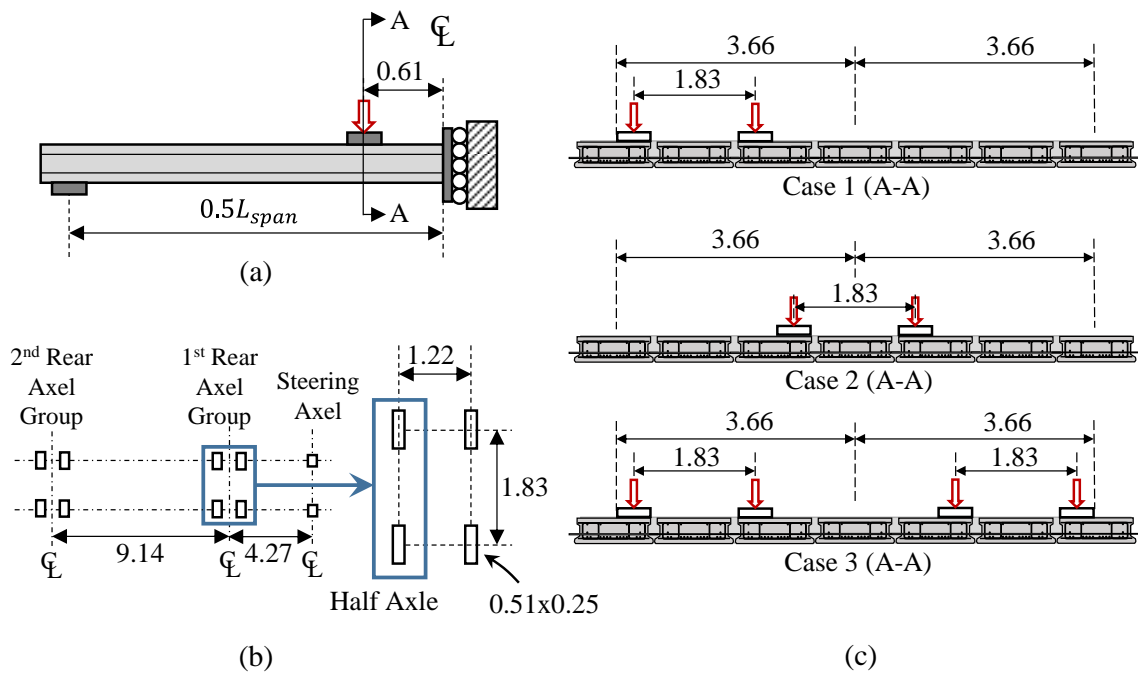


Figure 4.5: Schematics of example bridge for FEA analysis: (a) half-bridge model with boundary conditions, (b) load patch pattern, and (c) load cases (FSB shown, others similar; not to scale; units: m, 1 m = 3.281 ft.)

Two loading stages were applied to the system per load case:

- *Prestressing*: Effects of prestressing and weight for all beams were modeled during this stage. The UHPC joint material was modeled with a very low Young's modulus (i.e., 6.9 MPa [1 ksi]) as at this stage the joint was not cast.

System Loading: The system was fully loaded until reaching the defined load level. The UHPC material properties were changed back to their original hardened properties.

4.4.3 Meshing and Material Models

The mesh of the superstructure models was generated by assigning a semi-structured mesh of 30 hexahedra elements along the length of the model (with a minimum element size of 51 mm [2 in.]) for the DBT 35, NEXT D and FSB sections. An unstructured mesh of tetrahedra elements (with a minimum element size of 51 mm [2 in.]) for the AASHTO BI section was defined to increase analysis efficiency. A sample mesh for two of the models is shown in Figure 4.6.

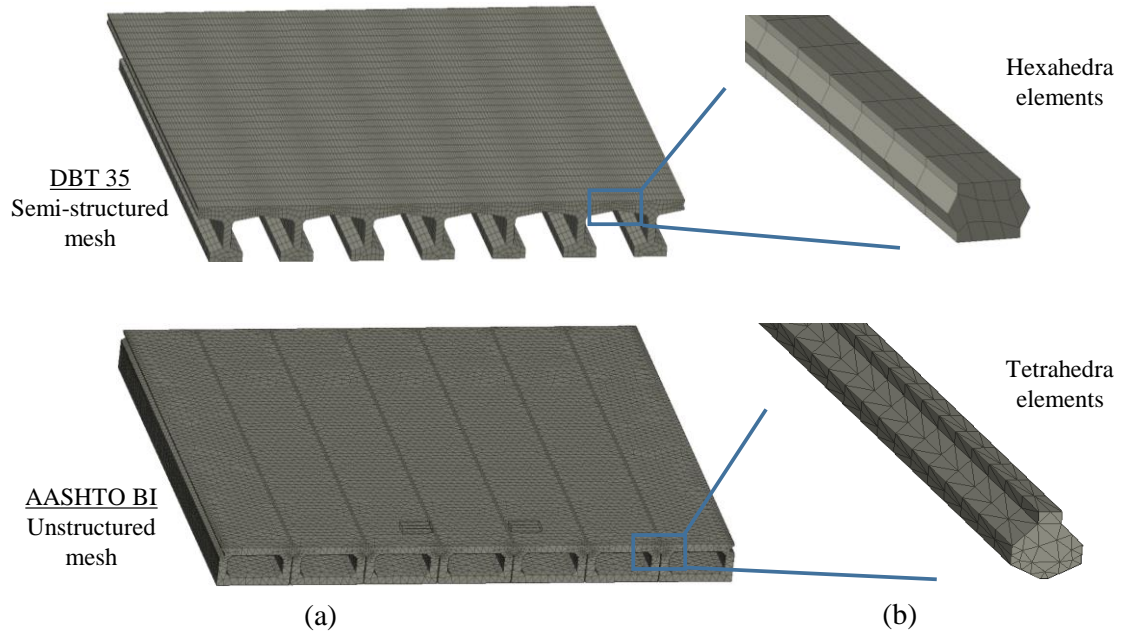


Figure 4.6: Mesh examples: (a) superstructure and (b) joint detail

The basic material properties for modeling the concrete, UHPC and steel reinforcement in the sections are summarized in Table 4.2. The precast sections were modeled using a conventional concrete model (CC3DNonLinCementitious2) with the described ultimate and compressive tensile stresses. The UHPC was also modeled using CC3DNonLinCementitious2, but with an increased compressive strength (f'_c), tensile strength (f_t), Young's Modulus (E), and fracture energy (G_F), as shown in Table 4.2. The CC3DNonLinCementitious2 material definition is based on two constitutive models for fracture (tension) and plastic (compression) behaviors combined through a simultaneous algorithm solution [84]. For a more realistic behavior, the values presented in Table 4.2 are based on calibrated software material properties for a typical precast, prestressed concrete beam and UHPC joint made of proprietary materials [10], which are assumed equal for simplicity in all superstructure systems.

Table 4.2: Summary of concrete and steel materials models used

| Material | Base Material Prototype | f_y (MPa) | f'_c (MPa) | f_t (MPa) | E (GPa) | G_F (kN/m) |
|----------------------|-------------------------|-------------|--------------|-------------|-----------|--------------|
| Beams* | CC3DNonLinCementitious2 | -- | 78.6 | 5.5 | 42.0 | 0.080 |
| UHPC Joints | CC3DNonLinCementitious2 | -- | 155.1 | 9.0 | 50.7 | 0.125 |
| Prestressing Strands | CCReinforcement | 1675.4 | -- | -- | 196.5 | -- |
| Steel Reinforcement | CCReinforcement | 450.9 | -- | -- | 199.9 | -- |

Note: f_y = yielding strength; f'_c = concrete compressive strength at 28 days; f_t = concrete tensile strength at 28 days; E = modulus of elasticity; *same material for all beams. (1 ksi = 6.9 MPa; 1 kip = 4.4 kN; 1 in. = 0.025 m)

4.5 Numerical Results and Discussion

4.5.1 Effects of Distribution Factors

A summary of all properties and distribution factor calculations for all four superstructure systems are shown in Table 4.3. All beams span 15.2 m (50 ft.) and are 1219 mm (48 in.) wide. The NEXT D 96 is equivalent to two 1219-mm (48-in.) single-stem beams, so its distribution factors are for one stem (i.e., half of the NEXT D 96).

Table 4.3: Section parameters and distribution factor summary

| Parameter | DBT 35x48 | NEXT D 96* | AASHTO BI 48 | FSB 18x48 |
|-----------|--|---|--|--|
| N_b | 7 | 8 | 7 | 7 |
| A | 0.195 m ² (302.50 in. ²) | 0.187 m ² (289.65 in. ²) | 0.449 m ² (695.19 in. ²) | 0.497 m ² (770.54 in. ²) |
| I | 0.007 m ⁴ (16,917.43 in. ⁴) | 0.004 m ⁴ (9,918.85 in. ⁴) | 0.027 m ⁴ (64,351.69 in. ⁴) | 0.009 m ⁴ (21,663.56 in. ⁴) |
| I_p | 0.011 m ⁴ (26,371.28 in. ⁴) | 0.006 m ⁴ (15,120.94 in. ⁴) | 0.099 m ⁴ (237,206.30 in. ⁴) | 0.058 m ⁴ (140,364.90 in. ⁴) |
| J | 0.003 m ⁴ (7,937.98 in. ⁴) | 0.005 m ⁴ (11,637.57 in. ⁴) | 0.010 m ⁴ (24,616.23 in. ⁴) | 0.026 m ⁴ (62,785.91 in. ⁴) |
| b | 0.635 m (25 in.) | 0.349 m (13.75 in.) | 1.219 m (48 in.) | 1.219 m (48 in.) |
| K_g | 0.069 m ⁴ (165,899.47 in. ⁴) | 0.026 m ⁴ (63,395.08 in. ⁴) | - | - |

| | | | | |
|--------------------------------------|------------------------|------------------------|----------------------|----------------------|
| k | - | - | 1.69 | 1.69 |
| e_g | 0.564 m (22.19 in.) | 0.345 m (13.59 in.) | - | - |
| t_s | 0.229 m (9 in.) | 0.203 m (8 in.) | - | - |
| S | 1.384 m (4.54 ft) | 1.308 m** (4.29 ft) | 1.237 m (4.06 ft) | 1.237 m (4.06 ft) |
| $g_{interior_single}$ | 0.342 | 0.315 | 0.366 | 0.220 |
| $g_{interior_multi}$ | 0.436 | 0.399 | 0.357 | 0.316 |
| FEA $g_{interior}$ | 0.305 | 0.235 | 0.197 | 0.195 |
| d_e | 0.344 m (1.13 ft) | 0.192 m (0.63 ft) | 0.344 m (1.13 ft) | 0.344 m (1.13 ft) |
| e_{single} | - | - | 0.354 m (1.16 ft) | 0.354 m (1.16 ft) |
| e_{multi} | 0.271 m (0.89 ft) | 0.256 m (0.84 ft) | 0.332 m (1.09 ft) | 0.332 m (1.09 ft) |
| $g_{exterior_single}$ | 0.214 | 0.184 | 0.425 | 0.256 |
| $g_{exterior_multi}$ | 0.390 | 0.335 | 0.387 | 0.343 |
| FEA $g_{exterior}$ | 0.350 | 0.275 | 0.248 | 0.244 |

Note: * Half beam (one stem) is only used. ** average spacing of stems was used

Where: N_b = number of beams or girders; A = gross area; I_p = gross inertia; J = St. Venant's torsional inertia; b = beam width; K_g = longitudinal stiffness parameter; k = stiffness parameter; t_s = depth of concrete slab; S = spacing of beams or webs; d_e = horizontal distance from the centerline of the exterior web of exterior beam at deck level to the interior edge of traffic barrier.

The DBT section had the largest distribution factors for both interior and exterior beams from the FEA results, which would suggest less load being transferred between adjacent beams compared to the other systems. The slab beam (FSB) system had the smallest measured distribution factors from the FEA results, which would suggest the best load transfer between adjacent beams. The distribution factors based on the FEA results were below the actual AASHTO values for all cases, with the largest difference observed in the AASHTO BI section (approximately 42 percent) and the smallest difference in the FSB section.

4.5.2 Effects on Transverse Section and Joint Demand

The FEA results were analyzed for the three load cases for all four section shapes. Only results from the critical load cases for each section type are shown in this section.

The largest transverse tensile stresses were observed in Load Case 3 for stemmed decked sections atop the central joint-precaster region, as shown in Figure 4.7 (a) for NEXT D and Figure 4.8 (a) for DBT sections, respectively. At peak load on NEXT D section, the top fibers of the precast sections at the center region developed transverse tensile stresses up to 2.86 MPa (415 psi), as shown in Figure 4.7 (b), which was also occurring at the top corners of Joint B, shown in Figure 4.7 (c), maintaining a decreasing tension profile across the joint thickness to the bottom. Top transverse compression and bottom transverse tension stresses up to 1.72 MPa (249 psi) stress were observed atop Joint A; Joint C had a similar response. Overall, stresses remained under cracking stresses in the precast NEXT D beam section and the joint, with the largest transverse tensile stress concentrations at boundary between Joint B and the adjacent NEXT D beams.

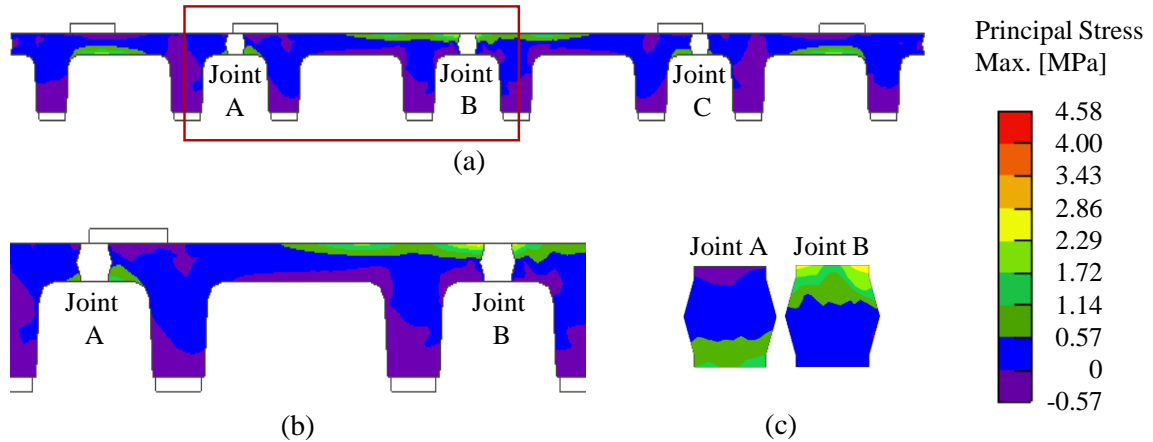


Figure 4.7: Maximum principal stress map at midspan for Load Case 3 – NEXT D section: (a) full width cross section, (b) zoomed in precast-joint region (other side similar), and (c) joint A and B cross-section stress maps (1 MPa = 0.15 ksi)

At peak load on DBT section using Load Case 3, the top fibers of the precast sections at the center region developed transverse tensile stresses up to 2.86 MPa (415 psi), as shown in Figure 4.8 (b). The stresses were higher at the top corners of Joint C, as shown in Figure 4.8 (c), with stresses topping 3.43 MPa (498 psi). Top transverse compression stresses and bottom transverse tension stresses up to 4.58 MPa (664 psi) were observed in Joint B, with similar stresses in Joint E. Overall, stresses remained under cracking stresses in the precast DBT beams and joints between beams, with the largest transverse tensile stress concentration at the boundary between Joint B and the adjacent DBT beams.

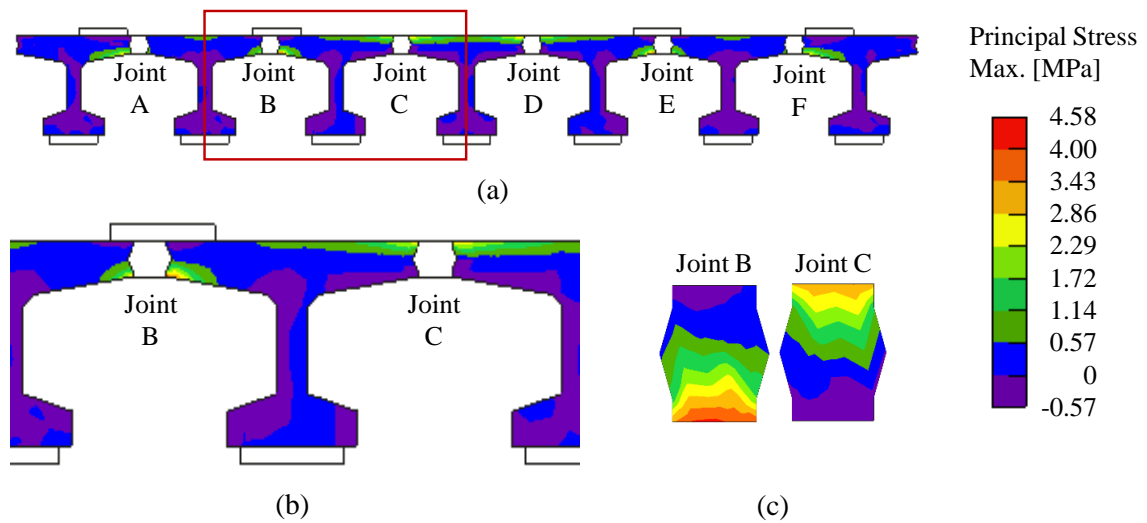


Figure 4.8: Maximum principal stress map at midspan for Load Case 3 – DBT section: (a) full width cross section, (b) zoomed in precast-joint region (other side similar), and (c) joint B and C cross-section stress maps (1 MPa = 0.15 ksi)

The largest transverse tensile stresses were observed in Load Case 2 for flat decked sections, occurring in the bottom central joint regions, as shown in Figure 4.9 (a) for FSB and Figure 4.10 (a) for AASHTO BI sections. At peak load on FSB section using Load Case 2, transverse compressive stresses developed across the top of the superstructure and transverse tensile stresses across the bottom of the superstructure, with a maximum transverse tensile stress of 1.72 MPa (249 psi) on the three central FSBs, as shown in Figure 4.9 (b). There was a higher transverse tensile stress observed toward the bottom of the joint region, transverse tensile stresses up to 4.00 MPa (581 psi) were observed in Joint C and Joint D at the joint reinforcement level, as shown in Figure 4.9 (c).

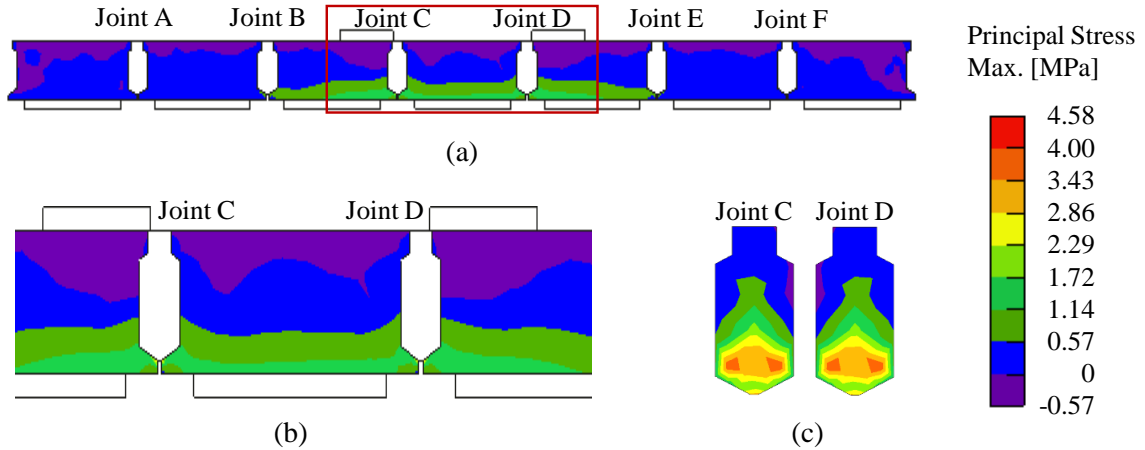


Figure 4.9: Maximum principal stress map at midspan for Load Case 2 – FSB section: (a) full width cross section, (b) zoomed in precast-joint region (other side similar), and (c) joint A and B cross-section stress maps (1 MPa = 0.15 ksi)

At peak load on AASHTO BI section using Load Case 2, transverse compressive stresses developed across the top of the superstructure and transverse tensile stresses up to 2.29 MPa (332 psi) near the bottom of the joint regions between interior beams, as shown in Figure 4.10 (b). These joints do not extend to the bottom of the precast section and the precast box section has a void in the middle, so the transverse stresses are concentrated in the top portion of the section (above the void) and the adjacent joints, as shown in Figure 4.10 (c).

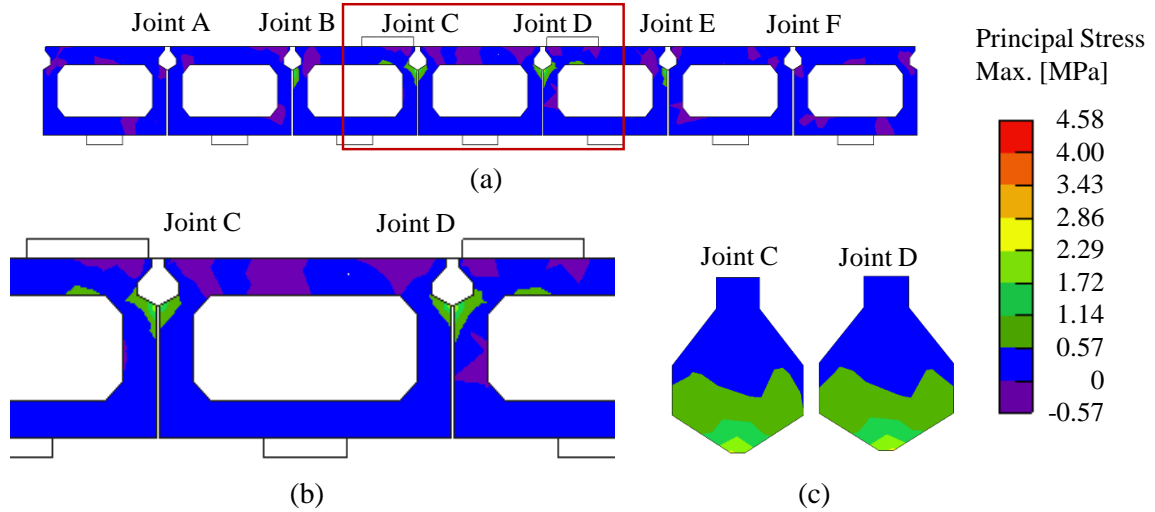


Figure 4.10: Maximum principal stress map at midspan for Load Case 2 – AASHTO BI section: (a) full width cross section, (b) zoomed in precast-joint region (other side similar), and (c) joint A and B cross-section stress maps (1 MPa = 0.15 ksi)

4.6 Conclusions and Recommendations

An analytical and numerical study was conducted to investigate four precast, prestressed concrete cross section shapes that can be used in short-span accelerated bridge construction applications. The sections were assessed to see the section efficiency and number of strands required for different bridge span lengths. Based on the analytical analysis, the following conclusions have been made:

- The decked bulb tee beam and box beam section shapes were the most efficient of the sections for all span lengths, with the DBT superstructure being the best performer.
- The solid slab required for the FSB section and the thick webs of the NEXT D beam resulted in these two sections being the least efficient of the four sections investigated.

- Although the solid slab section resulted in the least efficient section and required the most strands, it did allow for the shallowest section depths for spans less than 22.9 m (75 ft.), making it an ideal option for bridges with narrow clearances or low profiles.

A FEA analysis was also conducted to investigate load distribution and transverse precast section and joint demands with a single two-lane, 15.2-meter-long (50-foot-long) superstructure span. Based on the software analyses, the following conclusions have been made:

- The slab beam (FSB) section had the smallest distribution factors from FEA results, suggesting they had the best load transfer between adjacent beams in the superstructure system.
- Overall transverse tensile stresses remained well under cracking stresses for all four sections.
- No significant discontinuity in the stress contour was observed in the sections with large precast members and small joint regions (e.g., DBT, AASHTO BI, and NEXT D) due to stiffness difference of materials. However, the joint of the FSB system showed a larger tensile stress contour in the UHPC matrix than the precast section.
- The DBT precast section developed the largest tensile stress concentrations at the bottom of the outermost exterior joints with Load Case 3. The FSB precast section developed most of the tensile stress concentrations at the bottom of the joint matrix at reinforcement level with Load Case 2.

- Small joint regions with angular geometry changes (e.g., stemmed decked sections and AASHTO BI) will develop high tensile stress concentrations at the changing corners.

All four superstructure systems explored in this research could be used effectively for ABC of short-span bridges. The selection of the best cross section to use would be based on specific project constraints and regional factors (e.g., available cross sections at local precasters). The work presented in this chapter can help the engineer make a better-informed decision where multiple cross sections may be available.

4.7 Data Availability Statement

Some or all data used during the study are available from the corresponding author by request.

- Data from analytical study
- Data from FEA analysis

4.8 Acknowledgement

The authors would like to thank the Florida Department of Transportation for their financial support of this project. The opinions, findings and conclusions expressed in this publication are those of the author(s) and not necessarily those of the Florida Department of Transportation or the U.S. Department of Transportation.

5. JOINT DESIGN OPTIMIZATION FOR ACCELERATED BRIDGE CONSTRUCTION OF SLAB BEAM BRIDGES¹

*Francisco Chitty², Christina Freeman³, and David Garber⁴

5.1 Abstract

The Florida Slab Beam (FSB) has been developed by the Florida Department of Transportation (FDOT) to be used for short-span bridges (less than about 19.8 m [65 ft.] long). The FSB system consists of shallow precast, prestressed concrete inverted-tee beams that are placed adjacent to each other and then involve reinforcement and concrete being placed in the inner joints and deck all in one single cast. Ultra-high-performance concrete (UHPC) is becoming more widely used in bridge construction applications due to its remarkable structural performance. Many departments of transportation have tested and deployed the use of UHPC in bridges around the US. Most of these applications have been to connect precast members (e.g., slabs to beams and slabs, adjacent beams, caps to columns, etc.). A modified FSB design is desired to eliminate the cast-in-place (CIP) deck and allow for UHPC to be used in the joint region, which will allow for accelerated construction and decrease the impact of construction on traffic. Different joint details and

¹ This material may be downloaded for personal use only. Any other use requires prior permission of the American Society of Civil Engineers. This material may be found at DOI: 10.1061/(ASCE)BE.1943-5592.0001561 [10]

² Corresponding Author. PhD Candidate, Civil and Environmental Engineering, Florida International University, Miami, FL, USA. Email: fchit001@fiu.edu

³ Structures Research Engineer, Structures Research Center, Florida Department of Transportation, Tallahassee, FL, USA. Email: christina.freeman@dot.state.fl.us

⁴ Associate Professor, Civil and Environmental Engineering, Florida International University, Miami, FL, USA. Email: dgarber@fiu.edu

cross-section geometries were analyzed and experimentally evaluated to determine feasible joint details with UHPC for slab beam bridges used in accelerated construction. Results from numerical modeling, strength, and fatigue experimental testing of the transverse joint performance of four different UHPC joints in two different depth slab beam bridges are presented. The straight-side and shear-key UHPC joint details were found to behave similar to or better than the current FSB joint detail.

5.2 Introduction

There are over 600,000 bridges in the US with about 40 percent of them at least 50 years old and about nine percent of them being structurally deficient [85]. In Florida, the majority of the structurally deficient or functionally obsolete bridges are short-span bridges, including slab beam systems with deficient load transfer capacity due to strength decay in their joints; approximately 90 percent of these bridges are less than 18 m (60 ft.) long [86]. There has been a need to develop solutions for rapidly replacing, repairing, or retrofitting these structures while minimizing the impact to traffic during construction. Accelerated bridge construction (ABC) techniques, specifically prefabricated bridge elements and systems (PBES), can provide such a solution. Slab beam superstructures, one type of prefabricated element, can be used with ultra-high performance concrete (UHPC) to create a resilient superstructure system that can offer accelerated construction with enhanced serviceability performance. The development of a joint detail for such a slab beam system that enhances load transfer capacity through numerical modeling and experimental testing of joints in flexure is summarized in this paper.

5.2.1 Slab Beam Superstructures

Slab beams have been used in bridge superstructure construction since prestressing began in the United States in the 1950s. Slab beam superstructures are characterized by having shallow depth, prestressed, precast concrete, and are placed side-by-side with a concrete joint cast in between them. Due to their shallow depths, the beam section is typically suitable for bridge spans less than 22.9 m (75 ft.) in length. Texas [87], Minnesota [60], Virginia [36], and Florida departments of transportation have used different slab beam configurations with different longitudinal joint and transverse tie mechanisms to ensure appropriate load transfer between adjacent members. The Florida Department of Transportation (FDOT) bridge inventory has developed six iterations of slab beam bridges that have been built since the 1950s [86]. The first of these slab beam bridges was the prestressed rectangular slab unit, shown in Figure 5.1 (a). This system did not have a cast-in-place (CIP) concrete deck and was connected through a longitudinal, 254 mm (10 in.) wide, concrete closure pour. The width of the joint was dependent on the required development length of the transverse steel projecting in the closure pour. In 1958, the system was modified to enhance its capacity by adding a 102-mm (4-in.) CIP reinforced concrete deck that was cast with the joint as shown in Figure 5.1 (b). The joint was modified by extending the bottom concrete ledges such that forming underneath the superstructure was not required and transverse post-tensioned tie bars in sleeves were used as the transverse joint reinforcement. Later in the 1950s, a lighter version of the slab unit called Sonovoid (voided slab) began to be used, shown in Figure 5.1 (c). Sonovoids have a reduced weight due to cylindrical voids running along the length of the beam and an asphalt layer in place of the 102-mm (4-in.) thick CIP deck; the asphalt overlay was used to

accommodate differential camber between adjacent beams. The overall joint geometry was decreased to small shear keys filled with grout. The same transverse post-tensioned tie bar detail was used to provide for the force transfer between adjacent beams. These cross-sections developed by FDOT regional offices were used for the next few decades. The next major development in the FDOT slab beam systems was the Prestressed Slab Unit (PSU), shown in Figure 5.1 (d), which first appeared in 2008 and was standardized in 2009. The PSU was simpler to construct in the field as it eliminated the need for transverse tie bars. The load transfer between adjacent members relied on a grouted shear key and a 153-mm (6-in.) thick CIP reinforced concrete deck that acted in composite action with the slab beams.

There have been some issues observed with existing slab beam systems in Florida [86], [88] shown in Figure 5.1 (a) – (d). The transverse capacity of the joint has decayed rapidly during service loading in some deployed bridges, indicated by longitudinal cracking at the joints along the length of the beams. This behavior would suggest that the slab beam superstructure system is not behaving as a composite unit, but rather load is being primarily carried by the beam on which it is directly applied.

Poor performance of these systems led FDOT to the development of an alternate system in 2005, the Florida Slab Beam (FSB), shown in Figure 5.1 (e). The FSB was developed for use on low volume, short-span bridges (less than about 19.8 m [65 ft.] long). It consists of shallow precast, prestressed concrete inverted-tee beams that are placed side by side, allowing the bottom lip to serve as a bottom form for the CIP joint and deck. A steel reinforcement cage is placed in the joint region with an additional steel reinforcement mat

for the top deck. A monolithic concrete joint and slab are cast after all the reinforcement is placed.

The section shares some characteristics with the Precast Composite Slab Span System (PCSSS) developed by Minnesota in 2005 [48], [59], [89], shown in Figure 5.1 (f), which was the first shallow inverted-T prestressed concrete system with straight web sides and bottom ledges that served as stay-in-place formwork. The main difference between the FSB and the PCSSS system is that the PCSSS has projecting rebar hooks that extend transversely through the joint creating a lapped splice, while the projecting rebar hooks in the FSB do not extend beyond the edge of the bottom lip. The detail in the FSB was intended to improve constructability by eliminating the potential of projecting rebars from adjacent members interfering with each other.

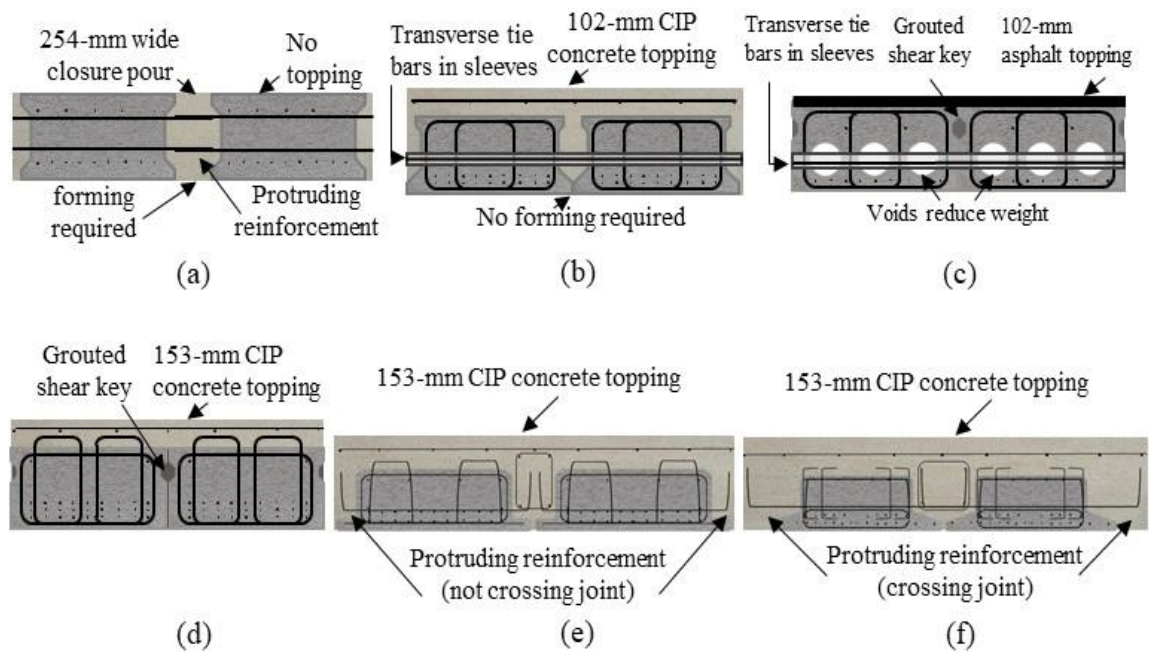


Figure 5.1: Slab beam system evolution in Florida: (a) prestressed rectangular slab unit (1955), (b) prestressed keyed slab unit (1958), (c) prestressed voided slab units – Sonovoid (1958), (d)

prestressed slab unit – PSU (2008), (e) Florida Slab Beam – FSB (2015), based on Goldsberry [51], and (f) precast composite slab span system – PCSS (2005).

After the PCSSS development, MnDOT implemented the system in two pilot bridge projects with one of the bridges instrumented and monitored to investigate the in-service performance and possible reflective cracks on the CIP deck [89]. It was found that cracking initiated in CIP deck regions immediately above the vertical sides of the beam webs over the ledged joints, and the researchers determined that these cracks resulted from restrained concrete shrinkage and environmental effects rather than traffic loads [48], [89]. Ten additional bridges were constructed between 2005 and 2011, giving a total of 12 bridges constructed in Minnesota with a version of the PCSSS system. Five of these bridges were inspected in 2011 to determine their performance [90]. Halverson et al. (2012) found there to be extensive cracking and efflorescence located on the bottom of the superstructure near joints in the inspected bridges. An optimized inverted T-beam was later proposed by researchers from Virginia with revised web section that included tapered sides. This solution was shown to decrease stress concentrations that could occur in abrupt geometry changes in the slab beam web [36], [91], but researchers still found that stresses from temperature and time effects were still significant [91].

5.2.2 Research Motivation, Objective, and Significance

The research discussed in this paper had two primary motivations: (1) the poor performance of previously used slab beam systems for short-span bridges evidenced by reflective cracking along the joint line in in-service bridges and (2) the desire to create a short-span bridge solution for accelerated construction. The primary objective of the research discussed in this paper was to develop a cross section for short-span bridges (less than 22.9

m [75 ft.] in length) and a joint design utilizing UHPC with satisfactory strength and fatigue performance, which allows for accelerated construction of the superstructure. UHPC was selected as the joint material for this research as it has been previously used in accelerated bridge construction applications to connect other precast members (e.g., full-depth precast deck panels, adjacent box beams). The research discussed in this paper is significant as it addresses the future construction of short-span bridges, which make up the vast majority of structurally deficient and functionally obsolete bridges.

5.2.3 Previously Investigated Joint Details with UHPC

Ultra-High-Performance Concrete (UHPC) is becoming more widely used due to its high compressive and tensile strength, improved long-term durability, low permeability, and high flowability. Also, UHPC has been used for constructing prefabricated bridge elements and overlays, but its primary application to date has been for the joints between prefabricated elements [1]. The high tensile strength of UHPC decreases the required joint size and improves the joint durability between prefabricated elements; UHPC has been shown to provide a stronger connection than the prefabricated members themselves [92].

There have been several research efforts that have investigated UHPC joints between full-depth precast concrete deck panels [62], [93] and adjacent box beams [8]. A study conducted by Aaleti and Sritharan [62] determined the four most popular joint geometries used in panel-to-panel connections with different steel rebar configurations: lap spliced bars, headed bars, non-contact lap spliced bars, and hooked bars. A UHPC joint geometry with non-contact, lap spliced transverse rebar was later developed to connect adjacent box

bridge superstructures [8]; the details of this joint were based on previously discussed joint geometries.

Guidelines for UHPC field-cast joint construction were developed based on the extensive research conducted by the Federal Highway Administration (FHWA) [4]. These guidelines were developed based on findings from the previously mentioned research on joint connections, additional reinforcement pull out and development testing [94], and UHPC material testing [95].

5.3 Development of UHPC Joint Geometry and Reinforcement Detail

The design embedment lengths, cover, lap splice length, and spacing between non-contact lap spliced bars in UHPC were chosen as recommended by Graybeal [4] as a starting point. The recommended and provided values for the #16 (#5) joint reinforcement ($d_b = 15.9$ mm [0.625 in.]) are shown in Table 5.1; the joint regions proposed for testing use #16 (#5) rebar as the primary joint reinforcement. These design recommendations are valid for a UHPC mix with 2-percent (by volume) steel fiber reinforcement and a compressive strength of at least 96.46 MPa (14 ksi). This value allows for accelerated construction applications, as a typical UHPC mix can reach above 96.46 MPa (14 ksi) within the first few days after casting [96].

Table 5.1: Design values for UHPC connections (based on [4])

| Parameter | Formula | Value | Provided |
|-------------------|-----------------|--|----------------------|
| Embedment length | $l_d = 8d_b$ | $8 * 15.9 \text{ mm} = 127.2 \text{ mm}$ | 127.2 mm or 161.9 mm |
| Cover | $\geq 3d_b$ | $3 * 15.9 \text{ mm} = 47.7 \text{ mm}$ | 47.6 mm |
| Lap splice length | $l_s = 0.75l_d$ | $0.75 * 127.2" = 95.4 \text{ mm}$ | 101.6 mm or 133.3 mm |

| | | | |
|---------------------------|-------|---------|---------|
| Max. clear spacing | l_s | 95.2 mm | 60.3 mm |
|---------------------------|-------|---------|---------|

Note: l_d = embedment length; l_s = lap splice length; 1 in. = 25.4 mm

Two categories of joint geometries were developed for investigation in this project: (1) straight joint sides with no shear key and (2) traditional shear key shape. The width of the joints with straight sides and no shear key was based on the required embedment length and splice length of the joint reinforcement. As UHPC allows for a shorter embedment and development lengths, only a 153-mm (6-in.) wide joint was required, resulting in two joint geometries called FDOT 1 (F1) and FDOT 2 (F2), as shown in Figure 5.2 (a) and (b). A bottom lip was still provided in these joints to allow for the joint to be constructed without bottom forming of the joint. Two different thickness bottom lips were provided: a 102-mm (4-in.) lip with reinforcement extending into it in joint F1, and a 51-mm (2-in.) lip without reinforcement extending into the lip in joint F2, shown in Figure 5.2 (a) and (b), respectively. The thinner bottom lip dimension allowed for the joint reinforcement to be moved further down in the section but did not allow for reinforcement to be extended into the lip.

One traditional shear key detail was chosen to allow for a larger embedment length of the joint reinforcement while keeping a similar joint area. This detail was based on a previously recommended detail for the connection between adjacent box beams [4], [8], and it is called Alternate 1 (A1) as shown in Figure 5.2 (c). The splice length of the joint reinforcement was the same as joint F1 and F2 previously described. The depth of the joint reinforcement in joint A1 (162 mm [6.4 in.]) was larger than that of joint F1 (158 mm [6.2 in.]). A second shear key detail, shown in Figure 5.2 (d) and called Alternate 2 (A2), was developed to:

(1) lower the height of the joint reinforcement, (2) increase the splice length of the reinforcement, and (3) strengthen the top flange portion of the joint.

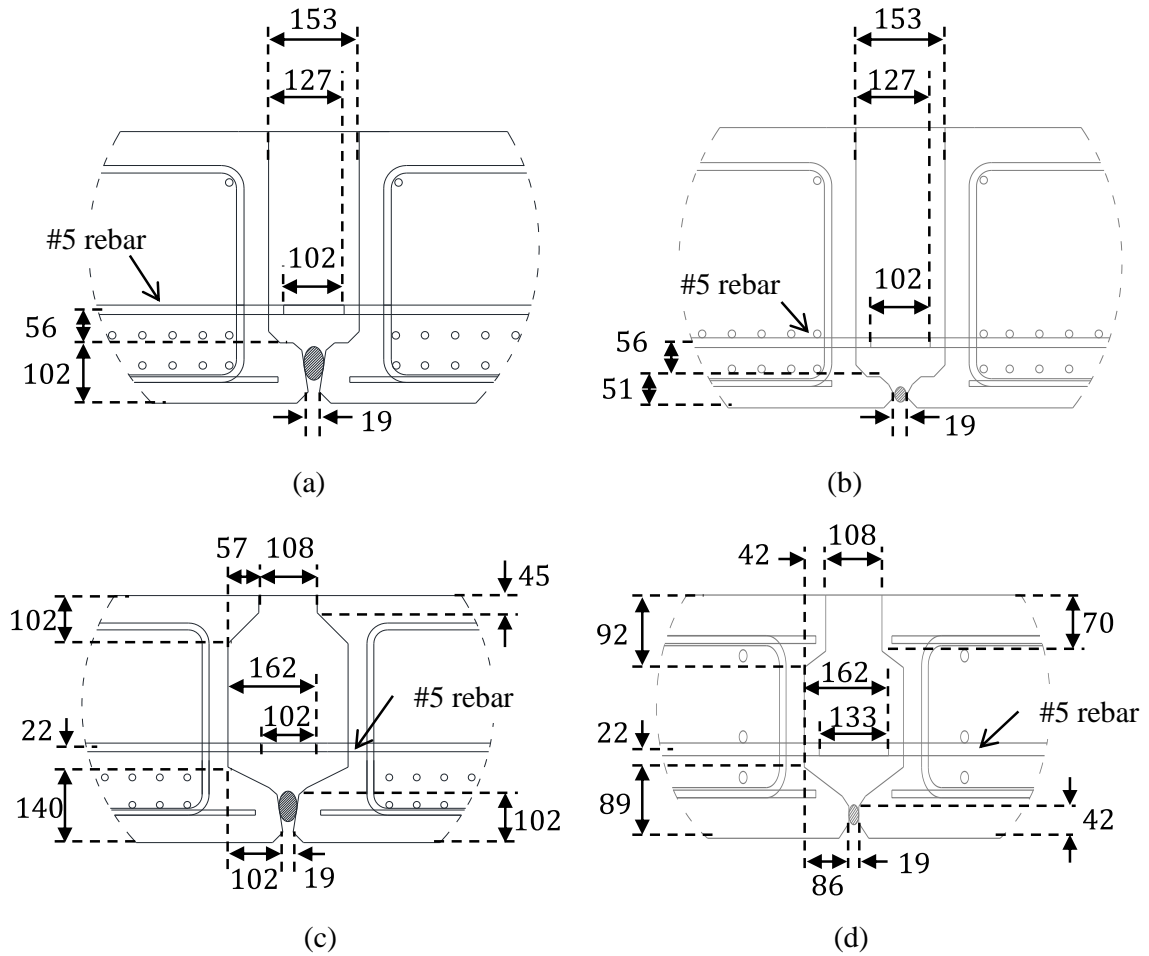


Figure 5.2: Details for joint: (a) FDOT 1 (F1), (b) FDOT 2 (F2), (c) Alternate 1 (A1), and (d) Alternate 2 (A2). (units: mm, 1 mm = 0.0394 in)

The performance of the proposed UHPC joint specimens was compared to the performance of a control specimen, called FSB, which had a joint designed using the original FSB construction detail. This detail requires #16 (#5) hooked joint reinforcement with a bend diameter of 64 mm (2.5 in.) extending 127 mm (5 in.) from the precast beams with a height measured from the base of the member of 165 mm (6.5 in.), as shown in Figure 5.1 (e).

The reinforcement installed in the field includes hooped bars in the joint, longitudinal joint reinforcement along the length of the beam, and deck reinforcement all of which are #16 (#5) bars. The joint and CIP deck are then cast at the same time.

These joint details were evaluated through the following numerical and experimental investigations using 305-mm (12-in.) and 457-mm (18-in.) deep specimens with reinforcement details similar to those recommended by the original FSB construction guidance.

5.4 Numerical Investigation

Finite element analysis (FEA) was first used to determine the failure mechanism of the proposed joint geometries. FEA served to initially evaluate the performance of the joints and to determine the geometry of the specimens (length, width, and depth) to ensure a flexural failure mechanism with expected failure loads within the testing frame capabilities.

5.4.1 Numerical Methods

The response of all the laboratory specimens were first estimated using a commercial non-linear FEA package named ATENA® specially designed for modeling reinforced concrete elements in the elastic, post-cracking, and ultimate capacity ranges. The software uses the Fracture-Plastic Constitutive Model: tensile (fracturing) and compressive (plastic) behavior [80], which is suitable to simulate concrete cracking, crushing under high confinement, and crack closure due to crushing in other material directions.

5.4.2 Specimen Geometry

Numerical models were developed for eight joint geometries to be tested in two groups: (1) 457-mm (18-in.) deep beams (Control FSB, F1, F2, and A1), and (2) 305-mm (12-in.) deep beams (F1, F2, A1, and A2), as shown in Figure 5.3. These joint specimens consisted of two beams with the same joint geometry placed side by side and loaded to study the transverse flexural capacity of the joints. There are three main slab-beam depths in the current FSB Specifications [54]. The control FSB specimen was designed using a 305-mm (12-in.) deep standard FSB section with a 1,520-mm (60-in.) wide (FSB 12x60) and a 152-mm (6-in.) deep CIP deck, giving an overall thickness of 457 mm (18 in.). The smallest and largest slab beam depths in the current FSB Specification (305 mm and 457 mm [12 in. and 18 in.]) were chosen for the investigation of the other UHPC joint specimens without CIP decks.

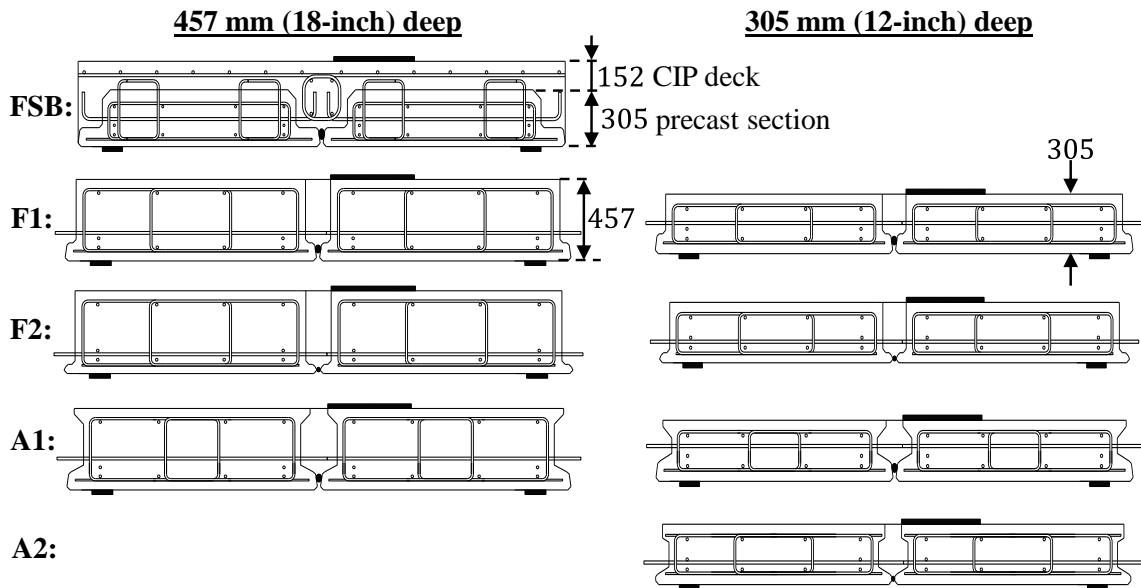


Figure 5.3: Specimen details for analytical and experimental program. (units: mm, 1 mm = 0.0394 in)

The FSB control served as a comparison for the 457-mm (18-in.) deep UHPC joint specimens. The overall thickness of the section is designated as the first number in the specimen's name (e.g., 12F1 is a 12-inch thick specimen with joint F1).

Ten total 15-mm (0.6-in.) diameter prestressing strands were located parallel to the joint in the beam section. Four strands were spread out across the top of the section, four strands at the bottom of the section and two strands in the outside of the section 51 mm (2 in.) above the bottom row of strands, as shown in Figure 5.3.

5.4.3 Meshing and Material Models

The mesh of all the models were generated automatically using the default mesh size (102 mm [4 in.]) per element with a tetrahedra geometry. The material properties used for modeling the concrete, UHPC, and steel reinforcement in the sections are summarized in Table 5.2. The FSB section and conventional joint concretes were modeled using a conventional concrete model (CC3DNonLinCementitious2) with the described ultimate and compressive tensile stresses. The UHPC was also modeled using CC3DNonLinCementitious2, but with an increased compressive strength (f'_c), tensile strength (f_t), modulus of elasticity (E) and fracture energy (G_F), as shown in Table 5.2. The CC3DNonLinCementitious2 material consists of two constitutive models for fracture (tension) and plastic (compression) behaviors combined through a simultaneous algorithm solution [84]. The crack initiation in the fracture model is computed using the Rankine failure criterion, which is described by a pyramid region formed by three stress planes in a stress space, or Rankine failure surface. A crack is formed when a maximum principal tensile stress (in any of the main three stress directions delimited by the failure surface at

any finite element) exceeds the tensile strength (f_t) of concrete [84]. The crack opening is then determined by the crack band size and the fracture strain as suggested by Hordijk [97].

Table 5.2: Summary of concrete and steel material models used

| Material | Base Material Prototype | f_y (MPa) | f'_c (MPa) | f_t (MPa) | E (GPa) | G_F (kN/m) |
|----------------------------|-------------------------|----------------|-----------------|----------------|--------------|-----------------|
| Beams* | CC3DNonLinCementitious2 | -- | 58.6 | 3.8 | 30.0 | 0.080 |
| Conventional Joint | CC3DNonLinCementitious2 | -- | 27.6 | 2.2 | 30.0 | 0.050 |
| UHPC Joint | CC3DNonLinCementitious2 | -- | 126.2 | 5.5 | 42.7 | 0.125 |
| Steel Reinforcement | CCReinforcement | 413.7 | -- | -- | 199.9 | -- |

Note: f_y = yielding strength; f'_c = concrete compressive strength at 28 days; f_t = concrete tensile strength at 28 days; E = modulus of elasticity; *same material for all beams: Control FSB and specimens with modified joint geometry; 1 ksi = 6.9 MPa; 1 kip = 4.4 kN; 1 in. = 0.025 m.

All the steel rebar in the models were specified as typical Grade 60 reinforcement without steel hardening. The longitudinal prestressing strands were modeled as inactive strands (without active prestressing force) as the models were used to assess the transverse behavior of the section and the joint strength.

The interface was modeled as a perfect bond between the UHPC and precast section, which was assumed because previous testing has shown that UHPC has a good bond to conventional concrete with proper aggregate exposure finish with at least 6-mm (0.25-in.) amplitude. Hence, the need for proper surface preparation for bond in joint specimens [4].

5.4.4 Transverse Joint Capacity

The transverse joint capacity between two adjacent members was investigated through these numerical analyses using a similar joint testing protocol conducted by Graybeal [92].

The boundary conditions, loading condition, and overall specimen geometry (for 1,422-mm [56-in.] long specimens) are shown in Figure 5.4 (a) and (b). Two beam segments with a short length (1,422 mm and 2,845 mm [56 in. and 112 in.]) were placed side by side with a UHPC joint connecting them (or CIP deck and joint for the FSB control specimen). The supports were located toward the outside of the beams running parallel to the joint; note that this is perpendicular to the orientation of the bearings in a bridge in the field as this test measures the transverse response at bridge mid-span between two beams. The load was then placed on the center edge of the joint region (aligning the outer wheel patch border to the joint boundary line) to test both the shear transfer and flexure capacity of the joint. The load is applied through a load plate the size of an HS-20 wheel patch (508 mm by 254 mm [20 in. by 10 in.]), as shown in Figure 5.4 (b) based on the AASHTO LRFD Bridge Design Specifications (American Association of State Highway and Transportation Officials) [98] oriented in the direction of traffic parallel to the joint. Joints were tested using these support and load conditions for specimens with 1,422-mm and 2,845-mm (56-in. and 112-in.) lengths to determine the ultimate strength of the joint, joint ductility through the load-deflection response (based on deformation after non-linear stage), and failure mechanism determined by the crack pattern at failure. A sample crack pattern and load-deflection response are shown in Figure 5.4 (c) and (d). The 2,845-mm (112-in.) long specimens appeared to be experiencing closer to a punching shear failure than a flexure failure of the joint. The 1,422-mm (56-in.) long specimens were all experiencing a clear flexure failure within the capacity of the available load frame used in the experimental investigation. A flexure failure was desired for this testing, so the 1,422-mm (56-in.) length was chosen for the construction of the experimental specimens.

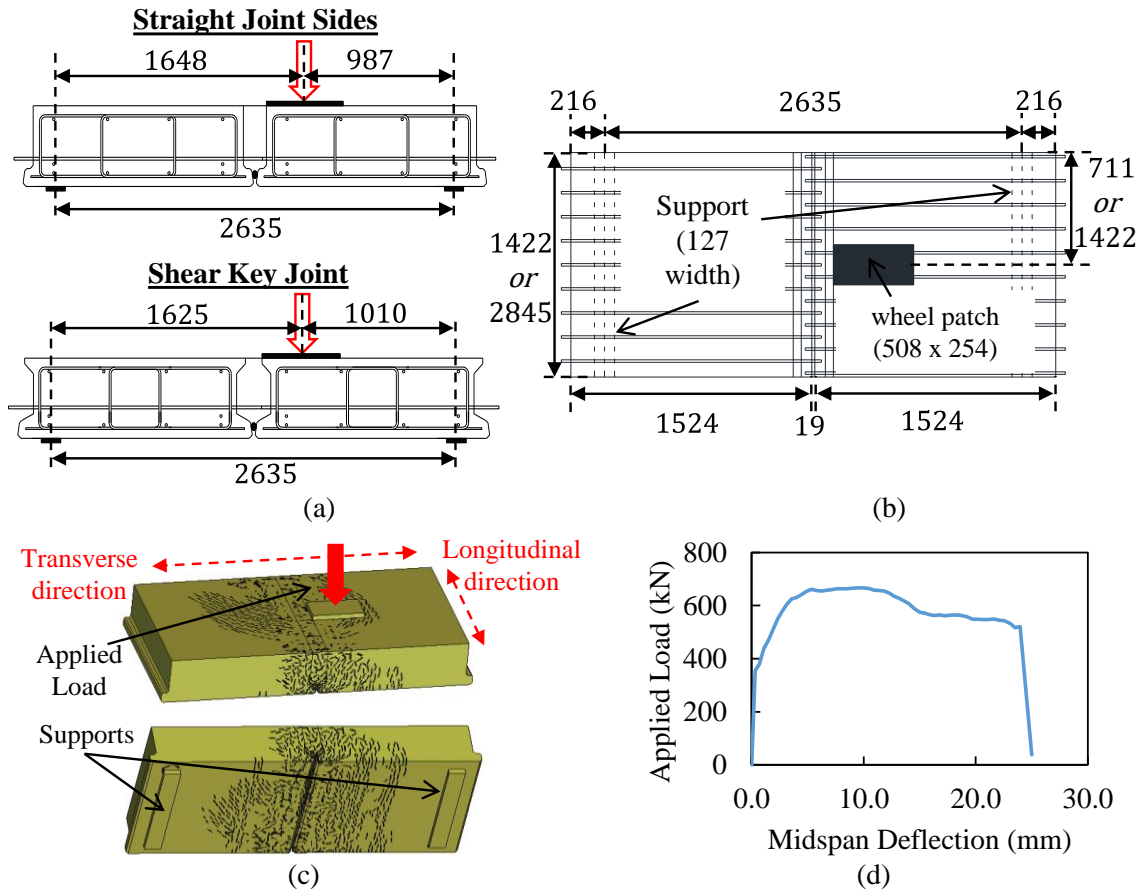


Figure 5.4: Transverse capacity evaluation: (a) applied load relative to joint and supports, (b) top view of wheel patch location, (c) 18F1 top and bottom expected cracking pattern before failure (others similar), and (d) 18F1 estimated load-deflection response (others similar). (length units: mm, 1 mm = 0.0394 in)

The principal stress that developed in the joints under different load conditions was also investigated through the FEA. The maximum principal stress for the four joint shapes in the 305-mm (12-in.) deep specimens are shown in Figure 5.5. There was a concentrated stress that developed at service loading at the bottom of the UHPC joint immediately above the bottom ledge. This concentrated stress was due to a perfect bond being assumed between the top of the ledge and the UHPC joint. As a result, the top of the ledge was not specified as an exposed aggregate finish for the beams constructed for the experimental

investigation. Additionally, cracking and concentrated stresses were observed in the top lip of joint A1, shown in Figure 5.5 (b). Joint A2 was developed using FEA to modify the joint to decrease these stress concentrations in the top lip of the joint. The FEA results were validated through the experimental investigation.

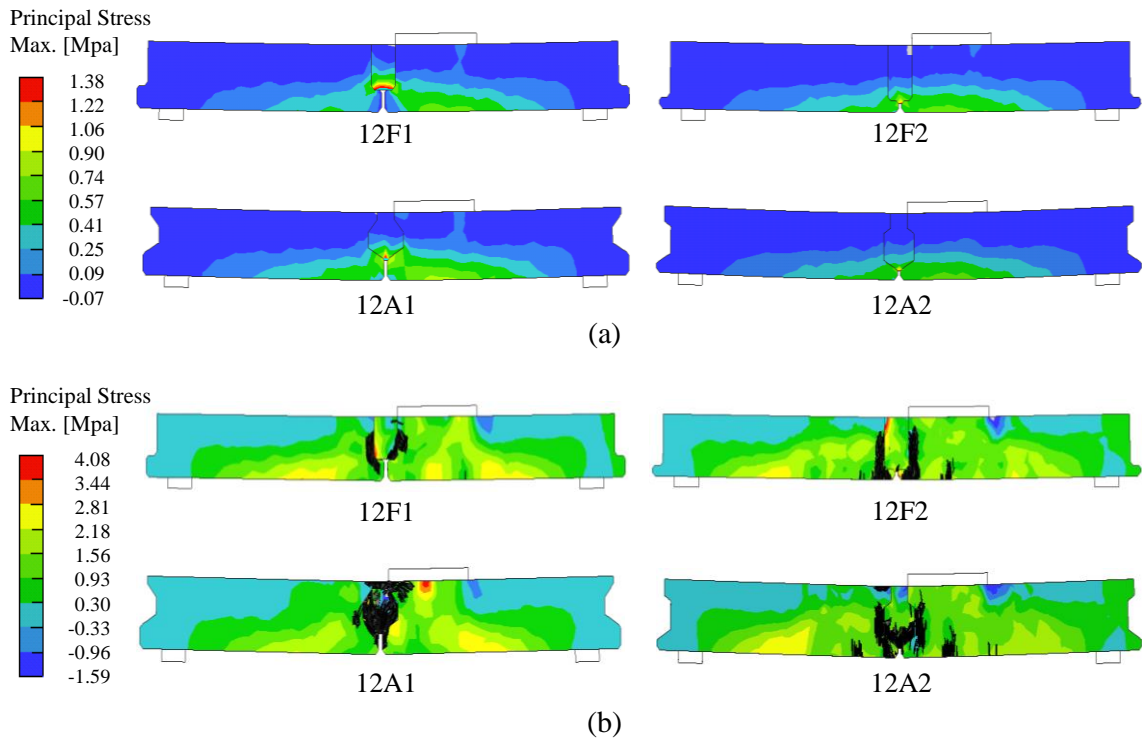


Figure 5.5: Maximum principal stress at the load point in 305-mm (12-inch) deep specimens from FEA at (a) service load of 35.6 kN (8 kips) and (b) ultimate load (load dependent on joint type) with cracking in the plane shown in black (1 MPa = 0.15 ksi)

5.5 Experimental Investigation

5.5.1 Specimen Design and Material Properties

Sixteen (16) prestressed slab-beam sections, 1,422-mm (56-in.) long by 1,524-mm (60-in.) wide, were built by a local precaster to construct the joint systems using two beams each, shown in Figure 5.2. Six of these beams were 457-mm (18-in.) deep (18F1, 18F2, and

18A1 pairs). The other 10 were precast at 305-mm (12-in.) deep (12F1, 12F2, 12A1, 12A2, and FSB pairs). The FSB section was precast at 305-mm (12-in.) deep and then a 152-mm (6-in.) deep CIP deck was cast on top with the joint giving the overall tested section a depth of 457 mm (18 in.). The thicknesses for all the specimens were summarized in Figure 5.3. The reinforcement details for each modified joint beam was based on the original FSB design [54]. Two joint tests were conducted for each pair of precast beams, designated by the last number in the specimen's name (e.g., 18F2-1 is the first test on the 18F2 set of specimens).

The precast concrete mix specified for all the beam specimens was FDOT Concrete Class VI with a minimum compressive strength at 28 days of 58.6 MPa (8,500 psi) and maximum water/cement ratio of 0.37 kg/kg (lb/lb). The required concrete mix for the CIP deck in the original FSB joint was FDOT Class II (bridge deck) with a minimum compressive strength at 28 days of 31 MPa (4,500 psi) and maximum water/cement ratio of 0.44 kg/kg (lb/lb). The UHPC mix used for the joint connections was specified to be Ductal® JS1000, which is a proprietary UHPC mixture commonly used for field-cast closure pours for prefabricated bridge element connections. The UHPC mix ingredients, dosages, and mixing procedure were all provided by the manufacturer. The specified and assumed concrete compression strength for the precast section and joint material are shown in Table 5.3.

Table 5.3: Material properties for experimental specimens

| Specimen | Section f'_c (MPa) | | Joint f'_c (MPa) | | Thickness of section (mm) | Joint Preparation |
|---------------|----------------------|----------|--------------------|----------|---------------------------|-------------------------------|
| | Specified | Measured | Specified | Measured | | |
| FSB-1 | 58.6 | 85.5 | 27.6 | 44.8 | 457.2* | Sandblasted ¹ |
| FSB-2 | 58.6 | 87.6 | 27.6 | 9.7 | 457.2* | Sandblasted ¹ |
| 18A1-1 | 58.6 | 77.9 | 144.8 | 164.1 | 457.2 | Sandblasted ^{1,2} |
| 18A1-2 | 58.6 | 75.8 | 144.8 | 160.6 | 457.2 | Sandblasted ^{1,3} |
| 18F1-1 | 58.6 | 82.0 | 144.8 | 169.6 | 457.2 | Sandblasted ^{1,2} |
| 18F1-2 | 58.6 | 80.7 | 144.8 | 165.5 | 457.2 | Sandblasted ^{1,3} |
| 18F2-1 | 58.6 | 82.0 | 144.8 | 175.8 | 457.2 | Sandblasted ^{1,2} |
| 18F2-2 | 58.6 | 84.1 | 144.8 | 171.7 | 457.2 | Sandblasted ^{1,3} |
| 12A1-1 | 58.6 | 86.2 | 144.8 | 160.0 | 304.8 | Sandblasted ^{1,2} |
| 12A1-2 | 58.6 | 95.1 | 144.8 | 178.6 | 304.8 | Sandblasted ^{1,3} |
| 12F1-1 | 58.6 | 85.5 | 144.8 | 160.0 | 304.8 | Sandblasted ^{1,2} |
| 12F1-2 | 58.6 | 86.2 | 144.8 | 187.5 | 304.8 | Sandblasted ^{1,3} |
| 12F2-1 | 58.6 | 81.4 | 144.8 | 164.8 | 304.8 | Sandblasted ^{1,2} |
| 12F2-2 | 58.6 | 86.2 | 144.8 | 168.9 | 304.8 | Sandblasted ^{1,3} |
| 12A2-1 | 58.6 | 77.2 | 144.8 | 166.9 | 304.8 | Paste Retarder ^{3,4} |
| 12A2-2 | 58.6 | 84.1 | 144.8 | 175.8 | 304.8 | Paste Retarder ^{3,4} |

Note: f'_c = concrete compressive strength at 28 days; *thickness of section includes 152.4 mm CIP deck; ¹sandblasting resulted in an exposed aggregate finish with less than 1.6 mm roughness; ²joint UHPC was mixed with improper admixtures; ³joint UHPC was mixed with proper admixtures; ⁴Use of paste retarder resulted in an exposed aggregate finish with 3.2 mm roughness; 1 in. = 25.4 mm; 1 ksi = 6.9 MPa.

The precast beam fabrication, beam delivery to the FDOT Structures Research Center (SRC), UHPC joint casting, and FSB deck fabrication are shown in Figure 5.6. Three sizes of Grade 60 mild steel reinforcement were used to build all the precast specimens: #10 (#3), #13 (#4), and #16 (#5) reinforcement. Ten fully bonded, pre-tensioned, 15-mm (0.6-in.) diameter Grade 270 strands were used in the precast sections with a small amount of

prestressing (103.4 MPa [50 ksi]), as shown in Figure 5.3. The strands were needed to support the mild reinforcement in the beam section, but likely did not play a role in the transverse capacity of the joint strength.

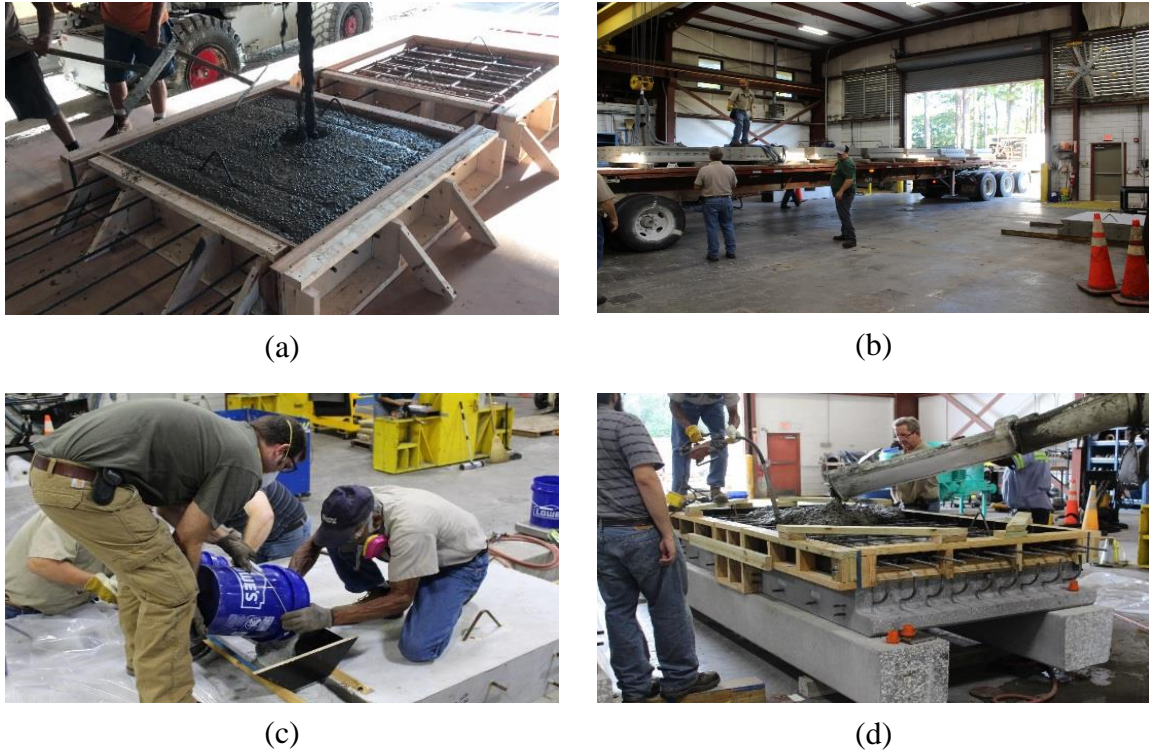


Figure 5.6: Construction of joint specimens: (a) precast specimen concrete pour, (b) delivery of slab-beam specimens to FDOT SRC, (c) casting of field-cast UHPC, and (d) FSB deck casting

5.5.2 Test Setup and Loading Protocol

The supports and testing frame used for the experimental program are shown in Figure 5.7. The test setup consisted of two main supports parallel to the joint and holding the specimens in a simply-supported configuration with a vertical clearance of 1,118 mm (44 in.) from the ground to the bottom of the specimen; this allowed to monitor displacements and cracks underneath the joint for ease. Each support was grouted to the strong floor to ensure levelness and avoid undesired movement or rotations. The simply-supported

specimens were loaded by a hydraulic jack with a 2,046.2-kN (460 kip) static and fatigue capacity and a variable stroke length of 254 mm (10 in.). The load application point was a steel plate with a 508-mm by 254-mm (20-in. by 10-in.) surface area and 51-mm (2-in.) thickness with a bottom neoprene bearing pad of the same size. The load area is similar to the wheel patch of an AASHTO HS-20 truck [98].

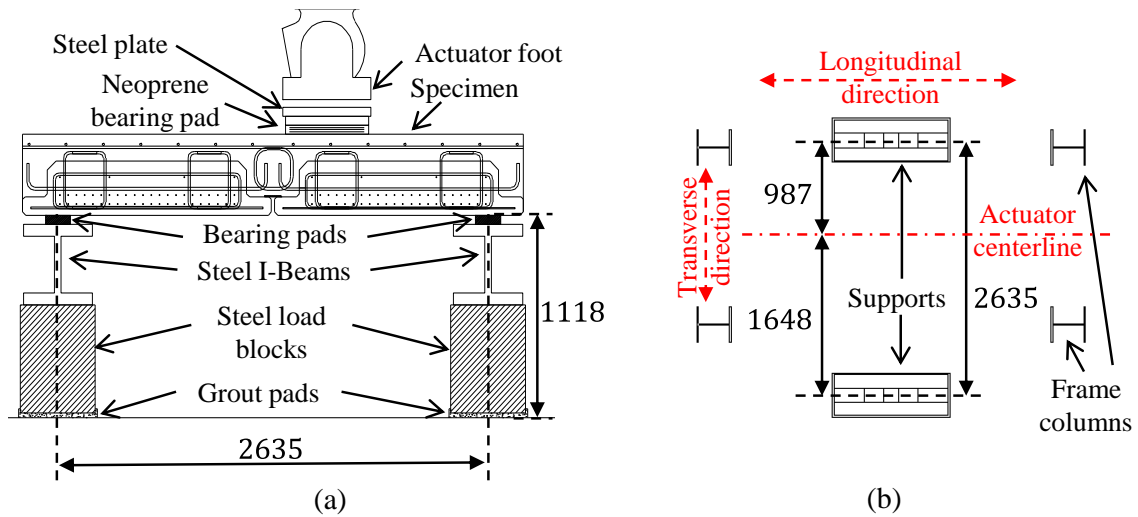


Figure 5.7: Testing frame layout: (a) supports elevation and specimen layout and (b) supports plan layout (actuator centerline parallel to longitudinal joint). (units: mm, 1 mm = 0.0394 in)

Specimens were tested to determine their ultimate strength and fatigue performance. Strength testing consisted of the application of a monotonic load at an approximate rate of 0.9 kN/s (0.2 kips/s). Loading was typically applied in 44.5-kN (10-kip) increments until 65 percent of the expected ultimate capacity. The specimen being tested was inspected for cracks, cracks marked, and pictures taken in between each load step until 65 percent was reached. The specimen was then gradually loaded until failure.

Two joint tests were performed on each pair of beams as both beam sides were built with the specified joint geometry. After the first test was performed, the connected specimens

were cut on one side of the joint region (if the beams did not break apart during test). Then, the beams were rotated so that the unaffected joints were aligned, the joint was cast, and a second test performed. All the specimens were evaluated in the strength test twice, except for 12F1, 12A1, and 12A2. These three specimens were tested once for strength alone and once for fatigue and strength.

The loading protocol for fatigue testing was designed to assess the fatigue performance of the joint on a low-volume, 4-lane urban collector bridge over a 100-year service life, to see if this fatigue loading would lead to cracking, debonding between the UHPC and precast system, or other degradation of the joint performance. This first stage of fatigue loading consisted of 1.1 million cycles of load between 8.9 kN and 56.2 kN (2 kip and 12.64 kip) at 2 Hz. The upper limit value was obtained using a single HS-20-wheel load amplified to include a dynamic load allowance of 33 percent. This dynamic load allowance should have been 15 percent for fatigue limit states, but the results with the 33 percent dynamic load allowance are conservative.

The second stage of fatigue loading was used to evaluate the effect of cycling from below to above the cracking load on crack and damage growth, debonding of joint reinforcement, and overall degradation of the system performance. The fatigue load range was selected based on the static test results. The lower fatigue load was selected approximately 10 percent less than the cracking load measured from the static tests. The load range was selected such that the stress range in the joint reinforcement was 137.9 MPa (20 ksi), a stress range recommended by Helgason et al. [99] to avoid fatigue of the reinforcement itself since this was not the purpose of this fatigue testing. The stress range was determined

based on strain measurements in the joint reinforcement during the static testing. Using this stress range, a load range of 84.5 kN to 133.4 kN (19 kip to 30 kip) was selected for these specimens. The scheduling of the laboratory testing allowed for a total of 2 million cycles for all the fatigue stages for each specimen, so 900,000 cycles at this post-cracking load range were applied to each of the three specimens tested in fatigue.

The ultimate strength of the specimens after the fatigue loading were then determined through a static loading protocol similar to that described earlier. This post-fatigue static testing was performed to see if fatigue testing had any negative influence on the ultimate strength of the joint.

5.5.3 Instrumentation

Four types of sensors were used to measure the response of the joint specimens: unidirectional concrete surface strain gauges oriented perpendicular to the joint, unidirectional rebar strain gauges installed on each joint rebar, linear crack opening transducers across the bottom joint between beams, and laser displacement transducers to measure the vertical deflections at different locations of the specimen. The laser displacement transducers were placed at three locations along the joint on the top of the specimen. The hydraulic jack had a built-in load cell capable of measuring the load being applied to the joint sample.

5.6 Experimental Results and Discussion

A summary of the measured flexural strengths found through the experimental testing is shown in Figure 5.8 alongside the estimated flexural strength from FEA and stress block calculations per AASHTO § 5.6.3.2.3 [98]. Results from the first and second test on each

joint are shown with a different shading used to highlight when the second test was performed after fatigue testing of a joint. The load versus deflection response for all of the experimental specimens are shown in Figure 5.9 (a) for the 457-mm (18-in.) specimens and Figure 5.9 (b) for the 305-mm (12-in.) specimens. The load-deflection curve for the FSB specimen is also shown as a comparison point for the 457-mm (18-in.) deep UHPC joints.

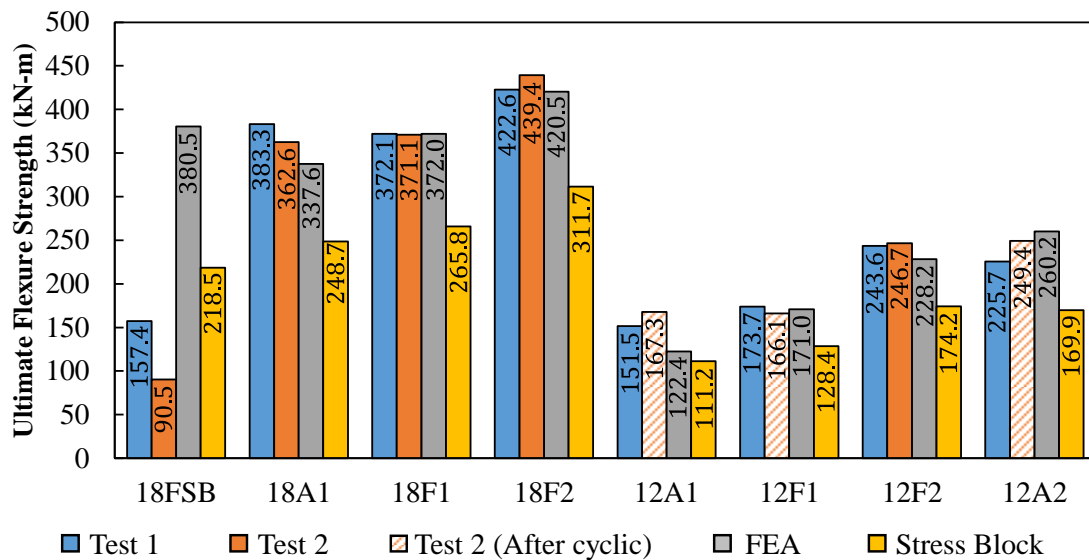


Figure 5.8: Ultimate flexural strength comparison. (1 kN-m = 0.738 k-ft)

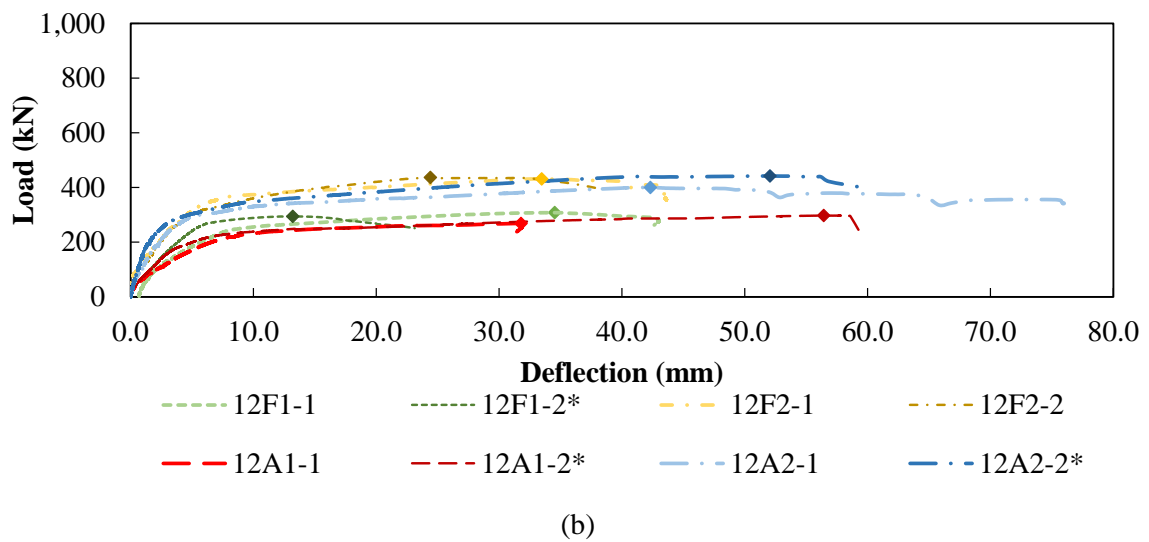
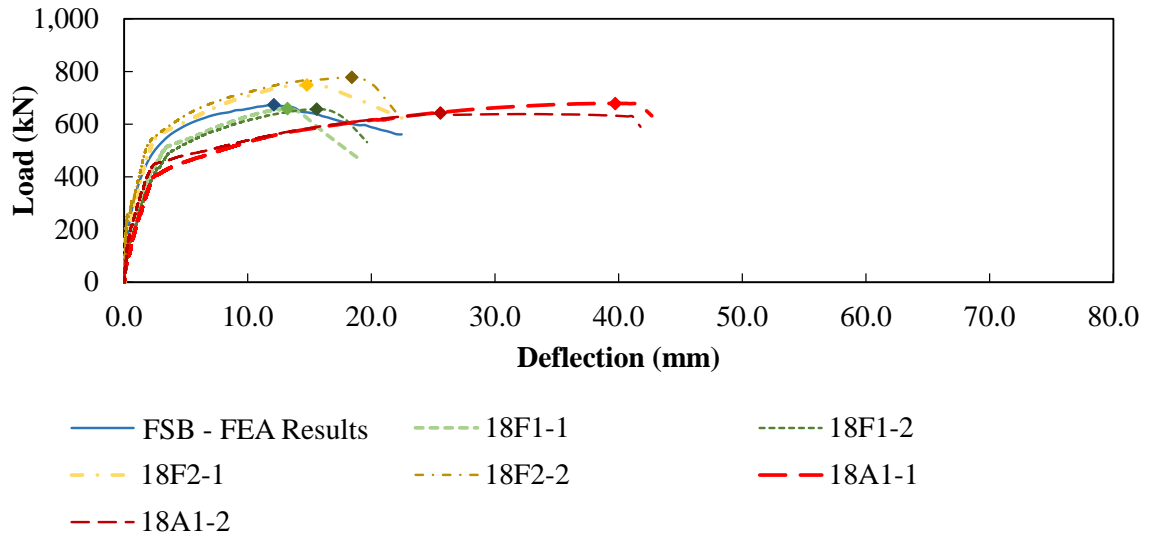


Figure 5.9: Load versus deflection responses with maximum loads for (a) 457-mm (18-inch) deep and (b) 305-mm (12-inch) deep specimens; *Monolithic response after fatigue testing completed

5.6.1 Performance of Numerical Modeling

There was an overall good agreement between the numerical results and the experimental results other than for the FSB specimens, see Figure 5.8. The predicted ultimate flexural strength in the 457-mm (18-in.) specimens was in good agreement with the experimental response (less than 10 percent difference): 18F1 with 372 kN-m (3,293 k-in) predicted

versus 371.5 kN-m (3,288 k-in) average from tests, 18F2 with 420.5 kN-m (3,722 k-in) versus 431 kN-m (3,815 k-in) average from tests, and 18A1 with 337.6 kN-m (2,988 k-in) versus 373 kN-m (3,301 k-in) average from tests. There was also good agreement of the predicted and tested experimental ultimate flexural strength for the 305-mm (12-inch) specimens: 12A1 with 122.5 kN-m (1,084 k-in) versus 159.6 kN-m (1,413 k-in) average from tests, 12F1 with 171 kN-m (1,514 k-in) versus 169.9 kN-m (1,504 k-in) average from tests, 12F2 with 228.2 kN-m (2,020 k-in) versus 245.1 kN-m (2,169 k-in) average from tests, and 12A2 with 260.2 kN-m (2,303 k-in) versus 237.6 kN-m (2,103 k-in) average from tests. There was a significant difference between the estimated and measured response for the FSB specimens, due to a different failure mechanism occurring in the tested FSB specimens than predicted by the FEA. The FEA results for the FSB specimens were used as the comparison point for the developed UHPC joints due to the overall good agreement between the FEA and experimental results for the other specimens. An estimated strength was also determined using the rectangular stress block approach for calculating nominal flexural strength; this estimated strength was less than the measured strength for all test specimens other than the FSB specimens.

5.6.2 Performance of Current FSB Joint Detail

Both FSB control specimen tests failed due to a development failure of the joint reinforcement before yielding of the joint reinforcement occurred, as shown in Figure 5.10 (a). The specimens had the same slope as the FEA model estimate until a crack developed at the location of one hook, which was the beginning of the development failure. The specimens then continued to maintain load as the specimen continued to deflect resulting

from the hook pulling out of the joint. The original FSB design guidelines (FDOT, 2016a) specify #16 (#5) joint reinforcement with a 90-degree hook and typical 64-mm (2.5-in.) bend diameter, as shown in Figure 5.10 (b). The hooked joint reinforcement from adjacent beams is spliced together with hoop bars and straight bars extending the length of the joint placed between the hook and the hoop. This detail was designed to ensure proper force transfer between adjacent beams. The actual bend diameter of this joint reinforcement was larger than specified, as shown in Figure 5.10 (c). This larger bend diameter resulted in the joint reinforcement not being able to develop, which led to a lower transverse flexural capacity than expected. The larger bend diameter resulted in the constructed hook having lower bearing stresses in the bend region and less length for stresses on the back of the tail of the hook to prevent the tail from kicking out; both of these factors would have contributed to the development failure of the hook. Additionally, the longitudinal reinforcement, placed inside the bend radius of the joint reinforcement to improve the splice behavior, bent during testing making it less effective at aiding with the splice connection. Additional joint reinforcement was added to the joint for FSB-2 to improve the splice behavior, but a much lower concrete strength was received for this joint than was specified, which further contributed to a lower failure load.

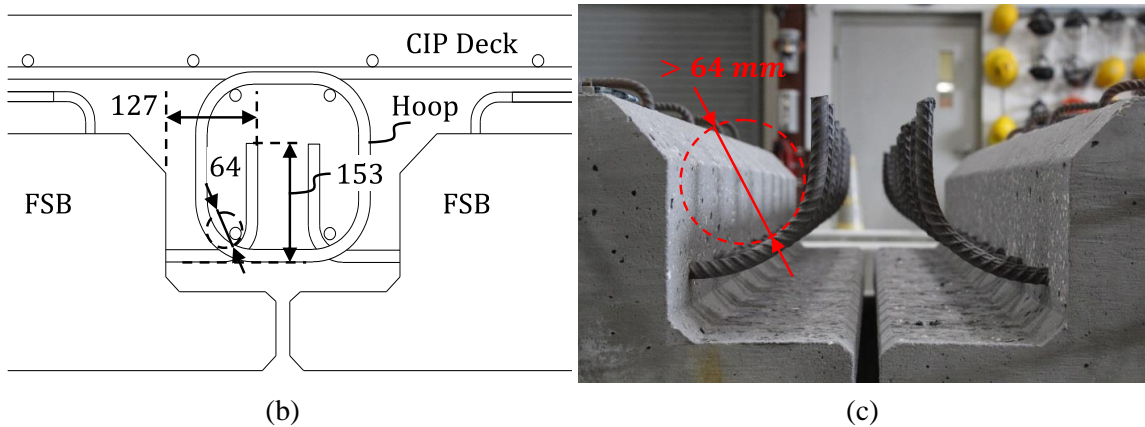
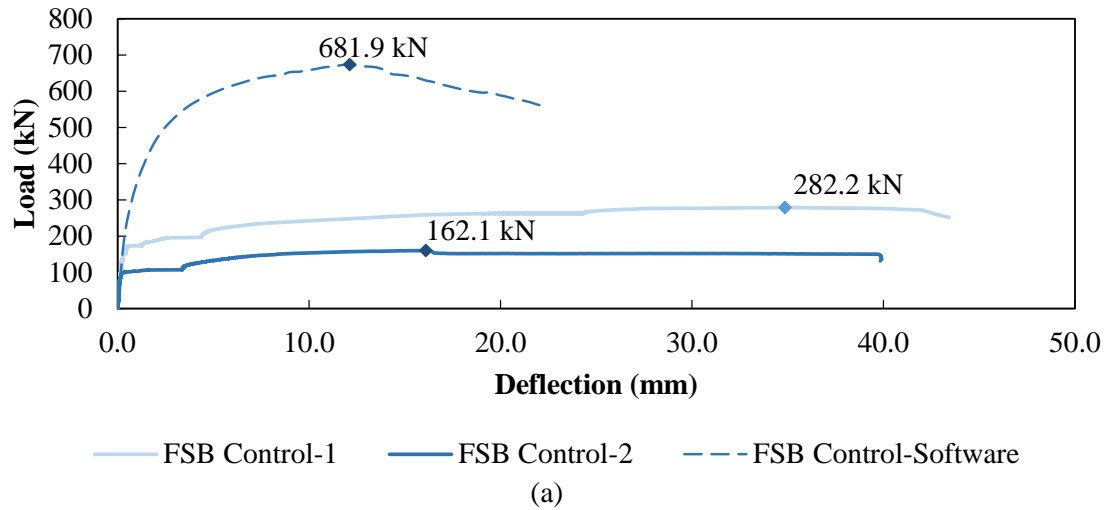


Figure 5.10: FSB joint performance: (a) load versus deflection response (b) specified joint detail with 64-mm bend diameter for hooks and (c) actual joint reinforcement with larger than 64-mm bend diameter for hooks. (length units: mm, 1 mm = 0.0394 in)

These test results highlight the importance of having the proper bend diameter, reinforcement detail and joint concrete strength for satisfactory performance of the joint. Although the proper bend diameter was not achieved in the test specimens for this research, there are no issues reported right now in the field with already deployed FSB systems. This may be due to a combination of the properly constructed detail exhibiting satisfactory behavior and the actual joint not experiencing the same level of load that was tested.

5.6.3 Performance of Developed Joint Details

When looking at the 457-mm (18-in.) deep specimens, the UHPC joints performed similar to or better than the predicted response for the FSB control specimen. The 18F2 joint had the highest capacity, with about a 10-percent higher capacity than the FSB control and other joints. This higher capacity was a result of an increased lever arm of the joint reinforcement, which translated to enhanced transverse flexural capacity. Though the increased lever arm came at the cost of constructability, as the 51-mm (2-in.) bottom lip with no reinforcement extending into it can be easily broken off during fabrication and shipping. The other 457-mm (18-in.) deep specimens (18F1 and 18A1) had similar capacities to the FSB control specimen as their lever arms only varied by about 10 mm (0.4 in.). The 18A1 joint had an increased ultimate deflection and deflection at ultimate load; 18A1 had the largest ultimate deflection and deflection at ultimate load of all the investigated UHPC joint details due to increased joint rebar embedment length.

The 305-mm (12-in.) deep specimens were tested to compare the flexural performance of the joint in the thinnest standard slab beam section that is standardized by FDOT. Because the current standard is a 305-mm (12-in.) deep precast section with a 153-mm (6-in.) thick CIP deck, no control comparison was possible for the 305-mm (12-in.) deep members. The lever arm of the joint reinforcement had a more pronounced impact on the flexural strength of these members: 12F2 and 12A2 had the largest lever arm for the joint reinforcement and had the highest strength. The available embedment and splice length impacted the ductility of the section: 12A2 had a larger splice length and an embedment length equal to or larger than the other joints and had the highest ductility. Finally, the ultimate strength of the joints

was not negatively impacted by the applied fatigue loading. 12A1, 12F1, and 12A2 all had similar ultimate strengths after fatigue loading (test 2) compared to their strengths without fatigue loading first (test 1).

There were two primary failure modes observed in the joint specimens:

1. **Failure due to lack of embedment or splice length:** Three different types of development failures were observed in the joint reinforcement, shown in Figure 5.11 (a), (b), and (c), due to a lack of embedment or splice length provided. In FSB-1 a failure occurred when crack developed at the location of the hook in the joint reinforcement, see Figure 5.11 (a). The reinforcement in 18F1-1, 12F1-2, and 12F2-2 experienced a development failure of the joint reinforcement when there was some combination of a splitting crack developing at the location of the reinforcement and a cone developed around the joint reinforcement along the length of the joint. 12F1-2 had a splitting crack visible on the outside of the joint at the level of the joint reinforcement, see Figure 5.11 (b). For 18F1-1 and 18F2-2, the UHPC remained bonded to some of the joint reinforcement, but a cone of UHPC around the reinforcement pulled away with some of the reinforcement from the joint causing a development failure, see Figure 5.11 (c) and (d); this type of development failure typically occurs when there is sufficient bond between the reinforcement and concrete but insufficient embedment or splice length. Many of these development failures started with cracking along the interface between the precast section and UHPC joint.

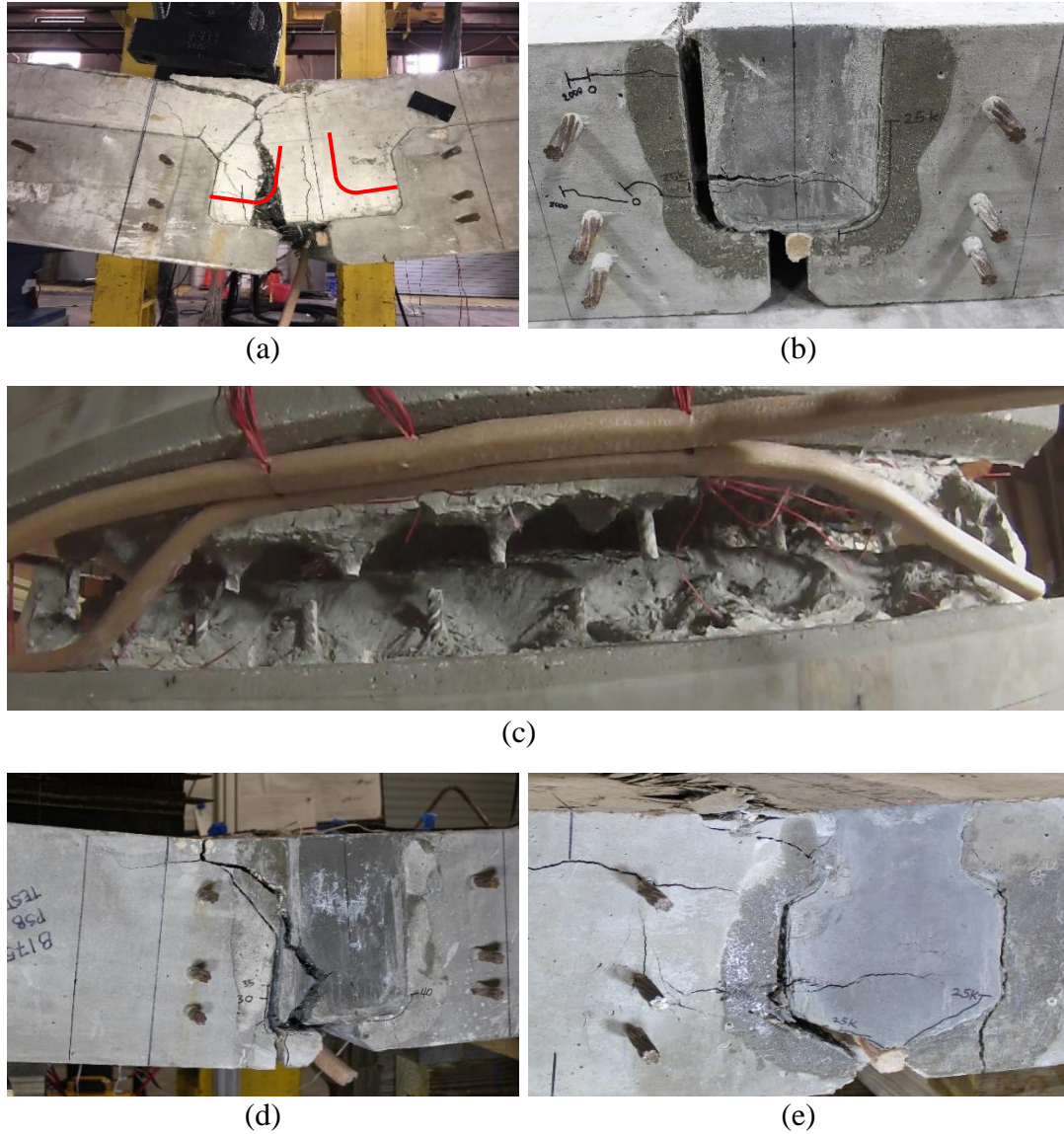


Figure 5.11: Failure mechanism observed during testing: (a) pullout of hooked reinforcement in FSB-1 (hooked joint reinforcement shown), (b) pullout of straight joint reinforcement caused by splitting crack in 12F1-1 (splitting crack shown after unloading), (c) pullout of straight joint reinforcement in 18F1-1 (bottom view shown), (d) pullout of straight joint reinforcement with conical failure in 12F2-2, and (e) crushing of concrete in top of section in 12A2-1

2. **Crushing of concrete at top of section:** Crushing of concrete along the top of the joint and fracture of joint reinforcement was the predominant failure in the specimens with a diamond shaped joints (18A1, 12A1, and 12A2), similar to Figure 5.11 (e). These specimens had a larger deflection at ultimate load and ultimate

deflection, as highlighted in Figure 5.9. Fracture of the joint reinforcement in these specimens was observed in these specimens when the load was removed, and they were removed from the test frame.

There were constructability issues and early cracking observed in the specimens with 51-mm (2-in.) thick bottom lips (12F2 and 18F2). The precaster commented that it was difficult to cast this specimen at only a 1,422-mm (56-in.) length and it would be very difficult for them to cast a full-length beam, as the lip can easily break off when the formwork is being removed. The bottom lip on one of the specimens (12F2) was damaged during shipping and placement of the beams; a repair was done on this specimen before casting of the UHPC joint. Additionally, cracking extended through the bottom lip in all these specimens, as shown in Figure 5.11 (c).

5.6.4 Interface Surface Finish and Bond to UHPC

The experimental testing also revealed the importance of surface finish and the workability of UHPC to achieve sufficient bond between the precast concrete and UHPC in the joint. Past research has shown that an exposed aggregate finish with a 6.3-mm (0.25-in.) magnitude surface roughness provides good texture for adequate bond between the precast element and the fresh UHPC [4]. This finish is traditionally achieved by painting a paste retarder on formwork prior to casting and then using a pressure washer to remove the soft cement paste within 24 hours of casting.

Fourteen (14) of the 16 beams were cast at the same time. Heavy sandblasting was used for the specimens 305-mm and 457-mm (12-in. and 18-in.) deep with F1, F2, and A1 joints, to achieve the specified 6.3-mm (0.25-in.) magnitude exposed aggregate finish that has

been recommended by previous researchers [4]. The finish that was achieved for these specimens, shown in Figure 5.12 (a), was less than 1.6 mm (0.0625 in.), not the specified 6.3-mm (0.25-in.) magnitude finish. Additionally, incorrect admixtures were initially sent with the UHPC that provided only a short working time and limited flowability of the UHPC for the first tests on these joint specimens. These two factors led to debonding between the precast section and UHPC joint in all these tests, as shown in Figure 5.12 (b) and (c). The proper admixtures for sufficient working time and flowability were obtained for casting of the joints for all the second tests, but debonding still occurred in these tests, which was likely a result of having a smoother joint surface finish than specified.

The recommended procedure for achieving the exposed aggregate finish was used for the last two specimens that were cast (12A2). A set-retarding admixture was painted on the side forms prior to casting. The forms were removed one day after casting, and the surface was pressure washed using constant 24.1 MPa (3,500 psi) water pressure at a controlled distance of application. A 3.2-mm (0.125-in.) magnitude exposed aggregate finish was achieved using the recommended procedure, shown in Figure 5.12 (d). Although the finish was not the recommended 6.3-mm (0.25-in.) magnitude, it still offered improved bond compared to the sandblasted finish, as shown in Figure 5.12 (e).

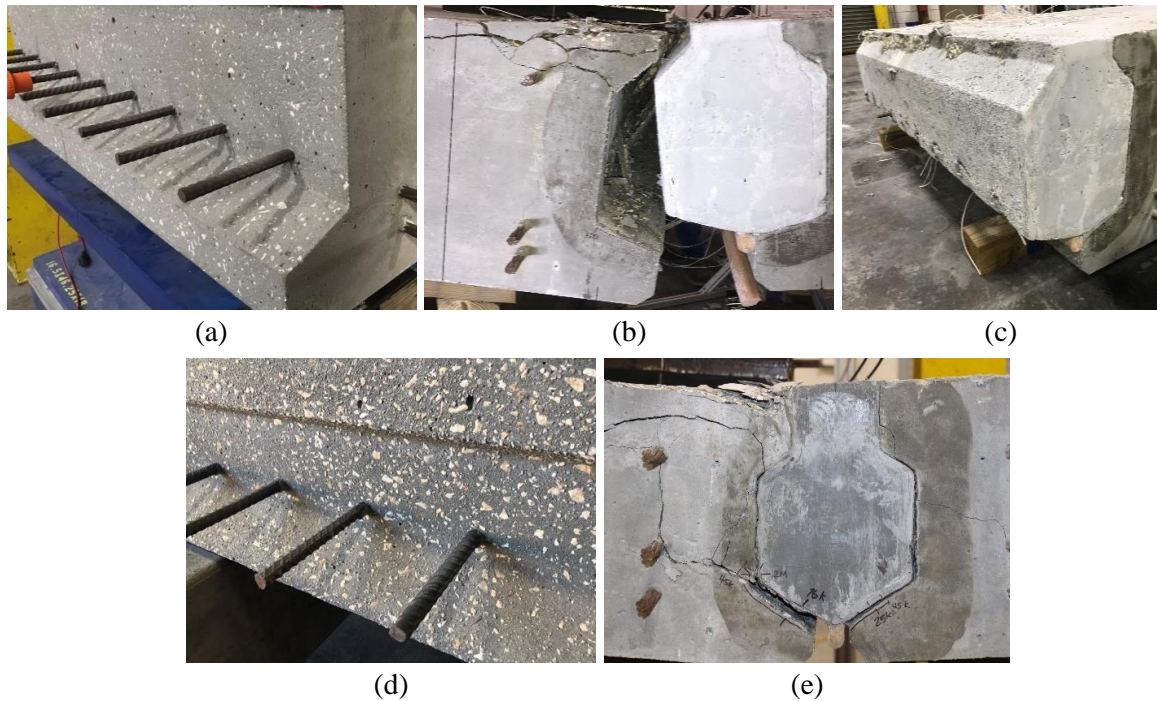


Figure 5.12: Impact of joint surface finish on performance: (a) surface finish obtained using heavy sandblasting, (b) debonding during testing of 18A1-1 (occurred in majority of these specimens with sandblasted finish), (c) failure plane of 18A1-1 after specimen removed from test setup, (d) surface finish obtained using paste retarder on forms for 12A2-2, (e) failure of 12A2-2.

Even though the precast joint surface finish did not seem to play a role in the ultimate capacity of the connection under monotonic load, it is thought to be a critical factor in the long-term service life of the joint. Insufficient bond may lead to early separation at the interface, which can expose the protruding steel to early pollution penetration like carbonation and/or chlorides in harsh marine environments. This can impact the transverse capacity and may lead to the slab beam superstructure no longer behaving as a solid unit.

5.6.5 Fatigue Performance of Joint Specimens

Fatigue testing was conducted on three of the 305-mm (12-in.) deep joint specimens: 12F1-2, 12A1-2, and 12A2-2. The normalized absolute stiffness for all three fatigue specimens is shown in Figure 5.13 (a) through (c), respectively. The stiffness was calculated every

thousandth cycle by dividing the difference between the upper and lower applied load by the corresponding difference between the upper and lower deflection. The normalized stiffness was found by dividing this calculated stiffness for every thousandth cycle by the stiffness of the first cycle, as described by Garber [101]. Cracking of these specimens or other degradation in overall behavior caused by fatigue loading would cause a change in the normalized stiffness. For 12A1-2 and 12A2-2, the change in normalized stiffness can be seen between the before and after cracking fatigue phases. 12F1-2 was accidentally cracked prior to fatigue loading generating two transverse cracks extending from the joint region to the precast section, seen at both joint end sides (at the level of joint reinforcement); this accidental crack pattern was similar to the pattern seen on 12A1-2 and 12A2-2 after concluding the after-cracking phase. Although the accidental load was not measured, the magnitude was larger than the specimen cracking load, thought to be between 178 and 222 kN (40 and 50 kips). The accidental load is the reason why there was no change in the normalized stiffness between the before and after cracking fatigue phases, and there was no further crack growth or decay of behavior during the cycle applications. Overall, there was no noticeable drop in the stiffness in any of the three joints that would indicate cracking in the joint during the before-cracking phase or decay in the joint strength capacity during the after-cracking phase.

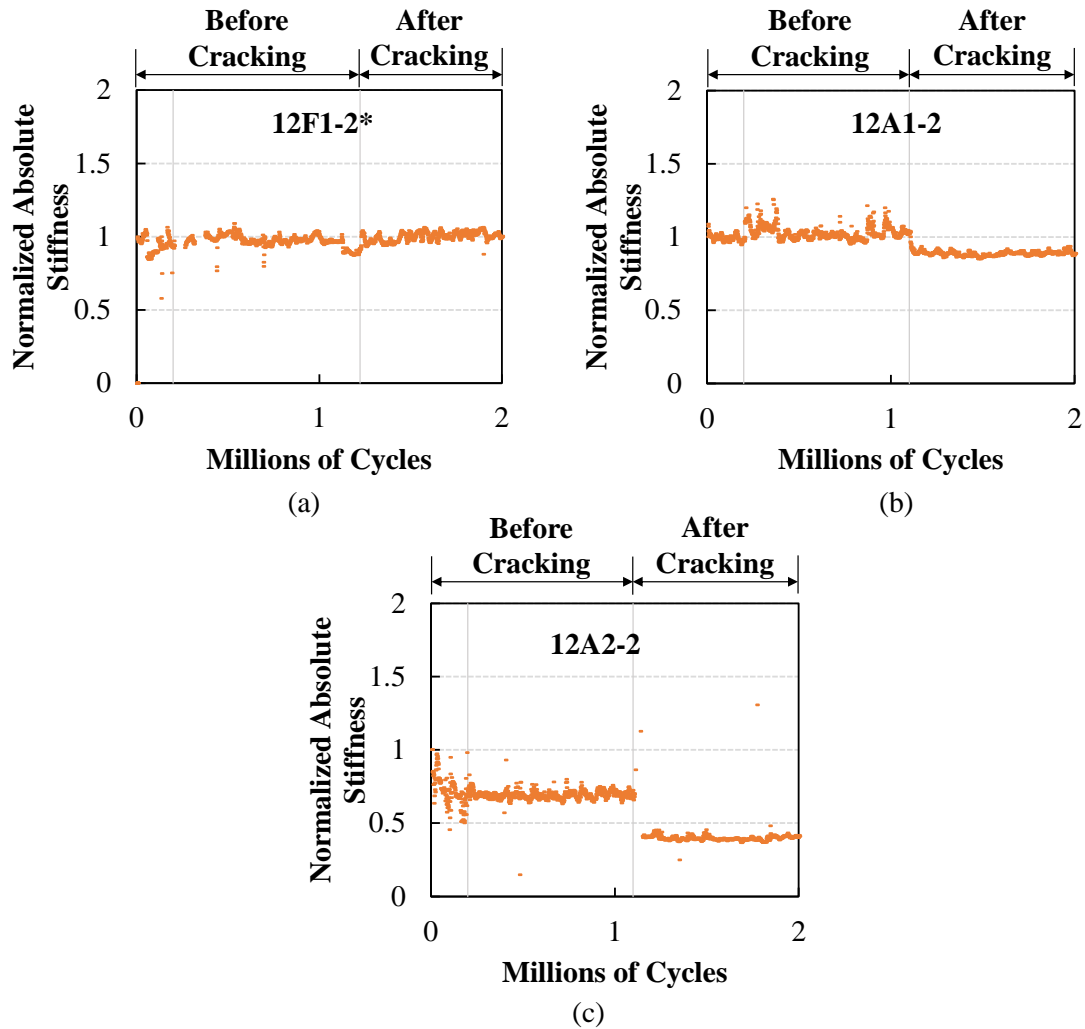


Figure 5.13: Normalized absolute stiffness every thousandth cycle of system for joints (a) 12F1-2, (b) 12A1-2, and (c) 12A2-2. *Cracked specimen due to accidental load

Also, as previously mentioned, the ultimate strength of each joint was tested following the fatigue testing. The ultimate strengths were comparable for specimens tested with and without prior fatigue testing: the ultimate strength of 12F1-2 decreased by about four percent after fatigue testing, and the ultimate strength of 12A1-2 and 12A2-2 both increased by about 10 percent. These measured ultimate strengths with and without fatigue

testing have similar variability to the two tests conducted without fatigue testing (18A1, 18F1, 18F2, and 12F2), as shown in Figure 5.8.

5.7 Conclusions

Several conclusions can be made based on the construction and experimental results of the joint tests:

- The control FSB joint (FSB-1 and FSB-2) did not perform as expected due to a larger bend diameter (FSB-1) and due to the compressive strength of the deck concrete being much lower than specified (FSB-2). These issues caused development failure of the joint reinforcement prior to yield.
- All 457-mm (18-in.) deep UHPC joints performed similar to or better than the predicted response of the FSB section using FEA (assuming no development failure occurred).
- Joint 18A1 (with a shear key and increased embedment length of the joint reinforcement) had the largest deflection at ultimate load and largest ultimate deflection of the 457-mm (18-in.) deep joints with a comparable ultimate strength.
- Joint 12A2 (with a shear key and increased embedment and splice length of the joint reinforcement) was the best performing joint of those tested. Although a 457-mm (18-in.) version was not tested experimentally, the benefits of this joint over 12A1 (with a shear key and shorter splice length of the joint reinforcement than 12A2) will likely translate well to the 457-mm (18-in.) version.

- A 51-mm (2-in.) thick bottom lip with no reinforcement extending into it presents challenges with constructability. A thicker bottom lip with reinforcement is recommended for similar slab beam members.
- Using heavy sandblasting on the precast beams with SCC resulted in an exposed aggregate finish of less than 1.6 mm (0.0625-in.). Using a paste retarding agent on similar beams provided a 3.2-mm (0.125-in.) magnitude exposed finish, which resulted in improved bond for the two specimens tested (12A2-1 and 12A2-2).
- The pre-cracking fatigue loading stage did not cause cracking or show any signs of deterioration in performance for 12A1-2 and 12A2-2. The after-cracking fatigue loading stage did not cause degradation of the overall behavior for 12A1-2, 12A2-2, and 12F1-2. Fatigue loading had little effect on the ultimate strength of joints 12A1-2, 12A2-2, and 12F1-2.

Based on the results of this testing, joint 12A2 (with a modified shear key shape and longer non-contact lap splice) appears to have the best performance and constructability. Future testing is planned on full-scale beams to determine actual joint demands and behavior, provide a comparison with the demand on the tested small-scale specimens, and develop complete design recommendations.

5.8 Notations

d_b = diameter of joint reinforcement

E = modulus of elasticity

f'_c = compressive strength of concrete

f_t = tensile strength of concrete

f_y = yield strength of steel reinforcement

G_F = fracture energy

l_d = required development or embedment length

l_s = required lap splice length

5.9 Data Availability Statement

Some or all data, models, or code generated or used during the study are available from the corresponding author by request.

- Videos from testing
- Select data from testing and FEA models

5.10 Acknowledgements

The research presented in this project was supported by the Florida Department of Transportation (FDOT). The authors would like to thank FDOT for their financial support and the team of engineers and staff at the Structures Research Center for their assistance in constructing and testing the specimens. The opinions, findings and conclusions expressed in this publication are those of the author(s) and not necessarily those of the Florida Department of Transportation or the U.S. Department of Transportation.

6. FULL-SCALE TESTING OF SLAB-BEAM BRIDGE SYSTEM FOR ACCELERATED BRIDGE CONSTRUCTION¹

*Francisco Chitty², Christina Freeman³, and David Garber⁴

6.1 Abstract

Adjacent prestressed concrete slab-beam sections have been used in the United States for short span bridge applications due to its inherent shallow profile and rapid construction. Many departments of transportation have deployed iterations of this system on bridges with spans ranging from 20 to 65 feet, which is generally built with longitudinal reinforced joints and a top deck poured in one single cast, developing composite action with the precast slab-beam elements. With the increased demand of rapid bridge replacements, an alternative design to expedite the construction process while improving structural performance for long-term durability is desired. Recently, a longitudinal joint detail that utilizes ultra-high-performance concrete (UHPC) was developed for a slab-beam system, eliminating the conventional concrete joint and cast-in-place (CIP) deck usage while decreasing the impact of construction on traffic without sacrificing strength capabilities. Three loading configurations were analyzed and experimentally evaluated to determine the UHPC joint performance between two 9150-mm (30-ft.) long slab beams adjacently

¹ Submitted to ASCE Bridge Engineering Journal.

² Corresponding Author. PhD Candidate, Civil and Environmental Engineering, Florida International University, Miami, FL, USA. Email: fchit001@fiu.edu

³ Structures Research Engineer, Structures Research Center, Florida Department of Transportation, Tallahassee, FL, USA. Email: christina.freeman@dot.state.fl.us

⁴ Associate Professor, Civil and Environmental Engineering, Florida International University, Miami, FL, USA. Email: dgarber@fiu.edu

connected without a CIP deck. Results from flexural strength and fatigue experimental testing of the longitudinal joint assessment are presented and compared. The UHPC joint detail was found to perform well during service and ultimate strength tests with no signs of deterioration in the UHPC-to-precast bond, demonstrating a promising joint detail with ease of implementation for similar systems. Later, a comparison study of four prestressed, precast superstructure systems for a two-lane, short-span bridge configuration for ABC was performed. The parameters considered in the analytical study and finite element analysis included flexural strength, section thickness, structural efficiency, load distribution factors, and longitudinal joint and section demand. The investigated sections all showed satisfactory behavior under service loads with different section shapes offering different benefits

6.2 Introduction

Bridge superstructure systems that use shallow, adjacently connected prestressed concrete slab sections have been used in the US since the beginning of the prestressed industry in the 1950s. Their low profile and ease for rapid construction represent a suitable and economical option for short-span bridges as they usually required minimal to no deck forming. Bridge practitioners and precast producers [31] previously standardized several of those products such as the adjacent solid and voided slab beams with preliminary design charts in accordance with current bridge design specifications [73], and they have been implemented by many state departments of transportation. Other states developed their own variants like Florida's Sonovoids and solid slabs [18], and Texas' shallow voided tee beams [87]. However, documented in-service performance of these systems has shown a

decay in the performance of the longitudinal connections between adjacent beams, which results in longitudinal reflective cracks in asphalt toppings along the joint lines. These cracks cause further performance decay by allowing the intrusion of moisture into the joints, which leads to corrosion of the joint reinforcement. Several states proposed changes to their slab joint geometries and required the use of transverse posttensioning, but this method added cost and time to the project without satisfactory results in terms of crack control [53].

A series of new slab-beam details was developed by several states following a 2004 investigation of new technologies in prefabricated bridge systems in France, Japan, and Germany sponsored by the Federal Highway Administration (FHWA) and AASTHO [102]. The Poutre-Dalle (“Beam Slab”) System was identified as a promising innovation of rapid bridge construction for the rapid replacement of short-span bridges. The Minnesota Department of Transportation (MnDOT) was the first to start developing a similar CIP slab span system in 2005 and was called the Precast Composite Slab Span (PCSS) system [48], [49], [89]. Other states then followed with their solutions such as Virginia’s inverted-tee [91], [103] and Florida’s slab-beam (FSB) sections for short-to medium-span applications [54] with several bridge deployments. These modern systems consist of shallow precast, prestressed concrete inverted-tee beams that are placed immediately adjacent to each other. Reinforcement is then placed in the joint and for the CIP deck, and then concrete is cast for the joint and CIP deck all in a single cast.

Although they are similar in terms of construction procedures, the joint reinforcement detail in the joint region varies slightly. The Poutre-Dalle system has transverse 180-degree

looped bars extending from the sides of the precast beams that ensure the transferring of forces either longitudinally or transversely between adjacent beams depending on the layout configuration, as shown in Figure 6.1 (a). The PCSS has a modification of the 180-degree hooked bars to 90-degree hooked bars, as shown in Figure 6.1 (b). This modification allows for a pre-tied reinforcement cage to be used while still resisting shear forces along the joint and controlling reflective cracks at the joint line. Both systems have joint reinforcement extending beyond the side edge of the precast member, which can make construction more difficult. The Virginia's inverted-tee modifies the PCSS from a straight-web shape to a tapered-web shape, decreasing stress concentrations created by the 90-degree entrant web corners in the former sections. No protruding joint reinforcement is provided other than the top shear transfer ties. The bottom ledges of adjacent slabs are welded together to create the transverse positive moment connection. The deck reinforcement is then provided with the shape of the tapered precast sides, as shown in Figure 6.1 (c). Similar to the PCSS, the FSBs have square edges with transverse joint reinforcing bars that protrude from the sides of the precast beam; however, the transverse reinforcement does not extend outside the bottom ledge of the section like in the PCSS. Also, a 51-mm (2-in.) chamfer is used at the top of the precast section to minimize abrupt changes in section geometry, as shown in Figure 6.1 (d). The Virginia inverted-tee beam and FSB do not have joint reinforcement extending beyond the ledges, which makes placement of the beams easier during construction.

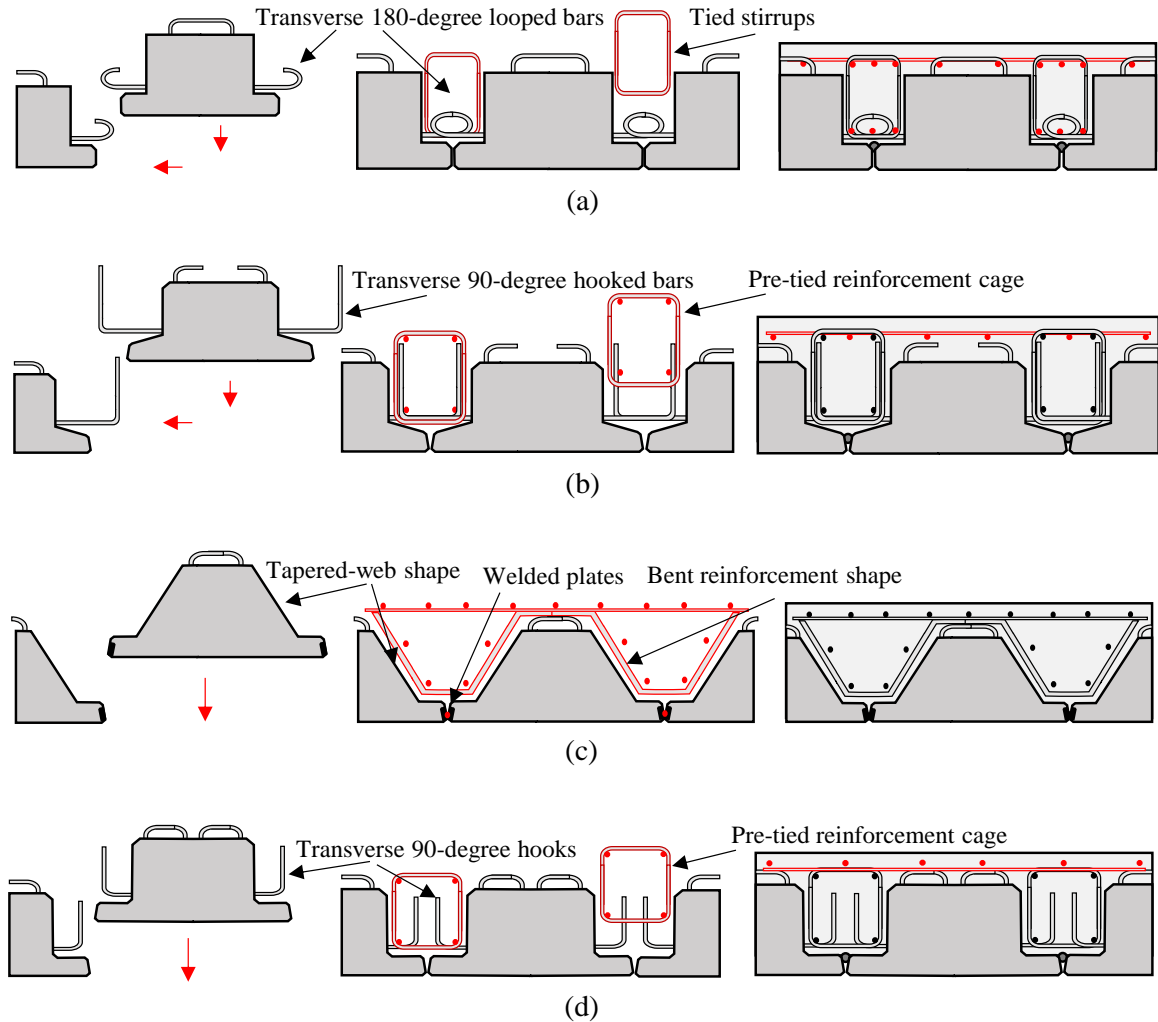


Figure 6.1: Joint system and CIP concrete topping system construction for: (a) Poutre-Dalle (French slab beam), (b) Minnesota PCSS, (c) Virginia inverted-tee, and (d) Florida Slab Beam

Researchers have highlighted several challenges experienced with these systems, such as economic feasibility for longer PCSS spans [49], reflective cracks due to thermal gradient effects on PCSS [47], damage at FSB corners due to large skewness [51], improper backer rod sizes between FSBs joint leading to CIP concrete leakage [51], and the general field requirement of large amounts of reinforcement and CIP deck placements [104]. Additionally, some systems have not been in service for long enough periods of time to be able to assess long-term performance [91]. Based on the previous mentioned construction

and in-service issues of slab-beam bridges, researchers have developed a modified joint design that eliminates the CIP deck (thus reducing the complexity of connections in integrated joint-CIP deck systems) and incorporating ultra-high-performance concrete (UHPC) for accelerated construction [10]. This novel joint geometry was developed by evaluating the transverse flexural performance of different connection details.

6.2.1 Research Motivation, Objective, and Significance

The motivation for the research was to test the slab beam joint detail developed through the transverse flexural tests using full-scale two-beam system tests. The main objectives of this research were to: (1) investigate the fatigue, service, and strength performance of a slab-beam bridge joint for rapid construction by conducting full-scale structural tests, (2) assess the bond serviceability performance of the UHPC joint, and (3) identify transverse tensile stresses caused by eccentrically placed loads simulating different support and traffic conditions. While there have been full-scale system tests on other beam systems (e.g., adjacent box beams), there have not been any previous system tests on shallow slab beam superstructures. This research will help advance the state-of-the-art in slab-beam joint design and construction for future superstructure deployments.

6.3 Experimental Program

The slab-beam joint system for accelerated construction evaluated in this research was developed and tested initially using transverse flexural tests for short beam segments [10], [104]. The FSB was used as a starting point for the section and joint design. The CIP topping was eliminated, and the longitudinal keyway geometry adapted for use with UHPC. Four different joint geometries and details were evaluated during this initial

transverse flexural testing on specimens with 305-mm (12-in.) and 457-mm (18-in.) depths. A test protocol similar to what Graybeal [3] used to test full-depth precast deck panel connections was used to evaluate the ultimate strength performance of all joints and fatigue performance of several of the joints. An optimized shear key incorporating non-contact lap spliced rebars as joint reinforcement, as shown in Figure 6.2 was found to have the highest transverse flexural strength, largest ductility at failure, and no observable deterioration in performance due to fatigue loading [10]. The 305-mm (12-in.) deep shear-key geometry was selected for the full-scale two-beam system tests in this research.

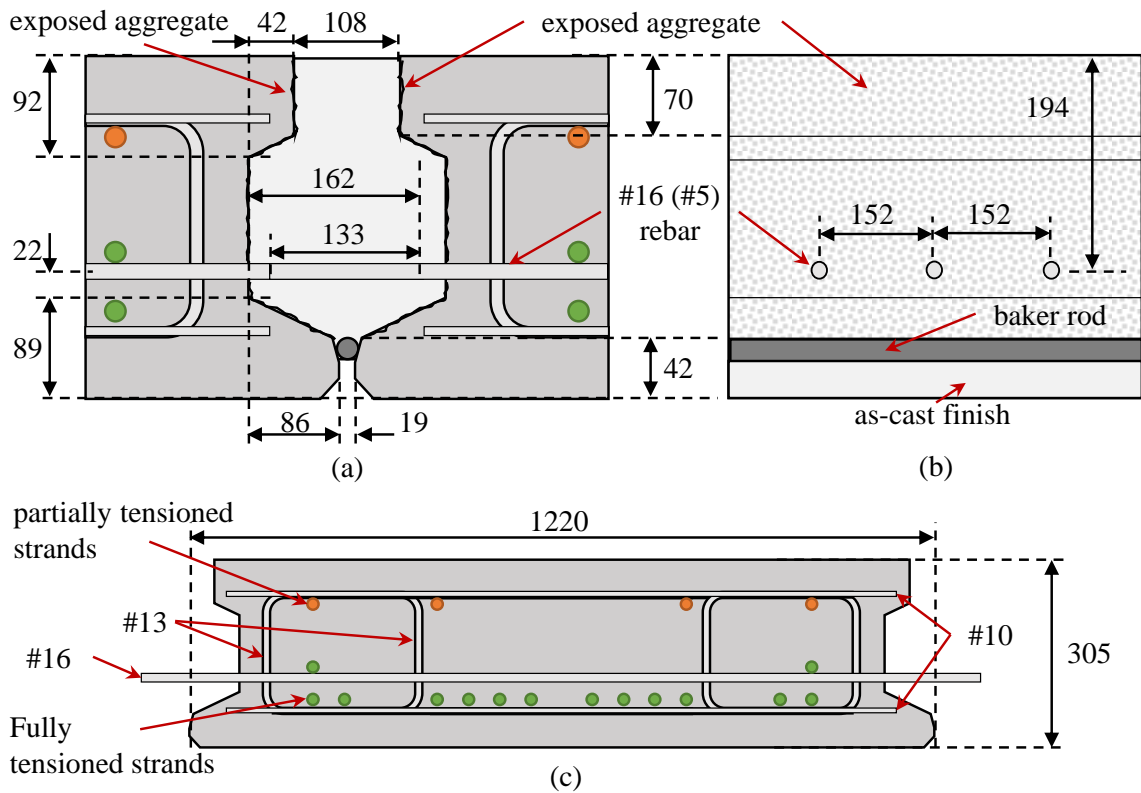


Figure 6.2: Slab-beam section details for two-beam system tests: (a) keyway detail, (b) side-joint detail, and (c) cross-section reinforcement detail. Note: design is for 9150-mm beam length (units: mm, 1 mm = 0.0394 in.)

6.3.1 Specimen Design and Material Properties

A total of eight 305-mm (12-in.) thick, 9150-mm (30-ft.) long by 1220-mm (4-ft.) wide FSBs were built by a local precaster in Florida. The section and joint design for the modified FSBs were based on the optimized joint geometry shown in Figure 6.2 and designed using current bridge design specifications [73] and FDOT design guidelines [82]. One set of five beams (FIU-1 through FIU-5) was designed with a prestress configuration per current specifications, with a layer of partially tensioned top strands. The second set of three beams (FIU-6 through FIU-8) had the same strand configuration as the first set of beams except they had fully prestressed top strands. Eighteen (18) fully bonded, Grade 270, seven-wire prestressing strands with 15-mm (0.6-in.) diameter were used per beam. FIU-1 through FIU-5 had 14 fully prestressed bottom strands to 1,396 MPa (202.5 ksi) and four partially prestressed top strands to 103.4 MPa (50 ksi). FIU-6 through FIU-8 had 14 fully prestressed bottom strands and four fully prestressed top strands to 1,396 MPa (202.5 ksi). Only four of the eight beams were used for the testing described in this paper: FIU-1 and FIU-2 for the first two-beam configuration test, and FIU-4 and FIU-5 for the second two-beam configuration test. The remaining four beams were used in the next phase of testing for this project.

Grade 60 mild steel (A615) was used for the transverse and shear reinforcement to assemble the reinforcement cage: #10 (#3) for ledges reinforcement, #13 (#4) for stirrups reinforcement, #16 (#5) for joint reinforcement, as shown in Figure 6.3 (c), and #19 (#6) for splitting reinforcement at beams ends. Wood formwork with the joint shape and holes with diameter larger than the transverse joint rebar was constructed and used for these

specimens. To achieve the proper joint surface treatment, a commercial paste retarder, BASF – Master Finish HV Pink (48), was painted on the wood forms to achieve at least a 6.3-mm (¼-in.) amplitude surface roughness, following FHWA guidelines on interface surface preparation [4], as shown in Figure 6.3 (a). Once the cage and forms were assembled, the concrete was cast and moist cured for at least 24 hours after casting, as shown in Figure 6.3 (b). FDOT Concrete Class VI with a minimum compressive strength at 28 days of 58.6 MPa (8,500 psi) and water-to-cement ratio of 0.37 kg/kg (lb/lb) was specified for all precast beams. Approximately 24 hours after casting, the side forms were removed and a pressure washer was used to remove the retarding agent with the unhydrated cement paste leaving the desired exposed aggregate finish, as shown in Figure 6.3 (c). The construction of the large-scale UHPC joints followed the guidelines described in the FHWA publication “Design and Construction of Field-Cast UHPC Connections” [4]. Joints for the two-beam systems were constructed by placing the beams side by side leaving a 19-mm (¾-in.) clear gap. A 25-mm (1-in.) backer rod was used to fill the gap between beams with a transparent leakage sealer used to fill any smaller gaps to make the joint watertight, as shown in Figure 6.3 (d). Wooden strips were placed on top of the beams beside the joint to provide an additional 6.3-mm (¼-in.) of joint depth, as shown in Figure 6.3 (e). The UHPC was then mixed and cast into the joint. Top plywood forms were used to keep the UHPC at the low points (i.e., the ends of the beams) at the correct height and allow for the filling of the rest of the joint, as shown in Figure 6.3 (f). One day after casting the UHPC joint, the overpoured section was ground down to level the joint surface with the precast section.



Figure 6.3: Slab beam and joint construction process: (a) reinforcement cage and wood formwork with painted paste retarder, (b) concrete cast in beams, (c) exposed aggregate finish, (d) joint geometry with non-contact lap spliced rebar, baker rod and leakage sealer, (e) wooden strips for UHPC overpour, and (f) top joint form closure application

A proprietary UHPC material commonly used for field-cast closure pours and joint connections was used in this research. The UHPC mixture ingredients, dosages, and mixing procedure were all provided by the manufacturer. One bulk bag of dry premix, equivalent to 49 smaller 22.7-kg (50-lb.) bags was used, which yielded a total of 0.48 cubic meters (17.05 cubic feet) necessary per joint construction. The UHPC mix design had a minimum compressive strength target of 145 MPa (21 ksi).

6.3.2 Test Setups and Loading Protocols

Several different support and loading configurations were used in each phase of testing. The first two-beam system (FIU-1/2) was simply supported with beams FIU-1 and FIU-2. Two different load configurations and protocols were used to test FIU-1/2, shown in Figure 6.4. The first load configuration (LC 2-4) included a full truck axle centered on the beams to maximize the tension on the top of the section, as shown in Figure 6.4 (b). The second

configuration (LC 2-1) had a half truck axle placed immediately next to the joint, as shown in Figure 6.4 (c). These configurations impersonated rear half- and full-axle loads of an HS-20 truck (AASHTO, 2017). The test setup consisted of two main supports located at each specimen end and holding the specimens in a simply supported configuration with enough vertical clearance from the ground to allow for monitoring displacements and cracks underneath the system, shown in Figure 6.4 (a). Each support was grouted to the strong floor to ensure specimen levelness and avoid undesired movement. A hydraulic actuator with a 2,046-kN (460 kip) capacity attached to a steel testing frame was used to apply the load to the specimens, utilizing different spreader beam arrangements to accommodate the desired load pattern. The load application points for LC 2-4 and LC 2-1 were steel plates with a 508-mm by 254-mm (20-in. by 10-in.) surface area and 51-mm (2-in.) thickness with bottom neoprene bearing pads of the same size.

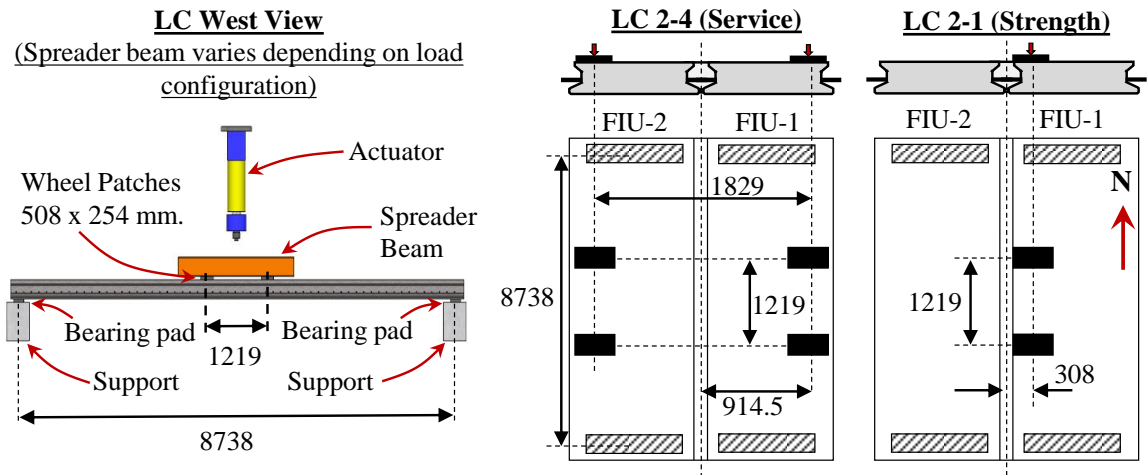


Figure 6.4: Testing frame layout for LC 2-4 (service loading) and LC 2-1 (ultimate strength) (units: mm, 1 mm = 0.0394 in.)

LC 2-4 was used to apply a service load to FIU-1/2 until transverse cracking occurred in the bottom of the beams at an approximate load of 267 kN (60 kips). LC 2-1 was used to

test the ultimate strength of the two-beam system and joint demand and performance at higher load levels. The load for static testing was applied at an approximate rate of 0.9 kN/s (0.2 kips/s). Several stops were made during static testing to inspect the growth of cracks in the beams. During ultimate strength testing, the crack displacement transducers extending across the joints were removed at 65 percent of the two-beam system capacity.

The second two-beam system (FIU-4/5) was constructed using beams FIU-4 and FIU-5. Several different support configurations were used with different service, fatigue, and strength load configurations to test FIU-4/5, as summarized in Table 6.1. The static loading schemes LC 2-1 and LC 2-4 used to test FIU-4 and FIU-5 were the same as those used for FIU-1/2, as shown in Figure 6.4. One additional static load configuration (LC 2-7) and two fatigue load configurations (FC 2-5 and FC 2-6) were also used for FIU-4/5:

1. *FC 2-5 (Unrestrained Fatigue Loading)*: This load and support configuration had load points like LC 2-4 with no restraints provided under the system at midspan, as shown in Figure 6.5 (a). Reverse sinusoidal fatigue loading was applied using two actuators with a 489.3-kN (110-kip) and 244.6 kN (55-kip) capacities and two spreader beams with an alternating 2-Hz sinusoidal wave, as shown in Figure 6.5 (b). The fatigue loading was applied through an applied displacement that corresponded with loads in each actuator of 89 kN (5 kips) (minimum load) and 200 kN (23.4 kips) (maximum load) with a plus or minus five percent allowable difference in applied displacement. A total of two million cycles were applied using FC 2-5 during Stages 2 and 3, which simulated normal service truck traffic conditions for a 100-year service life. LC 2-4 with a 272 kN (61.2-kip) total load

was used to determine the behavior of the system before (Stage 1) and after (Stage 4) fatigue testing with FC 2-5, simulating a rear FL120 full-axle permit load [83], which is equivalent in weight to 1.67 times an HS-20 truck. A similar load configuration (FC 2-5cr) was also used to cause transverse cracking in FIU-4 and not in FIU-5 in Stage 10. This loading consisted of increasing the load in both actuators to 89 kN (20 kips) and then increasing load only in one actuator to 200.2 kN (45 kips) while the other actuator was held at 89 kN (20 kips), as shown in Figure 6.5 (c).

2. *FC 2-6 (Restrained Fatigue Loading)*: This load and support configuration had similar load and end support points to FC 2-5, but with two additional interior supports provided underneath FIU-5 near midspan, as shown in Figure 6.5 (d). A constant load of 89 kN (5 kips) was maintained on FIU-5 with the midspan supports while a 2-Hz sinusoidal fatigue load was applied to the adjacent beam as shown in Figure 6.5 (e), with a maximum load of 104.1 kN (23.4 kips) and a minimum load of 89 kN (5 kips), as shown in Figure 6.5 (f). A total of two million additional HS-20 cycles were applied using FC 2-6 during Stage 6 and 7. This configuration included static monotonic FL120 loading ramps before (Stage 5) and after (Stage 8) fatigue testing to determine if there was any deterioration in the behavior of the system caused by the fatigue testing; these static load ramps are labeled FC 2-6st. A load configuration like FC 2-6st was also used to attempt to cause longitudinal cracking along the top of the joint (Stage 11), called FC 2-6cr. This load protocol consisted of increasing the load in both actuators to 222 kN (50 kips) at the same

time and then unloading. An additional 700,000 cycles were applied using FC 2-6 after the transverse and longitudinal cracking service tests (Stage 13 and Stage 14).

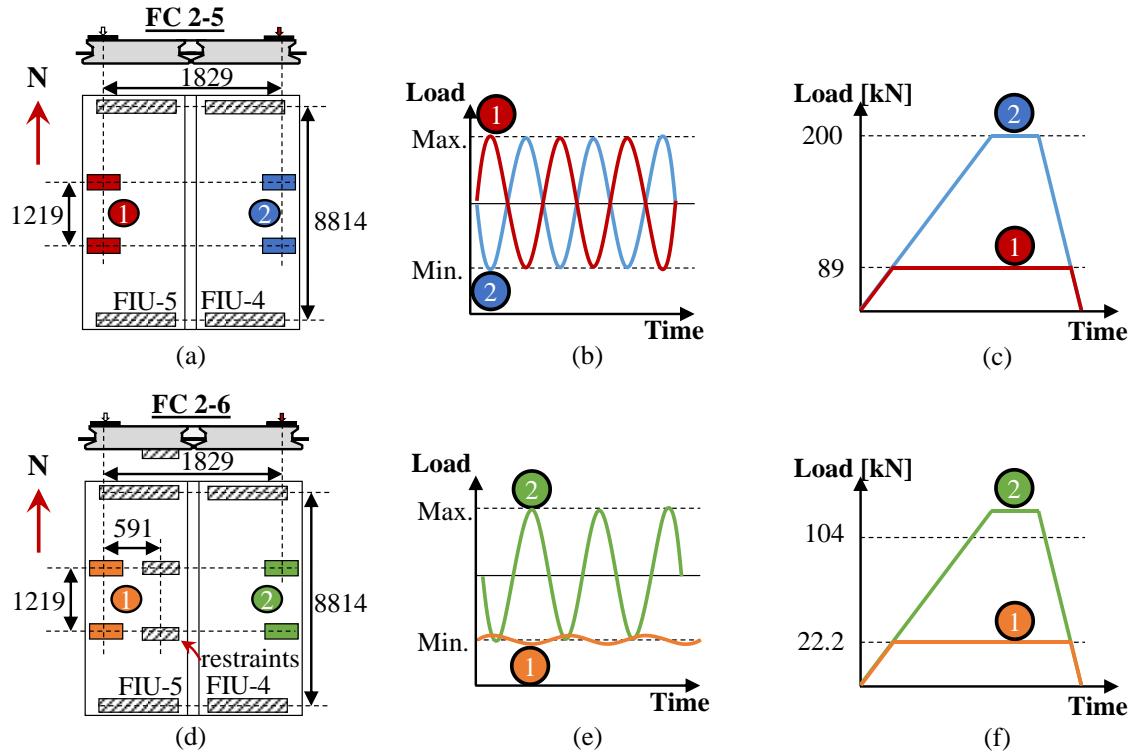


Figure 6.5: Test setup for configurations: (a) FC 2-5 plan/elevation views, (b) reverse sinusoidal load protocol for FC 2-5, (c) static transverse cracking load protocol for FC 2-5cr, (d) FC 2-6 plan/elevation views, (e) reverse sinusoidal load protocol for FC 2-6, and (f) static load protocol for FC 2-6st. (units: mm, 1 mm = 0.0394 in.)

3. *LC 2-7 (Continuous Span)*: This load configuration had similar load and end support points to LC 2-4, but one end was restrained for rotation. A continuous span was simulated in LC 2-7 by shifting one of the supports toward midspan and providing a vertical restraint at the end of the beam outside the support. The load was applied using two actuators and two spreader beams simultaneously with the configuration shown in Figure 6.6. A total load of 272 kN (61.2 kips) was applied at an approximate rate of 0.9 kN/s (0.2 kips/s), simulating a FL120 rear axle load.

Several monotonic load cycles were performed to see how the joint response would change if the system were used for simple-for-dead-continuous-for-live (SDCL) construction.

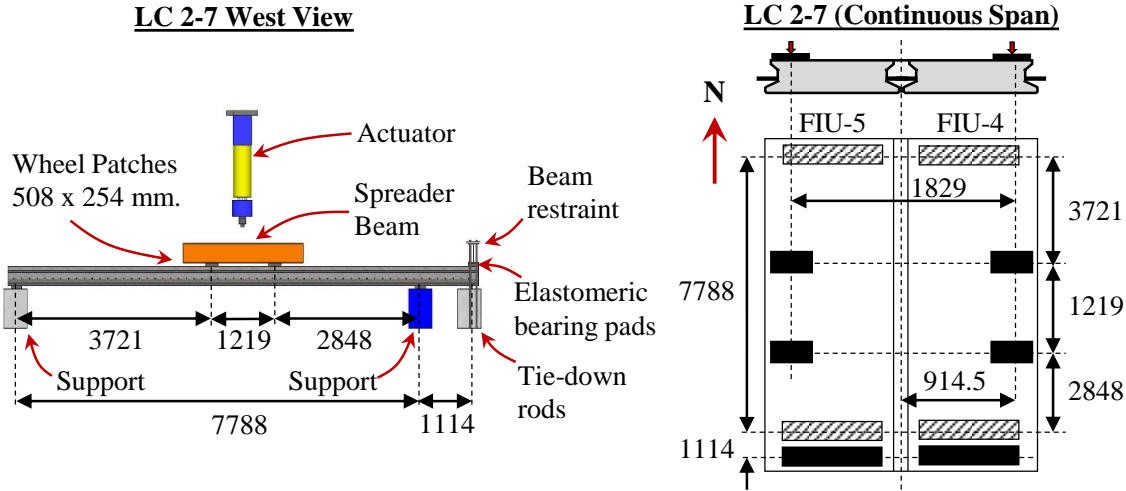


Figure 6.6: Testing frame layout for LC 2-7 (continuous span) (units: mm, 1 mm = 0.0394 in.)

The end restraint was created using a spreader beam spanning both precast beams tied down to the strong floor with threaded rods. Elastomeric bearing pads were placed between the spreader beam and the top of the specimen to distribute load and avoid damage.

After all fatigue and static ramps were performed, FIU-4/5 was tested to failure using the same LC 2-1 load protocol shown in Figure 6.4; all intermediate supports were removed prior to ultimate strength testing. This ultimate load response after all the fatigue testing was compared with the ultimate load response of the system without any fatigue loading (FIU-1/2).

Table 6.1: Service, fatigue, and strength testing schedule for FIU-4/5

| Stage | Description | Lower Limit Load ^{1,2} (Δ) | Upper Limit Load ^{1,2} (Δ) | Load Conditions | # Cycles |
|-------|------------------------------|--|--|-----------------|-----------|
| 1 | Static Elastic FL 120 | 0 kN (0.0 mm) | 136.1 kN (18.8 mm) | LC 2-4 | 5 |
| 2 | Fatigue Calibration | 22.2 kN (2.8 mm) | 104.1 kN (9.1 mm) | FC 2-5 | 200,000 |
| 3 | HS20 Truck Load | 22.2 kN (2.8 mm) | 104.1 kN (9.1 mm) | FC 2-5 | 1,800,000 |
| 4 | Static Elastic FL 120 | 0 kN (0.0 mm) | 136.1 kN (18.8 mm) | LC 2-4 | 2 |
| 5 | Static Elastic HS20 | 22.2 kN ³ (2.8 mm) | 104.1 kN ⁴ (9.1 mm) | FC 2-6st | 4 |
| 6 | Fatigue Calibration | 22.2 kN ³ (2.8 mm) | 104.1 kN ⁴ (9.1 mm) | FC 2-6 | 200,000 |
| 7 | HS20 Truck Load | 22.2 kN ³ (2.8 mm) | 104.1 kN ⁴ (9.1 mm) | FC 2-6 | 1,800,000 |
| 8 | Static Elastic HS20 | 22.2 kN ³ (2.8 mm) | 104.1 kN ⁴ (9.1 mm) | FC 2-6st | 2 |
| 9 | Static Elastic FL 120 | 0 kN (0.0 mm) | 136.1 kN (18.8 mm) | LC 2-7 | 3 |
| 10 | Transverse Crack Procedure | | | FC 2-5cr | 1 |
| 11 | Longitudinal Crack Procedure | | | FC 2-6cr | 2 |
| 12 | Static Inelastic FL 120 | 22.2 kN ³ (2.8 mm) | 158.3 kN ⁴ (10.2 mm) | FC 2-6st | 2 |
| 13 | Fatigue Calibration | 22.2 kN ³ (2.8 mm) | 104.1 kN ⁴ (9.1 mm) | FC 2-6 | 200,000 |
| 14 | HS20 Truck Load | 22.2 kN ³ (2.8 mm) | 104.1 kN ⁴ (9.1 mm) | FC 2-6 | 500,000 |
| 15 | Static Inelastic FL 120 | 89 kN (2.8 mm) | 200.2 kN ⁵ (11.4 mm) | FC 2-5cr | 1 |
| 16 | Ultimate Strength Test | | | LC 2-1 | 1 |

Notes: ¹Loads/displacements listed are for each actuator (not total); ²Acceptable load/displacement range for loading is starting load/displacement $\pm 5\%$; ³Lower load range for FC 2-6 determined from load required to bear against the center supports; ⁴Upper load range for FC 2-6 determined from lower load range plus 136.1 kN (30.6 kips) (service) or 81.8 kN (18.4 kips) (fatigue); ⁵Upper load range for FC 2-6 determined from maximum actuator capacity of 222.4 kN (50 kips). (1 kN = 0.2248 kip; 1 mm = 0.0394 in.)

The static load ramps (LR) are labeled in this paper based on the stage of the loading and the static load cycle that is being shown, e.g., results from the first static load ramp in Stage 4 will be labeled LR 4-1. The load configuration label will also be included with the load ramp label in the figures and text.

6.3.3 Instrumentation

Several different types of instrumentation were used in testing of the two-beam systems. Rebar strain gauges (RSGs) were installed on the joint reinforcement extending from each of the precast beams (at 25 mm away from the precast section joint face). Concrete surface gauges (CSGs) were installed on the top and bottom of the precast beams in the longitudinal direction (at each beam centerlines) and transverse directions (at 308 mm away from the joint centerline). Crack displacement transducers (CDTs) were installed across the joint region along the length of the top and bottom of the systems. Laser displacement transducers (LDTs) were placed at five different locations along the length and measured the displacement of the tops of the beams at three locations across the width of the system. The locations of the different types of gauges are included with the results. The hydraulic actuators had a built-in load cell capable of measuring the loads being applied to the two-beam system.

6.4 Experimental Results and Discussion

6.4.1 Effect of Cyclic Loading

A total of 4.7 million load cycles were applied to FIU-4/5 using two different fatigue load configurations without an intermediate support (FC 2-5) and with an intermediate support under FIU-5 (FC 2-6). The normalized stiffness at midspan of FIU-4/5 during the complete fatigue assessment is shown in Figure 6.7 (a). The stiffness was found based on the deflection and load measured by the actuator applying load to FIU-4 and FIU-5 individually. The stiffness was normalized by the starting stiffness of the system at the beginning of each fatigue cycle. A decrease in the normalized stiffness of the system (i.e., falling below 1.0) would suggest the cyclic loading is causing a deterioration in the performance of the system. The normalized stiffness remained between 0.94 and 1.11 for FIU-4 and between 0.93 and 1.07 for FIU-5 with no observable trend with increased number of cycles.

Several static load tests were performed before and after each of the fatigue loading stages to determine if there were any changes in the static response caused by the fatigue loading. The load versus displacement curves for FIU-4 and FIU-5 before and after FC 2-5 measured using LC 2-4 are shown in Figure 6.7 (b). The responses before (LR 1-1) and after (LR 4-1) the FC 2-5 fatigue loading stage essentially overlay each other, which suggests that there was no deterioration in the overall system performance caused by FC 2-5. This was also true for the additional load cycles applied through FC 2-6.

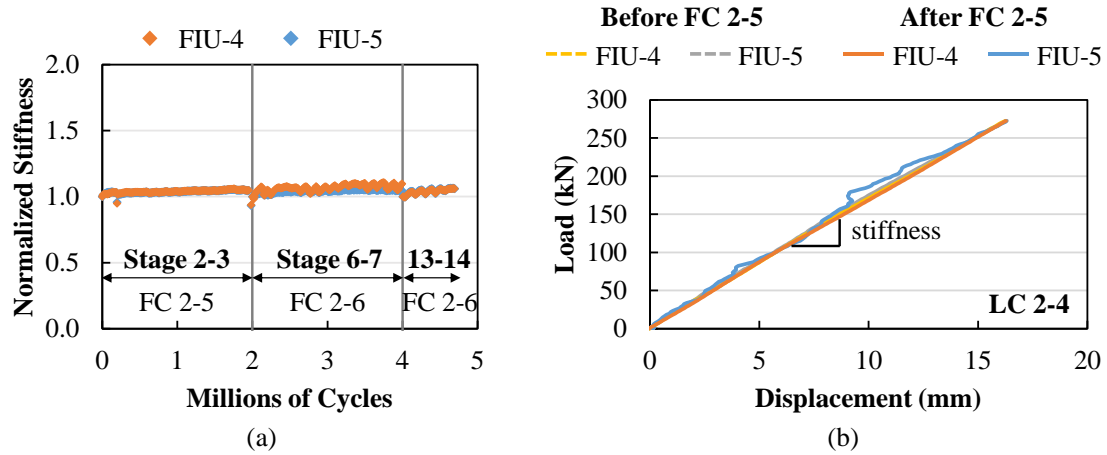


Figure 6.7: (a) Normalized stiffness at midspan versus fatigue cycles and (b) load versus midspan deflection before and after FC 2-5 fatigue loading (1 kN = 0.225 kips; 1 mm = 0.0394 in.)

The response from all the RSGs on joint reinforcement, CDTs across the top and bottom of the joint, and longitudinal and transverse CSGs on the top and bottom of the system were also monitored during the static and fatigue tests. The response throughout fatigue testing was summarized by plotting the change in strain divided by the change in applied load. A change in this normalized response would indicate that the fatigue loading was affecting the performance of the joint reinforcement, joint, or surrounding concrete. There was no observed change in the response caused by the fatigue loading stages. An example of the change in strain per change in applied load is shown in Figure 6.8 (a) for two transverse CSGs located next to the joint on top of FIU-4/5. There was little to no change in response with increasing number of load cycles within each of the fatigue load stages, e.g., the responses remained constant within Stage 2-3.

There was a change in the normalized response due to the different loading configurations. Adding the intermediate supports in FC 2-6 increased the transverse strain change with a larger transverse strain change measured above the intermediate supports in FIU-5. The

strain change increased again after the transverse cracking (FC 2-5cr) and longitudinal cracking (FC 2-6cr) load protocols.

The load versus strain curves in the same two transverse CSGs on top of FIU-4/5 before and after FC 2-5 measured using LC 2-4 are shown in Figure 6.8 (b). The curves essentially overlay each other indicating that the fatigue loading had no effect on the static load response. Similar results were observed in all the instrumentation.

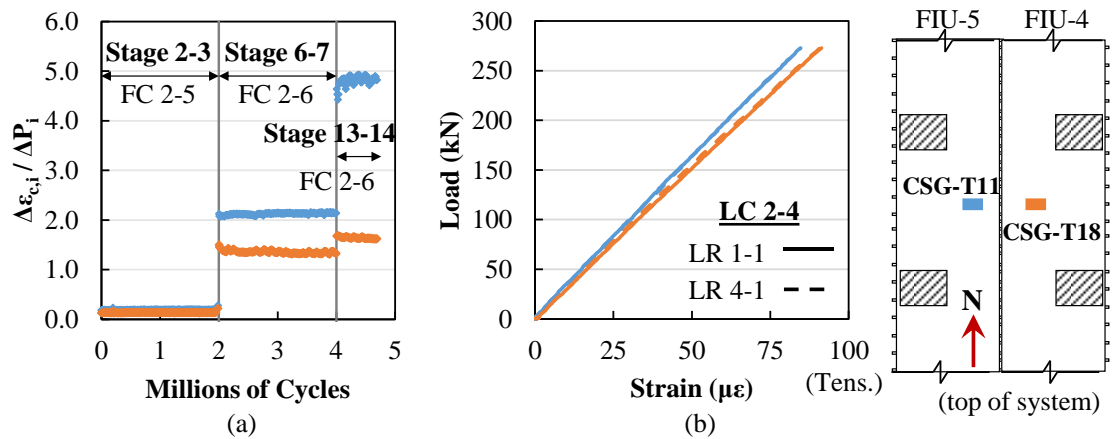


Figure 6.8: (a) Strain change of top transverse CSGs per change in applied load versus number of cycles and (b) load versus strain in top transverse CSGs before and after FC 2-5 fatigue loading (1 kN = 0.225 kips; 1 mm = 0.0394 in.)

6.4.2 Effect of Intermediate Support

FIU-4/5 was tested with simply supported end conditions and without intermediate supports (using LC 2-4 and FC 2-5) and with intermediate supports (FC 2-6). The load versus displacement curves for FIU-4/5 using LC 2-4 and FC 2-6st load configurations are shown in Figure 6.9 (a). The system had a similar response during both tests until FIU-5 began to bear against the intermediate supports, which occurred at approximately 50 kN (11.2 kips) of total applied load. At this point, the system response became stiffer where

the intermediate supports were present. The point of bearing was also noticeable in the longitudinal CSGs, as shown in Figure 6.9 (b). The longitudinal CSGs in the unrestrained beam (FIU-4) measured higher strains than those in the restrained beam. Less load was applied during LR 8-1 to ensure that no cracking occurred in the system; this initial load level was based on HS-20 truck loading with a half-axle load. The load level with the intermediate supports was increased to higher levels in Stage 11 with FC 2-6cr.

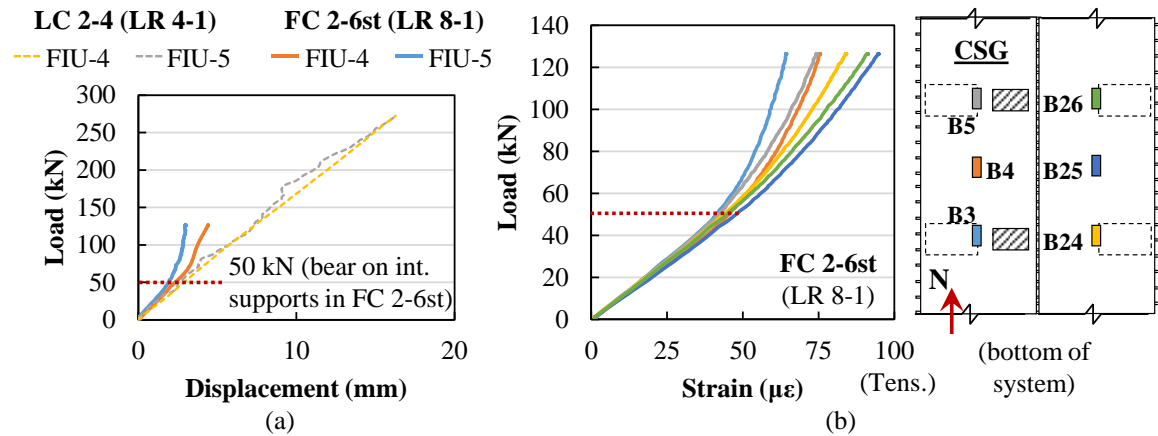


Figure 6.9: (a) Load versus displacement for FIU-4/5 with LC 2-4 and FC 2-6st load configurations and (b) load versus longitudinal concrete strain for longitudinal CSGs on bottom of system at midspan (1 kN = 0.2248 kips; 1 mm = 0.0394 in.)

The load versus average strain across the top of the joint in FIU-4/5 without (LC 2-4) and with (FC 2-6st) intermediate supports is shown in Figure 6.10. The presence of the intermediate supports did not affect the static response of the transverse gauges (CDTs and CSGs) on top of the system at the total load applied during FC 2-6st (126 kN [28.3 kips]); the strains measured at this load were comparable during both tests.

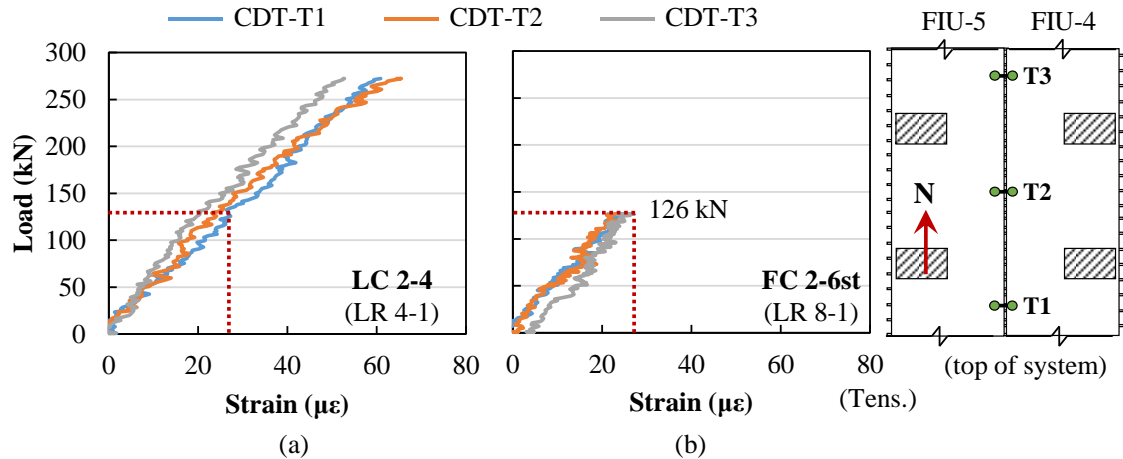


Figure 6.10: Load versus average strain across the joint for FIU-4/5 on top of the system measured using CDTs using (a) LC 2-4 and (b) FC 2-6st load configurations (1 kN = 0.2248 kips)

6.4.3 Joint Demand for Continuous Beams

The end rotation of FIU-4/5 was restrained in LC 2-7 by moving the bottom support toward midspan and adding a restraint on the top of the system outside of the bottom support, as shown in Figure 6.6. The load versus midspan displacement for the system with (LC 2-7) and without (LC 2-4) the end restraint on one end is shown in Figure 6.11 (a). The addition of the end restraint and decrease in span length (from 7.78 m [25.5 ft.] for LC 2-7 and 8.74 m [28.7 ft.] for LC 2-4) led to a 67-percent increase in stiffness for the system with end restraints, with the stiffness going from 16.7 kN/mm (95.4 k/in.) without end restraints (LC 2-4) to 27.9 kN/mm (159.3 k/in.) with an end restraint on one end (LC 2-7). The end restraint on one end of the system led to negative moment developing over the bottom end support. This negative moment was observed by tension being measured in the top of the system and compression on the bottom of the system at the ends of the beam. The bottom CSGs were located immediately opposite the top CSGs, so the average reading from the two top and two bottom CSGs located at a plane could be used with the height of the section

(305 mm [12 in.]) to calculate the average curvature along the length of the system, shown in Figure 6.11 (b) for the CSGs located near the end and at midspan. The average curvature at a total applied load of 272.4 kN (61.2 kips) was $-0.293 \mu\epsilon/\text{mm}$ ($-7.45 \mu\epsilon/\text{in.}$) at the location of T1/T22 and $1.618 \mu\epsilon/\text{mm}$ ($41.1 \mu\epsilon/\text{in.}$) at approximately the midspan (location of T4/T25). The system behaved linear-elastically through LC 2-7, as shown in Figure 6.11 (b), and there was no distress or longitudinal cracking observed in the location of the end restraint.

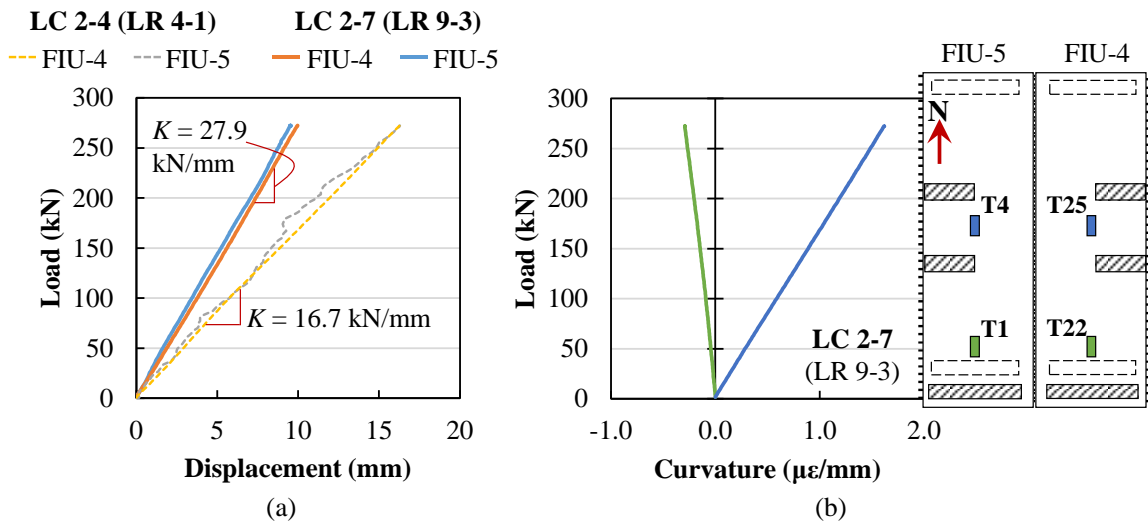


Figure 6.11: (a) Load versus displacement for FIU-4/5 with LC 2-4 and LC 2-7 load configurations and (b) load versus average curvature found using CSGs on top and bottom of system toward beam ends and midspan (1 kN = 0.2248 kips; 1 mm = 0.0394 in.)

The transverse system behavior was also measured using the transverse CSGs on the top and bottom of the system, CDTs along the length of the joint, and RSGs on the joint reinforcement. The transverse tensile strains measured during LC 2-7 (with end restraint) were less than those measured during LC 2-4 (without end restraints), as shown in Figure 6.12; strains at the peak load (272.4 kN [61.2 kips]) were between 78 and $90 \mu\epsilon$ for LC 2-

4 and between 58 and 65 $\mu\epsilon$ for LC 2-7, which is an average 37-percent decrease in the transverse strains. Similar results were observed in the other transverse gauges.

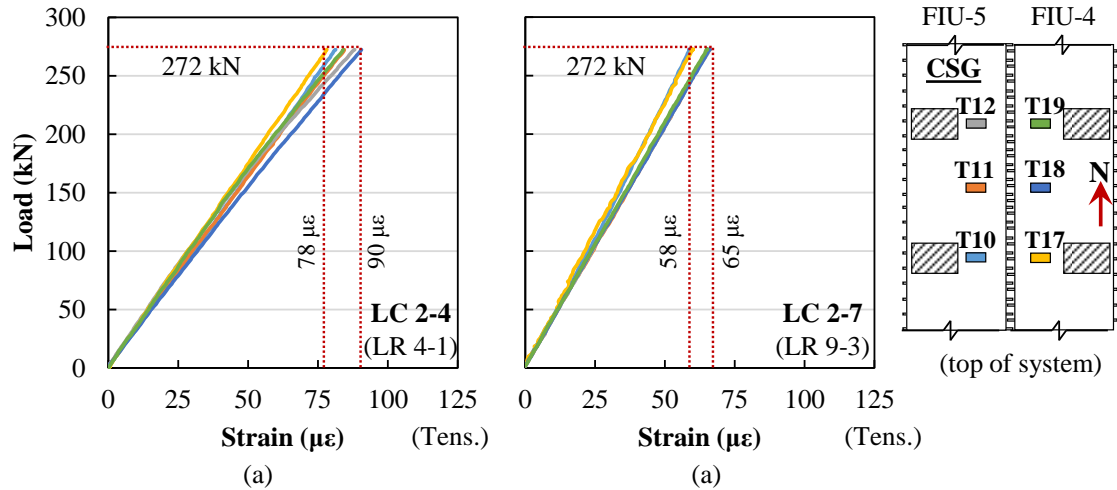


Figure 6.12: Load versus transverse concrete strain on top of FIU-4/5 for (a) LC 2-4 and (b) LC 2-7 (1 kN = 0.2248 kips)

6.4.4 Effect of Cracking on Joint Demand

Two different cracking load configurations were applied to FIU-4/5: FC 2-5cr to cause transverse cracking in one of the beams and FC 2-6cr to attempt to cause a longitudinal crack along the joint. The total load versus displacement curves for FC 2-5cr and FC 2-6cr are shown in Figure 6.13 (a). Interior supports under FIU-5 were provided during FC 2-6cr but not for FC 2-5cr. The point when FIU-4/5 begins to bear against the interior supports in FC 2-6cr is the point when there is a noticeable change in the system response, at around 50 kN (11.2 kips). Transverse cracking occurred on the bottom of FIU-4 due to FC 2-5cr at a total applied load of approximately 280 kN (62.9 kips). The cracking load during FC 2-5cr was determined using the longitudinal CSGs at midspan, shown in Figure 6.13 (b), based on when there was a dramatic increase or decrease in measured strain. An increase

in strain indicates a crack at the location of the CSG; a decrease in strain indicates a crack next to the CSG. CSG-B24 saw an increase in strain and CSG-B25 a decrease in strain starting approximately at 280 kN (62.9 kips). The cracking was visually inspected and marked, as shown in Figure 6.13 (b). No longitudinal cracking or joint distress was observed during either cracking load configurations (FC 2-5cr or FC 2-6cr).

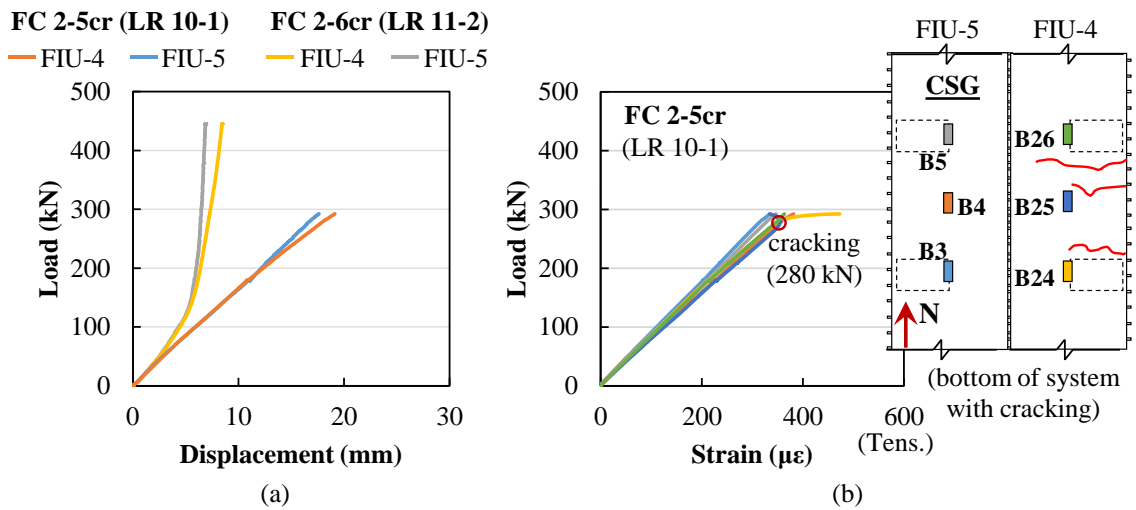


Figure 6.13: (a) Load versus displacement for FIU-4/5 with FC 2-5cr and FC 2-6cr load configurations and (b) load versus longitudinal concrete strain for longitudinal CSGs on bottom of system at midspan of beams (1 kN = 0.2248 kips; 1 mm = 0.0394 in.)

The transverse cracking occurred at a total applied load of 280 kN (62.9 kips) during the first application of FC 2-5cr (LR 10-1); since the system was uncracked before this load, the response during LR 10-1 can be considered the uncracked system response using load configuration FC 2-5cr. FC 2-5cr was used to apply load to the system again after both cracking load configurations and an additional 700,000 load cycles using FC 2-6; this static load ramp was LR 15-1. The influence of the transverse cracking on the system response could be determined by comparing the results from LR 10-1 and LR 15-1. The curves for total applied load versus average strain across the joint measured by three of the CDTs on

top of FIU-4/5 are shown in Figure 6.14 (a) for LR 10-1 and Figure 6.14 (b) for LR 15-1. Similar average strains were measured across the joint before and after the cracking load protocols and 700,000 load cycles; this would suggest that there was no degradation in the joint performance due to cracking or further fatigue loading. There were similar observations for the other transverse gauges in FIU-4/5 for LR 10-1 and LR 15-1.

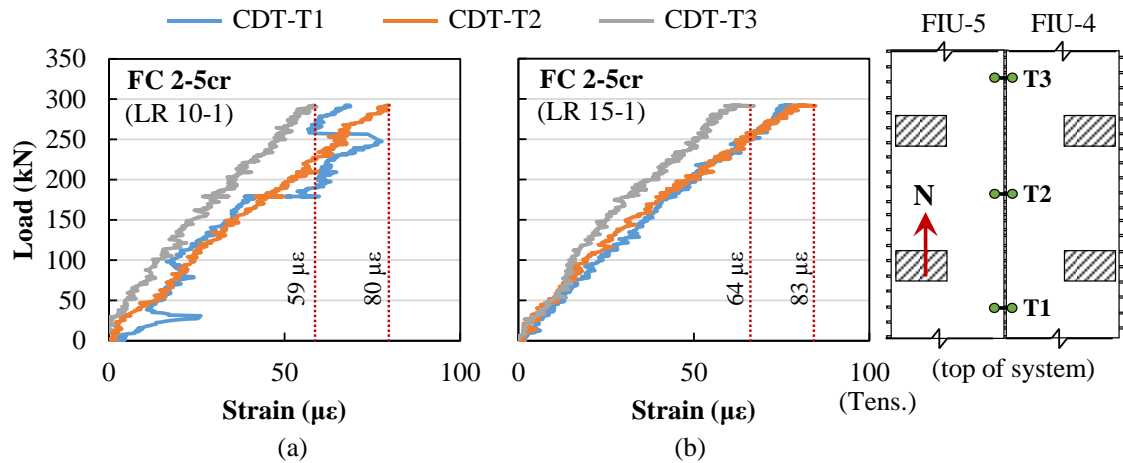


Figure 6.14: Load versus average strain across the joint for FIU-4/5 on top of the system measured using CDTs using FC 2-5cr (a) before (LR 10-1) and (b) after (LR 15-1) transverse cracking and subsequent fatigue loading (1 kN = 0.2248 kips)

6.4.5 Ultimate Strength Behavior

FIU-1/2 and FIU-4/5 were both tested to their ultimate flexural capacity using LC 2-1. The total applied load versus midspan deflection responses for FIU-1/2 and FIU-4/5 are shown in Figure 6.15 (a). The midspan deflection was measured toward the outside of each of the beams, so any differential deflection between the adjacent beams could be measured. There was a differential deflection between beams of 5 percent between FIU-4 and FIU-5 and 7 percent between FIU-1 and FIU-2 at 600 kN (134.9 kips), which shows that the joint provided good load transfer between the two beams during testing.

Photographs of the systems immediately after failure are shown in Figure 6.15 (b) for FIU-1/2 and Figure 6.15 (c) for FIU-4/5. Failure occurred at 703 kN (158 kips) for FIU-1/2 and 707 kN (159 kips) for FIU-4/5 and was triggered by crushing of the compression block for both systems. The concrete crushed across the entire top of the two-beam system with both the conventional concrete in the precast section and UHPC in the joint crushing. No other joint distress was observed during testing. There was a similar ultimate strength and overall behavior between FIU-1/2 and FIU-4/5, which shows that the system performance was not affected by the additional service and fatigue load configurations that were applied to FIU-4/5.

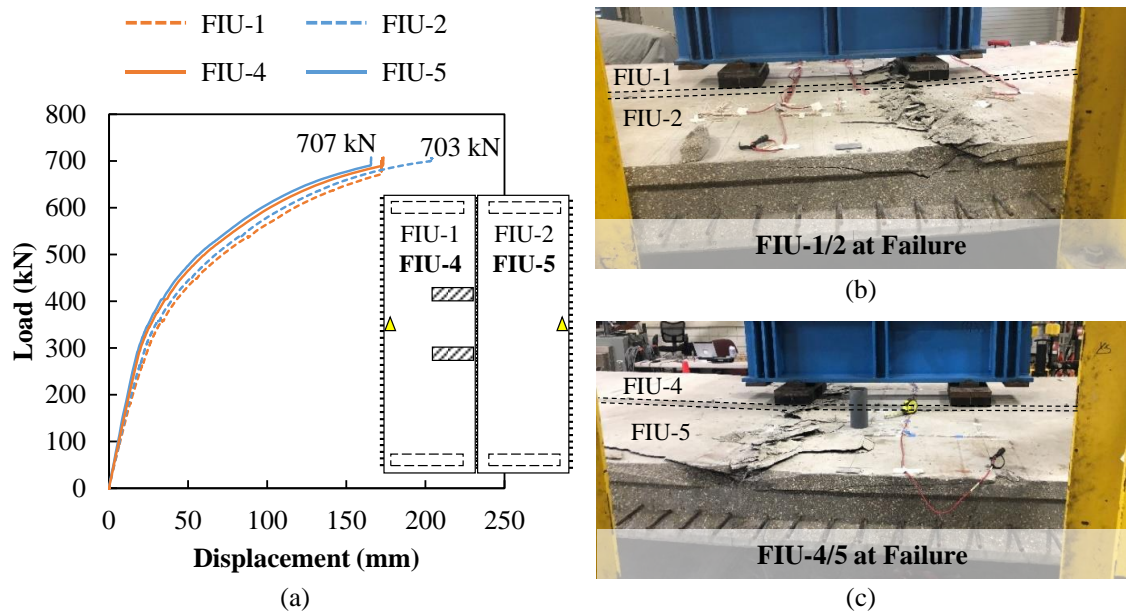


Figure 6.15: (a) Load versus displacement for ultimate strength tests on FIU-1/2 and FIU-4/5, (b) failure of FIU-1/2, and (c) failure of FIU-4/5 (1 kN = 0.2248 kips; 1 mm = 0.0394 in.)

Three concrete cores were taken from the center region of the systems after assessing the ultimate capacity, as shown in Figure 6.16 (a). These cores were taken at the precast-to-UHPC boundary region and extended through the entire depth of the system, as shown in

Figure 6.16 (b). A similar crack was observed in most of the cores from FIU-1/2 and FIU-4/5, shown in Figure 6.16 (c), (d), and (e). The crack was located between the top of the lip in the precast section and the UHPC joint and in some cases extended diagonally into the precast section. Although only three cores were taken at one precast-to-UHPC boundary region, cracks on top of the bottom lip surfaces would have been expected to appear if the cores were taken right at the middle of the joint matrix.

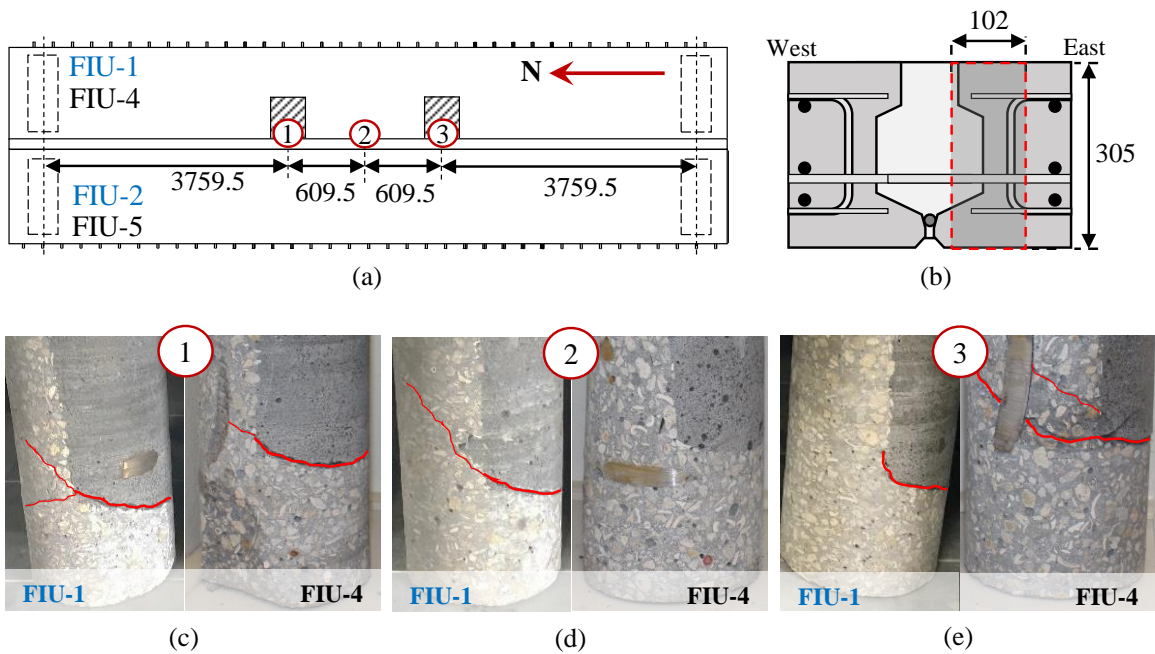


Figure 6.16: Crack patterns from cores at center region: (a) plan location of cores, (b) core location at boundary region, (c) north side core, (d) center side core, and (e) south side core. (units: mm, 1 mm = 0.0394 in.)

The total applied load versus measured strain in the joint reinforcement for FIU-1/2 under service (LC 2-4) and ultimate (LC 2-1) load configurations is shown in Figure 6.17 (a) and (b), respectively. Small compression strains were measured in the joint reinforcement under LC 2-4 and tensile strains measured in the joint reinforcement under LC 2-1. There was a slight jump in tension measured in some of the RSGs (e.g., RSG-13) at

approximately 360 kN (80.9 kips) using LC 2-1, as shown in Figure 6.17 (b); this may have been the point when the cracking observed in the joint interface cores occurred, but there were no signs of cracking observed in the transverse CSGs at this load.

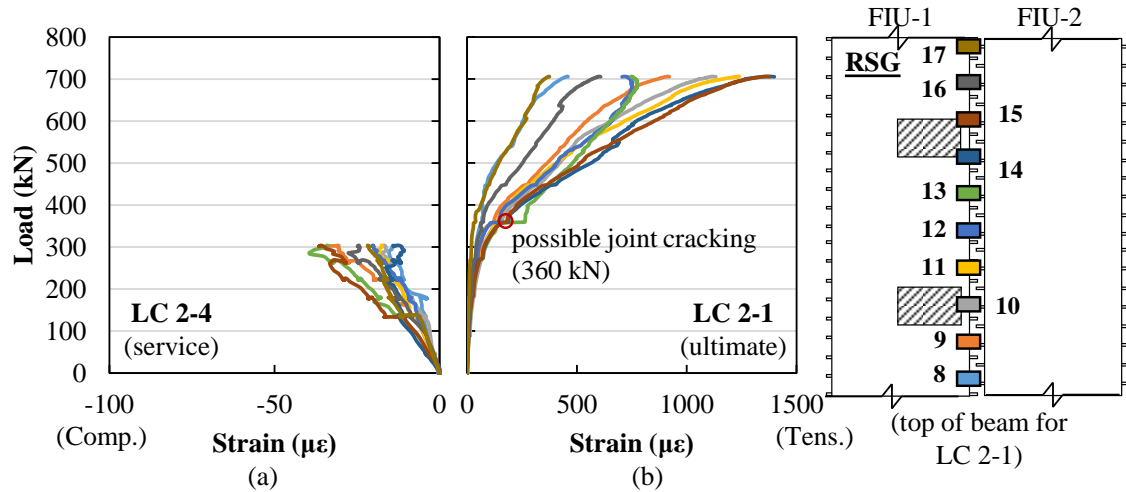


Figure 6.17: Load versus joint reinforcement strain for joint reinforcement region extending from FIU-1 in the center region for (a) LC 2-4 service load testing and (b) ultimate strength testing (1 kN = 0.2248 kips; 1 mm = 0.0394 in.)

6.5 Conclusions

Service and ultimate strength testing were performed on one two-beam system (FIU-1/2), and service, fatigue, and ultimate strength testing were performed on a second two-beam system (FIU-4/5). These tests were conducted to evaluate the full-scale system performance of a slab-beam section and UHPC joint that were previously developed based on small-scale transverse flexure testing. The following conclusions and recommendations can be made based on these two two-beam system tests.

- The system and joint performed well during service load and ultimate strength testing. No joint debonding or distress was observed in the joint region during any of the service, fatigue, and ultimate load testing. The concrete in the compression

block crushed across the entire width of the system (including the UHPC joint), which highlighted the quality of the bond between the UHPC and precast concrete. Additionally, the joint successfully transferred stress between beams; there was only a minor differential displacement between beams when only one beam was loaded using LC 2-1.

- FIU-4/5 had similar performance to FIU-1/2 during the ultimate strength testing, which shows that the 4.7 million cyclic loads, other service load configurations, and cracking tests did not impact the overall system and joint behavior.
- The joint demand (measured using the transverse CSGs, CDTs across the joint, and RSGs on the joint reinforcement) decreased when a moment restraint was provided on one end of FIU-4/5.
- Transverse tension was measured in the top of the beams (using CSGs) and across the top of the joint (using CDTs) and transverse compression across the bottom of the beams and across the bottom of the joints in all the load and support configurations for FIU-4/5 (LC 2-1, LC 2-4, FC 2-5, FC 2-6, and LC 2-7).

Transverse tension was below the estimated tensile cracking strain for the precast concrete for all service tests but exceeded this strain in the ultimate strength test (LC 2-1) at high levels of load (above service levels). Further numerical study should be done on deeper sections (e.g., 15-inch and 18-inch-deep sections) including stresses induced by temperature effects to see if a top layer of reinforcement is needed.

- Small compression strains ($< 50 \mu\epsilon$) were generally measured in the joint reinforcement for the service and fatigue load configurations (LC 2-4, FC 2-5, FC

2-6, and LC 2-7). Larger tensile strains ($> 300 \mu\epsilon$) were measured during LC 2-1 in the joint reinforcement with the highest strains measured near the load points. Strains remained under the yield strain for steel. The joint reinforcement also appeared to help inhibit the growth of cracks that developed between the top of the bottom lip and UHPC in the joint.

- There were no signs of bond deterioration between the joint reinforcement and UHPC in the joint during any of the fatigue, service, or strength testing.

These conclusions support the findings that the developed connection detail satisfies the load demand of 100 years of service life.

6.6 Data Availability Statement

Some or all data used during the study are available from the corresponding author by request.

- Videos from testing
- Selected data from testing

6.7 Acknowledgements

The research presented in this project was supported by the Florida Department of Transportation (FDOT). The authors would like to thank FDOT for their financial support and the team of engineers and staff at the Structures Research Center for their assistance in constructing and testing the specimens. The opinions, findings and conclusions expressed in this publication are those of the author(s) and not necessarily those of the Florida Department of Transportation or the U.S. Department of Transportation.

7. SUMMARY, CONCLUSIONS, AND RECOMMENDATIONS

A proposed slab-beam section and joint region for accelerated construction of short-span bridges was developed utilizing ultra-high performance concrete (UHPC) as the joint material based on an extensive comparison study on precast concrete superstructure systems, numerical modeling and joint design optimization, small-scale joint testing, and full-scale system testing. The proposed slab-beam section (without a composite cast-in-place deck) has possible span ranges between 6.1 m (20 ft.) for the 305-mm-deep (12-inch-deep) section and 16.8 m (55 ft.) for the 457-mm-deep (18-inch-deep) section.

A comparison study and finite element analysis of four prestressed, precast superstructure systems was performed to assess their flexural strength, section thickness, structural efficiency, load distribution factors, and joint and section demand. Numerical analyses were used to develop options for section and joint geometries and details. Several of the most promising joint details were evaluated through the small-scale joint testing program. Four longitudinal connection details were tested in the small-scale testing protocol: (a) two with straight sides and bottom ledges with varying thicknesses and (b) two with diamond-shape keyways with different transverse joint reinforcement depths and ledge geometries. The small-scale joint testing was performed on 305-mm (12-inch) and 457-mm-deep (18-inch-deep) sections and included both fatigue and ultimate strength testing protocols. The performance of the current FSB design standard was evaluated alongside the proposed joint details in the small-scale testing program. The best performing joint, shown in Figure 7.1, was further evaluated in the full-scale system testing program. Two two-beam systems with

the proposed joint detail were constructed and tested using service, fatigue, and ultimate strength loading protocols.

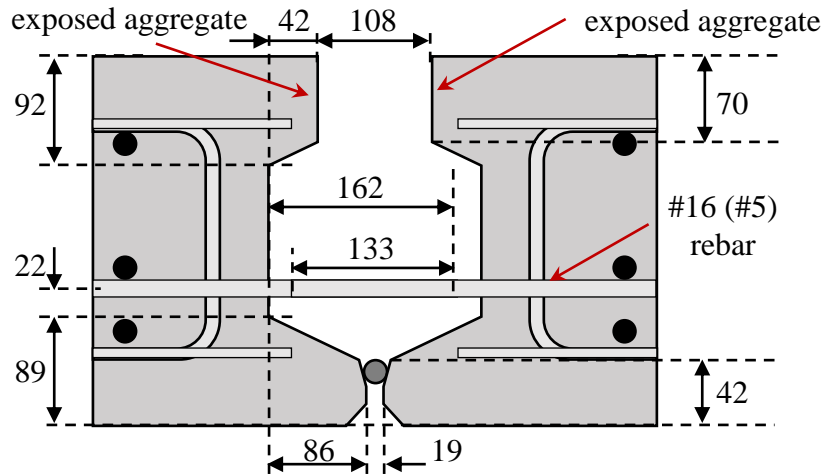


Figure 7.1: Proposed joint geometry based on small-scale joint testing and two-beam system tests (units: mm, 1 mm = 0.0394 in.)

This chapter summarizes the primary conclusions from the analytical study, numerical analyses, specimen construction, small-scale joint testing, and full-scale two-beam system testing.

7.1 Conclusions and Recommendations

The conclusions and recommendations are separated based on the three main components that the primary research consisted of: (1) analytical study of precast concrete superstructure systems, (2) joint design optimization and small-scale testing, and (3) full-scale system testing.

7.1.1 Analytical Study of Precast Concrete Superstructure Systems

The following conclusions can be made based on the parametric analysis:

- The proposed slab-beam section allowed for the shallowest section depths for spans less than 22.9 (75 ft.), making it an ideal section for superstructures with low clearances.
- The proposed slab-beam section had the smallest distribution factors from FEA results, suggesting that joint geometry provided the best load transfer mechanism between adjacent slab-beam elements.

The modified FSB design standard showed satisfactory behavior under service loads when compared to other popular adjacent precast, prestressed deck beam elements

7.1.2 Joint Design Optimization and Small-Scale Testing Protocol

The following conclusions can be made based on the design optimization and small-scale joint testing:

- The control FSB joint (based on the current FSB Design Standard) did not perform as expected due to a larger bend diameter (for both specimens) and due to the compressive strength of the deck concrete being much lower than specified (for one specimen). These issues caused development failure of the joint reinforcement prior to yield. The results from the numerical analysis were used as the point of comparison for the developed UHPC joints.
- All modified joints with UHPC had similar or greater strength and ductility compared to the current FSB design standard.
- The joints without shear keys with shorter available development and splice lengths for the joint reinforcement typically failed due to development failure of the joint reinforcement. Joints with shear keys and greater available development and splice

lengths typically failed due to crushing of the concrete or fracture of the joint reinforcement, which led to more ductile failures.

- The joint finish had a large effect on the behavior of the specimens. The sandblasted joint interface preparation was not sufficient to achieve the desired UHPC-to-precast bond. Debonding was observed in all the specimens with a sandblasted surface finish. A ¼-inch magnitude exposed aggregate finish was required to get satisfactory bond between the precast concrete and UHPC joint material.
- For the specimens that were fatigue loaded, fatigue loading did not cause degradation of specimen performance before or after cracking was intentionally caused. The fatigue loading did not affect the ultimate strength performance of the specimens.

The best performing joint from the small-scale joint testing, shown in Figure 7.1, was used in the full-scale system tests

7.1.3 Full-Scale Testing Protocol

Service and ultimate strength testing were performed on one two-beam system (FIU-1/2) and service, fatigue, and ultimate strength testing were performed on a second two-beam system (FIU-4/5). The following conclusions and recommendations can be made based on these two two-beam system tests.

- The joint performed well during service load and ultimate strength testing. No joint debonding or distress was observed in the joint region during any of the service, fatigue, and ultimate load testing. The concrete in the compression block crushed across the entire width of the system (including the UHPC joint), which highlighted

the quality of the bond between the UHPC and precast concrete. Additionally, the joint successfully transferred stress between beams; there was only a minor differential displacement between beams when only one beam was loaded.

- FIU-4/5 had similar performance to FIU-1/2 during the ultimate strength testing, which shows that the 4.7 million cycles and other service load and cracking tests did not impact the overall system behavior.
- Transverse tension was measured in the top of the beams (using CSGs) and across the top of the joint (using CDTs) and transverse compression across the bottom of the beams and across the bottom of the joints in all the load and support configurations for FIU-4/5 (LC 2-1, LC 2-4, FC 2-5, FC 2-6, and FC 2-7). Transverse tension was below the estimated tensile cracking strain for the precast concrete for all service tests but exceeded this strain in the ultimate strength test (LC 2-1) at high levels of load (above service levels).
- Transverse cracking of one beam (when the other beam remained uncracked) increased the transverse demand on the top of the adjacent precast beam when interior supports were provided. The transverse cracking caused a decreased stiffness in the unrestrained beam, which led to the increased transverse strains on the top of the restrained precast beam. However, strains remained less than the expected cracking strain and no longitudinal cracks were observed in the top of the beams. This shows that unequal stiffness between adjacent beams can lead to increased demand in the joint.
- Small compression strains ($< 50 \mu\epsilon$) were generally measured in the joint reinforcement for the service and fatigue load configurations (LC 2-4, FC 2-5, FC

2-6, and FC 2-7). Larger tensile strains ($> 300 \mu\epsilon$) were measured during LC 2-1 in the joint reinforcement with the highest strains measured near the load points. Strains remained under the yield strain for steel. The joint reinforcement also appeared to help inhibit the growth of cracks that developed between the top of the bottom lip and UHPC in the joint.

- There were no signs of bond deterioration between the joint reinforcement and UHPC in the joint during any of the fatigue, service, or strength testing.

Findings from these studies demonstrates that the proposed slab-beam and joint design is applicable for developing a standardized detail for UHPC connections in other slab-beam geometries.

7.1.4 Constructions and Design Recommendations

The following construction and design recommendations can be made based on the small-scale joint tests and full-scale system tests:

- *Proper bend diameter for current FSB Design Standard:* The joint reinforcement used in the current FSB Design Standard must have the correct bend diameter to help with the development of the joint reinforcement. Additionally, the longitudinal joint reinforcement may need to be increased to #19 (#6) bars to help with the development of the joint reinforcement. It is recommended that additional testing or bridge monitoring be done to validate the performance of the current FSB joint detail.
- *Use increased development and splice length of joint reinforcement in UHPC:* Using the currently recommended $8d_b$ embedment length and $0.75l_d$ splice length

allowed the reinforcement to develop its yield strength but resulted in pullout or development causing failure. An increased embedment and splice length resulted in fracture of the reinforcement and crushing of the concrete at failure. The proposed joint detail includes this increased available development and splice length.

- *Ensure proper surface finish of joint:* An exposed aggregate finish with 7-mm (¼-inch) magnitude is needed to ensure proper bond between the precast member and UHPC joint. Make sure the proper admixtures are used. An aggregate size of 32 mm (1 ¼ inch) may be needed to achieve the 7-mm (¼-inch) magnitude roughness. Casting mock-ups is recommended to ensure the precaster can provide the proper finish. Additionally, the surface should be pre-wetted to an SSD condition immediately before casting of the UHPC.
- *Minimum bottom flange thickness:* The bottom flange of the beam should have an average thickness greater than 51 mm (2 inches) and contain a #10 (#3) transverse reinforcing bar. This will prevent the bottom flange from breaking off during casting, transport, or construction of superstructure. The proposed joint detail includes a bottom flange design sufficient to prevent damage of the flange during casting and construction.
- *Check UHPC materials before casting:* Check that the proper dry pre-mix and compatible admixtures were received. Also check to make sure that the materials are not expired and do not have any large dry clumps.

These construction and design recommendations are provided to ensure better precast section quality and top in-service performance.

7.2 Recommendations for Future Work

The following items should be considered for future work:

- The proposed slab-beam section and joint geometry (see Figure 6.1) was only compared to three adjacent precast, prestressed concrete deck beam elements. Additional analytical studies involving steel sections and other modular superstructure systems should be done.
- The service and strength performance of the proposed joint geometry (see Figure 6.1) was evaluated analytically for a thicker section. Further numerical and experimental studies should be done on deeper sections (e.g., 381-mm [15-inch] and 457-mm-deep [18-inch-deep] sections) including stresses induced by temperature effects to see if a top layer of reinforcement is needed,
- The performance of the joint region was assessed with a proprietary UHPC as the joint material (JS1000 from Ductal). The performance of other proprietary and non-proprietary UHPC mixes as the joint material should also be investigated,
- The development length of the joint reinforcement was based on design recommendations made by FHWA, providing a minimum of $8d_b$ for deformed reinforcing bars with yield strength less than 75 ksi. However, additional research should be performed on bars with yield strengths larger than 75 ksi or epoxy-coated reinforcement, providing a larger development length of $10d_b$ as per FHWA design guidelines on field-cast connections.

- Although costs would vary based on project requirements, a cost study should be done based on regional factors (e.g., local precaster fabrication costs, UHPC materials, labor, future maintenance, and traffic impact costs),
- The proposed joint geometry was only assessed in a full-scale two-beam system testing. Additional multi-beam system testing should be investigated to assess the overall superstructure behavior,
- The specimens in the full-scale system testing were assessed under a one-end rotation constraint to simulate a continuity diaphragm scenario. Based on the results of the previous test, modifications should be investigated for using UHPC longitudinal and transverse joints in a multi-span bridge utilizing the simple for dead load and continuous for live load (SDCL) concept.
- Although the joint region was developed to withstand truck loads for a period of 100 years of service life, a retrofit action throughout this service life was not evaluated. It is recommended to impersonate a joint retrofit and compare the capacity of the repaired joint with a sound joint built.

REFERENCES

- [1] H. G. Russell and B. A. Graybeal, "Ultra-High Performance Concrete: A State-of-the-Art Report for the Bridge Community," Federal Highway Administration, FHWA-HRT-13-060, 2013.
- [2] A. Azizinamini, E. H. Power, G. F. Myers, and H. C. Ozyildirim, "Bridges for Service Life Beyond 100 Years: Innovative Systems, Subsystems, and Components," Transportation Research Board, 0309273633, 2014.
- [3] B. A. Graybeal, "Ultra-high-performance concrete connections for precast concrete bridge decks," *PCI J.*, vol. 59, no. 4, pp. 48–62, Fall 2014, doi: <https://doi.org/10.15554/pcij.09012014.48.62>.
- [4] B. A. Graybeal, "Design and construction of field-cast UHPC Connections," Federal Highway Administration, FHWA-HRT-14-084, Oct. 2014.
- [5] M. P. Culmo and R. L. Seraderian, "Development of the Northeast Extreme Tee (NEXT) Beam for Accelerate Bridge Construction," *PCI J.*, vol. 55, no. 3, pp. 86–101, 2010.
- [6] B. Graybeal, "Structural Behavior of a Prototype UHPC Pi-Girder," Federal Highway Administration, McLean, VA, FHWA-HRT-10-027, Nov. 2009.
- [7] J. Yuan and B. Graybeal, "Full-Scale Testing of Shear Key Details for Precast Concrete Box-Beam Bridges," *J. Bridge Eng.*, vol. 21, no. 9, Feb. 2016, doi: 10.1061/(ASCE)BE.1943-5592.0000906.
- [8] J. Yuan, B. Graybeal, and K. Zmetra, "Adjacent Box Beam Connections: Performance and Optimization," Federal Highway Administration, FHWA-HRT-17-093, Feb. 2018.
- [9] F. Chitty, I. Zapata, C. Freeman, and D. Garber, "Precast Concrete Superstructure Systems for Accelerated Construction of Short-Span Bridges," *Eng. Struct.*, 2021.
- [10] F. D. Chitty, C. J. Freeman, and D. B. Garber, "Joint Design Optimization for Accelerated Construction of Slab Beam Bridges," *Journal of Bridge Engineering*, vol. 25, no. 7, p. 04020029, 2020.
- [11] F. Chitty, C. Freeman, and D. Garber, "Full-Scale Testing of Slab-Beam Bridge System for Accelerated Bridge Construction," *J. Bridge Eng.*, 2021.
- [12] Federal Highway Administration, "Long-Term Bridge Performance Program," *LTBP InfoBridge*, 2020. <https://infobridge.fhwa.dot.gov/>
- [13] American Society of Civil Engineers (ASCE), "2021 Infrastructure Report Card," Reston, VA, 2021. [Online]. Available: <https://www.infrastructurereportcard.org/cat-item/bridges/>
- [14] American Society of Civil Engineers (ASCE), "2017 Infrastructure Report Card," Reston, VA, 2017. [Online]. Available: <https://www.infrastructurereportcard.org/cat-item/bridges/>

- [15] T. Doolen, B. Tang, A. Saeedi, and S. Emami, “To ABC or Not?,” *FHWA-HRT-12-001*, vol. 75, no. 3, Dec. 2011. [Online]. Available: <https://www.fhwa.dot.gov/publications/publicroads/11novdec/02.cfm>
- [16] Federal Highway Administration, “Framework for Prefabricated Bridge Elements and Systems (PBES) Decision-Making,” Federal Highway Administration, FHWA-IF-06-30, 2005. [Online]. Available: <https://www.fhwa.dot.gov/bridge/prefab/framework.cfm>
- [17] Federal Highway Administration, “Prefabricated Bridge Elements & Systems (PBES) Cost Study: Accelerated Bridge Construction Success Stories,” 2006. [Online]. Available: <https://www.fhwa.dot.gov/bridge/prefab/successstories/091104/index.cfm>
- [18] M. Roddenberry and J. Servos, “Prefabricated/Precast Bridge Elements and Systems (PBES) for Off-System Bridges,” Florida Department of Transportation, No. FSU Project ID 029858, Aug. 2012.
- [19] B. Chavel and J. Yadlosky, “Framework for Improving Resilience of Bridge Design,” Federal Highway Administration, Office of Bridge Technology, FHWA-IF-11-016, Jan. 2011.
- [20] R. Miller, G. Hlavacs, T. Long, and A. Greuel, “Full-Scale Testing of Shear Keys for Adjacent Box Girder Bridges,” *PCI J.*, vol. 44, no. 6, pp. 80–90, Dec. 1999.
- [21] B. Graybeal, “UHPC in the US Highway Infrastructure,” *Des. Build. UHPFRC*, pp. 221–234, 2009.
- [22] N. Grace, T. Enomoto, P. Baah, and M. Bebawy, “Flexural Behavior of CFRP Precast Prestressed Decked Bulb T-Beams,” *J. Compos. Constr.*, vol. 16, no. 3, pp. 225–234, 2012, doi: 10.1061/(ASCE)CC.1943-5614.0000266.
- [23] E. T. Visage, K. R. Perera, B. D. Weldon, and D. V. Jauregui, “Experimental and Analytical Analysis of the Flexural Behavior of UHPC Beams,” 2012, p. 403.
- [24] G. Zhang and B. A. Graybeal, “Development of UHPC Pi-Girder Sections for Span Length up to 41 m,” *Journal of Bridge Engineering*, vol. 20, no. 3, p. 04014068, 2015.
- [25] Z. Haber and B. Graybeal, “Performance of Grouted Connections for Prefabricated Bridge Deck Elements,” Federal Highway Administration, McLean, VA, FHWA-HIF-19-003, Nov. 2018.
- [26] Federal Highway Administration, “Recording and Coding Guide for Structure Inventory and Appraisal of the Nation’s Bridges,” Federal Highway Administration, Office of Engineering Bridge Division, FHWA-PD-96-001, 2000. [Online]. Available: <https://www.fhwa.dot.gov/bridge/mtguide.pdf>
- [27] G. Nasser, M. Tadros, and A. Sevenker, “The Legacy and Future of an American Icon: The Precast, Prestressed Concrete Double Tee,” *PCI J.*, vol. 60, no. 4, pp. 49–68, Aug. 2015.
- [28] Precast/Prestressed Concrete Institute (PCI), “Northeast Deck Bulb Tee Beam Details - Recommended Usage and Notes.” Precast/Prestressed Concrete Institute Northeast, Aug. 02, 2016. [Online]. Available:

- https://www.pci.org/PCI_Docs/PCI_Northeast/Technical_Resources/Bridge/2018_03_06_NEDBT_plot.pdf
- [29] Florida Department of Transportation (FDOT), “2010 FDOT Design Standards: Inverted-T Beam - Standard Details (Index No. 20320),” 2010.
- [30] F. Jaber, “Nebraska’s Inverted Tee Short-Span Bridge System,” *ASPIRE Magazine*, no. Spring, pp. 34–35, 2013.
- [31] Precast/Prestressed Concrete Institute (PCI), “PCI Design Handbook, 7th Edition,” Precast and Prestressed Concrete Institute (PCI), Chicago, 2010.
- [32] G. Zhang, B. Graybeal, and L. Chen, “Development of a Family of Ultra-High Performance Concrete Pi-Girders,” Federal Highway Administration, McLean, VA, FHWA-HRT-14-027, Dec. 2013.
- [33] Precast/Prestressed Concrete Institute (PCI), “Bridge Design Manual,” 2011.
- [34] Texas Department of Transportation (TxDOT), “Bridge Standards.” TxDOT, 2017. [Online]. Available: <http://www.txdot.gov/insdtdot/orgchart/cmd/cserve/standard/bridge-e.htm>
- [35] Ohio Department of Transportation, “Prestressed Concrete Box Beam Bridge Details.” Office of Structural Engineering, 2007. [Online]. Available: <http://www.dot.state.oh.us/Divisions/Engineering/Structures/standard/Bridges/Standard%20Drawings/PSBD-2-07.pdf>
- [36] F. Menkulasi, M. Mercer, C. Wollmann, and T. Cousins, “Accelerating Bridge Construction Using the Precast Inverted T-Beam Concept,” *Precast. Concr. Inst. PCI*, Sep. 2012.
- [37] M. Khan, *Accelerated Bridge Construction - Best Practices and Techniques*. Waltham, MA: Elsevier, 2015.
- [38] B. F. Bender and W. G. Kriesel, “Precast, Prestressed Box Beams - A State-of-the-Art Report,” *PCI J.*, 1969.
- [39] A. Avendaño *et al.*, “Pretensioned Box Beams: Prestress Transfer and Shear Behavior,” FHWA/TX-13/0-5831-3, 2013.
- [40] K. E. Hanna, G. Morcous, and M. K. Tadros, “Transverse Post-Tensioning Design and Detailing of Precast, Prestressed Concrete Adjacent Box-Girder Bridges,” *PCI J.*, vol. 54, no. 4, pp. 160–174, 2009.
- [41] J. Corvin, “Post-Tensioned Box Girders - Design Manual,” Sep. 2015.
- [42] Ductal, “Hawk Lake Bridge, Ontario, Canada - Joint Fill,” 2010. <http://www.ductal.com/en/engineering/hawk-lake-bridge> (accessed Sep. 01, 2016).
- [43] J. Lall, S. Alampalli, and E. DiCocco, “Performance of Full-Depth Shear Keys in Adjacent Prestressed Box Beam Bridges,” *PCI J.*, pp. 72–79, Mar. 1998.
- [44] Precast/Prestressed Concrete Institute Northeast (PCINE), “Northeast Extreme Tee (NEXT) Beam Details,” 2015.

- [45] Matiere, “The principle of Poutre-Dalle beam slab,” 2014. <http://www.matiere-tp.com/beam-slab/> (accessed Sep. 01, 2016).
- [46] M. S. Mercer, “Transverse Sub-Assemblage Testing of the Inverted-T Bridge System,” Doctoral dissertation, Virginia Tech, Blacksburg, VA, 2012.
- [47] M. Dimaculangan and T. Lesch, “Minnesota’s Precast Composite Slab Span System,” *ASPIRE*, p. 4, 2010.
- [48] C. French *et al.*, “Cast-in-Place Concrete Connections for Precast Deck Systems (Web-Only Document 173),” National Academies of Sciences, Engineering, and Medicine, Washington DC, 2011. [Online]. Available: <https://doi.org/10.17226/17643>
- [49] R. Piccinin and A. E. Schultz, “The Minnesota Inverted-Tee System: Parametric Studies for Preliminary Design,” *PCI J.*, vol. 57, no. 2, pp. 162–179, 2012.
- [50] F. Menkulasi, C. L. Roberts Wollmann, and T. Cousins, “Live-Load Distribution Factors for Composite Bridges with Precast Inverted T-Beams,” *J. Perform. Constr. Facil.*, p. 04016045, 2016.
- [51] B. Goldsberry, “Florida Slab Beam (FSB) - Development and Implementation,” presented at the Design Training Expo, 2015. [Online]. Available: <http://www.dot.state.fl.us/officeofdesign/Training/DesignExpo/2015/presentations/FSBDevelopmentandImplementation-BenGoldsberry.pdf>
- [52] V. Young, “Florida Slab Beam (FSB) - Superstructure Package,” presented at the Design Training Expo, 2016. [Online]. Available: [http://www.dot.state.fl.us/officeofdesign/training/DesignExpo/2016/Presentations/FloridaSlabBeams\(FSB\)SuperstructurePackage-VickieYoung.pdf](http://www.dot.state.fl.us/officeofdesign/training/DesignExpo/2016/Presentations/FloridaSlabBeams(FSB)SuperstructurePackage-VickieYoung.pdf)
- [53] H. T. Bollmann, “Precast Prestressed Slab Units,” Nov. 09, 1984. [Online]. Available: https://fdotwww.blob.core.windows.net/sitefinity/docs/default-source/structures/structuresmanual/archivedstructuresmanuals/structuresdirectives-pre1987hd.pdf?sfvrsn=9b0b58ba_2
- [54] Florida Department of Transportation (FDOT), “Instructions for Developmental Design Standards,” *Index D20450 Ser. Fla. Slab Beam*, Mar. 2016, [Online]. Available: <http://www.dot.state.fl.us/rddesign/DS/Dev/IDDS/IDDS-D20450.pdf>
- [55] R. V. Robertson, “Florida Slab Beam Superstructure System,” 2016. [Online]. Available: <http://www.dot.state.fl.us/officeofdesign/bulletins/SDB16-01.pdf>
- [56] M. Biswas, “Precast bridge deck design systems,” *PCI J.*, vol. 31, no. 2, pp. 40–94, 1986.
- [57] D. G. Hieber, J. M. Wacker, M. O. Eberhard, and J. F. Stanton, “State-of-the-art report on precast concrete systems for rapid construction of bridges,” Citeseer, 2005. [Online]. Available: <http://citeseerx.ist.psu.edu/viewdoc/download?doi=10.1.1.369.9839&rep=rep1&type=pdf>

- [58] S. S. Badie and M. K. Tadros, “NCHRP Report 584: Full-Depth, Precast-Concrete Bridge Deck Panel Systems,” National Cooperative Highway Research Program (NCHRP), Report 584, 2008.
- [59] C. M. Bell, C. E. French, and C. K. Shield, “Application of precast decks and other elements to bridge structures,” University of Minnesota, Minneapolis, MN, MN/RC-2006-37, Sep. 2006.
- [60] Federal Highway Administration (FHWA), “MnDOT/FHWA Precast Slab System Workshop Summary Report,” 2015. <https://www.fhwa.dot.gov/bridge/prefab/slab.cfm>
- [61] M. Royce, “Implementing ultra-high-performance concrete for accelerated bridge construction in New York,” *PCI J.*, pp. 38–47, 2014.
- [62] S. Aaleti and S. Sritharan, “Design of Ultrahigh-Performance Concrete Waffle Deck for Accelerated Bridge Construction,” *Transp. Res. Rec. J. Transp. Res. Board*, vol. 2406, pp. 12–22, 2014, doi: 10.3141/2406-02.
- [63] B. Graybeal, “UHPC in the US highway transportation system,” 2008, pp. 11–17.
- [64] S. S. Badie, M. K. Tadros, and R. M. M. Usdan, “Full-depth, precast concrete bridge deck panel systems,” *Concr. Int.*, vol. 31, no. 04, pp. 53–58, 2009.
- [65] Z. Haber, “Ultra-High Performance Concrete (UHPC),” presented at the Design Training Expo, 2016.
- [66] B. Graybeal, “Development of Non-Proprietary Ultra-High Performance Concrete for Use in the Highway Bridge Sector,” 2013.
- [67] E. Brühwiler, “‘Structural UHPFRC’: Welcome to the post-concrete era!,” 2016.
- [68] M. A. Saleem, A. Mirmiran, J. Xia, and K. Mackie, “Ultra-high-performance concrete bridge deck reinforced with high-strength steel,” *ACI Struct. J.*, vol. 108, no. 5, p. 601, 2011.
- [69] T. L. Vande Voort, M. T. Suleiman, and S. Sritharan, “Design and performance verification of ultra-high performance concrete piles for deep foundations,” 2008.
- [70] S. Alampalli, J. O’Connor, and A. P. Yannotti, “Fiber reinforced polymer composites for the superstructure of a short-span rural bridge,” *Compos. Struct.*, vol. 58, no. 1, pp. 21–27, 2002.
- [71] B. A. Graybeal, “Behavior of Field-Cast Ultra-High Performance Concrete Bridge Deck Connections Under Cyclic and Static Structural Loading,” Office of Infrastructure Research & Development, McLean, VA, Final Report FHWA-HRT-11-023, 2010.
- [72] A. Semendary, E. Steinberg, and K. Walsh, “Implementing Ultra High Performance Concrete (UHPC) with Dowel Bars in Longitudinal Joints (Shear Key) in an Adjacent Box Beam Bridge,” presented at the International Interactive Symposium on Ultra-High Performance Concrete, Des Moines, Iowa, 2016. doi: 10.21838/uhpc.2016.71.
- [73] A. A. of S. H. and T. O. (AASHTO), “AASHTO LRFD Bridge Design Specification, Customary U.S. Units, 8th Edition,” Washington, D. C., 2017.

- [74] Bridgesight Inc., “PGSuper Resource Center,” 2014. <http://www.pgsuper.com/> (accessed Jun. 17, 5AD).
- [75] Florida Department of Transportation (FDOT), “Prestressed Beam-LRFD v5.1,” 2017.
- [76] Y. F. Guyon, “Prestressed Concrete,” *Jointly Publ. Contract. Rec. Ltd John Wiley Sons Inc*, vol. 1, p. 239, 1953.
- [77] B. G. Rabbat and H. G. Russell, “Optimized Sections for Precast, Prestressed Bridge Girders,” *PCI J.*, pp. 88–104, Jul. 1982.
- [78] M. L. Ralls, L. Ybanez, and J. J. Panak, “The New Texas U-Beam Bridges: An Aesthetic and Economical Design Solution,” *PCI J.*, vol. 38, no. 5, pp. 20–29, Sep. 1993.
- [79] W. Podolny and J. M. Muller, *Construction and Design of Prestressed Concrete Segmental Bridges*. New York: John Wiley & Sons, Inc., 1994.
- [80] V. Cervenka, L. Jendele, and J. Cervenka, “ATENA Program Documentation - Theory,” Cervenka Consulting, Dec. 2016.
- [81] N. Grace, E. Jensen, and D. K. Noamesi, “Flexural Performance of Carbon Fiber-Reinforced Polymer Prestressed Concrete Side-by-Side Box Beam Bridge,” *J. Compos. Constr. - ASCE*, vol. 15, no. 5, pp. 663–671, Oct. 2011.
- [82] Florida Department of Transportation (FDOT), “Structures Design Guidelines - FDOT Structures Manual,” 2017.
- [83] Florida Department of Transportation (FDOT), “Bridge Load Rating Manual,” *State Load Rat. Eng.*, Jan. 2020, [Online]. Available: <http://www.fdot.gov/maintenance/LoadRating.shtm>
- [84] J. Cervenka and V. Papanikolaou, “Three Dimensional Combined Fracture-Plastic Material Model for Concrete,” *Int. J. Plast.*, vol. 24, pp. 2192–2220, 2008, doi: 10.1016/j.ijplas.2008.01.004.
- [85] American Society of Civil Engineers (ASCE), “2017 Infrastructure Report Card,” 2017.
- [86] S. Nolan, C. Freeman, A. Kelley, and M. Rossini, “Advancing Small Bridges (Florida Down Under),” presented at the 5th International fib Congress, Melbourne, AU, Oct. 2018.
- [87] Texas Department of Transportation (TxDOT), “Prestressed Concrete Decked Slab Beam Standards,” table14e, Mar. 2018. [Online]. Available: <https://www.dot.state.tx.us/insdtdot/orgchart/cmd/cserve/standard/bridge-e.htm>
- [88] Florida Department of Transportation (FDOT), “SURVEY: FDOT Superstructure Types for Short and Medium Spans,” 2013.
- [89] M. Smith, W. Eriksson, C. Shield, and C. French, “Monitoring and Analysis of Mn/DOT Precast Composite Slab Span System (PCSSS),” University of Minnesota, Minneapolis, MN, MN/RC 2008-41, Sep. 2008.

- [90] M. Halverson, C. French, and C. Shield, “Full-Depth Precast Concrete Bridge Deck System: Phase II,” University of Minnesota, Minneapolis, MN, Final Report MN/RC 2012-30, Oct. 2012.
- [91] F. Menkulasi, T. Cousins, and R. Wollmann, “Implementation of a Precast Inverted T-Beam System in Virginia: Part II: Analytic and Field Investigation,” Virginia Polytechnic Institute and State University, Blacksburg, VA, Final Report FHWA/VTRC 19-R2, Aug. 2018.
- [92] B. A. Graybeal, “Behavior of Ultra-High Performance Concrete Connections between Precast Bridge Deck Elements,” presented at the 2010 Concrete Bridge Conference: Achieving Safe, Smart & Sustainable Bridges, 2010.
- [93] B. A. Graybeal, “Ultra-high-performance concrete connections for precast concrete bridge decks,” *PCI J.*, Fall 2014.
- [94] J. Yuan and B. Graybeal, “Bond Behavior of Reinforcing Steel in Ultra-High Performance Concrete,” Office of Infrastructure Research & Development, McLean, VA, Final Report FHWA-HRT-14-090, Oct. 2014.
- [95] Z. Haber, I. De la Varga, B. Graybeal, B. Nakashoji, and R. El-Helou, “Properties and Behavior of UHPC-Class Materials,” Federal Highway Administration, FHWA-HRT-18-036, Mar. 2018.
- [96] B. A. Graybeal, “Material property characterization of ultra-high performance concrete,” Federal Highway Administration, No. FHWA-HRT-06-103, 2006.
- [97] D. Hordijk, “Local Approach to Fatigue of Concrete,” Dissertation, Technische Universiteit Delft, The Netherlands, 1991.
- [98] American Association of State Highway and Transportation Officials (AASHTO), “AASHTO LRFD Bridge Design Specification, Customary U.S. Units, 7th Edition,” Washington, D. C., 2014.
- [99] T. Helgason, J. M. Hanson, N. F. Somes, W. G. Corley, and E. Hognestad, “Fatigue Strength of High-Yield Reinforcing Bars,” *NCHRP Rep.*, no. 164, 1976.
- [100] Florida Department of Transportation (FDOT), “Developmental Design Standards,” *Index No D20450 Ser. Fla. Slab Beam*, Mar. 2016, [Online]. Available: <http://www.dot.state.fl.us/rddesign/DS/Dev/IDDS/IDDS-D20450.pdf>
- [101] D. Garber, J. Gallardo, D. Deschenes, and O. Bayrak, “Experimental Investigation of Prestress Losses in Full-Scale Bridge Girders,” *ACI Struct. J.*, vol. 112, no. 5, p. 12, 2015.
- [102] M. L. Ralls *et al.*, “Prefabricated Bridge Elements and Systems in Japan and Europe,” Federal Highway Administration, Alexandria, VA, Technical Report FHWA-PL-05-003, Mar. 2005.
- [103] F. Menkulasi and D. Kuruppuarachchi, “Development of Alternative Concrete Bridge Superstructure Systems for Short and Medium Span Bridges,” *Eng. Struct.*, vol. 143, p. 20, Apr. 2017, doi: 10.1016/j.engstruct.2017.04.029.

- [104] F. Chitty, C. Freeman, and D. Garber, “Joint Demand in Slab Beam Bridges,” Aug. 2019, p. 17. [Online]. Available: https://www.pci.org/PCI_Docs/Papers/2019/13_Final_Paper%20Chitty.pdf
- [105] Florida Department of Transportation (FDOT), “Plans Preparation Manual, Volume 1.” Roadway Design Office, Jan. 01, 2017. [Online]. Available: <http://www.fdot.gov/roadway/ppmmanual/2017PPM.shtm>
- [106] G. P. Tilly, “Fatigue of Steel Reinforcement Bars in Concrete: A Review,” *Fatigue Fract. Eng. Mater. Struct.*, vol. 2, no. 3, pp. 251–268, 1979.
- [107] *Code of Federal Regulations - Title 23 - Highways*. Washington DC: National Archives and Records Administration, 2020.
- [108] Florida Department of Transportation (FDOT), “FDOT Design Manual, Volume 1.” Roadway Design Office, Jan. 01, 2020. [Online]. Available: https://fdotwww.blob.core.windows.net/sitefinity/docs/default-source/roadway/fdm/2020/2020fdm102glossary.pdf?sfvrsn=448ee2_2
- [109] F. H. A. (FHWA), “Traffic Data Computation Method - Pocket Guide,” US Department of Transportation, Federal Highway Administration, Washington D.C., FHWA-PL18-027, Aug. 2018.
- [110] Florida Department of Transportation (FDOT), “Project Traffic Forecasting Handbook,” Florida Department of Transportation, Tallahassee, FL, 2019.
- [111] S. Badie, G. Morcou, and M. Tadros, “Simplified Full-Depth Precast Concrete Deck Panel Systems,” Transportation Research Board, Washington D.C., NCHRP Research Report 895, 2018.
- [112] Florida Department of Transportation (FDOT), “Portland Cement Concrete - Florida Slab Beam Superstructure System,” Dev346SRA, Jan. 2016. [Online]. Available: <http://www.fdot.gov/programmanagement/OtherFDOTLinks/Developmental/Files/Dev346SRA.pdf>
- [113] Florida Department of Transportation (FDOT), “Standard Specifications for Road and Bridge Construction,” *Sect. 901 Coarse Aggreg.*, Jul. 2018.
- [114] ASTM International, “ASTM C33 / C33M-18, Standard Specification for Concrete Aggregates,” *West Conshohocken Pa*, 2018, doi: 10.1520/C0033_C0033M-18.

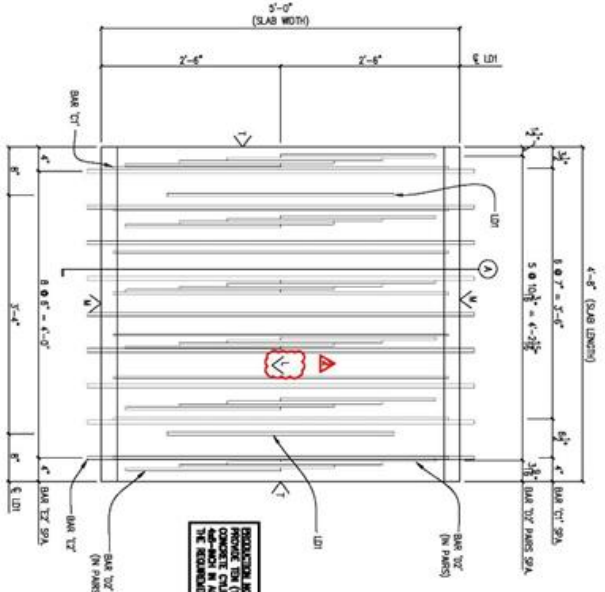
APPENDIX

A. Construction Drawings

The construction drawings for the small-scale and full-scale beam tests are provided in this section.

A.1 Construction Plans for Small-Scale Joint Test Specimens

These specimens were cast in two sets. The first set included all specimens other than the specimens with joint A2.



REINFORCING PLAN VIEW

CONSTRUCTION NOTES:
 1. SHEET BARS TO BE LONGITUDINALLY AS REQUIRED TO CLEAN BARS TO
 2. SHEET BARS TO BE LONGITUDINALLY AS REQUIRED TO CLEAN BARS TO

SLAB BEAM SCHEDULE

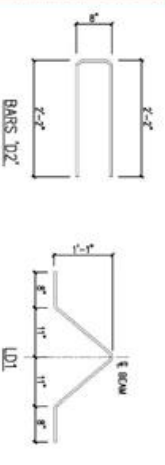
| MARK | QTY. | LENGTH @ E | WIDTH | DL. NOS. |
|---------|------|------------|---------|-----------|
| REBAR 1 | 1 | 4'-0" | 3.500 # | DLR. C.V. |

**REBAR SCHEDULE
(FOR ONE MEMBER ONLY)**

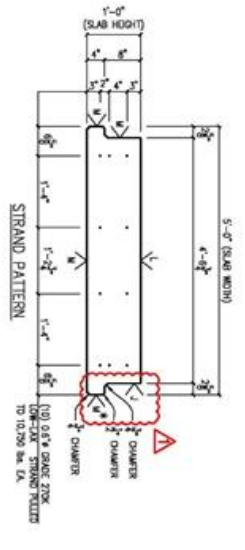
| ITEM | QTY. | PART ID. | SIZE | LENGTH | REMARKS |
|------|------|----------|-------------|--------|---------------|
| C1 | 8 | REBAR 1 | #3 | 4'-0" | STRAIGHT BARS |
| D2 | 24 | REBAR 4 | #3 | 5'-0" | SEC. RIGHT |
| E2 | 9 | REBAR 5 | #3 | 5'-0" | STRAIGHT BARS |
| L01 | 2 | STRAND | 5/8" STRAND | 4'-1" | SEC. RIGHT |

NOTE: ALL BAR DIMENSIONS ARE OUT-TO-OUT
 LENGTH IS IN FEET, INCHES (FT., IN.) UNLS.

REVISED DRAWINGS
 AUGUST 4, 2017
DESTROY ALL OTHERS



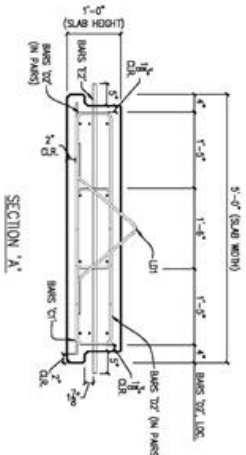
CONSTRUCTION NOTE:
 ADDITIONAL
 CONCRETE CHAMBERS OF SIZE
 4'-0" X 1'-0" IN ACCORDANCE WITH
 THE REQUIREMENTS WITH C&G



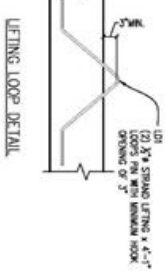
DEFINING SEQUENCE

CONCRETE CLASS VI
 F_c (28 DAYS) = 6,500 PSI
 F_d (RELEASE) = 6,000 PSI

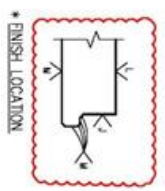
SHIELDING LEGEND
 - - - WIRE REQUIRED



SECTION A-A



LETTING LOOP DETAIL



* ENGLISH LOCATION

STANDARD ENGLISH SYMBOLS:
 NOTE: ALL CONCRETE SURFACE FINISHES SHALL
 CONFORM TO FDOT STANDARD SPECIFICATION
 400-152
 DATE: 7/29/17
 FINISHES:
 ▽ = FORM FINISH
 ▽ = SMOOTH FLAT
 ▽ = AS CAST

| | | | |
|--|---|--------------------------------------|---|
| | PRECAST SLAB DETAIL DURA-STRESS Inc. CA 95028 P.O. BOX 400779 LAS VEGAS, NV 89140-0779 PHONE (352) 781-1422 FAX (352) 781-0080 <small>STRUCTURAL ENGINEERING AND ARCHITECTURAL PRECAST CONCRETE PRODUCTS</small> | | REV. DESCRIPTION DATE BY CHK. 1/1 REVISIONS AS SHOWN 8/4/17 POL 2/1 REVISIONS AS SHOWN 8/4/17 |
| | JOB NAME: N/A LOCATION: N/A ARCHITECT: N/A ENGINEER: N/A CONTRACTOR: N/A PROJ. NO.: N/A | DRAWING NO.: B1757 SHEET: 2 OF 13 | |

CONCRETE NOTES:
 1. REINFORCEMENT TO BE PLACED TO CLEAR BASE 1".
 2. SPLIT BAR 1" LONGITUDINALLY AS REQUIRED TO CLEAR BAR TOP FLANGE.

SLAB BEAM SCHEDULE

| MARK | QTY. | LENGTH @ E | WEIGHT | OL. VOL. |
|------|------|------------|---------|----------|
| PS93 | 1 | 4'-4" | 3.295 # | 0.01 CFT |

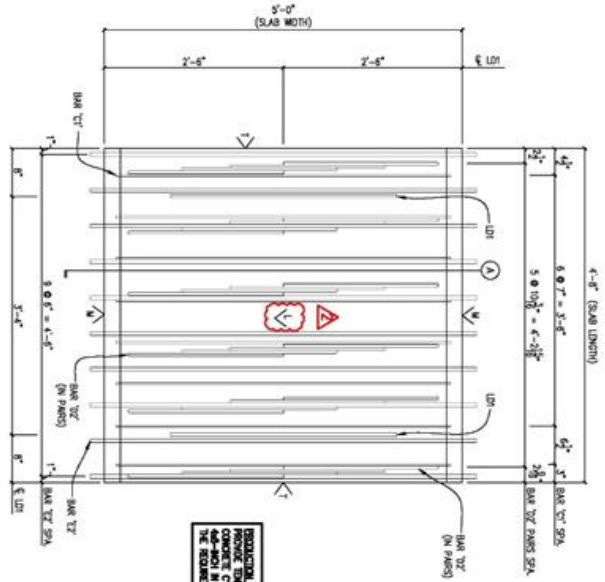
REBAR SCHEDULE

(FOR ONE MEMBER ONLY)

NOTE: ALL BAR DIMENSIONS ARE OUT-TO-OUT
 LENGTH IS IN FEET, INCHES (FT. IN.) UNL.

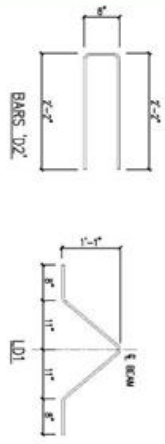
| ITEM | QTY. | PART ID. | SIZE | LENGTH | REMARKS |
|------|------|----------|------|--------|---------------|
| C1 | 8 | REBAR 3 | #3 | 4'-4" | STRAIGHT BARS |
| C2 | 24 | REBAR 4 | #4 | 5'-0" | SEE RIGHT |
| C3 | 10 | REBAR 5 | #5 | 5'-4" | STRAIGHT BARS |

| ITEM | QTY. | PART ID. | SIZE | LENGTH | REMARKS |
|------|------|----------|-------------|--------|-----------|
| LN1 | 2 | STRAND | 5/8" STRAND | 4'-1" | SEE RIGHT |

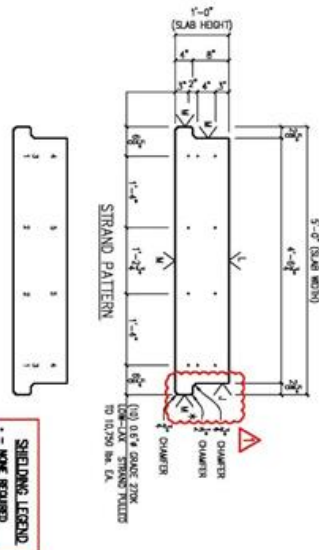


REINFORCING PLAN VIEW

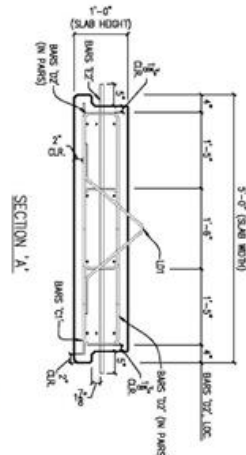
REVISED DRAWINGS
 AUGUST 4, 2017
 DESTROY ALL OTHERS



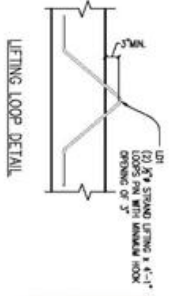
PROTECTIVE NOTES:
 1. REMOVE EXCESSIVE CONCRETE CHANGERS OF SIZE FROM REINFORCEMENT BEFORE CASTING.



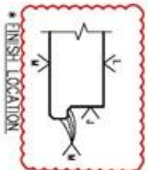
STRAND PATTERN



SECTION 'A-A'



LETTING LOOP DETAIL



FINISH LOCATION

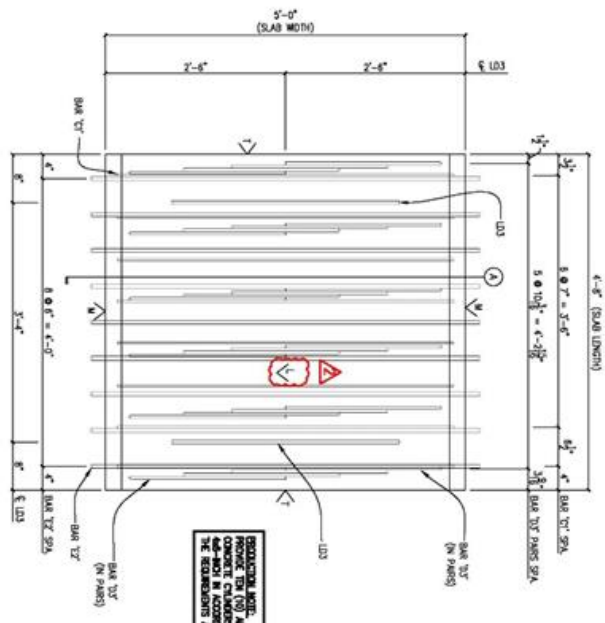
STANDARD FINISH SYMBOLS:
 NOTE: ALL CONCRETE SURFACE FINISHES SHALL CONFORM TO F.O.D.T. STANDARD SPECIFICATION 400-152
 DATE: 1/7/07/07
 FINISHED

▽ = FOG FINISH
 ▽ = SMOOTH FLOAT
 ▽ = AS CAST

DEFINING SEQUENCE
 CONCRETE CLASS VI
 F₁ (28 DAYS) = 6,500 PSI
 F_{0.1} (RELEASE) = 0,000 PSI
 * * * MORE REQUIRED

SHIELDING LEGEND
 * * * MORE REQUIRED

| | | | |
|--|--|--|--|
| | PRECAST SLAB DETAIL DURA-STRESS Inc. CA 95028 P.O. BOX 40279 • LEESSBURG, FL 34749-0279 PHONE (352) 787-1422 FAX (352) 787-0080 <small>STRUCTURAL PROFESSIONAL AND ADMINISTRATIVE PRECAST CONCRETE PRODUCTS</small> | | REV. 1 DESCRIPTION: REVISED AS SHOWN DATE: 8/4/17 BY: FOL CHK: |
| | JOB NAME: N/A LOCATION: N/A ARCHITECT: N/A ENGINEER: N/A CONTRACTOR: N/A PROJ. NO: N/A | | JOB NO: N/A DRAWING NO: B1757 SHEET: 3 OF 13 |



REINFORCING NOTES:
 1. BARS LONGITUDINALLY AS REQUIRED TO CLEAR BAR #2.
 2. SHEET BAR #1 LONGITUDINALLY AS REQUIRED TO CLEAR BAR #2 PANS.

SLAB BEAM SCHEDULE

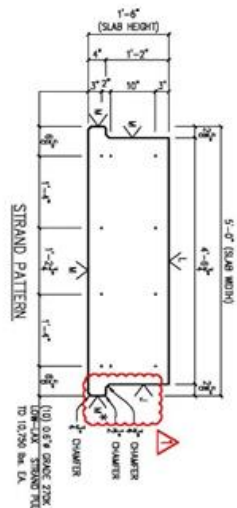
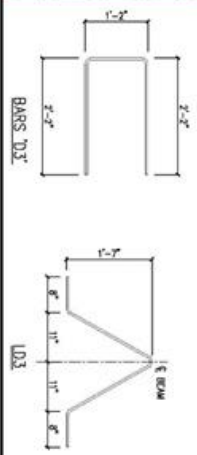
| MARK | QTY | LENGTH @ E | WEIGHT | OL. NOS |
|------|-----|------------|---------|----------|
| FROM | 1 | 4'-0" | 4.881 # | L21 C1-C |

REBAR SCHEDULE (FOR ONE MEMBER ONLY)
 NOTE: ALL BAR DIMENSIONS ARE OUT-TO-OUT
 LENGTH IS IN FEET, INCHES (FT. IN.) UNLS.

| ITEM | QTY | PART ID. | SIZE | LENGTH | REMARKS |
|------|-----|----------|--------|--------|---------------|
| C1 | 8 | REBAR 3 | #3 | 4'-0" | STRAIGHT BARS |
| C2 | 24 | REBAR 4 | #4 | 5'-0" | SEE RIGHT |
| C3 | 9 | REBAR 5 | #5 | 5'-0" | STRAIGHT BARS |
| L21 | 2 | STAND | 5"x11" | 4'-11" | SEE RIGHT |

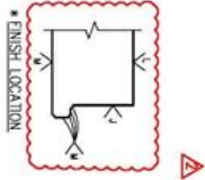
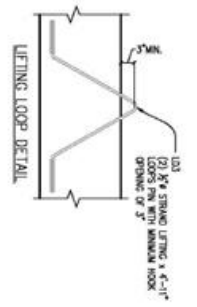
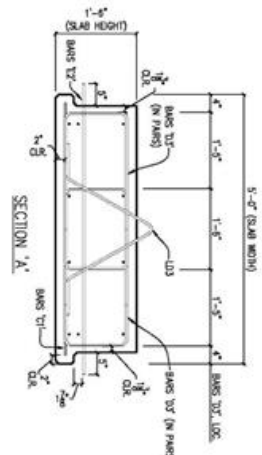
REINFORCING PLAN VIEW

REVISED DRAWINGS
 AUGUST 4, 2017
 DESTROY ALL OTHERS



CONCRETE CLASS VI
DEFINING SEQUENCE
 F_c (28 DAYS) = 8,500 PSI
 F_d (RELEASE) = 8,000 PSI

SHIELDING LEGEND
 - - - NONE REQUIRED



STANDARD FINISH SYMBOLS
 NOTE: ALL CONCRETE SURFACE FINISHES SHALL CONFORM TO FDOT STANDARD SPECIFICATION 400-152

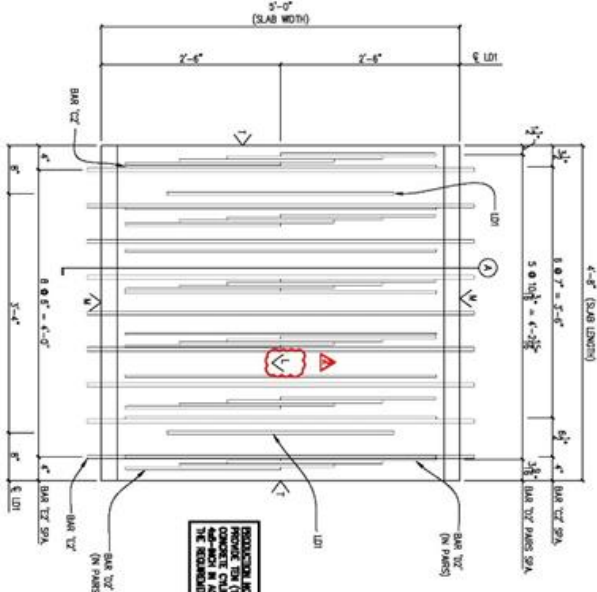
M = FORM FINISH
 S = SMOOTH FLOAT
 V = AS CAST

| | |
|-------------|-----|
| JOB NAME: | N/A |
| LOCATION: | N/A |
| ARCHITECT: | N/A |
| ENGINEER: | N/A |
| CONTRACTOR: | N/A |
| PROJ. NO.: | N/A |

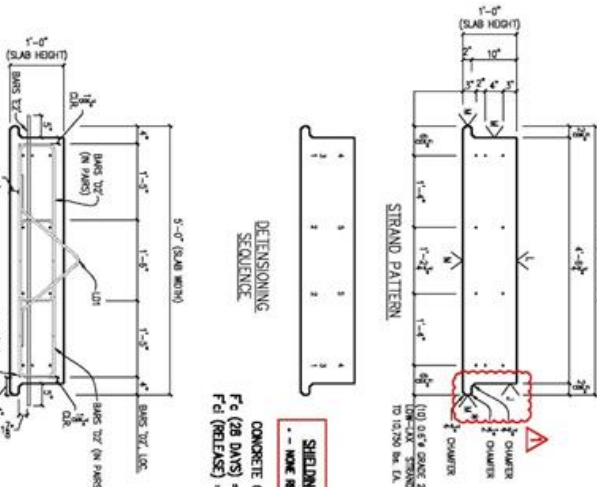
PRECAST SLAB DETAIL
DURA-STRESS Inc.
 CA 95028
 P.O. BOX 480779 LEESBURG, FL 34749-0779
 PHONE (352) 783-1425 FAX (352) 783-2883
 STRUCTURAL ANALYSIS AND ARCHITECTURAL PRECAST CONCRETE PRODUCTS

| REV | DESCRIPTION | DATE | BY | CHK. |
|-----|------------------|--------|-----|------|
| 1 | REVISED AS SHOWN | 8/4/17 | PKL | |
| 2 | REVISED AS SHOWN | 8/4/17 | | |



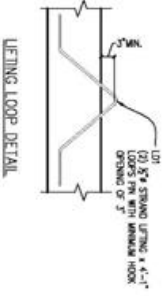


REINFORCING PLAN VIEW

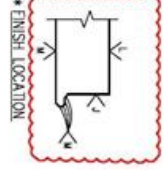


SECTION 'A-A'

REVISED DRAWINGS
AUGUST 4, 2017
DESTROY ALL OTHERS



LIFTING LOOP DETAIL



* ENGLISH LOCATION

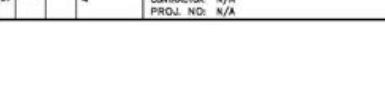
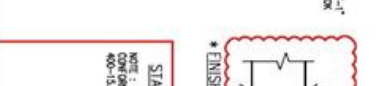
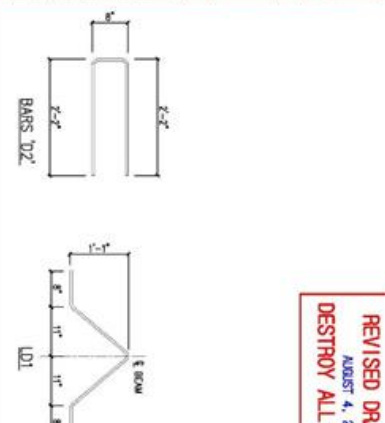
SLAB BEAM SCHEDULE

| MARK | QTY | LENGTH @ E | WEIGHT | QTY | QTY |
|------|-----|------------|---------|---------|-----|
| PROB | 1 | 4'-0" | 3.344 # | QAB C/A | |

REBAR SCHEDULE (FOR ONE MEMBER ONLY)

| ITEM | QTY | PART ID. | SIZE | LENGTH | REMARKS |
|------|-----|----------|-------------|--------|---------------|
| C2 | 8 | REBAR 3 | #3 | 4'-4" | STRAIGHT BARS |
| D2 | 24 | REBAR 4 | #4 | 5'-0" | SEE RIGHT |
| E2 | 8 | REBAR 5 | #3 | 5'-4" | STRAIGHT BARS |
| L01 | 2 | STRAND | 5/8" STRAND | 4'-1" | SEE RIGHT |

NOTE: ALL BAR DIMENSIONS ARE OUT-TO-OUT LENGTHS IN FEET INCHES (FT., IN.) UNLS.



PRECAST SLAB DETAIL

DURA-STRESS Inc.
CA 95038
P.O. BOX 480778 LOS ANGELES, FL 34748-0778
PHONE (352) 787-1422 FAX (352) 787-5085
STRUCTURAL PARTS AND ARCHITECTURAL PRECAST CONCRETE PRODUCTS

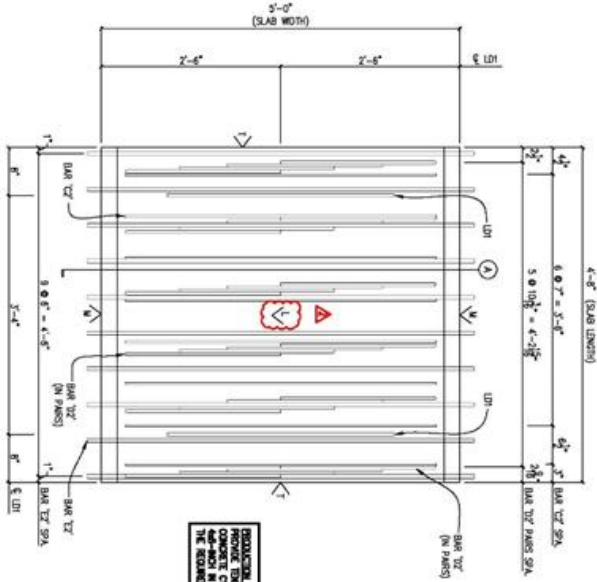
| REV | DESCRIPTION | DATE | BY | CHK. |
|-----|------------------|--------|-----|------|
| 1 | REVISAS AS SHOWN | 8/4/17 | POL | |
| 2 | REVISAS AS SHOWN | 8/4/17 | | |

CONCRETE CLASS VI
F_c (28 DAYS) = 8,500 PSI
F_d (RELEASE) = 6,000 PSI

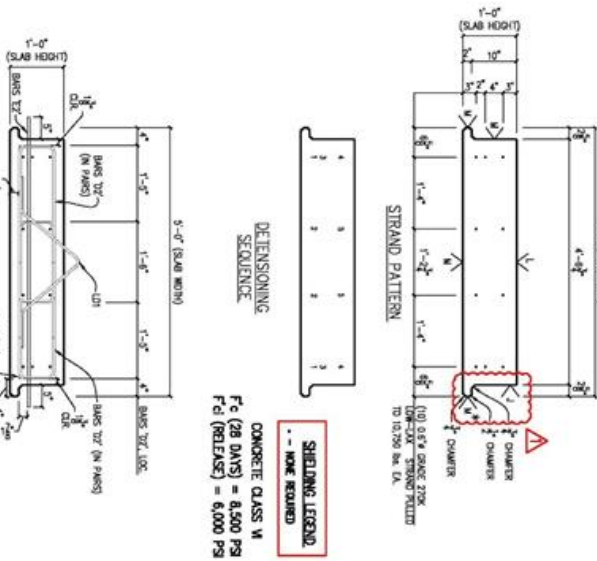
SHIELDING LEGEND
- - - HOOK REQUIRED

STANDARD FINISH SYMBOLS:
NOTE: ALL CONCRETE SURFACE FINISHES SHALL CONFORM TO F.O.D.T. STANDARD SPECIFICATION 400-152
DATE: 7/29/17
DESIGNED:
JOB NAME: N/A
LOCATION: N/A
ARCHITECT: N/A
ENGINEER: N/A
CONTRACTOR: N/A
PROJ. NO.: N/A

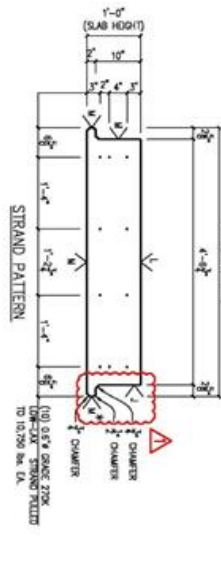
58 JOB NO: **B1757**
SHEET: 6 of 13



REINFORCING PLAN VIEW



SECTION 'A'



STRAND PATTERN

REVISIONS:
 1. REVISIONS TO BE MADE IN ACCORDANCE WITH THE REVISIONS LISTED ON SHEET 7-D13.

SHIELDING LEGEND
 - - - - - NOT REQUIRED

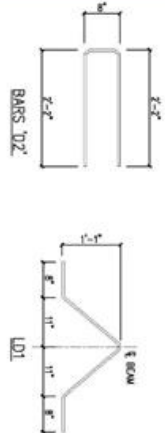
CONCRETE CLASS VI
 F_c (28 DAYS) = 8,500 PSI
 F_d (RELEASE) = 6,000 PSI

REINFORCING NOTES:
 1. SHIRT BAR 1\"/>

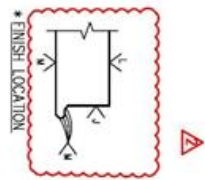
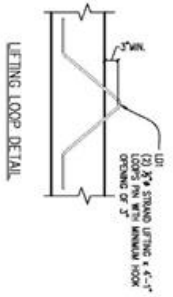
| SLAB BEAM SCHEDULE | | | | |
|--------------------|------|------------|--------|-----------|
| MARK | QTY. | LENGTH @ E | WEIGHT | DL. VOL. |
| REBAR 1 | 1 | 4'-8" | 3.34 # | 0.00 C.Y. |

REBAR SCHEDULE (FOR ONE MEMBER ONLY)
 NOTE: ALL BAR DIMENSIONS ARE OUT-TO-OUT. LENGTH IS IN FEET, INCHES (FT., IN.) UNLS.

| ITEM | QTY. | PART ID. | SIZE | LENGTH | REMARKS |
|------|------|----------|------|--------|---------------|
| C1 | 8 | REBAR 1 | #3 | 4'-8" | STRAIGHT BARS |
| D1 | 24 | REBAR 4 | #3 | 5'-0" | SEC. NORTH |
| E1 | 10 | REBAR 3 | #3 | 5'-0" | STRAIGHT BARS |



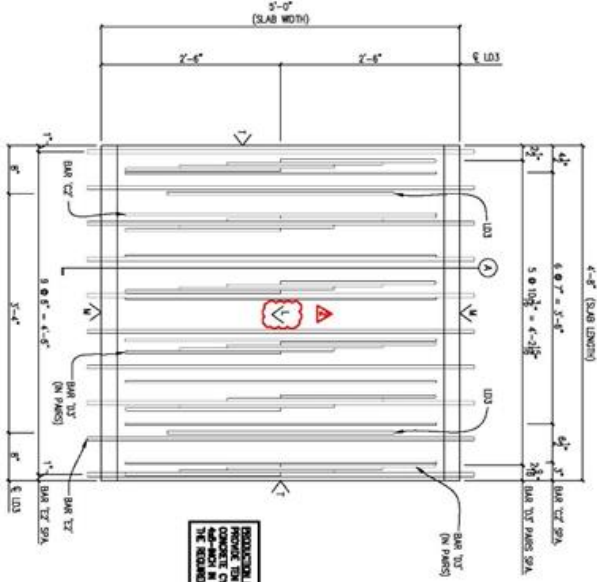
REVISED DRAWINGS
 MUST 4, 2017
 DESTROY ALL OTHERS



STANDARD FINISH SYMBOLS
 NOTE: ALL CONCRETE SURFACE FINISHES SHALL CONFORM TO FLAT STANDARD PREPARATION 400-152

◊ = FORM FINISH
 ◊ = SMOOTH FLAT
 ◊ = AS CAST

| | | | | | | |
|--|---|--|--|--------------------------|------------------|--------------|
| | PRECAST SLAB DETAIL DURA-STRESS Inc. CA 95028 P.O. BOX 480779 LEESBURG, FL 34748-0779 PHONE (352) 781-1429 FAX (352) 781-2085 STRUCTURAL ENGINEERING AND ARCHITECTURAL PRECAST CONCRETE PRODUCTS | | REV. 1 DESCRIPTION 1 REVISED AS SHOWN 2 REVISED AS SHOWN | DATE 8/4/17 8/4/17 | BY POL POL | CHK. |
| | JOB NAME: N/A LOCATION: N/A ARCHITECT: N/A ENGINEER: N/A CONTRACTOR: N/A PROJ. NO.: N/A | DRAWN BY: N/A CHECKED BY: N/A DATE: 1/27/2017 RELEASED: | 55 498 NOS 81757 SHEET: 7-D13 | | | |



REINFORCING PLAN VIEW

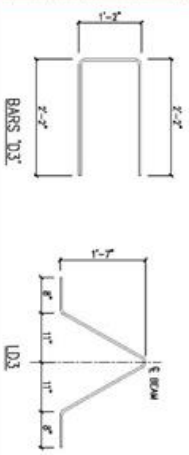
EXPLANATORY NOTES:
 1. SHEET BAR #27 BARS LONGITUDINALLY AS REQUIRED TO CLEAR BAR #2.
 2. SHEET BAR #2 LONGITUDINALLY AS REQUIRED TO CLEAR BAR #3 PLANK.

REVISED DRAWINGS
 AUGUST 4, 2017
DESTROY ALL OTHERS

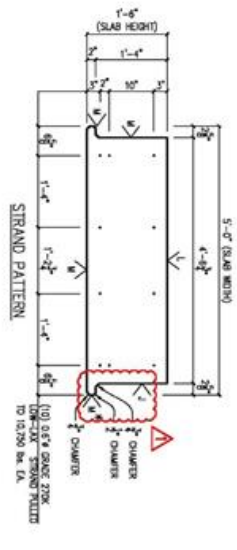
| SLAB BEAM SCHEDULE | | | | | |
|--------------------|-----|------------|---------|-----------|--------|
| MARK | QTY | LENGTH @ E | WEIGHT | CL. 95 | CL. 95 |
| P909 | 1 | 4'-6" | 4.840 # | 1.20 C.V. | |

| REBAR SCHEDULE (FOR ONE MEMBER ONLY) | | | | | |
|--------------------------------------|-----|----------|-------------|--------|---------------|
| ITEM | QTY | PART ID. | SIZE | LENGTH | REMARKS |
| C2 | 8 | REBAR 3 | #3 | 4'-4" | STRAIGHT BARS |
| D3 | 24 | REBAR 4 | #4 | 5'-6" | SEE RIGHT |
| E2 | 10 | REBAR 5 | #5 | 5'-4" | STRAIGHT BARS |
| L03 | 2 | STRAIGHT | 5/8" STRAND | 4'-11" | SEE RIGHT |

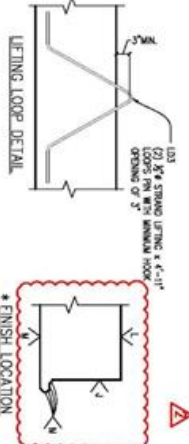
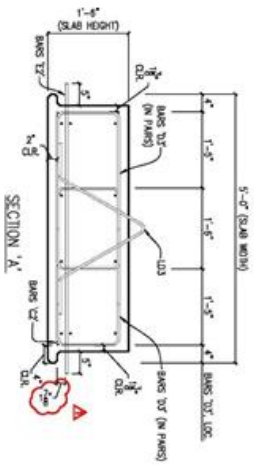
NOTE: ALL BAR DIMENSIONS ARE OUT-TO-OUT LENGTH IS IN FEET INCHES (F.T., IN.) UNLS.



PRODUCTION NOTE:
 REBAR AND STRAND CONCRETE CHAMBERS OF SIZE 4'-0" X 5'-0" IN ACCORDANCE WITH THE REQUIREMENTS FOR BAR CUT.



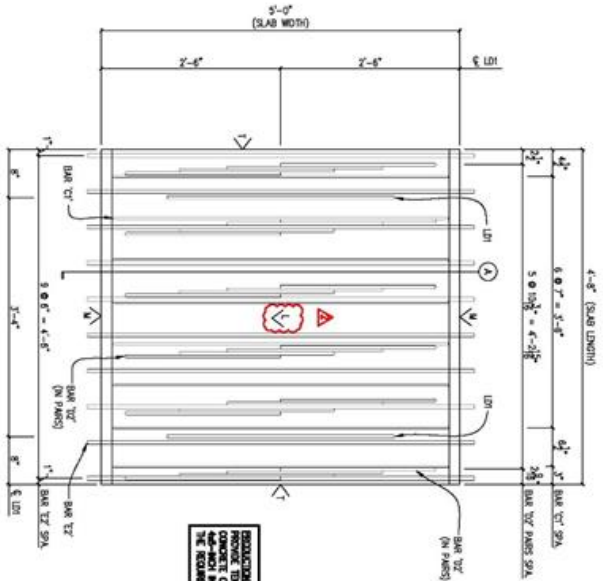
SHIELDING LEGEND
 - - - NONE REQUIRED
 CONCRETE CLASS VI
 F_c (28 DAYS) = 8,500 PSI
 F_d (RELEASE) = 6,000 PSI



STANDARD FINISH SYMBOLS:
 NOTE: ALL CONCRETE SURFACE FINISHES SHALL CONFORM TO F.O.D.T. STANDARD SPECIFICATION 400-152
 - - - FORM FINISH
 - - - SMOOTH FLOAT
 - - - AS CAST

| | | | |
|--|--|--|--|
| <p>JOB NAME: N/A LOCATION: N/A ARCHITECT: N/A ENGINEER: N/A CONTRACTOR: N/A PROJ. NO: N/A</p> | <p>PRECAST SLAB DETAIL DURA-STRESS Inc. CA 95028 P.O. BOX 480779 LOS ANGELES, FL 34748-0779 PHONE (352) 787-1422 FAX (352) 787-5085 STRUCTURAL ENGINEERING AND ARCHITECTURAL PRECAST CONCRETE PRODUCTS</p> | <p>REV. DESCRIPTION DATE BY CHK. 1/1 REVISIONS AS SHOWN 8/4/17 POL 2/1 REVISIONS AS SHOWN 8/4/17</p> | |
|--|--|--|--|

DATE: 7/29/17
 DRAWN BY: B1757
 SHEET: 9 OF 13

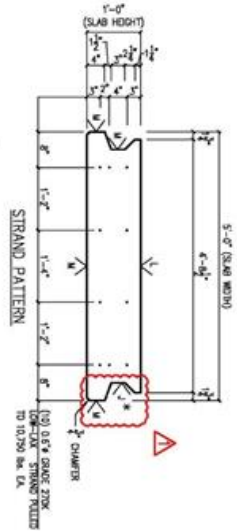
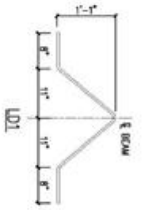
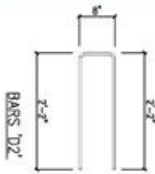


REINFORCING PLAN VIEW

EXPLANATORY NOTES:
 1. SHEET BAR 1\"/>

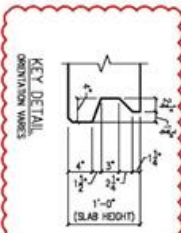
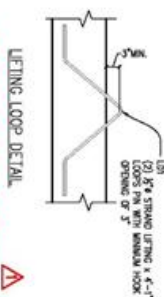
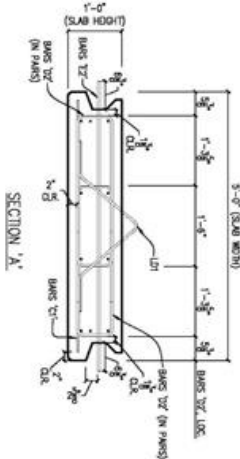
| SLAB BEAM SCHEDULE | | | | | |
|---|-----|------------|---------|--------|---------------|
| MARK | QTY | LENGTH @ E | WEIGHT | | |
| PH01 | 1 | 4'-8" | 3.269 # | | |
| REBAR SCHEDULE (FOR ONE MEMBER ONLY) NOTE: ALL BAR DIMENSIONS ARE OUT-TO-OUT LENGTH IS IN FEET, INCHES (F.T., IN.) UNLS. | | | | | |
| ITEM | QTY | PART ID. | SIZE | LENGTH | REMARKS |
| C1 | 8 | REBAR 3 | #3 | 4'-8" | STRAIGHT BARS |
| C2 | 24 | REBAR 4 | #4 | 5'-0" | SEE RIGHT |
| C3 | 10 | REBAR 5 | #3 | 5'-0" | STRAIGHT BARS |
| STRAND SCHEDULE ITEM 2 STRAND #4 STRAND 4'-1" SEE RIGHT | | | | | |

REVISED DRAWINGS
 AUGUST 4, 2017
DESTROY ALL OTHERS



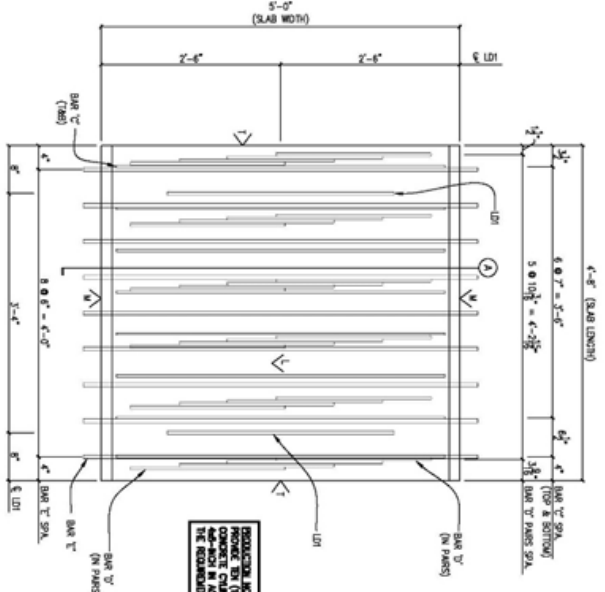
SHIELDING LEGEND
 - - NONE REQUIRED
 CONCRETE CLASS VI
 F_{cd} (28 DAYS) = 8,500 PSI
 F_{cd} (RELEASE) = 6,000 PSI

DEFENSIONING SEQUENCE
 SET KEY DETAIL



STANDARD FINISH SYMBOLS
 NOTE: ALL CONCRETE SURFACE FINISHES SHALL CONFORM TO FDOT STANDARD SPECIFICATION 400-15.2
 DATE: 1/7/2017
 FINISHING: [Symbol] = FORM FINISH
 [Symbol] = SMOOTH FLOAT
 [Symbol] = AS CAST

| | | | |
|---|--|--|--|
| <p>DURA-STRESS Inc. P.O. BOX 490779 LEESBURG, FL 34748-0779 PHONE (352) 787-1422 FAX (352) 787-5080 STRUCTURAL PRECAST/STRESSING AND ADDED/REINFORCED PRECAST CONCRETE PRODUCTS</p> | JOB NAME: N/A LOCATION: N/A ARCHITECT: N/A ENGINEER: N/A CONTRACTOR: N/A PROD. NO.: N/A | REV: [] DESCRIPTION: REVISD AS SHOWN DATE: 8/4/17 BY: PKL CHK: [] | |
| | OS JOB NO.: B1757 SHEET: 11 of 13 | | |



EXPLANATORY NOTES:
 1. SPLIT BAR 'V' PARS LONGITUDINALLY AS REQUIRED TO CLEAR BARS 'E'.
 2. SPLIT BAR 'C' LONGITUDINALLY AS REQUIRED TO CLEAR BAR 'V' PARS.

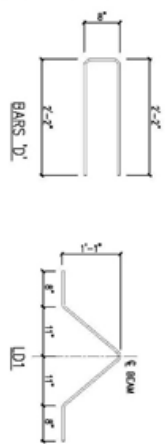
SLAB BEAM SCHEDULE

| MARK | QTY. | LENGTH @ E | WEIGHT | CL. TO S |
|---------|------|------------|---------|-----------|
| REBAR 1 | 1 | 4'-8" | 3.540 # | 0.80 C.V. |

REBAR SCHEDULE (FOR ONE MEMBER ONLY)
 NOTE: ALL BAR DIMENSIONS ARE OUT-TO-OUT (LENGTH IS IN FEET, INCHES (FT., IN.) UNLS.)

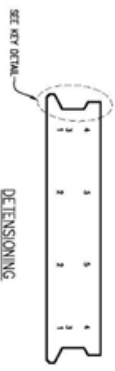
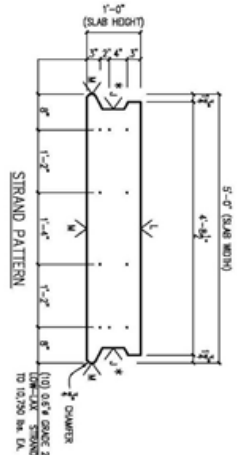
| ITEM | QTY. | PART ID. | SIZE | LENGTH | REMARKS |
|------|------|----------|------|--------|---------------|
| C | 15 | REBAR 3 | #3 | 4'-7" | STRAIGHT BARS |
| D | 24 | REBAR 4 | #4 | 5'-0" | SET RIGHT |
| E | 9 | REBAR 5 | #5 | 5'-0" | STRAIGHT BARS |

**FOR YOUR
 FEBRUARY 19, 2018
 APPROVAL**



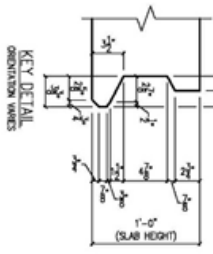
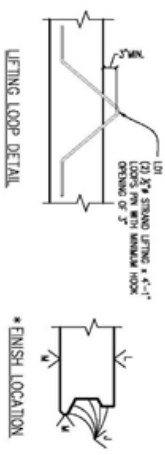
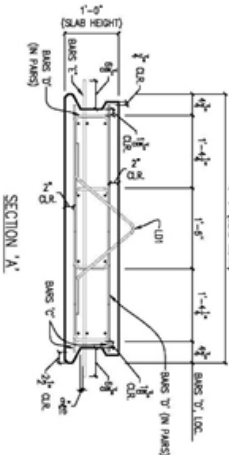
REINFORCING PLAN VIEW

EXPLANATORY NOTE:
 ADDITIONAL CONCRETE CHANGES OF SIZE AND LOCATION IN ACCORDANCE WITH THE REQUIREMENTS WITH C.A.



CONCRETE CLASS VI
F_c (28 DAYS) = 8,500 PSI
F_d (RELEASE) = 6,000 PSI

SHIELDING LEGEND
 - - - NONE REQUIRED



STANDARD ENGLISH SYMBOLS
 NOTE: ALL CONCRETE SURFACE FINISHES SHALL CONFORM TO F.O.D.T. STANDARD SPECIFICATION 400-15.2
 M = HEAVY SANDCAST
 N = FORM FINISH
 V = SMOOTH FLOAT
 T = AS CAST

| | |
|---------------|--------|
| JOB NAME: | N/A |
| LOCATION: | N/A |
| ARCHITECT: | N/A |
| ENGINEER: | N/A |
| CONTRACTOR: | N/A |
| PROJ. NO.: | N/A |
| ISS. AND NO.: | 81779 |
| DATE: | 2/7/18 |
| DESIGNED BY: | |
| CHK. BY: | |
| APP. BY: | |
| DATE: | 1/12 |

PRECAST SLAB DETAIL
DURA-STRESS Inc.
 CA 95028
 P.O. BOX 480779 LOS ANGELES, CA 90048-0779
 PHONE (352) 782-1422 FAX (352) 782-5095
 STRUCTURAL PARTS AND ARCHITECTURAL PRECAST CONCRETE PRODUCTS

| REV | DESCRIPTION | DATE | BY | CHK. |
|-----|-------------|------|----|------|
| | | | | |



A.2 Construction Procedure for Joints of Small-Scale Specimens

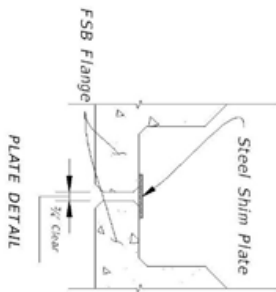
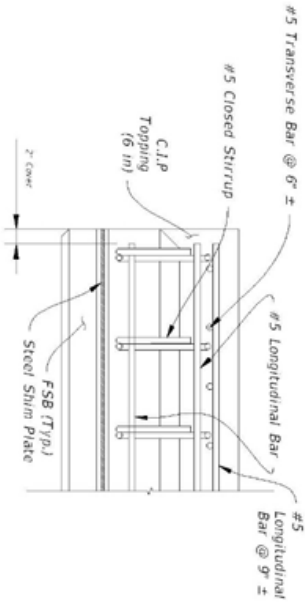
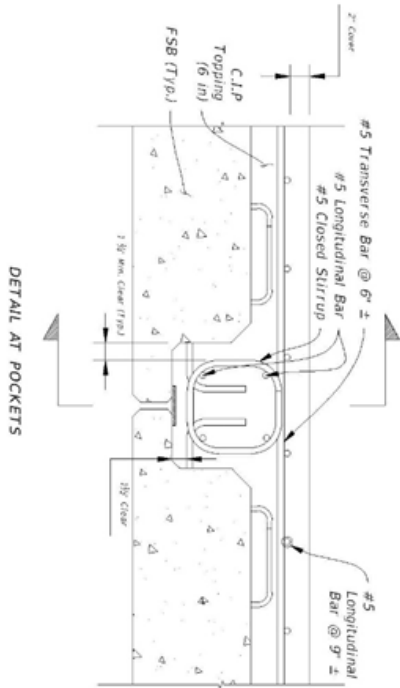
DETAIL AT POCKET

CONSTRUCTION STEPS

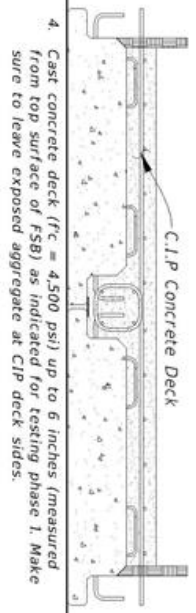
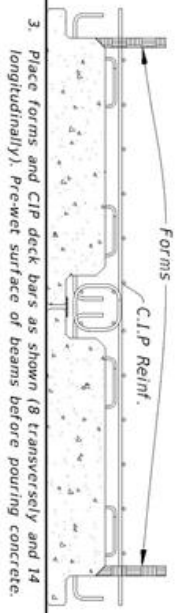
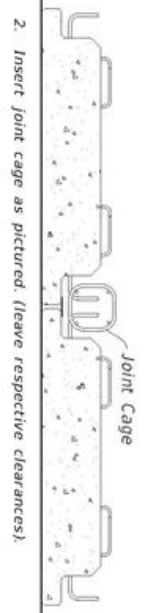
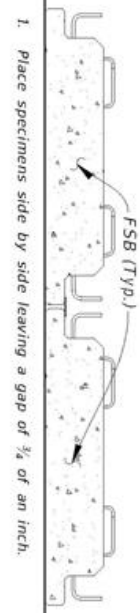
1. Place specimens side by side leaving a gap of 1/4 of an inch
2. Place form with channel shape and pre-wet before pouring UHPC
3. Cast UHPC (Ductal) in pocket as shown

Note: Apply same procedure to all FDOT specimens. Provide five (5) UHPC cylinders of size 3x6-inch per joint.

| PROJECT | | SECTION | | REVISIONS | | DATE | |
|------------------|----|------------------------------|----|--|----|--------------|----|
| NO. 111 | 11 | 11 | 11 | 11 | 11 | 11 | 11 |
| PROJECT NAME | | SECTION NAME | | REVISIONS | | DATE | |
| STATE OF FLORIDA | | REPARTMENT OF TRANSPORTATION | | F.S.B. Construction Procedure - FDOT 2 (18 in) | | Sheet 1 of 1 | |
| DESIGNED BY | | CHECKED BY | | APPROVED BY | | DATE | |
| DRAWN BY | | SCALE | | PROJECT NO. | | SHEET NO. | |
| DATE | | PROJECT | | SHEET | | OF | |

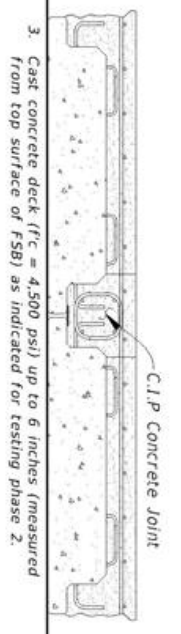
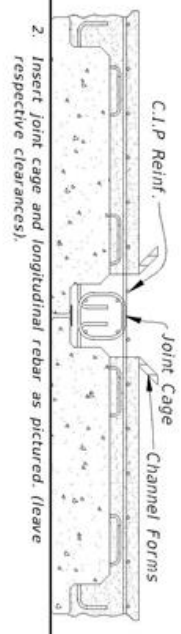
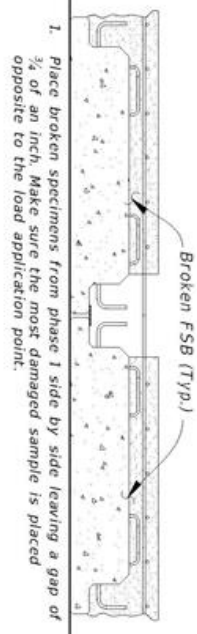


| DATE | | BY | | REVISION | | DATE | | BY | | REVISION | | DATE | | BY | | REVISION | | | | | | | | | | | | | |
|--|-------------------------------------|------------------|--|----------|--|------|--|----|--|----------|--|------|--|----|--|----------|--|--------------|-------------------------|------------------|--|-----------------|-------------------------------------|-----------------|--|-------------|------------|------------------|------------|
| 08/21/17 | CT | 1000 | MSQ | DESIGN | | | | | | | | | | | | | | | | | | | | | | | | | |
| <table border="0" style="width: 100%;"> <tr> <td style="width: 25%;">OWNER</td> <td style="width: 25%;">STATE OF FLORIDA</td> <td style="width: 25%;">PROJECT</td> <td style="width: 25%;">FSB Construction Procedure - Current FSB (CIP DECK)</td> </tr> <tr> <td>DESIGNER</td> <td>REPAIRMENT OF TRANSPORTATION</td> <td>CONTRACT</td> <td>FSB WITH UJRPC JOINT CONNECTION</td> </tr> <tr> <td>DATE</td> <td>N/A</td> <td>PROJECT #</td> <td>N/A</td> </tr> </table> | | | | | | | | | | | | | | | | | | OWNER | STATE OF FLORIDA | PROJECT | FSB Construction Procedure - Current FSB (CIP DECK) | DESIGNER | REPAIRMENT OF TRANSPORTATION | CONTRACT | FSB WITH UJRPC JOINT CONNECTION | DATE | N/A | PROJECT # | N/A |
| OWNER | STATE OF FLORIDA | PROJECT | FSB Construction Procedure - Current FSB (CIP DECK) | | | | | | | | | | | | | | | | | | | | | | | | | | |
| DESIGNER | REPAIRMENT OF TRANSPORTATION | CONTRACT | FSB WITH UJRPC JOINT CONNECTION | | | | | | | | | | | | | | | | | | | | | | | | | | |
| DATE | N/A | PROJECT # | N/A | | | | | | | | | | | | | | | | | | | | | | | | | | |
| <table border="0" style="width: 100%;"> <tr> <td style="width: 25%;">SCALE</td> <td style="width: 25%;">AS SHOWN</td> <td style="width: 25%;">SHEET NO.</td> <td style="width: 25%;">3</td> </tr> </table> | | | | | | | | | | | | | | | | | | SCALE | AS SHOWN | SHEET NO. | 3 | | | | | | | | |
| SCALE | AS SHOWN | SHEET NO. | 3 | | | | | | | | | | | | | | | | | | | | | | | | | | |



CONSTRUCTION STEPS - Phase 1

Note: Provide five (5) concrete cylinders of size 4x8-inch per phase of casting.



CONSTRUCTION STEPS - Phase 2

| | | | | | | | |
|---|-------------|---------------|--------------------------|---|-------------|---------------|--------------------------|
| DATE | | REVISED | | DATE | | REVISED | |
| 08/29/17 | CF | HW | SR | HW | SR | HW | SR |
| PROJECT INFORMATION | | | | PROJECT INFORMATION | | | |
| PROJECT NO. | 17-00000000 | PROJECT NAME | FLORIDA TURNPIKE PROJECT | CONTRACT NO. | 17-00000000 | CONTRACT NAME | FLORIDA TURNPIKE PROJECT |
| CONTRACT NO. | 17-00000000 | CONTRACT NAME | FLORIDA TURNPIKE PROJECT | CONTRACT NO. | 17-00000000 | CONTRACT NAME | FLORIDA TURNPIKE PROJECT |
| STATE OF FLORIDA | | | | STATE OF FLORIDA | | | |
| DEPARTMENT OF TRANSPORTATION | | | | DEPARTMENT OF TRANSPORTATION | | | |
| CONTRACT NO. | 17-00000000 | CONTRACT NAME | FLORIDA TURNPIKE PROJECT | CONTRACT NO. | 17-00000000 | CONTRACT NAME | FLORIDA TURNPIKE PROJECT |
| FSB Construction Procedure - Current FSB - Phases | | | | FSB Construction Procedure - Current FSB - Phases | | | |
| FIU - FSB with UHPC Joint Connection | | | | FIU - FSB with UHPC Joint Connection | | | |
| SHEET NO. | | | | SHEET NO. | | | |
| 4 | | | | 4 | | | |

B. Fatigue Loading Scheme for Small-Scale Joint Specimens

One of the goals of the small-scale fatigue testing was to simulate truck traffic loading on the UHPC joint over the expected 100-year service life of the bridge. Note that the fatigue testing was limited to 2 million cycles of load applied and a maximum 2 Hz load rate, due to schedule and laboratory limitations. The FSB section was originally restricted to off-system bridges with a low average daily traffic (ADT) and average daily truck traffic (ADTT) [54]. Off-system projects are bridges not located on the State Highway System (SHS) or the National Highway System (NHS). According to the FDOT Plans Preparation Manual, Volume 1, Glossary of Terms [105], the standards for low volume highways in annual average daily volumes in collector systems are summarized in Table B.1. These characteristics were the basic values of the fatigue loading scheme definition. Two main assumptions were made in terms of truck traffic number and the range of the fatigue load and are described in the following sections.

Table B.1: FDOT standards for low volume highways (AADT: Annual Average Daily Traffic)

| Highway Type | | Low Volume AADT |
|-------------------|-----------------|-----------------|
| Collector - Urban | 2-Lane Facility | 11,000 |
| | 4-Lane Facility | 37,000 |
| Collector - Rural | 2-Lane Facility | 8,000 |
| | 4-Lane Facility | 30,000 |

B.1 Assumption for Truck Traffic Number

The highest AADT was selected from Table B.1 to ensure the bridge could be used in all locations with 4-lane configurations; the AADT of a 4-lane urban collector is 37,000. FDOT Plans Preparation Manual [105] recommends that the truck traffic be taken as 10

percent of the AADT or the daily count (24-hour count). As a result, the average annual daily truck traffic (AADTT) was 3,700 trucks. This quantity accounts for bidirectional truck traffic, and because the specimen dimension is less than one-lane width (2.7 meters [8' – 10 ¾"]), the truck numbers must be decreased to unidirectional traffic. The most recent AASHTO LRFD Bridge Design Specifications (§C3.6.1.4.2) [98] states that one direction of traffic carries more than one-half of the bidirectional AADT; thus, designing for 55 percent of the bidirectional AADT is recommended. This factor allows the bidirectional truck traffic number to drop from 3,700 to 2,035 unidirectional truck traffic. Using this AADTT over the 100-year service life give a total of 203,500 trucks passing over the UHPC joint. Note that this does not include traffic growth data for the intended design life, so an assumption will be done to account for any uncertainties.

B.2 Assumption for Fatigue Load Range

The type of truck load used in the fatigue testing was the HL-93 as specified in AASHTO LRFD Bridge Design Specifications (§3.6.1.4) [98], Each truck has two axle groups of 32 kips and each axle group has four-wheel loads with two of them closely spaced. Because one truck width does not fit entirely in the fatigue specimen width, a half-width truck was used. Therefore, the wheel patch that was used was the same as the strength testing accounting for the largest wheel area and stress. Since each half-width truck has four 51 by 25 centimeters (20-inch wide by 10-inch) long wheel loads, the number of cycles for a 100-year service life test is four times 203,500 trucks, which is 814,000 cycles. Due to uncertainties of traffic growth previously described, the number of cycles was increased to 900,000 cycles, which translated to about a 10-percent increase. Because the maximum

number of cycles permitted was 2,000,000, three different fatigue load ranges were executed, which will be discussed in the following section.

B.3 Fatigue Loaf Testing Protocol

The fatigue loading scheme is shown in Table B.2. The *first load range step* (calibration) was to make sure that sensors were reading correctly, cycled load was stable, and the specimens were behaving as expected for the prescribed load range. Fatigue loading was paused for one day following the calibration stage for the data to be processed. The beams were also visually inspected for cracking or any other damage that occurred; cracking and damage were marked, labeled, photographed, and documented. There were no complications experienced in the calibration stages for these specimens, so the fatigue testing continued with the second step (before cracking performance).

Table B.2: Fatigue Loading Scheme

| Loading type | Load Range Steps | Lower Limit Load | Upper Limit Load | Frequency | # Cycles |
|--------------|---------------------------------|------------------|--------------------|-----------|----------|
| Fatigue | 1 - Calibration | 2 kip | 12.64 kip | 2 Hz | 200,000 |
| | 2 – Before Cracking Performance | 2 kip | 12.64 kip | 2 Hz | 900,000 |
| | 3 – After Cracking Performance | 19 kip | 31 kip | 1 Hz | 900,000 |
| Strength | 4 – Overload Performance | 0 kip | 100 % Failure Load | N/A | N/A |

The *second load range step* in the fatigue testing was aimed at evaluating the behavior of the joint under the expected fatigue loading and cycles for a 100-year service life. The fatigue load was under the cracking load for these specimens, so the fatigue testing was

also used to see if the fatigue loading would cause cracking or debonding between the UHPC and precast system. The range of loading for this second cycle was calculated using Equation B-1.

$$P = (1 + IM) * P_{wheel} \quad \text{Equation B-1}$$

$$P = (1 + 0.33) * 8 \text{ k} = 10.64 \text{ kips}$$

P was added to the lower limit to calculate the upper limit, as shown in Equation B-2.

$$P_{upper} = (1 + IM) * P_{wheel} + P_{lower} \quad \text{Equation B-2}$$

$$P_{upper} = 10.64 \text{ k} + 2 \text{ k} = 12.64 \text{ kips}$$

where:

IM = Dynamic Load Allowance = 0.33 from AASHTO LRFD Bridge Design Specifications (§3.6.2.1) [98]

P_{wheel} = HL-93 rear axle wheel load = 8 kips

P_{lower} = lower cyclic load

P_{upper} = upper cyclic load

The *third load range step* was used to evaluate the effect of cycling from below to above the cracking load on crack growth, bond loss of joint reinforcement, and overall degradation of the system performance. The fatigue load range was selected based on the fatigue stress range in the reinforcement, as discussed above.

After all the fatigue load ranges are applied, the specimens were subjected to static load until failure. The static load test procedure was the same as the other static load tests.

B.4 Assumption for Truck Traffic Number

The upper load range was based on the strain and stress ranges in the reinforcing steel. There have been several previous studies investigating the low-cycle and high cycle fatigue strength of reinforcing steel [99], [106]. Since the available cycles for the upper load range was 900,000 cycles, lower and upper loads were selected to cause a stress range in the reinforcement that would have a theoretical fatigue life greater than 1,000,000 cycles. The goal of this fatigue testing was not to fatigue the reinforcement, but to see if the bond between the reinforcement and the UHPC was adversely affected by fatigue loading.

An NCHRP study was conducted by Helgason et al. [99] investigating the fatigue strength of reinforcing bars in concrete. The results from this study are summarized in Figure B.1. They found that the fatigue strength of the bars was affected by the grade reinforcement, size of bar, stress range (f_r) and low applied stress.

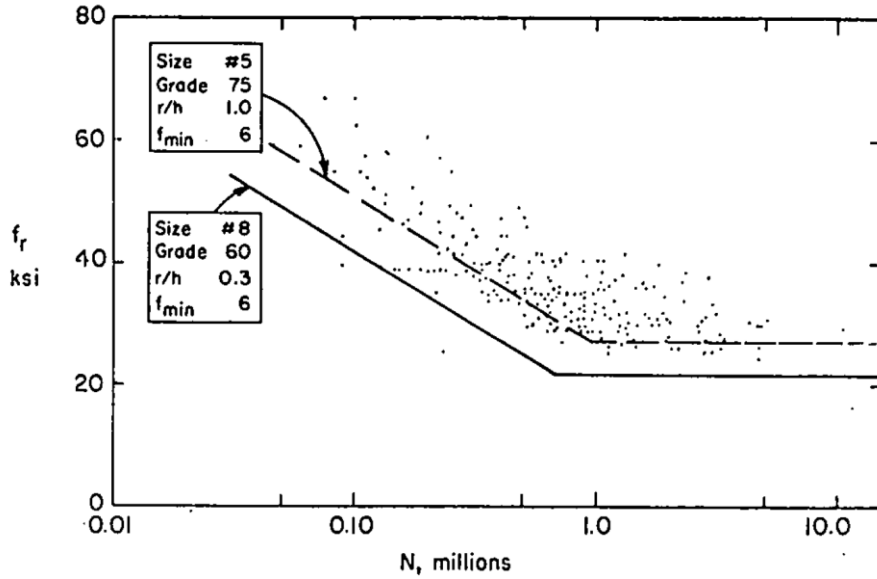


Figure B.1: Summary of results and recommended design provision [99]

The results from this testing were used to develop a recommended design equation, shown in Equation B-3.

$$f_r = 21 - 0.33f_{min} + 8(r/h) \quad \text{Equation B-3}$$

Where:

f_r = stress range (ksi)

f_{min} = corresponding minimum tensile stress (positive) or maximum compressive stress (negative) (ksi)

r/h = ratio of base radius to height of rolled-on deformations (taken as 0.3 if unknown)

Using this expression and looking at the test results, a stress range of 138 MPa (20 ksi) in the reinforcement was selected for the after-cracking fatigue loading. This stress range was used to get the load range recommended in the following section.

The fatigue load range was based on an average 138-MPa (20-ksi) stress range in the steel, which corresponds to a strain range of 690 microstrain. The load range was selected based on this strain range using the strain versus load response of the reinforcement from the static tests, shown in Figure B.2. The load range was shifted to ensure that both the visual cracking load and the cracking load from the concrete surface gauges were within the load range. A load range of 131 MPa (19 kips) to 214 MPa (31 kips) was selected for all the fatigue specimens.

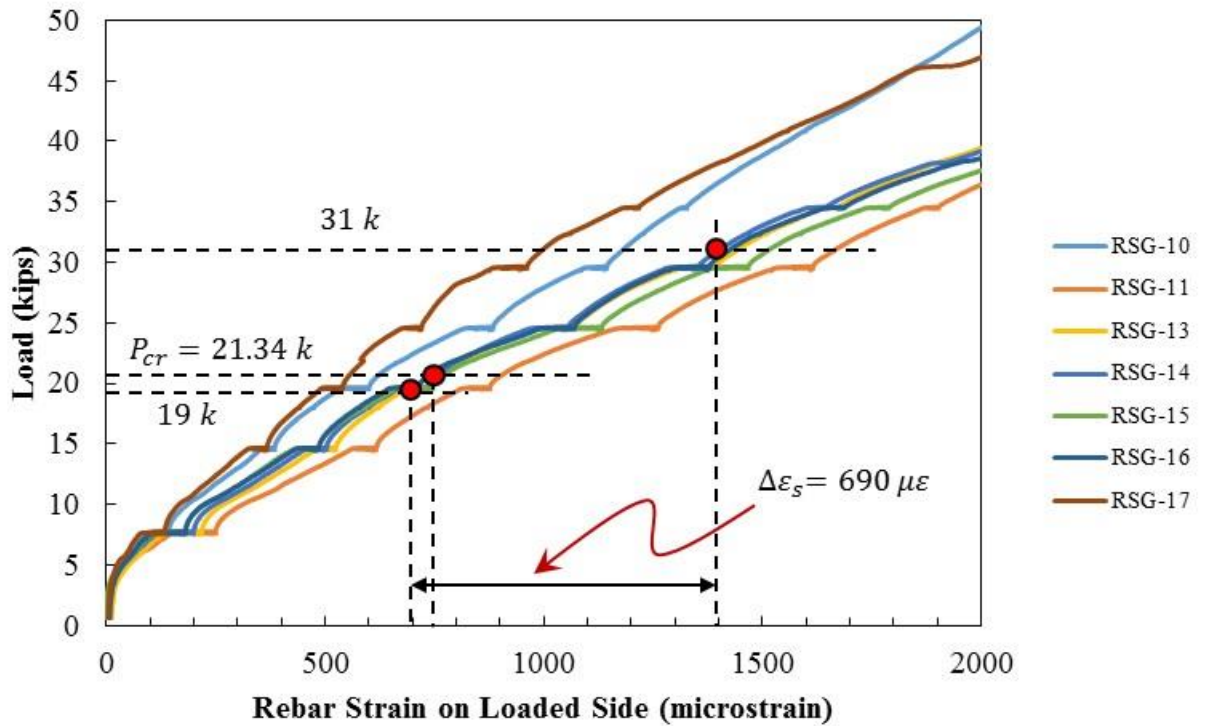


Figure B.2: Procedure for selecting load range from rebar strain range (for 12F1)

C. Fatigue Loading Scheme for Full-Scale Joint Specimens

The second full-scale two-beam system test was used to evaluate the fatigue and strength behavior of the system. The strength and fatigue protocols will be like those used for the small-scale joint testing program. Three main testing stages are proposed to assess the fatigue performance of the FSB for accelerated construction over a 100-year design lifespan.

C.1 Fatigue Loading Scheme

The goal of the test was to simulate truck traffic loading during a period of 100 years of service life acting on the large-scale UHPC connection. Originally, the FSB superstructure system was restricted to off-system bridges with a low Average Daily Traffic (ADT) and Average Daily Truck Traffic (ADTT) [54], and according to the Code of Federal Regulations (CFR) Title 23 §470.103 [107], off-system projects are bridges not located on the State Highway System (SHS) or the National Highway System (NHS), classified as local roads or rural minor collectors. Low volume and high volume roadways are classified by the FDOT Plans Preparation Manual, Volume 1, Glossary of Terms [108], based on functionality (freeway, arterial, and collector) and type of facility (two-lane, four-lane, six-lane, and eight-lane facilities), as summarized in Table C.1.

Table C.1 FDOT standards for low and high-volume highways (AADT: Annual Average Daily Traffic)

| Facility | | Urban | | Rural | |
|-----------|-----------------|-----------------|------------------|-----------------|------------------|
| | | Low Volume AADT | High Volume AADT | Low Volume AADT | High Volume AADT |
| Freeway | 4-Lane Facility | 57,000 | 69,000 | 46,000 | 56,000 |
| | 6-Lane Facility | 86,000 | 103,000 | 69,000 | 83,000 |
| | 8-Lane Facility | 114,000 | 138,000 | 92,000 | 111,000 |
| Arterial | 2-Lane Facility | 16,000 | 20,000 | 9,000 | 14,000 |
| | 4-Lane Facility | 37,000 | 43,000 | 38,000 | 47,000 |
| | 6-Lane Facility | 55,000 | 64,000 | 58,000 | 71,000 |
| | 8-Lane Facility | 69,000 | 80,000 | -- | -- |
| Collector | 2-Lane Facility | 11,000 | 16,000 | 8,000 | 13,000 |
| | 4-Lane Facility | 37,000 | 45,000 | 30,000 | 38,000 |

The previous assumption made in the small-scale fatigue testing protocol was to use the highest low-volume Annual Average Daily Traffic (AADT) number of 37,000 for a collector functional classification, limiting such study to a lower operating roadway. However, an increased AADT was scheduled to be used as baseline for the large-scale fatigue testing protocol, and this characteristic is the basic value of the fatigue loading scheme definition. Three main assumptions are made in terms of truck traffic number, design truck types, and the cycle count and are described in the next sections.

C.2 Assumption for Truck Traffic Number

The total truck traffic number for a 100-year design is obtained from a two-stage computation in which the AADT is first calculated for the requested design lifespan, and then the Annual Average Daily Truck Traffic (AADTT) is obtained. This will be transformed to the total truck traffic number to be used in the following cycle count section.

C.1.2 Estimating the AADT for 100-year design life

Although the FSB superstructure is currently permitted for collectors as per definition [54] [107], the tested performance of the modified FSB joint for accelerated construction showed no transverse flexural strength decay over an approximated period of 100 years for low-volume, urban collectors (see Task 4e). Therefore, the truck traffic number will be now evaluated for a freeway functional classification with larger AADT volume, being a high-volume eight-lane urban facility of 138,000 AADT. Previously in Task 4e, an assumption was made to consider traffic growth by rounding up the final truck traffic number to the nearest hundred. However, the AASHTO LRFD Bridge Design Specifications (§C3.6.1.4.2) [73] states that traffic growth data is usually not predicted for the bridge design life, taken as 75 years unless otherwise specified by the owner. Hence, the selected 138,000 AADT can be maintained up until the year 75th in the design. To account for traffic growth in the additional 25-year-design period due to uncertainties, a forecasted AADT is needed for the year 100th using the Equation C.1, recommended in the Traffic Data Computation Method [109], shown below:

$$AADT_{Future} = AADT_{Current} * (1 + AACR)^n \quad \text{Equation C.1}$$

Where:

$AADT_{Future}$ = Annual Average Daily Traffic for the forecasted year (vehicles/day)

$AADT_{Current}$ = Annual Average Daily Traffic for the current year (vehicles/day)

$AACR$ = Annual Average Change Rate

n = number of forecasted years

A typically accepted value for number of forecasted years is 20, which covers 18 to 25 years from the time of data forecast [109]. The AACR is usually computed by using the statewide modeling programs and data provided by metropolitan planning organizations (MPOs) for each selected facility [109]. In this case, a generally accepted rate provided by two practicing engineers is 1.5 percent. Therefore, the forecasted AADT for the year 100th of design life is:

$$AADT_{Future} = 138,000 * (1 + 0.015)^{20} = 185,865,99 \approx 185,866$$

This result represents a total theoretical AADT increase of 35 percent or 47,866 over a period of 18 to 25 years above the year 75th, which is suitable to account for uncertainties due to traffic growth or traffic pattern changes.

C.1.3 Estimating the AADT for 100-year design life

The AADTT can be determined by multiplying the AADT by the fraction of trucks in the traffic. The AASHTO LRFD Bridge Design Specifications (§C3.6.1.4.2) [73] states that the fraction of trucks in traffic is 15 percent for Urban-Interstate-Highway class, and applying this percentage to the 75-year design period AADT, the bidirectional AADTT is

20,700. Also, the Specifications states that one direction of traffic carries more than one-half of the bidirectional AADT; thus, designing for 55 percent of the bidirectional AADT is recommended [73]. Therefore, the unidirectional AADTT is 11,385 for a 75-year lifespan. However, for the additional 25-year-design period AADTT and unidirectional AADTT, if the annual traffic average increases, so does the fraction of trucks until the final forecasted AADT. As a result, the unidirectional truck traffic was computed over time until the 100th year using a 1.5 percent AADT increment for future years above the 75th. Table C.2 includes the unidirectional AADTT computation for the additional 25-year design lifespan needed in the overall 100-year design.

Table C.2: Total Unidirectional AADTT Calculation for 100-Year Design Life

| Design Year | Future AADT | Bidirectional AADTT | Unidirectional AADTT |
|--------------------|--------------------|----------------------------|-----------------------------|
| 75 | 138,000 | 20,700 | 11,385 |
| 76 | 140,070 | 21,011 | 11,556 |
| 77 | 142,171 | 21,326 | 11,729 |
| 78 | 144,304 | 21,646 | 11,905 |
| 79 | 146,468 | 21,970 | 12,084 |
| 80 | 148,665 | 22,300 | 12,265 |
| 81 | 150,895 | 22,634 | 12,449 |
| 82 | 153,159 | 22,974 | 12,636 |
| 83 | 155,456 | 23,318 | 12,825 |
| 84 | 157,788 | 23,668 | 13,017 |
| 85 | 160,155 | 24,023 | 13,213 |
| 86 | 162,557 | 24,384 | 13,411 |
| 87 | 164,995 | 24,749 | 13,612 |
| 88 | 167,470 | 25,121 | 13,816 |
| 89 | 169,982 | 25,497 | 14,024 |
| 90 | 172,532 | 25,880 | 14,234 |
| 91 | 175,120 | 26,268 | 14,447 |
| 92 | 177,747 | 26,662 | 14,664 |
| 93 | 180,413 | 27,062 | 14,884 |
| 94 | 183,119 | 27,468 | 15,107 |
| 95 | 185,866 | 27,880 | 15,334 |

| | | | |
|---------------|---------|----------|----------|
| 96 | 185,866 | 27,880 | 15,334 |
| 97 | 185,866 | 27,880 | 15,334 |
| 98 | 185,866 | 27,880 | 15,334 |
| 99 | 185,866 | 27,880 | 15,334 |
| 100 | 185,866 | 27,880 | 15,334 |
| Overall Total | -- | 625,239* | 343,882* |

**Does not include the values in the 75th year, which is already accounted for in the 75-year design lifespan*

The amount of trucks in 100 years of service life is equal to the AADTT multiplied by 75 years plus the additional AADTT increasing over time during a period of 25 years as calculated in Table C.1, shown below and rounded up to the nearest thousandth as per FDOT recommendation [110]:

$$N^{\circ} Trucks_{100\ years} = (11,385 * 75\ years) + 343,882 = 1,197,757 \approx 1,198,000$$

This truck traffic volume represented the amount of unidirectional truck traffic for a design life of 100 years. As trucks have four lanes available, AASHTO LRFD Bridge Design Specifications (Table 3.6.1.4.2-1) [73] states the fraction of truck traffic in a single lane for this configuration is 80 percent. Therefore, one lane of traffic will carry 958,400 trucks over the entire design period.

C.3 Assumption for Cycle Count

Different researchers have tested the service performance of bridge joints using several cycles counts to simulate truck traffic incidence. Yuan et al. [7], [8] applied nearly seven million cycles to different box beam connection settings, boundary conditions, and load ranges, by subdividing the analysis in different loading stages and cycle counts. Haber and Graybeal [25] performed low load-level cycles and later at least two million cycles of fatigue loading to assess the large-scale performance of 75 deck panel connection

assemblies. Each assembly was subjected to three different loading protocols varying the load level and cycle number. Miller et al. [20] analyzed the shear key performance of full-scale adjacent box girders by applying two million cycles, and subdividing the analysis in different intervals to check if any joint cracks or decaying transverse load transfer mechanism was occurring. Badie et al. [111] assessed the cyclic performance of a simplified connection detail between full-depth precast concrete deck panels and beams. To expedite the fatigue test, the fatigue load was magnified by a factor that decreased the cycles number, which resulted in 1.9-million magnified cycles, or 6.86-million design fatigue cycles. Although no correlation between traffic and cycles number was established in either studies, the cyclic performance seems to be tested above at least two million cycles, or until strength degradation is observed using the traffic load but not frequency, thus representing sufficient fatigue performance.

The number of trucks passing directly over at least one FSB bridge joint during a 100-year service life was approximated above to be 958,400. This number can be correlated to a certain amount of fatigue load cycles, and because each truck has two rear axles of either 32 kips (HS20) or 53.3 kips (FL120), one load cycle of the fatigue loading scheme can be counted as one axle from one truck riding over a typical bridge lane. Therefore, 958,400 trucks represent 1,916,800 rear axles or cycles over the 100-year service lifespan of a bridge. However, the test specimen is limited to one joint (two-beam configuration) of a full-width bridge, so an assumption must be made regarding the load configuration. If the rear-axle centerline is aligned with the joint centerline as shown in Figure C.1 (a), the wheel patches will be located on the outside of both beams as shown in Figure C.1 (b); this will create transverse tensile strain at the top and compression strain at the bottom specimen

regions when it is loaded, as shown in Figure C.1 (c). This loading configuration was identified as Load Configuration 2-4 and was described in detail in §6.3.2.

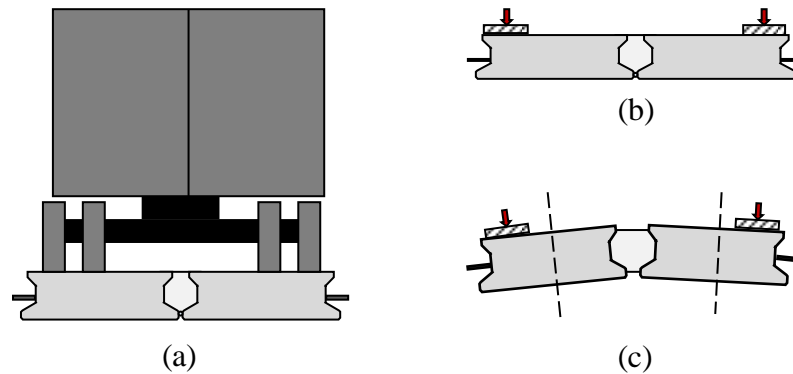


Figure C.1: Load Configuration 2-4 with (a) truck rear axle aligned at the joint centerline, (b) specimen load point locations, and (c) deformed specimen due to applied load

Although transverse tensile strain was seen at the top region with Load Configuration 2-4, both beams were deflecting at the same time during the load application. The effect of the rear axle over the joint can be further exploited if the beams deflect independently when the load is applied, similar to Load Configuration 2-4. This will subject the joint to a stress reversal during each cycle's application. To model such effect, a half-axle can be applied on each beam independently, simulating two trucks riding over the joint loading one side first to peak while the other side is loaded to minimum, as shown in Figure C.2 (a). The wheel patches will still be located on the outside of both beams, but the load is applied at different times, as shown in Figure C.2 (b). This should create a transverse moment that is detrimental to the joint strength caused by the beams deflecting independently, as shown in Figure C.2 (c).

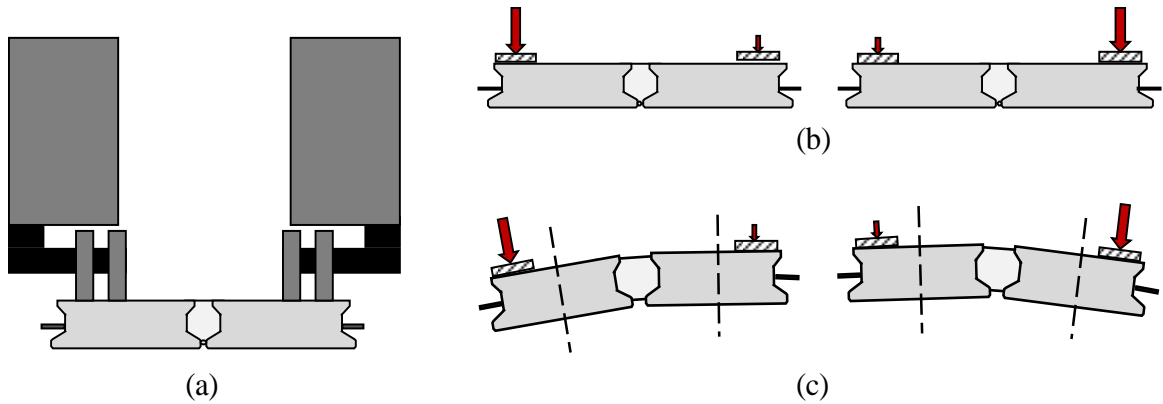


Figure C.2: Alternating Load Configuration 2-3 with (a) half-truck rear axles outside the joint centerline, (b) specimen load point locations, and (c) deformed specimen due to applied load

The complete load cycle calculation for the fatigue test is based on the below step-by-step procedure for an urban 8-lane freeway facility:

| <u>75-Year Design Life</u> | <u>Additional 25-Year Design Life</u> |
|--|--|
| From Table C.1: | $AADT_{Future} = AADT_{Current}$ |
| $AADT_{Bi} = 138,000$ | $* (1 + AACR)^n$ |
| As traffic growth data is usually not | $AADT_{Current} = AADT_{Bi} = 138,000$ |
| predicted for the design life of bridges (75 | $AACR = 1.5\%$ |
| years), then the total average traffic for the | $n = 20 \text{ years (accounts for 18 – 25}$ |
| year 75 th is: | $\text{years})$ |
| $ADT_{Bi} = 138,000 * 75$ | $AADT_{Future} \approx 185,866 \text{ (year 100th)}$ |
| $ADT_{Bi} = 10,350,000$ | |

The percentage of truck traffic is 15 percent for Urban-Interstate-Highway class; hence:

$$ADTT_{Bi} = 10,350,000 * 15\%$$

$$ADTT_{Bi} = 1,552,500 \text{ trucks}$$

One direction of traffic carries more than one-half of $ADTT_{Bi}$, or 55 percent; hence:

$$ADTT_{Uni} = 1,552,500 * 55\%$$

$$ADTT_{Uni} = 853,875 \text{ trucks}$$

Total cumulative of bidirectional truck traffic using 15 percent (from Table C.2) is:

$$ADTT_{Bi} = 605,239 \text{ trucks}$$

One direction of traffic carries more than one-half of $ADTT_{Bi}$, or 55 percent; hence the cumulative unidirectional truck traffic is (from Table C.2):

$$ADTT_{Uni} = 343,882 \text{ trucks}$$

Therefore, the estimated total amount of truck traffic in 100 years of design life rounded up to the nearest thousand is:

$$N^{\circ} \text{ Trucks}_{100 \text{ years}} = 853,875 + 343,882 = 1,197,757 \approx 1,198,000 \text{ trucks}$$

The above result represents the amount of unidirectional (four lanes) truck traffic for a design life of 100 years. Based on the assumption that at least two lanes have alternating trucks, the fraction of truck traffic in two lanes is taken as 80%: therefore:

$$N^{\circ} \text{ Trucks} = 1,198,000 * 80\% = 958,400 \text{ trucks}$$

As each truck has two rear axles, the total amount of axles is:

$$N^{\circ} \text{ Axles} = 958,400 * 2 = 1,916,800 \text{ axles}$$

Finally, the total number of axles is equalized to the total number of cycles and rounded to the nearest millionth, as shown below:

$$N^{\circ} \text{ Axles} = N^{\circ} \text{ cycles} = 1,916,800 \approx 2,000,000 \text{ cycles}$$

This total amount of cycles is used in the large-scale fatigue testing protocol.

Where:

| | | |
|------------------|---|---|
| $AACR$ | = | Annual Average Change Rate |
| $AADT_{Bi}$ | = | Bidirectional Annual Average Daily Traffic (vehicles/day) |
| $AADT_{Current}$ | = | Annual Average Daily Traffic for the current year (vehicles/day) |
| $AADT_{Future}$ | = | Annual Average Daily Traffic for the forecasted year (vehicles/day) |
| ADT_{Bi} | = | Bidirectional Average Daily Traffic (vehicles/day) |
| $ADTT_{Bi}$ | = | Bidirectional Average Daily Truck Traffic (vehicles/day) |
| $ADTT_{Uni}$ | = | Unidirectional Average Daily Truck Traffic (vehicles/day) |
| n | = | number of forecasted years |

C.4 Assumption for Fatigue Load Ranges

The goal of this fatigue testing is to determine if there is a degradation in joint performance under service conditions during a 100-year design period. Degradation of joint performance could include debonding at the joint interface, which would allow for the ingress of chlorides, and a decreasing ability of the joint to transmit load from one beam to the other. A fatigue load range was established based on HS20 truck loading and a monotonic service load range based on the FL120 truck.

During the service load assessment in the previous strength test, two monotonic load ramps using Load Configuration 2-4 were applied to the two-beam specimen until first cracking of the system was observed. Transverse cracks underneath the specimen at midspan were observed when the actuator force was at 68.5 kips, after which the specimen behavior went non-linear. Although some minor longitudinal bottom cracks were observed at 30, 40, and 50 kips near midspan, no joint debonding was detected during testing, as measured by top and bottom Crack Displacement Transducers (CDT). Also, the joint reinforcement response data from the Rebar Strain Gauges (RSG) in both east and west joint center sides showed insignificant rebar engagement, indicating the concrete withstood the majority of the tensile stresses across the joint. The performance of the uncracked system is desired for the fatigue testing stages of this research, so a load range will be selected less than the previously observed 68.5-kip cracking load.

C.4.1 Selection of FL120 Load Range

The FL120 is the truck load selected for service static performance, which is intended to simulate permit traffic truck driving over the joint during its lifespan. Because two actuators are planned to be used with Load Configuration 2-4, each actuator load range will be between unloaded condition (zero kips) to an upper limit that must not surpass the above-mentioned cracking load divided by two, ending up in 34.25 kips. The upper load range for the static load ramps is calculated using Equation C.2.

$$P = (1 + IM) * P_{wheel} \quad \text{Equation C.2}$$

$$P = (1 + 0.15) * 26.65 \text{ k} = 30.65 \text{ kips} < 34.25 \text{ kips}$$

where:

IM = Dynamic Load Allowance = 0.15 from AASHTO LRFD Bridge Design Specifications (§3.6.2.1) [73]

P_{wheel} = FL120 rear axle wheel load = 13.325 kips (x2)

P = Actuator load for FL120

C.4.2 Selection of HS20 Load Range

The HS20 is the truck load selected for cyclic performance with the alternating load configuration 2-4 (FC 2-5). For the minimum load level, the bearing pads located at the beam supports should be compressed by the beams to ensure proper load bearing capacity and avoid any uneven load distribution at the supports. Also, the bearing pads simulating the wheel patches located at the top must not shift from the load application points. An actuator load of 5 kips was selected as the lower load range, similar to the small-scale testing phase and the load used by other researchers [7], [8], [25].

The upper load range for the cyclic loading is calculated using the same Equation C.2

$$P = (1 + 0.15) * 16 k = 18.40 kips$$

P is added to the lower limit to calculate the upper limit, as shown in Equation C.3

$$P_{upper} = (1 + IM) * P_{wheel} + P_{lower} \quad \text{Equation C.3}$$

$$P_{upper} = 18.40 k + 5 k = 23.40 kips < 34.25 kips$$

where:

P_{wheel} = HS20 rear axle wheel load = 8.0 kips (x2)

P_{lower} = lower cyclic load

P_{upper} = upper cyclic load

These load ranges were used in the fatigue load testing protocol described in §6.3.2.

D. Concrete and Reinforcement Material Properties for Beam Specimens

The relevant material properties for the concrete and reinforcement used to construct the precast sections, CIP deck for the FSB, and joints for the optimization study (§5.5.1) are presented in this section.

D.1 Concrete Mixture Properties

The specified mix design for all the precast sections was FDOT Concrete Class VI and for the CIP deck was FDOT Concrete Class II in concordance with FDOT Developmental Specifications [100], [112]. Each precast beam was built by a local precaster using self-consolidating concrete with a target compressive strength at 28 days of 8,500 psi. The mixture design is shown in Table D.1. Note that the coarse aggregate, which was product FDOT Code 12 [113] and followed ASTM #67 specification [114], had a maximum aggregate size of ¾-inch.

Table D.1: Concrete mixture design for Class VI concrete used in precast sections

| Component | Quantity |
|---|-----------------|
| Cement – Type II | 735 lbs. |
| Fly Ash – Class F | 165 lbs. |
| C12 - #67 Stone | 1324 lbs. |
| F01 – Silica Sand (Concrete) | 1270 lbs. |
| Darex AEA – Admixture for Concrete – Air Entraining | 2 fl. oz. |

| | |
|---|-----------------------|
| ZYLA 610 – Admixture for Concrete – Type D | 36 fl. oz. |
| ADVA Cast 600 – Admixture for Concrete Type F | 50 fl. oz. |
| Water | 36 gallons (300 lbs.) |

The concrete used for the CIP deck and joint of the FSB specimens was specified with a target compressive strength at 28 days of 4,500 psi. The concrete mixture design provided by the ready-mix plant is shown in Table D.2.

Table D.2: Concrete mixture design for Class II concrete used for CIP deck and joint in FSB control specimens

| Component | Quantity |
|---|-----------------|
| Cement – Type I/II | 635 lbs. |
| Coarse Aggregate | 2220 lbs. |
| Fine Aggregate | 1420 lbs. |
| Fly Ash – Class F | 155 lbs. |
| Darex AEA – Admixture for Concrete – Air Entraining | 4 fl. oz. |
| WRDA64 – Admixture for Concrete | 40 fl. oz. |
| Water | 24 gallons |

One of the bottom ledges needed to be repaired in the 12F2-1 specimens due to fracture when the beams were being prepared for UHPC casting. A concrete mixture, shown in Table D.3, was used to repair the ledge and proceed with the UHPC cast.

Table D.3: Mixture design to repair ledge in 12F2-1

| Component | Quantity |
|------------------|-----------------|
| Vibropruf-11 | 50 lbs. |
| Sand | 7 lbs. |
| Pea Gravel | 20 lbs. |
| River Rock | 10 lbs. |
| Water | 8.85 lbs. |

The UHPC mixture was specified to be Ductal[®] JS1000, which is a proprietary UHPC mixture commonly used for field-cast closure pours for prefabricated bridge element connections. This UHPC mixture contains the following components:

- *Premix (dark-grey)*: pre-blended cement, sand, ground quartz, and silica fume
- *Liquid Admixture*: high range water reducer
- *Steel fibers*: 0.008 in. diameter x 0.5 in. long; tensile strength > 290 ksi
- *Water and/or ice*: Ice required when batching in warm/hot weather

D.2 Steel Reinforcement Properties

Three sizes of Grade 60 mild steel reinforcement were used to build all the precast specimens: #3, #4, and #5 reinforcement. Six fully bonded pre-tensioned strands were used in the precast section with a small amount of prestressing (50 ksi) to simulate some level of prestressing in the longitudinal direction. The measured properties for the steel reinforcement were provided by the precaster, shown in Table D.4. The #5 reinforcement was taken from four different lots.

Table D.4: Steel Material Data

| Description | Yield (psi) | Tensile (psi) |
|---------------------------------|--------------------|----------------------|
| #3 Rebar A615M Gr60 | 64,400 | 100,600 |
| #4 Rebar A615M Gr60 | 70,800 | 100,200 |
| #5 Rebar A615M Gr60 (a) | 66,900 | 97,400 |
| #5 Rebar A615M Gr60 (a) | 65,400 | 96,600 |
| #5 Rebar A615M Gr60 (a) | 66,000 | 96,300 |
| #5 Rebar A615M Gr60 (a) | 66,700 | 98,200 |
| .600 7 wire 270 low lax. strand | 251,000 | 275,000 |

(a) Rebars from four different lots/heats were used

VITA

FRANCISCO DE JESUS CHITTY GOZALO

Born, San Félix, Venezuela

| | |
|-------------|--|
| 2008 - 2013 | B.S., Civil Engineering Andres Bello Catholic University Ciudad Guayana, Venezuela |
| 2014 - 2016 | M.S., Civil Engineering Florida International University Miami, FL, USA |
| 2016 - 2021 | Doctoral Candidate Florida International University Miami, FL, USA |
| 2021 | Teaching Assistantship – Florida International University, Miami, FL, USA |
| 2020 - 2021 | Tau Beta Pi Fellow – The Engineering Honor Society |
| 2019 | Outstanding Achievement Scholarship – Florida Structural Engineering Association |
| 2018-2019 | Graduate Student of the Year – ASCE Florida Section – Miami-Dade Branch |
| 2017 | Poster and Travel Award – PCI Convention & National Bridge Conference |

PUBLICATIONS AND PRESENTATIONS

Chitty F., Freeman C., Garber D., (2021), *Full-Scale Testing of Slab-Beam Bridge System for Accelerated Bridge Construction*, submitted to ASCE Journal of Bridge Engineering.

Chitty F, Zapata I, Freeman C, Garber D., (2021), *Precast Concrete Superstructure Systems for Accelerated Construction of Short-Span Bridges*, to be submitted to Engineering Structures Journal.

Chitty F., Freeman C., Garber D., (2020), *Joint Design Optimization for Accelerated Construction of Slab Beam Bridges*, ASCE Journal of Bridge Engineering, vol. 25, no. 7. DOI: 10.1061/(ASCE)BE.1943-5592.0001561

Chitty F., Freeman C., and Garber D., (2019), *Performance of Longitudinal Joint in ABC Slab Beam Bridges*, ABC International Bridge Conference.

Chitty F., Garber D., Freeman C., (2019), *Joint Demand in Slab Beam Bridges*, PCI Committee Days.

Chitty F., Garber D., Freeman C., (2019), *UHPC Shear Key Design Optimization for Slab Beam Bridges*, ASCE/SEI Structures Congress.

Garber D., Freeman C., Chitty F., (2019), *Modification of Florida Slab Beam Incorporating Ultra High-Performance Concrete*, TRB 98th Annual Meeting.

Garber D., Freeman C., and Chitty F., (2019), *Longitudinal Joint Design of Slab Beam Bridge for Accelerated Construction*, FPCA Annual Membership Meeting, Invited guest speaker.

Chitty F., Garber D., Freeman C., (2018), *Development of UHPC Joint Detail for Florida Slab Beam Bridge*, PCI Annual Convention.

Garber D., Chitty F., (June 2018), *Concrete I-Beam for Bridge Construction*, US Patent 9,988,775.

Chitty F., Freeman C., Garber D., (2018), *Development of Longitudinal Joint Details for Florida Slab Beam Incorporating Ultra-High-Performance Concrete*, TRB 97th Annual Meeting, Latest Accelerated Bridge Construction Innovations from Research.

Chitty F., Freeman C., Garber D., (2018), *Analysis of Efficient Prestressed Concrete Superstructures for Short-Span Bridges for Accelerated Construction*, TRB 97th Annual Meeting, Latest Accelerated Bridge Construction Innovations from Research.